UNIVERSITAT DE BARCELONA

Molecular characterization of neurofibromatosis type 1–associated malignant peripheral nerve sheath tumours and functional identification of genes involved in their pathogenesis

Ernest Terribas Pérez

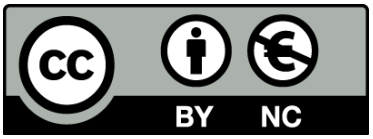

MOLECULAR CHARACTERIZATION OF NEUROFIBROMATOSIS TYPE 1–ASSOCIATED MALIGNANT PERIPHERAL NERVE SHEATH TUMOURS AND FUNCTIONAL IDENTIFICATION OF GENES INVOLVED IN THEIR PATHOGENESIS

Ernest Terribas Pérez

2015

MOLECULAR CHARACTERIZATION OF NEUROFIBROMATOSIS TYPE 1–ASSOCIATED MALIGNANT PERIPHERAL NERVE SHEATH TUMOURS AND FUNCTIONAL IDENTIFICATION OF GENES INVOLVED IN THEIR PATHOGENESIS

Memòria presentada per

Ernest Terribas Pérez

Per optar al títol de

Doctor per la Universitat de Barcelona

Tesi realitzada a l'Institut de Medicina Predictiva i Personalitzada del Càncer
sota la direcció del Dr. Eduard Serra i Arenas

Programa de Doctorat en Biomedicina
Facultat de Farmàcia
Universitat de Barcelona

Director/Tutor	Doctorand
Eduard Serra i Arenas	Ernest Terribas Pérez

Novembre 2015

"Defensa el teu dret a pensar,
perquè fins i tot pensar de manera errònia
és millor que no pensar"

Hipàtia d'Alexandria, 355 – 415

"Sólo podemos ver poco del futuro,
pero lo suficiente para darnos cuenta
de que hay mucho que hacer"

Alan Turing, 1912 – 1954

A mis padres

Arriba el moment d'escriure les últimes línies d'aquesta tesi, i amb aquestes, els agraïments a tots aquells que he tingut a prop durant aquests cinc anys i escaig. Vull agraïr en primer lloc a l'Edu la possibilitat que em va brindar ara fa gairebé set anys de ser, en les seves paraules, el *pal de paller* del seu laboratori de recerca. També vull agraïr-li l'oportunitat d'haver realitzat la tesi sota la seva direcció. Han estat molts mesos de feina, amb moments bons i altres no tant, però val a dir que tot acaba sent més fàcil quan sempre reps un *gràcies* per la feina feta i quan sents que confien en tu. Gràcies, Edu, per ser la gran persona que ets. Gràcies als meus companys de grup per aguantar-me tot aquest temps, en especial a en Bernat, per tota la teva ajuda plasmada en aquesta tesi i per les nostres discussions científiques; a la Imma, per ser la millor companya que es pot tenir, per la teva complicitat i amistat; al meu company de fatigues tesils, en Josep, que durant aquests anys ha passat de ser pupil a ser col·lega; a la Meri, per la teva ajuda constant i pels teus consells; i a l'Eli, pel teu suport. També gràcies a tots aquells que heu format part del Serralab i que ja no hi sou: Jaume, Carles, Rocío... en especial a l'Helena, per haver-me aguantat en primera persona durant uns quants mesos. Gràcies també als altres membres del grup NF, els que hi són i els que ja no: a la Conxi, per la teva confiança; a la meva estimada i també *potablava* Juani; i al perla del Joan, per la teva amistat i per ser un excel·lent company d'aventurilles.

Gràcies als companys de l'IMPPC, institució que en breu serà història. Gràcies per la vostra ajuda, pel vostre suport, i pels grans moments viscuts fora de la feina, liant-la pel Raval o jugant al vòlei… A tots aquells que heu passat pel MAP lab: gràcies sobretot a la meva estimada Berta, per la teva gran amistat i per ser un exemple en molts aspectes, i a la Mar, por tu amistad y tu gran camaradería; també al meu estimat Quim, a la *estupenda* Marta, a l'esbojarrada Elvira, a la meva *darky* Yaiza, al *follonero* Sergi, Mireia, Llorenç, Inês, Anna, Raquel, Miquel Àngel,… També gràcies als companys del Buschbeck lab: en especial a la Vane, o sigui, la *vanesa valero querida en el mundo entero*, per la seva amistat; a mi amiga Melanija, a quien se quiere muy fácil, també a la meva estimada Anna, Catherine, David, Julien, Roberto, Sarah, Marcus,… I gràcies a la resta de companys de l'institut que cada dia feu recerca malgrat les dificultats: Emili, Gabrijela, Sonia, Jessica, Érica, Sara, Francisco, i a tota la resta de companys de l'IMPPC. Gràcies també als companys de l'IJC i de l'IGTP.

A dues grans persones i professionals que sense la seva ajuda no hagués estat possible no només aquesta tesi sinó moltes altres en aquesta institució: gracias Patri, por tu amistad i gràcies, Bárbara, per ser tan gran. Als companys dels serveis de suport a la recerca, tant de l'IMPPC com de l'IGTP: gràcies Gerard, Marco, Sheila, Raquel, Gabriel, Lauro, Maria Pilar, Anna, Eugeni, i a tots els companys d'administració i IT, en especial al Juan, per comprar tan bé. Gracias Oliver, Irina, y gracias a mi querida Milagros. Gracias Antonia. Gràcies als companys del comitè d'empresa, que cada dia vetllen per la dignificació dels treballadors que contribuïm a fer ciència en aquest centre i fora del mateix.

Vull agraïr també als meus orígens professionals en la recerca. Gràcies a tots aquells que heu passat per l'IRO-IDIBELL-ICO i que heu compartit moments amb mi. En especial vull agraïr l'amistat i el suport de la meva flor de comarques amb ànima camaca, la Magüi, y de mi flor manchega preferida, la Bego. Gràcies a la Mariona i a la resta d'ex-companys de l'IRO, a la Sara i a la resta d'ex-companys del LRT-1 de l'ICO, i a l'Eva i resta de companys del LRT-2 de l'ICO. Gracias también a Sara Larriba por darme mi primera oportunidad profesional, i a l'Oriol Casanovas per ensenyar-me molt del que avui sé.

En darrer lloc, però no per això menys important, vull agraïr als meus amics (molts d'ells ja esmentats) per ser-ho i per ser-hi, pel seu suport i pels seus consells: als que esteu aquí a prop meu i els que esteu més lluny: moltes gràcies a tots! Muchas gracias a mi familia: a mi padre, quien hoy estaría muy orgulloso del más pequeño de la casa; y a mi madre, por su constante apoyo y por su amor incondicional. Gracias mamá y papá por proporcionarme vuestro mayor tesoro: los valores que me han conducido hasta aquí. Gracias a mis hermanos y cunyats, que siempre están ahí cuando se les necesita, i als meus nebots. Y gracias a Julio César, mi *piri*, por compartir los últimos años de este proyecto, los más difíciles, por tu paciencia, y por tu constante apoyo y comprensión.

TABLE OF CONTENTS

ABBREVIATIONS

^{18}F-FDG	fluorine-18-labeled-fluorodeoxyglucose
BAF	B-allele frequency
BLAT	BLAST-like alignment tool
BSA	bovine serum albumin
CALM	café-au-lait macule
cAMP	cyclic adenosin monophosphate
CFC	cardio-facio-cutaneous syndrome
CGH	comparative genomic hybridisation
CNV	copy number variation
CPC	chromosomal passenger complex
Cq	quantification cycle
CSRD	cystein-serine rich domain
DMEM	Dulbecco's modified Eagle medium
DMSO	dimethyl sulfoxide
DNA	deoxyribonucleic acid
dNF	dermal neurofibroma
DTT	dithiothreitol
E	efficiency
FAP	familial adenomatous polyposis
FBS	fetal bovine serum
FISH	fluorescence in situ hybridization
GAP	GTPase activating protein
GEF	guanine exchange factor
GEM	genetically engineered mouse
GIST	gastrointestinal tumour
GRD	GAP Related Domain
H3K27me3	trimetylation of lysine 27 of histone 3
H3K9ac	acetylation of lysine 9 of histone 3
H3K9me2	dimetylation of lysine 9 of histone 3
HBOC	hereditary breast and ovarian cancer
HDAC	histone deacetylase
HFF	human foreskin fibroblast
HNPCC	hereditary nonpolyposis colon cancer
IC_{50}	half maximal inhibitory concentration
JCML	juvenile chronic myelomonocytic laeukemia
LDR	linear dynamic range
LINE	long interspersed element
LOH	loss of heterozygosity
LREA	long-range epigenetic activation
LRES	long-range epigenetic silencing
LRR	log R ratio
miRNA	micro RNA

MLPA	multiplex ligation-dependent probe amplification
MMPA	microsatellite multiplex PCR analysis
MPNST	malignant peripheral nerve sheath tumour
mRNA	messenger ribonucleic acid
NF	normalization factor
NF1	neurofibromatosis type 1
NF2	neurofibromatosis type 2
NLS	nuclear localization signal
NRE	normalized relative expression
NRQ	normalized relative quantity
NSML	Noonan syndrome with multiple lentigines
NTC	non-targeting control
PBS	phosphate buffered saline
PET	positron emission tomography
pNF	plexiform neurofibroma
PNS	peripheral nervous system
PRC1	Polycomb repressor complex 1
PRC2	Polycomb repressor complex 2
PREDA	position related data analysis
qPCR	quantitative polymerase chain reaction
RCN	relative copy number
RF	rescaling factor
RMA	robust multi-array average
RNA	ribonucleic acid
RQ	relative quantity
RT	retrotranscription
RTK	receptor tyrosine kinase
SC	Schwann cell
SCM	Schwann cell medium
SCNA	somatic copy number alteration
SINE	short interspersed nuclear element
siRNA	small interfering RNA
SKP	skin-derived precursor
SNP	single nucleotide polimorphism
STR	short tandem repeat
SVA	SINE/variable number of tandem repeats/Alu
SWAN	subset-quantile within array normalization
TI	transcriptional imbalance
TSG	tumour suppressor gene
UPL	Universal Probe Library
UTR	untranslated region

LIST OF FIGURES AND TABLES

INTRODUCTION

1. Hereditary cancer syndromes

The cell is the basic structural, functional and reproductive unit of life. In multicellular organisms cells are organized in tissues and organs and evolution has provided them with sophisticated regulatory mechanisms to control their properties, such as interaction, motility or division. However, these mechanisms may sometimes fail. We call cancer to a collection of diseases characterized by an uncontrolled division of cells, which can also invade surrounding tissues or even spread to distant organs.

Cancerous cells are able to both maintain proliferative signals and elude those that are antiproliferative. They can resist cell death and present a limitless replicative potential. Moreover, they can induce the generation of new blood vessels from pre-existing ones, which is known as angiogenesis, and activate the invasion to adjacent tissues and the dispersion to other organs, known as metastasis (Hanahan and Weinberg, 2000). During the last decade three more properties of cancerous cells have been proposed: genome instability, deregulation of cell metabolism and avoidance of immune destruction. Moreover, a new important concept known as “tumour microenvironment”, which considers their capacity of promoting inflammation by the recruitment of normal cells, has emerged (Hanahan and Weinberg, 2011). Another major concept is the “cancer stem cell”, which implies that not all cells present in a tumour would be tumourigenic but only a specific subgroup with self-renewal properties, the cancer stem cells, would be the ones generating the tumour (Tan et al., 2006).

In the predisposition to develop cancer there is a combination of inherited and environmental factors. Considering these two factors cancer can be classified into sporadic, familial or hereditary. Sporadic cancers account for 70-80% of all cancers and they appear over the lifetime of single individuals as a result of an accumulation of mutations in genes mainly due to environmental factors. About 10-20% of cancers are considered familial, since they appear in several members within a family. In these cancers there is a clear aggregation that can be caused by unidentified genetic factors, including more than a single gene, or due to the exposure of family members to a particular environment. Finally, hereditary cancer, which accounts for 5-10% of all cancers, appears in individuals within a family with a clear inheritance pattern and normally environmental factors represent a minor role.

Hereditary cancer syndromes are genetic inherited disorders that predispose the affected individuals within a family to develop cancer due to inherited mutations in particular genes. The mutated genes responsible for cancer syndromes can be oncogenes or, mostly, tumour suppressor genes (TSGs). Oncogenes are mutated forms of proto-oncogenes, which work as promoters of cell proliferation and survival in normal cells. These proto-oncogenes can induce cancer when they acquire dominant gain-of-function mutations. Examples of oncogenes are *RET*, *KIT* and *MET*. TSGs prevent normal cells from the acquisition of tumourigenic properties; hence loss-of-function mutations in TSGs can lead to tumourigenesis. TSGs can be classified in "gatekeepers" and "caretakers" (Kinzler and Vogelstein, 1996). Gatekeeper genes inhibit cell proliferation, induce apoptosis and promote differentiation, such as *RB* or *APC*. Caretaker or stability genes are responsible for the maintenance of DNA integrity and are involved in repairing DNA damage, such as *MLH1* or *ATM*. A third group of TSGs called "landscapers" that would be involved in the control of tumour microenvironment, has been proposed (Michor et al., 2004).

The majority of cancer syndromes are caused by pathogenic mutations in TSGs. They present a dominant inheritance pattern, where the presence of only one mutated allele is needed to develop the disorder. However, and according to Knudson's second-hit inactivation, the loss of both alleles of a TSG is necessary for tumour development (Knudson, 1971), thus TSGs act in a recessive manner at the cellular level.

Examples of hereditary cancer syndromes are hereditary breast and ovarian cancer (HBOC), hereditary nonpolyposis colon cancer (HNPCC) or Lynch syndrome, familial adenomatous polyposis (FAP) and the neurofibromatoses.

2. Neurofibromatoses and RASopathies

The neurofibromatoses are a group of three hereditary cancer syndromes characterized by the development of tumours in the nervous system. Neurofibromatosis type 1 (NF1; MIM 162200), Neurofibromatosis type 2 (NF2; MIM 101000) and schwannomatosis (MIM 162091 and 615670) share an occurrence of tumours in tissues derived from the neural crest, especially from Schwann cells (SCs) or their precursors.

NF1, also known as von Recklinghausen disease, is caused by mutations in the *NF1* gene (Viskochil et al., 1990; Cawthon et al., 1990b; Wallace et al., 1990). *NF1* is located at 17q11.2 region (Barker et al., 1987; Wallace et al., 1990) and its product neurofibromin is mainly a negative regulator of RAS protein (Ballester et al., 1990; Martin et al., 1990; Xu et al., 1990; Bollag and McCormick, 1991). The most characteristic clinical manifestation of NF1 is the presence of multiple benign tumours in the peripheral nerves called neurofibromas. NF2 is caused by mutations in the *NF2* gene (Trofatter et al., 1993; Rouleau et al., 1993). *NF2* is located at 22q12.2 and encodes the protein merlin, a scaffolding protein that links actin filaments to the cell membrane (Trofatter et al., 1993; Rouleau et al., 1993). The appearance of bilateral schwannomas in the vestibular nerves, which are highly homogeneous SC tumours, is the most distinctive trait of NF2 patients. Schwannomatosis is caused by mutations in both *SMARCB1* and *LZTR1* genes. *SMARCB1* is located at 22q11.23 region (Versteege et al., 1998) and encodes a subunit of the SWI/SNF chromatin-remodelling complex. About 50% of inherited cases of the disease are related to *SMARCB1* (Hulsebos et al., 2007; Sestini et al., 2008; Hadfield et al., 2008). In the 80% of cases with no mutation in *SMARCB1*, mutations in the *LZTR1* gene have been recently found (Piotrowski et al., 2014). Located closely to *SMARCB1*, at 22q11.21, *LZTR1* has been related to the stabilization of the cellular Golgi complex. The main clinical manifestations of schwannomatosis are similar to those of NF2 with the appearance of multiple schwannomas, but rarely at the vestibular nerve.

NF1 can also be classified as a RASopathy. The RASopathies are a group of developmental disorders caused by mutations in genes that encode components of the RAS/MAPK pathway. For some of them there is genetic heterogeneity and can be caused by mutations in several RAS/MAPK genes. Other RASopathies are associated with mutations in single genes of the pathway. RASopathies predispose patients to short stature, cognitive impairment, and also to the development of some tumours (Simsek-Kiper et al., 2013). Taken together the prevalence of RASopathies is about 1:1000 (https://rasopathiesnet.org). In addition to NF1, RASopathies also include, among others, Noonan syndrome, Cardio-Facio-Cutaneous (CFC) syndrome, Costello syndrome, Noonan syndrome with multiple lentigines (NSML; also named LEOPARD syndrome), and Legius syndrome.

3. Neurofibromatosis type 1: clinical manifestations

NF1 is a genetic disorder inherited as autosomal dominant, with half of the cases being *de novo*. Its incidence at birth is of 1:2500 individuals and its minimum prevalence of 1:4000 – 1:5000 individuals (Huson et al., 1989). It presents a complete penetrance at the age of eight (DeBella et al., 2000). NF1 shows a high variability in its clinical manifestations, affecting several tissues and being the most distinctive a high predisposition to develop neural crest-derived tumours, especially in the Peripheral Nervous System (PNS).

The most frequent clinical traits are alterations of skin pigmentation called café-au-lait macules (CALMs) and skin-fold freckling, hamartomas of the iris called Lisch nodules, and the development of multiple peripheral nerve sheath tumours. Among these tumours, dermal neurofibromas (dNFs) are the most frequent, affecting almost all (~99%) NF1 patients and whose number is variable, ranging from tens to thousands among patients. Around 30% of NF1 patients have clinically visible plexiform neurofibromas (pNFs; Huson et al., 1988), which originate from multiple nervous fascicles and are thought to be originated during embryonic development (Riccardi, 1992). dNFs do not progress towards malignancy but certain pNFs transform into a type of soft-tissue sarcoma called malignant peripheral nerve sheath tumours (MPNSTs), that can also arise *de novo* or from internal neurofibromas. NF1 patients have an 8–13% lifetime risk of developing an MPNST (Evans et al., 2002), which is the leading cause of NF1-related mortality.

Concerning NF1 tumourigenesis, in addition to dNFs, pNFs and MPNSTs, NF1 patients can also develop other tumours, such as optic pathway gliomas, gastrointestinal tumours (GISTs), pheochromocytomas, glomus tumours of the digits, juvenile chronic myelomonocytic laeukemia (JCML), glioblastomas and rhabdomyosarcomas (reviewed in Brems et al., 2009). It has also been associated a higher risk of developing breast cancer in NF1 patients than in the general population (Sharif et al., 2007; Wang et al., 2012). Other traits associated to NF1 are specific osseous lesions (including dysplastic scoliosis, sphenoid wing dysplasia and long bones dysplasia, such as tibial pseudoarthrosis), short stature, macrocephaly, cardiovascular pathologies and cognitive problems.

The diagnostic criteria of NF1 approved in the US National Institutes of Health (NIH) Consensus Conference in 1987 (NIH, 1988) are:

- Six or more CALMs greater than 5 mm in prepubertal individuals and over 15 mm in postpubertal individuals
- Two or more neurofibromas of any type or one pNF
- Freckling in the axillary or inguinal regions
- Optic glioma
- Two or more Lisch nodules (iris hamartomas)
- A distinctive osseous lesion such as sphenoid dysplasia or thinning of long bone cortex with or without pseudoarthrosis
- A first-degree relative (parent, sibling or offspring) with NF1 according to the above criteria

An individual is diagnosed with NF1 if two or more of these criteria are present.

4. *NF1* gene

4.1. Genomic region, gene structure and expression

The *NF1* gene is located at the pericentromeric region q11.2 of chromosome 17. It spans ~300Kb and it is considered a large gene, consisting of 60 exons (including three alternatively spliced exons 9a, 23a and 48a). Three genes, transcribed from the complementary DNA strand with respect to the *NF1* gene, *OMGP*, *EV12A*, and *EV12B*, are embedded in the large intron 27b (Cawthon et al., 1990a; Cawthon et al., 1991; Viskochil et al., 1991). The promoter region is located in a ~10Kb CpG-rich region (Rodenhiser et al., 1993) and contains several conserved binding motifs to transcription factors (Hajra et al., 1994). The 3'UTR region spans 3.5kb. Exons 21 to 27a encode a functional domain called GAP Related Domain (GRD). The *NF1* gene is located in a genomic region that contains three low-copy repeats (called REP-A, REP-B and REP-C), which are paralogous regions that flank *NF1*. These repeats, together with *SUZ12* gene and *SUZ12P1* pseudogene, are responsible for the generation of large deletions (also known as microdeletions) that arise via nonallelic homologous recombination (see section 4.3. and **Figure 2**).

Several *NF1* pseudogenes located at different chromosomes, including 2, 12, 14, 15, 18, 21, and 22, have been described (Legius et al., 1992; Gasparini et al., 1993; Suzuki et al., 1994; Purandare et al., 1995; Cummings et al., 1996; Kehrer-Sawatzki et al., 1997). These *NF1*-related sequences present different degrees of sequence homology with *NF1* and are suggested to have arisen by duplication and transposition of the *NF1* locus. Some of them are transcribed (Yu et al., 2005) but they are not totally processed and consequently they are not functional, although they can hinder the genetic analysis of the *NF1* gene.

The expression of *NF1* is found in nearly all adult tissues but it is especially relevant in the brain and the PNS (Wallace et al., 1990; Daston et al., 1992). The full-length *NF1* mRNA transcript is about 11 to 13 kb and five different isoforms have been identified (Nishi et al., 1991; Gutman et al., 1993; Danglot et al., 1995; Kaufmann et al., 2002), being the main ones type I and type II. Type I isoform contains 57 exons and type II contains, in addition, the alternative spliced exon 23a, which is introduced within the GRD (Nishi et al., 1991). This type II isoform is the most abundant NF1 transcript found in adult tissues (Teinturier et al., 1992) and it is translated to a neurofibromin that presents a lower capacity of negatively regulate RAS than type I isoform (Uchida et al., 1992; Andersen et al., 1993).

4.2. Neurofibromin

The product of *NF1* gene is the protein neurofibromin. This protein has 2818 aminoacids and a molecular mass of 250-280 kDa (DeClue et al., 1991; Gutmann et al., 1991). It is ubiquitously expressed, but its main expression is in the nervous system in neurons, oligodendrocytes and nonmyelinating SCs (Daston et al., 1992; Nordlund et al., 1993). It is highly conserved among vertebrates (Bernards et al., 1993).

Two neurofibromin domains have been so far well characterized at a functional level: the GRD (Ballester et al., 1990; Martin et al., 1990; Xu et al., 1990) and the contiguous SEC14-PH domain (Aravind et al., 1999). The GRD has 360 aminoacids, it is conserved among species and it contains an arginine finger structure that interacts with RAS protein (Scheffzek et al., 1998). This interaction stabilizes the transition state of the GTPase reaction and favours the RAS-GTPase activity; so active RAS-GTP is

inactivated to RAS-GDP. The SEC14-PH domain is composed of the Sec14p homologous segment and a PH-like domain, it is contiguous to the GRD and it has 256 aminoacids. SEC14-PH is involved in lipid-regulated processes and it has been shown to promote the interaction of neurofibromin to the cell phospholipids (D'Angelo et al., 2006; Welti et al., 2007).

Other functional binding domains in neurofibromin have been proposed, such as to syndecan (Hsueh et al., 2001); a nuclear localization signal (NLS; Vandenbroucke et al., 2004); a cystein-serine rich domain (CSRD) as a PKA recognition site (Izawa et al., 1996); to cytoskeletal proteins, such as tubulin (Gregory et al., 1993; Bollag et al., 1993), actin (Gutmann et al., 2001; Li et al., 2001) and keratin (Koivunen et al., 2000); to the molecular motor kinesin-1 (Hakimi et al., 2002); and to other regulators of RAS/MAPK pathway, such as SPRED1 (Stowe et al., 2012).

Neurofibromin is a GTPase Activating Protein (GAP) that negatively regulates RAS activation (**Figure 1**). Its degradation is mediated by the ubiquitin-proteasome pathway (Cichowski et al., 2003). RAS is a cytoplasmic protein anchored to the inner cell membrane that transduces extracellular signals from the membrane receptors to intracellular pathways (**Figure 1**). RAS proteins act as binary molecular switch that can alternate active states, when bound to GTP, and inactive states, when bound to GDP (**Figure 1**). These changes are regulated by two kind of mediators: Guanine Exchange Factors (GEFs), which promotes the release of GDP, enabling the binding of GTP, and GAP proteins, which stimulate hydrolysis of GTP bound to RAS.

RAS proteins are involved in several signalling pathways that control different cellular processes. The main ones are the RAS/RAF/MEK/ERK pathway (also known as RAS/MAPK), especially involved in cell proliferation and the RAS/PI3K/AKT/mTOR pathway, that especially promotes cell survival and growth (**Figure 1**). Gain-of-function mutations of *RAS* gene and loss-of-function mutations in *NF1* result in an increased activity of RAS and a permanent stimulation of the signalling pathways that can lead to tumourigenesis. In fact, it has been observed that loss of neurofibromin is correlated with high levels of RAS in NF1-associated tumours and derived cells (Basu et al., 1992; DeClue et al., 1992; Guha et al., 1996).

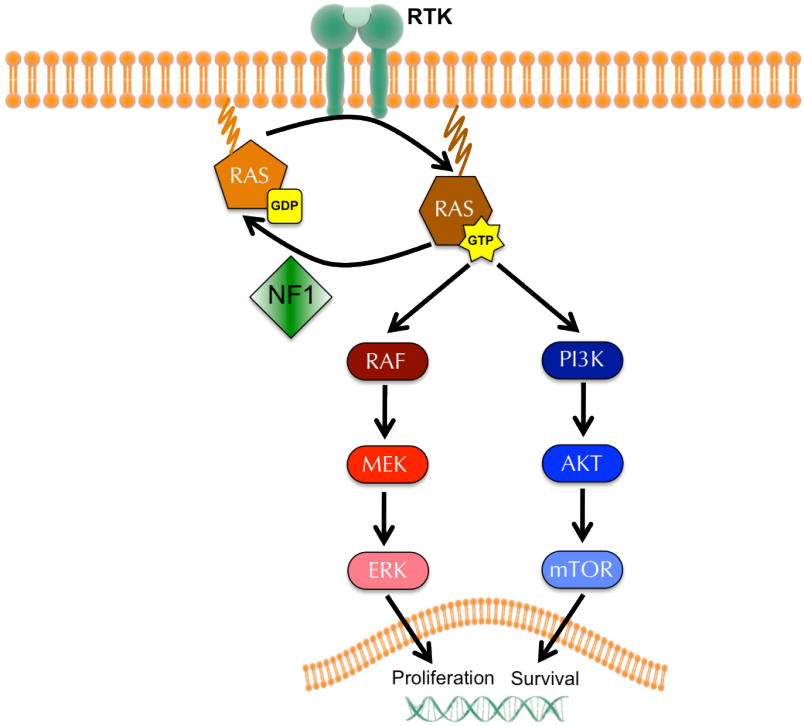

Figure 1. Regulation of RAS signalling pathways by neurofibromin. Activation of RAS requires exchange of GDP for GTP downstream from receptor tyrosine kinase (RTK) activation. The hydrolysis of GTP to GDP is catalysed by neurofibromin. Activated RAS regulates the downstream ERK and PI3K pathways involved in cell proliferation and survival, respectively. Modified from Katz et al., 2009.

Neurofibromin has also been shown to regulate the cAMP pathway by regulating adenylyl cyclase (AC) activity in yeast (Tanaka et al., 1989; Tanaka et al., 1990), in *Drosophila* (Guo et al., 1997) and in mice (Tong et al., 2002). The AC/cAMP/PKA pathway has many roles, especially in cell metabolism, proliferation and differentiation. Increased levels of cAMP inhibit the proliferation of most cell types, and it has been proposed that altered levels of cAMP can lead to cancer.

4.3. Constitutional mutational spectrum

The mutation rate of *NF1* is one of the highest among human genes (Friedman, 1999). The detection of mutations is complex because of the large size of the gene, the diverse spectrum of mutations identified so far, and the presence of pseudogenes. There is a high number of mutations distributed throughout the *NF1* gene and few of

them are recurrent. However, *NF1* does not seem to present any mutational hot spot (Messiaen and Wimmer, 2008).

NF1 patients show a wide spectrum of constitutional mutations. The majority (~93%) are point mutations, including splicing (~27%), insertion/deletions (~26%), nonsense (~21%), and missense mutations (18%). The remaining mutations consist of intragenic deletions/duplications (~2%) and microdeletions that span *NF1* and neighbouring genes (~5%; Messiaen and Wimmer, 2008). In a recent study, a targeted next-generation sequencing (NGS) of *NF1* in 246 patients obtained similar percentages of these types of constitutional mutations (Pasmant et al., 2015). Approximately 90% of *NF1* microdeletions (Types-1, -2, and -3) are recurrent and arise via nonallelic homologous recombination between low-copy repeats (REPs) or between the *SUZ12* gene and *SUZ12P1* pseudogene (**Figure 2**). REP-A and REP-C regions mediate Type-1 deletions, which are the most frequent (~77%; **Figure 2**). These regions span 1.4 Mb and contain *NF1* and 14 other protein-coding genes (Dorschner et al., 2000; Lopez Correa et al., 2000; Jenne et al., 2001). Type-2 deletions are less frequent (~9%) and typically appear in the context of somatic mosaicism. The distance between their breakpoints, which are located at the *SUZ12* gene and its pseudogene *SUZ12P1*, spans 1.2 Mb (Petek et al., 2003; **Figure 2**). The REP-B and REP-C regions are involved in the rare Type-3 deletions (~4%), which are 1.0 Mb in length (Bengesser et al., 2010; Pasmant et al., 2010; Zickler et al., 2012; **Figure 2**). In the remaining ~10% of constitutional *NF1* microdeletions, the so-called atypical deletions, the REPs are not involved in the generation of the breakpoint (Pasmant et al., 2010; Zickler et al., 2012; **Figure 2**). A new type of microdeletion, caused by insertions associated to SVA (SINE/variable number of tandem repeats/Alu) retrotransposons in the breakpoints, has been recently identified (Wimmer et al., 2011; Vogt et al., 2014; Hsiao et al., 2015).

Sometimes, constitutional mutations are not inherited directly from the germline and occur post-zygotically. When this happens the affected individual is composed of two genetically different cell populations, resulting in mosaicism. This can be somatic, if only somatic cells are affected; germline, when the mutation affects the gametes; or gonadosomatic, if the mutation is affecting both the somatic and the germ lines. In NF1, examples of the three types are found (Kehrer-Sawatzki and Cooper, 2008) and

mosaicism can present as a mild generalized NF1 phenotype if all embryonic layer derivatives are affected (NF1 generalized mosaicism), or can be characterized by the limitation of NF1 signs to specific areas of the body when only some of the layer derivatives are affected by the mutation (NF1 segmental mosaicism).

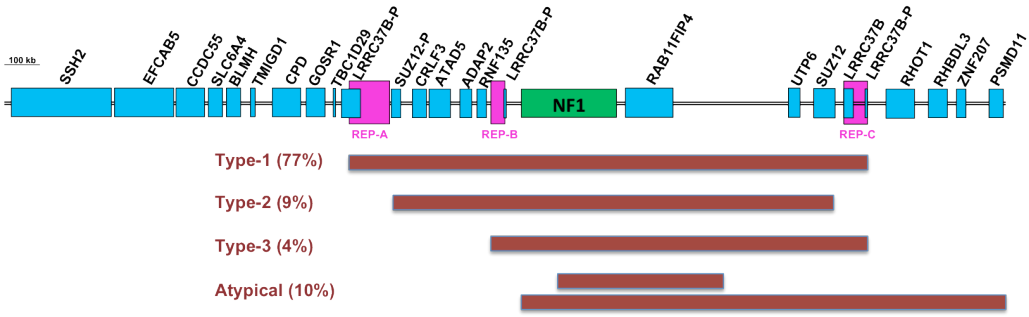

Figure 2. *NF1* region and types of constitutional microdeletions. Schematic representation of the *NF1* region at 17q11.2. *NF1* gene is represented by a green box, protein-coding genes are represented by blue boxes, and paralogous regions REPs are represented by pink boxes. Brown long rectangles show the four types of *NF1* constitutional microdeletions: Type-1 (mediated by REP-A and REP-C), Type-2 (mediated by the *SUZ12* gene and its pseudogene *SUZ12-P*), Type-3 (mediated by REP-B and REP-C) and atypical (neither the REPs nor *SUZ12/SUZ12-P* are involved in the deletion).

4.4. Somatic mutational spectrum

Several findings indicate that the *NF1* gene is a TSG. It is inactivated in all NF1-associated tumours, all bearing somatic second-hit mutations affecting the wild type allele (reviewed in De Raedt et al., 2008). The number of *NF1* somatic mutations identified so far is, however, limited because of the few number of analysis performed in tumours such as dNFs, and the presence of cellular heterogeneity in these tumours. Biallelic inactivation of the *NF1* gene is a key event in the development of dNFs (Colman et al., 1995; Sawada et al., 1996; Serra et al., 1997; Daschner et al., 1997; John et al., 2000) and pNFs (Daschner et al., 1997; Kluwe et al., 1999b; John et al., 2000), being SCs the ones bearing the second-hit inactivation (Kluwe et al., 1999a; Serra et al., 2000; Wallace et al., 2000; Maertens et al., 2006a). MPNSTs also show somatic mutations in *NF1* (Legius et al., 1993; Lothe et al., 1995). In CALMs the somatic mutation occurs in the melanocytes (Maertens et al., 2007; De Schepper et al., 2008). In tibial pseudoarthrosis double inactivation of *NF1* has also been found (Stevenson et al., 2006). Other NF1 traits, such as GISTs, pheochromocytomas, JCML, and glomus tumours of the digits, have also been observed to bear the biallelic

inactivation of the gene (De Raedt et al., 2008; Brems et al., 2009; Laycock-van Spyk et al., 2011).

Several studies have analyzed *NF1* somatic mutations in dNFs, concluding that ~75% are due to point mutations (i.e., nonsense, missense, small insertion/deletion, and splicing mutations) and intragenic deletions, and the remaining ~25% are evidenced by loss of heterozygosity (LOH; Serra et al., 2001; Maertens et al., 2006a; De Raedt et al., 2006; Thomas et al., 2010; Garcia-Linares et al., 2011; Thomas et al., 2012). The mechanistic causes of LOH are mitotic recombination in ~65% of cases and genomic deletions of 80 kb to 8 Mb in the remaining ~35% (De Raedt et al., 2006; Garcia-Linares et al., 2011). Biallelic inactivation evidenced by LOH has not been found in *NF1* microdeletion patients (De Raedt et al., 2006). LOH has also been detected in 30-60% of pNFs (Kluwe et al., 1999b; Rasmussen et al., 2000; Steinmann et al., 2009). In MPNSTs, 60-90% of the *NF1* second-hit inactivation is due to genomic deletions (Upadhyaya et al., 2008b; Bottillo et al., 2009). No epigenetic mechanisms as causative of a somatic inactivation of the *NF1* gene have been reported in NF1-associated tumours (Horan et al., 2000; Harder et al., 2004; Fishbein et al., 2005).

4.5. Genotype-phenotype correlations

There is a high clinical heterogeneity in NF1, even among individuals carrying the same mutation. Members from a same family or unrelated patients bearing the same *NF1* mutation can present different number and location of clinical manifestations (Szudek et al., 2000; Szudek et al., 2002; Szudek et al., 2003). Epidemiologic studies suggest that the underlying cause of this phenotypic variability can be due to different factors, such as age or environmental conditions. A molecular cause can be explained by the effect of modifier genes that could exert a more subtle effect by changing the efficiency of different steps in tumourigenesis and other traits, such as CALMs (Easton et al., 1993; Wiest et al., 2003).

Despite of this, some genotype-phenotype correlations regarding the constitutional mutation have been reported so far. The main one involves the ~5% of NF1 patients bearing constitutional microdeletions that encompass *NF1* and neighbouring genes. These patients, compared to the general NF1 population, present a more severe

clinical phenotype, including dysmorphic features (Kayes et al., 1994; Leppig et al., 1997; Pasmant et al., 2010), learning disabilities (Kayes et al., 1994; Pasmant et al., 2010), cardiovascular malformations (Venturin et al., 2005), childhood overgrowth (Pasmant et al., 2010) and a higher number of dNFs and pNFs at an earlier age (Wu et al., 1995; Leppig et al., 1997). In addition, and most importantly, *NF1* microdeletion patients present an increased lifetime risk for the development of MPNSTs (De Raedt et al., 2003). Besides these large deletions, two point mutations have also been significatively correlated with specific NF1 phenotypes. The intragenic deletion c.2970-2972delAAT leads to a 3-bp in-frame deletion in exon 17 and it is correlated with the presence of CALMs and the absence of dNFs and pNFs (Upadhyaya et al., 2007). Recently, two new missense mutations, c.5425C>T and C>G, that lead to the p.Arg1809Cys aminoacid substitution in neurofibromin, have been significatively associated with also a mild phenotype, consisting of the presence of CALMs, the absence of dNFs and pNFs and, in some cases, facial Noonan-like features (Rojnueangnit et al., 2015; Pinna et al., 2015).

5. Neurofibroma

5.1. Molecular and cellular pathogenesis

Neurofibroma is the most common NF1-associated tumour and the most characteristic trait of NF1. It is a benign tumour arising in peripheral nerves. Normal peripheral nerves are well-organized structures that contain neuronal axons. Each axon is surrounded by one SC, forming a protective sheath and a nerve fiber. Several nerve fibers cluster into nerve fascicles and each fascicle is then enclosed by concentric layers of perineurial cells. Multiple fascicles, fastened by connective tissue, constitute an individual nerve. Different cell types are found in nerve fascicle, including SCs, neural and perineurial cells, fibroblasts, endothelial cells and, sometimes, mast cells. During neurofibroma formation, the interaction among these cells is disrupted and the normal nerve structure is consequently lost. SCs are dissociated from nerves and the perineurium is disturbed. The most abundant cell type representing the 60-80% of neurofibroma cells is SC (Krone et al., 1983; Peltonen et al., 1988), which expresses the S100 protein. S100 can be immunohistochemically detected. Perineurial cells,

fibroblasts, mast cells, and an abundant extracellular matrix rich in collagen are also present in the neurofibroma.

A double inactivation of the *NF1* gene has been found in neurofibromas (Colman et al., 1995; Sawada et al., 1996; Serra et al., 1997). Subsequent molecular analyses showed that only a subpopulation of SCs bore the biallelic inactivation of the *NF1* gene ($SC^{NF1-/-}$), while other SCs ($SC^{NF1+/-}$) and fibroblasts within the neurofibroma did not present the second-hit mutation (Serra et al., 2000). Moreover, SCs lacking neurofibromin showed increased RAS activity and proliferative advantage compared to other neurofibroma cell components (Sherman et al., 2000; Muir et al., 2001). The advance of *Nf1*-deficient mouse models also supports that $SC^{NF1-/-}$ or a precursor is the initiating cell type in neurofibroma formation (Zhu et al., 2002).

Neurofibroma formation would be triggered by a second-hit inactivation of *NF1* in SCs or precursor cells (**Figure 3**), which may initiate the development of the tumour by activating a cascade of changes in other cell types as a result of their interdependency (Cichowski and Jacks, 2001). *NF1* heterozygosity in the tumour environment contributes to neurofibroma development in mouse models (Zhu et al., 2002). Infiltrated mast cells have been considered as an important player in neurofibroma formation (Riccardi, 1981; Johnson et al., 1989) and it has been demonstrated that in mice, $SC^{NF1-/-}$ alter neurofibroma microenvironment by secreting Kit ligand (KitL), which stimulates mast cell migration (Yang et al., 2003). $SC^{NF1-/-}$ have also been found to secrete other growth factors that promote angiogenesis (Mashour et al., 2001; Kawachi et al., 2003). Thus, the *NF1* haploinsufficiency present in neurofibroma environment would promote its formation in mice, but it should be addressed if this also occurs in human neurofibromas, given the differences that RAS-driven tumour types show between mice and humans (Hamad et al., 2002).

5.2. Neurofibroma subtypes: dNF and pNF

There is still no agreement among pathologists and clinicians on how to classify the different types of neurofibromas. Traditionally two neurofibromas subtypes have been defined: dermal neurofibromas (dNFs) and plexiform neurofibromas (pNFs).

Dermal neurofibromas are benign tumours affecting nearly all NF1 patients (**Figure 3**). Their size ranges from one millimetre to some centimetres and their number is also variable. Both size and number of dNFs increase with age. They typically arise in single peripheral nerves from the skin during puberty. Some dNFs can cause malformation and itching, but they have not been reported to acquire a malignant transformation. They have also been suggested to be hormone-responsive, as their number and growth increase during puberty and pregnancy (Dugoff and Sujansky, 1996). More recently, some studies have also suggested that multipotent skin-derived precursors (SKPs) present in the hair follicles may contribute to dermal neurofibromas both in mice and humans (Le et al., 2009; Jouhilahti et al., 2011).

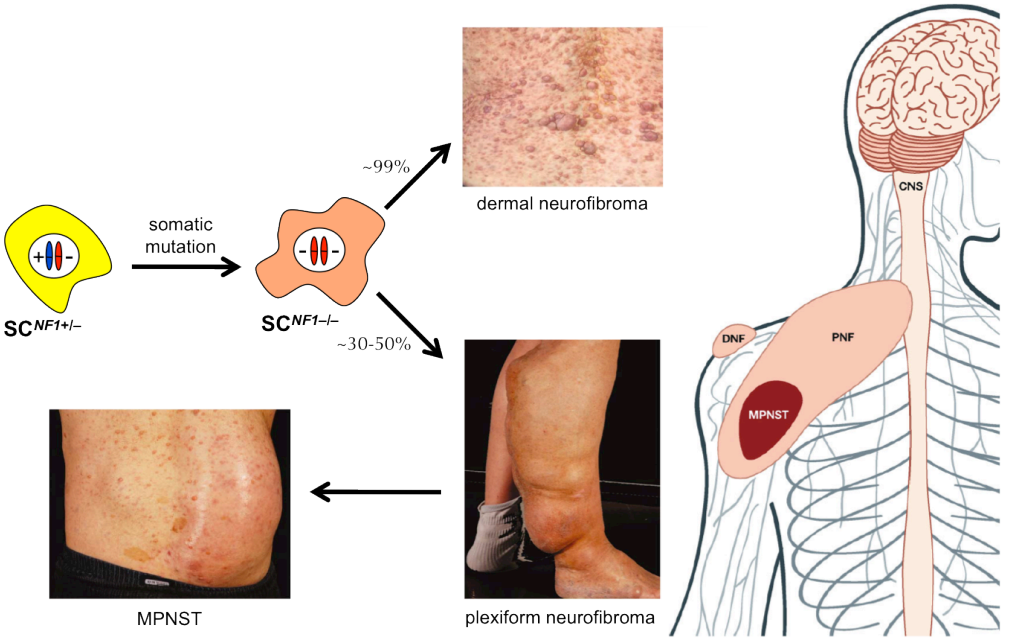

Figure 3. Tumourigenesis of the PNS in NF1 patients. NF1 is caused by loss of function of the *NF1* gene. A second-hit inactivation of *NF1* in Schwann cells (SCs) from NF1 patients is necessary for the development of a neurofibroma. Dermal neurofibromas (dNFs) are the most common benign peripheral nerve sheath lesions and appear in the skin of virtually all NF1 patients. Plexiform neurofibromas (pNFs) affect the total length of a peripheral nerve in almost half of the patients. Some pNFs have a significant propensity to undergo malignant transformation to MPNST, which can also arise outside of this context. Modified from Katz et al., 2009. Images taken from Ferner, 2007.

Plexiform neurofibromas are benign tumours affecting around 30-50% of NF1 patients (Huson et al., 1988; Ferner, 2007; **Figure 3**). They are bigger than dNFs and can spread along a total length of a peripheral nerve. They are thought to be congenital and arise in multiple nerve fascicles during childhood. A recent study in mice has

shown that a specific population of SC precursors in embryonic nerve roots are the cells of origin of pNFs (Chen et al., 2014). They are not hormonally responsive. About 10% of patients bearing pNFs have been reported to develop MPNSTs (Evans et al., 2002).

A third class of neurofibroma, called subcutaneous neurofibroma, has also been defined. These tumours localize in lower layers of skin and are thought to be the cause of pain and neurological problems. Individuals with subcutaneous neurofibromas are more likely to have also MPNSTs (Tucker et al., 2005).

5.3. pNF malignant transformation to MPNST

A specific type of neurofibroma, called atypical neurofibroma has also been defined. This tumour is pathologically characterized by the presence of more hypercellular regions than a dNF or a pNF, with cells having bigger and hyperchromatic nuclei, but with no mitoses detected. At the clinical level, they are often symptomatic presenting with pain. They also frequently show an increased glucose uptake on fluorine-18-labeled-fluorodeoxyglucose (^{18}F-FDG)-positron emission tomography (PET) scan (Ferner et al., 2008). These tumours have been suggested to be a transition state between a benign pNF and a MPNST (Nielsen et al., 1999; Brems et al., 2009; Beert et al., 2011).

6. MPNST

MPNST is a rare and aggressive tumour that account for 3-10% of all soft-tissue sarcomas (Katz et al., 2009). It is mostly developed in limbs and trunk (Ducatman et al., 1986; Sorensen et al., 1986) and around 50% are associated to NF1 patients, while the other 50% develop sporadically (Ducatman et al., 1986). The average lifetime risk of developing an MPNST in NF1 patients is 8-13% (Evans et al., 2002; **Figure 3**), being this risk two or three times higher in patients bearing an *NF1* microdeletion (De Raedt et al., 2003). Its estimated annual incidence is of 0.16%, compared with 0.001% in the general population (Ducatman et al., 1986). The mean age of MPNST diagnosis in NF1 patients is of 26 years old (Evans et al., 2002) and it is difficult to clinically diagnose, due to the presence of multiple benign tumours in the PNS. Clinical signs of

MPNST development are changes in neurofibroma texture, rapid tumour growth, recent pain and neurological deficit. Due to its invasive growth, propensity to metastasize, and limited sensitivity to chemotherapy and radiation, MPNST has a poor prognosis (Brems et al., 2009). MPNST is the leading cause of NF1-related mortality, being the 5-year survival rate of NF1 patients with MPNST of 21% (Evans et al., 2002; Friedrich et al., 2007). By using ^{18}F-FDG-PET scan, MPNSTs can be differentiated from most benign neurofibromas (Ferner et al., 2008).

MPNSTs are highly hyperploid tumours characterized by the occurrence of many chromosomal aberrations. First cytogenetic and fluorescence in situ hybridization (FISH) analyses showed complex karyotypes with several chromosomal rearrangements, including translocations, duplications and numerical gains and losses (Glover et al., 1991; Plaat et al., 1999; Mechtersheimer et al., 1999; Mertens et al., 2000). Unlike specific translocations found in other sarcomas (Barretina et al., 2010), no consistent chromosomal aberrations have been so far associated to MPNST pathogenesis. However, many studies using cytogenetics (Plaat et al., 1999), chromosomal comparative genomic hybridisation (CGH; Mechtersheimer et al., 1999; Schmidt et al., 2000), array CGH (Kresse et al., 2008; Mantripragada et al., 2009; Beert et al., 2011; Du et al., 2013), and single nucleotide polimorphism (SNP) array (Upadhyaya et al., 2012) have identified some recurrent somatic copy number alterations (SCNAs). These SCNAs include known TSGs and oncogenes drivers of MPNST pathogenesis and may also include some other candidate genes. The most recurrent SCNAs found are gains in chromosomes 7, 8q and 17q and losses in 1p, 9p, 10 and 11q, being genomic gains more abundant than losses in the MPNST genome.

6.1. Genes contributing to MPNST pathogenesis

6.1.1. Tumour suppressor genes

Somatic second-hit mutations in *NF1* gene have been found in 40-90% of NF1-associated MPNSTs (Legius et al., 1993; Upadhyaya et al., 2008a; Bottillo et al., 2009; Zhang et al., 2014; Lee et al., 2014) but this seems to be insufficient for MPNST formation, hence an accumulation of additional genetic alterations is needed. In

addition to *NF1* gene, the most recurrent genetic alterations found in MPNSTs are in the tumour suppressor genes *CDKN2A*, *TP53* and *PTEN*.

Alterations in the *CDKN2A* locus have been frequently detected in MPNSTs. *CDKN2A* encodes two proteins: p16/INK4A and p14/ARF. Protein p16 [or inhibitor of CDK4A (INK4a)] is a cell cycle inhibitor that inhibits pRb pathway, leading to cellular senescence. Protein p14, result of an alternate open reading frame (ARF) of the *CDKN2A* gene, is also a cell cycle inhibitor that activates p53 function. This locus has been found deleted in 40-80% of MPNSTs analyzed in various studies (Berner et al., 1999; Kourea et al., 1999; Nielsen et al., 1999; Perrone et al., 2003; Holtkamp et al., 2008; Mantripragada et al., 2008; Beert et al., 2011; Lee et al., 2014). Point mutations and promoter methylation have scarcely detected as mechanisms of *CDKN2A* inactivation (Berner et al., 1999; Kourea et al., 1999; Perrone et al., 2003; Lee et al., 2014). It is also important to highlight that in a recent study, *CDKN2A* has also been deleted in nearly all pre-malignant atypical neurofibromas studied, suggesting that this alteration is an early event in the malignant transformation of pNF to MPNST (Beert et al., 2011). Deletions in the *RB* gene, which encodes another negative regulator of cell cycle, pRb, have also been detected in MPNSTs (Mawrin et al., 2002; Mantripragada et al., 2008).

Many studies have also found *TP53* to be altered in MPNSTs. *TP53* encodes p53 protein, an important regulator of both DNA repair and apoptosis mechanisms. Some first studies using cytogenetics or microsatellite analysis showed the presence of LOH in the short arm of chromosome 17 (17p), where *TP53* is located, suggesting a possible role of this gene in MPNST pathogenesis (Menon et al., 1990; Jhanwar et al., 1994; Lothe et al., 1995). Point mutations in *TP53* have also been found (Legius et al., 1994; Birindelli et al., 2001; Lothe et al., 2001; Holtkamp et al., 2007; Upadhyaya et al., 2008a; Verdijk et al., 2010). However, the percentage of MPNST bearing mutations in *TP53* is highly variable among studies, due to the small number of tumours analyzed or to the restriction to specific exons in the mutational analyses. Taken together, these studies found point mutations in *TP53* in less than 20% of the NF1-associated MPNSTs analyzed. LOH in *TP53* has been found in a higher percentage of MPNSTs (40-55%) than point mutations (Holtkamp et al., 2008; Upadhyaya et al., 2008a; Beert et al., 2011). In a recent study, the combination of whole exome sequencing, SNP

array and RNA-seq techniques detected *TP53* deletions and point mutations in 46% and 27% of 26 NF1-associated MPNSTs, respectively (Lee et al., 2014), confirming the results found in previous studies. However, biallelic *TP53* inactivation is low (Lothe et al., 2001; Lee et al., 2014) and it has been suggested that *TP53* haploinsufficiency, in cooperation with alterations in other genes, would be sufficient for MPNST tumourigenesis (Brosius et al., 2014; Rahrmann et al., 2014). Amplifications in *MDM2*, a negative regulator of *TP53*, have also been found (Wallander et al., 2012).

Alterations in *PTEN* gene, which encodes a phosphatase that negatively regulates PI3K and consequently inhibits pro-survival signalling, have also been detected in ~50% of MPNSTs analyzed either for deletions (Holtkamp et al., 2008; Perrone et al., 2009) or promoter methylation (Bradtmoller et al., 2012).

The advances of several genetically engineered mice (GEM) models support the role of the TSGs *NF1*, *CDKN2A, TP53*, and *PTEN* in MPNST development. These are the knockouts Nf1+/–; p53+/– (Cichowski et al., 1999; Vogel et al., 1999) and Nf1+/–; $p16^{Inka4}$/$p19^{Arf}$–/– (Joseph et al., 2008) and the conditional knockouts Nf1 fl/fl; Pten fl/fl; Dhh-Cre and Nf1 fl/fl; Pten fl/+; Dhh-Cre (Keng et al., 2012a).

6.1.2. Oncogenes

In addition to TSGs, some oncogenes have also been found altered in MPNSTs. Most of them encode receptor tyrosine kinases (RTKs) or their ligands, which are both involved in proliferation, survival, migration and invasion, among other cellular properties. Some of these genes, such as *EGFR*, *PDGFR* or *VEGF*, are overexpressed in MPNSTs, leading to the activation of their downstream effectors (reviewed in Katz et al., 2009).

EGFR is amplified in at least 30% of the NF1-asociated MPNSTs analyzed so far (Perry et al., 2002; Holtkamp et al., 2008; Perrone et al., 2009; Du et al., 2013). The *ERBB2* gene, which encodes the EGFR family receptor HER2, has also been found amplified (Storlazzi et al., 2006; Holtkamp et al., 2008). Amplifications in *PDGFR* (Holtkamp et al., 2006; Mantripragada et al., 2008; Perrone et al., 2009; Zietsch et al., 2010; Upadhyaya et al., 2012) and other receptors, such as *KIT* (Holtkamp et al., 2006;

Zietsch et al., 2010), *MET* (Mantripragada et al., 2008; Upadhyaya et al., 2012) or *IGF1R* (Yang et al., 2011) have also been found. Moreover, recent functional evidences of a role of these oncogenes in MPNST pathogenesis have been showed: *EGFR* (Holtkamp et al., 2008; Byer et al., 2013; Du et al., 2013; Wu et al., 2014; Rahrmann et al., 2014); *ERBB2* (Stonecypher et al., 2005) and its ligand Neuregulin-1 (*NRG1*; Eckert et al., 2009; Kazmi et al., 2013; Brosius et al., 2014); *PDGFRB* (Ohishi et al., 2013); MET (Torres et al., 2011). Activating gain-of-function point mutations have not been detected in these oncogenes in cell lines derived from MPNSTs, suggesting that the main mechanism underlying their activation would be by genomic amplification (Sun et al., 2012).

In addition, some other genes showing to be amplified and/or overexpressed in MPNSTs have been proposed to have an oncogenic role in MPNST pathogenesis, which in some cases is also supported by recent functional studies. Examples are the gene *TOP2A*, that encodes DNA topoisomerase II alpha, an helicase frequently targeted with anticancer agents (Skotheim et al., 2003; Storlazzi et al., 2006; Kresse et al., 2008; Kolberg et al., 2015); *BIRC5*, that encodes the antiapoptotic protein survivin that have also a role in promoting cell division (Levy et al., 2004; Storlazzi et al., 2006; Kresse et al., 2008; Kolberg et al., 2015); *AURKA*, which encodes the promitotic protein Aurora Kinase A (Levy et al., 2004; Patel et al., 2012; Mohan et al., 2013); and the chemokine receptor gene *CXCR4* (Mo et al., 2013; Hattermann et al., 2013).

6.1.3. Other genes

In addition to TSGs and oncogenes, other genes have been associated with MPNST pathogenesis. Some neural crest stem cell markers, such as *TWIST1* and *SOX9* are overexpressed in MPNSTs and have been found to be functionally involved in cell chemotaxis and cell survival, respectively (Miller et al., 2006; Miller et al., 2009). *EYA4*, a potential transcriptional target of *SOX9* involved in development, is also overexpressed in MPNSTs (Miller et al., 2010). Activation of the Wnt/beta-catenin signalling pathway, involved in many cellular processes including differentiation, proliferation and migration, and also with cancer, have also been associated with MPNST pathogenesis (Watson et al., 2013; Luscan et al., 2014).

MicroRNAs (miRNAs) have been demonstrated to have an important role in cancer, either if they act as TSGs when their function is lost, or as oncogenes if the gain function. Some miRNAs have been found to be downregulated in MPNSTs, such as miR-34a (Subramanian et al., 2010), miR-204 (Gong et al., 2012), miR-29c (Gong et al., 2012) and miR-210 (Wang et al., 2013). An overexpressed miRNA found to be oncogenic in MPNSTs is miRNA-21 (Itani et al., 2012).

6.2. Epigenetics

Alterations in DNA methylation and histone modifications are a common feature in cancer. Hence, inactivation of TSGs and activation of oncogenes can be caused by mutations and also by epigenetic modifications. In general, gene promoter hypermethylation is associated to transcriptional silencing, while gene hypomethylation is associated to overexpression. In addition to DNA methylation, histones can be also post-translationally modified to regulate the conformation of the chromatin. Some histone marks are associated to gene expression, such as acetylation of lysine 9 of histone 3 (H3K9ac). Other modifications are associated to transcriptional repression, such as dimethylation of lysine 9 of histone 3 (H3K9me2) or trimethylation of lysine 27 of histone 3 (H3K27me3).

Some players in chromatin remodelling mechanisms have been postulated to have an important role in MPNST pathogenesis. This is the case of *SUZ12* gene. *SUZ12* is located at 17q11.2 region, closely to *NF1,* and it has been found to be the gene responsible for the elevated risk for MPNST development in *NF1* microdeletion patients (De Raedt et al., 2003; De Raedt et al., 2014) and to act as a TSG cooperating with *NF1* and *CDKN2A* in the development of MPNSTs (De Raedt et al., 2014; Lee et al., 2014; Zhang et al., 2014). *SUZ12* is a component of the Polycomb Repressor Complex 2 (PRC2), a group of proteins with histone methyltransferase activity that trimethylate lysine 27 of histone H3 (H3K27me3), thus marking chromatin to be transcriptionally silent. Mutations in other PRC2 components, such as *EED* gene, have also been associated to MPNST development (De Raedt et al., 2014; Lee et al., 2014). Another member of PRC2, *EZH2*, have recently found to act, in this case, as an oncogene in MPNST tumourigenesis (Zhang et al., 2014; Zhang et al., 2015).

Another group of chromatin remodelers, the histone deacetylases (HDACs), which are enzymes that remove the acetyl group from acetylated lysines from histones, have also proposed to have a role in MPNST pathogenesis (Lopez et al., 2011), especially the HDAC8 member (Lopez et al., 2015).

Regarding the association of DNA methylation with MPNST pathogenesis, the most robust finding is the inactivation of *PTEN* by promoter methylation found in some MPNSTs (Bradtmoller et al., 2012). In addition, only one study has been published so far comparing the methylomes of MPNSTs and neurofibromas, in which no significant global hypomethylation was observed in MPNSTs, in contrast to what has been reported for other tumours, although hypomethylation was significant in satellite repeats (Feber et al., 2011). Recently, the overexpression of *TAGLN* gene, which encodes the actin-associated protein transgelin, has been associated to hypomethylation in its promoter region in NF1-associated MPNSTs (Park et al., 2014). In another study, hypermethylation of the gene promoter of *RASSF1A*, a TSG involved in cancer development, has been found in 60% of MPNSTs analyzed and has also been associated to a poor prognosis (Danielsen et al., 2015).

6.3. Sporadic MPNST

Half of MPNSTs within the general population occur sporadically and are not associated to NF1 patients (Ducatman et al., 1986). Although sporadic MPNSTs are histologically indistinguishable from those NF1-associated, they present some different clinical features. Sporadic MPNSTs are less aggressive than NF1-associated ones, being their 5-year survival rate of 42%, compared to 21% in NF1 patients (Evans et al., 2002). Possible explanations of this difference in prognosis are that NF1-associated MPNSTs have a greater propensity to metastasize than sporadic ones, as well as they are more difficult to detect in NF1 patients due to their tumour burden and that most of these NF1-associated MPNSTs arise in preexisting pNFs (Ducatman et al., 1986). Moreover, sporadic MPNSTs appear later in a lifetime of an individual: the mean age of diagnosis is of 62 years old, compared to 26 in NF1 patients (Evans et al., 2002).

Sporadic MPNSTs have also been found to bear somatic mutations in the *NF1* gene, indicating that these somatic events share common characteristics with the NF1-associated ones (Bottillo et al., 2009; Zhang et al., 2014; Lee et al., 2014). Regarding SCNAs in sporadic MPNSTs, the most recurrent gains and losses are similar to those from NF1-associated MPNST (reviewed in Yang and Du, 2013). Mutations in the TSGs *CDKN2A* (Lee et al., 2014), *TP53* (Birindelli et al., 2001; Holtkamp et al., 2007; Lee et al., 2014; Verdijk et al., 2010) and *SUZ12* (Lee et al., 2014; Zhang et al., 2014) have also been found in sporadic MPNSTs. Genomic amplifications encompassing *EGFR*, *PDGFR*, *MET*, *IGF1R* and other oncogenes are also present in sporadic MPNSTs (reviewed in Yang and Du, 2013).

The conditional GEM knockout model with a total loss of *PTEN* expression and the overexpression of *EGFR*, *Pten* fl/fl; Dhh-Cre; Cnp-EGFR, is able to generate MPNSTs sporadically (Keng et al., 2012b). This suggests a potential important role of these two genes in sporadic MPNSTs.

6.4. Therapeutical approaches for MPNSTs

Due to its invasive growth, propensity to metastasize, and limited sensitivity to chemotherapy and radiation, MPNSTs from NF1 patients have a poor prognosis (Brems et al., 2009). Up to now, only surgical resection is the basis of MPNST clinical management.

Some clinical trials with single agents have been performed so far with no conclusive results after phase II. These include a study targeting EGFR with erlotinib (Albritton et al., 2006); a trial using sorafenib that inhibits the RTKs VEGFR2, C-KIT and PDGFR and the RAS effectors C-RAF and B-RAF (Maki et al., 2009) and another clinical trials also targeting C-KIT with imatinib (Chugh et al., 2009). There are now some ongoing clinical trials for the treatment of MPNSTs, which have completed phase I and include several combined therapies with two or three chemical inhibitors. Among them, there are one trial co-targeting hedgehog signalling and gamma-secretase, two trials combining the inhibition of RTKs with chemotherapy and a fourth trial using mTOR inhibitors together with the inhibition of the heat shock protein HSP90 (www.ctf.org).

In an effort to *in vitro* study different biological characteristics and potential drugs for MPNST treatment, several cell lines have been derived from human tumours. These lines, although they can be heterogeneous in some of their biological features, they recapitulate most of the genomic and transcriptomic profiles of the primary MPNSTs from they have been established, especially at early passages, and they have been claimed as a primary tool for the identification of genes and molecular pathways involved in MPNST pathogenesis and potential therapeutic targets (Miller et al., 2006). Some of the currently available NF1-associated MPNST-derived cell lines are S462 (Frahm et al., 2004), T265 (Badache and De Vries, 1998), ST88-14 (Fletcher et al., 1991), sNF96.2 (Perrin et al., 2007), 90-8 (Glover et al., 1991), and NMS-2 (Imaizumi et al., 1998). Some other cell lines have also been derived from sporadic MPNSTs, such as STS26T (Dahlberg et al., 1993), HS-Sch-2 (Sonobe et al., 2000) and HS-PSS. Many *in vitro* treatments with different agents have been performed so far using these MPNST cell lines.

A step forward in the identification of potential therapeutic targets is the use of *in vivo* pre-clinical models. New potential therapeutic targets have been recently identified with either GEM modelling MPNST development or MPNST xenograft mice (especially from MPNST cell lines), which are summarized in **Table 1**.

The use of a combined treatment inhibiting two (or more) molecular targets is stressed in these approaches. Our group has recently developed the first orthoxenograft mouse model from primary MPNSTs, where sorafenib, in combination with doxorubicin or rapamycin, was found to reduce tumour growth (Castellsague et al., 2015). These assays, either in transgenic or xenograft mice, generate a source of potential treatments to be tested in further clinical trials. This is the case for mTOR and Hsp90 combined treatment (De Raedt et al., 2011), which is now being tested in a clinical trial, as mentioned above. Most of these treatments combine the inhibition of the activated RAS signalling due to *NF1* loss of function (either MAPK or mTOR signalling) with the inhibition of another target involved in other cellular processes.

Mouse model		Target (inhibitor)	Reference
Genetically engineered mice		mTOR (rapamycin)	Johannessen et al., 2008
		mTOR (rapamycin) + Hsp90 (IPI-504)	De Raedt et al., 2011
		CXCR4 (AMD3100)	Mo et al., 2013
		mTOR (everolimus) + Mek (PD03259010)	Watson et al., 2014
		Mek (PD03259010) + Brd4 (JQ1)	De Raedt et al., 2014
		Brd4 (JQ1)	Patel et al., 2014
MPNST cell lines	Subcutaneous xenografts	HDACs (PCI-24781, SAHA, MS-275)	Lopez et al., 2011
		MET/VEGFR2 (XL184)	Torres et al., 2011
		BIRC5 (YM155)	Ghadimi et al., 2012b
		AURKA (MLN8237)	Patel et al., 2012
		PI3K/mTOR (XL765)	Ghadimi et al., 2012a
		MEK (PD03259010)	Jessen et al., 2013
		RTK (imatinib)	Ohishi et al., 2013
		RTK (imatinib) + RTK/KIT (PLX3397)	Patwardhan et al., 2014
		JAK2/STAT3 (FLLL32)	Wu et al., 2014
		mTOR (everolimus) + proteasome (bortezomib) + RT*	Yamashita et al., 2014
		HDAC8 (PCI-34051, PCI-48012)	Lopez et al., 2015
		EZH2 (3-deazaneplanocin A)	Zhang et al., 2015
Primary MPNSTs	Subcutaneous xenografts	mTOR (rapamycin)	Bhola et al., 2010
		CDK4/6 (palbociclib)	Perez et al., 2015
	Orthoxenografts	AURKA (MLN8237)	Mohan et al., 2013
		RTK (sorafenib) + mTOR (rapamycin)$^{+}$	Castellsague et al., 2015

Table 1. Recent pre-clinical *in vivo* treatments for NF1-associated MPNSTs. Molecular targets and chemical inhibitors used for the treatment of MPNSTs in pre-clinical mouse models including genetically engineered mice and xenograft mice. *RT, radiotherapy; $^{+}$, combination of sorafenib plus doxorubicin was also studied.

7. Role of kinesins in cell division and cancer

Kinesins are proteins that act as molecular motors travelling unidirectionally along microtubules in a cell. The kinesin superfamily has more than 650 members (Miki et al., 2005) and in humans 45 kinesin genes have been identified, with some members being involved in disease (Hirokawa et al., 2010). Kinesins have been classified into 14 subfamilies, from kinesin-1 to kinesin-14, according to phylogenetic analysis of the motor domain (Lawrence et al., 2004). They have two main roles in cell physiology: intracellular vesicle and organelle transport (Hirokawa et al., 2009) and cell division (Wordeman, 2010).

Name	Other name	Functions in cell division	Expression status in cancer
KIF2A		Microtubule minus end-depolymerizing motor required for bipolar spindle formation	Overexpression promotes the development of squamous cell carcinoma of the tongue
KIF2B		Involved in kinetochore–microtubule dynamics to promote mitotic progression	
KIF2C	MCAK	Microtubule depolymerizing motor required for chromosome congression and alignment	Prognostic marker in colon cancer. Overexpressed in gastric cancer and during breast tumourigenesis
KIF4A*		Participates in chromosome condensation, anaphase spindle formation and cytokinesis	Amplified and overexpressed in cervical cancer. Prognostic marker for lung cancer
KIF10	CENPE	Participates in microtubule–kinetochore capture and mitotic checkpoint signalling	Downregulated in hepatocellular carcinoma. Overexpressed in certain types of breast cancer
KIF11	EG5	Required for the separation of duplicated centrosomes during spindle formation	Highly expressed in blast crisis chronic myelogenous leukaemia. Overexpressed in pancreatic cancer
KIF14		Required for chromosome congression and alignment and cytokinesis	Predictor of grade and outcome in breast cancer and ovarian cancer. Prognostic marker in lung cancer
KIF15		Required for maintenance of spindle bipolarity	Breast cancer tumour antigen
KIF18A		Involved in chromosome congression	Overexpressed in colorectal cancer. Associated with tumour grade and poor survival in breast cancer
KIF18B		Involved in the regulation of microtubule dynamics	
KIF20A	MKLP2	Essential for cytokinesis	Overexpressed in pancreatic cancer
KIF20B	MPP1	Probably required for completion of cytokinesis	Overexpressed in bladder cancer
KIF22	KID	Generates polar injection forces essential for chromosome congression and alignment	
KIF23	MKLP1	Essential for cytokinesis	Overexpressed in glioma
KIFC1	HSET	Essential for bipolar spindle assembly and proper cytokinesis	Highly predictive of brain metastasis of lung cancer. Overexpression leads to docetaxel resistance in breast cancer cells

Table 2. Function of human kinesins in cell division and expression in cancer. Name of mitotic kinesins (and other aliases for some of them). The main function in cell division and their expression reported in some cancers is shown. Modified from Rath and Kozielski, 2012. * KIF4B has same functions than KIF4A.

At present, 16 kinesins have been involved in participating at different stages of mitosis and cytokinesis (**Table 2,** reviewed in Rath and Kozielski, 2012). Among their several functions are the bipolar spindle formation and maintenance in prophase, driven by kinesins KIF11 (also known as EG5), KIF2A, KIFC1 (aka HSET) and KIF15; the chromosome congression and alignment in metaphase, conducted by kinesins KIF10 (aka CENPE), KIF14, KIF18A and KIF18B and KIF22 (aka KID); or the cytokinesis, driven by KIF14, KIF23 (aka MKLP1), KIF20A (aka MKLP2), KIF20B (aka MPP1) and

KIFC1. Some members have multiples roles during cell division, such as KIFC1, KIF14; or the members KIF4A and KIF4B, which have been both involved in regulating chromosome structure and dynamics in metaphase, anaphase and cytokinesis. Moreover, some kinesins have dual functions, in both cell division and intracellular trafficking during neuronal development, like KIF2A, KIF4A or KIF4B.

Over the past years, some of the kinesins involved in cell division have been found deregulated in several cancers, such as breast, hepatic, pancreatic, bladder and colorectal cancer and some leukaemias (summarized in **Table 2**). Hence kinesins have emerged as potential targets for the development of antitumoural drugs. There are currently several ongoing and completed clinical trials with different compounds inhibiting the kinesin KIF11, one compound inhibiting KIF10 and one peptide as a KIF20B inhibitor (Rath and Kozielski, 2012; clinicaltrials.gov).

8. Searching driver genes of tumourigenesis by using regional genomic information

Several studies from the past few years have revealed that some regions of the human genome, ranging from kilobases to megabases, can be variable in terms of their copy number across individuals. These copy number variations (CNVs) represent inter-individual differences in gene number and expression at the constitutional level that can have an impact on the phenotypic variation, including disease predisposition. In contrast, SCNAs, present in somatic tissues, are different from constitutional CNVs and they do not represent a natural constitutional variation on copy number, but aberrant alterations in the number of copies of specific genomic regions, which are found enriched in the genomes from tumours. SCNAs are frequent in many cancers and the identification of these genomic regions that undergo alterations in specific cancers represents a powerful way to discover genes contributing to tumour development and maintenance (Beroukhim et al., 2010).

The influence of SCNAs in the expression of the genes they contained has been studied in several solid tumours. About 40-60% of highly amplified genes in breast cancer samples have shown to be also overexpressed (Hyman et al., 2002; Pollack et

al., 2002) or have been associated to gene-expression subtypes (Bergamaschi et al., 2006). Specific SCNAs have been significantly associated to direct copy number-driving changes in gene expression in glioblastoma multiforme (Lee et al., 2008b; de Tayrac et al., 2009), laryngeal squamous cell carcinoma (Jarvinen et al., 2006) and bladder (Lee et al., 2008b), prostate (Phillips et al., 2001; Chaudhary and Schmidt, 2006; Rose et al., 2010) and colon cancer (Loo et al., 2013). In an elegant study, homozygous and heterozygous deletions in the *NF1* gene were correlated to neurofibromin expression levels in a set of soft-tissue sarcomas other than MPNSTs (Barretina et al., 2010). SCNAs in some chromosomes from multiple myeloma have also been correlated to gene expression levels (Samur et al., 2013). Moreover, the impact of SCNAs on the proteome of breast cancer cell lines has been also studied (Geiger et al., 2010).

In addition, it is well known that epigenetics also influences gene expression. As a general rule, specific hypermethylation of promoter CpG islands are associated to gene silencing at single level. Nevertheless, inactivation of the gene expression of a large genomic region can also be caused by epigenomic mechanisms. This is the case of long-range epigenetic silencing (LRES), a phenomenon by which DNA hypermethylation and chromatin remodeling suppress the expression of genes placed contiguous in specific gross genomic locations, which was defined and first identified in colorectal cancer (Frigola et al., 2006). LRES has also been detected in prostate (Coolen et al., 2010), bladder (Stransky et al., 2006), breast (Novak et al., 2008; Hsu et al., 2010), gastric (Park et al., 2011; Kang et al., 2015), and in a subtype of renal (Dallosso et al., 2009) cancer. Thus, in some tumours, loss of gene expression would occur through LRES with similar implications as a genomic deletion. In a similar manner, a mechanism called long-range epigenetic activation (LREA), characterized by the gain of active chromatin histone marks and loss of repressive marks within genomic regions encompassing some oncogenes, have been recently identified in prostate cancer (Bert et al., 2013).

In order to obtain a better insight in cancer biology it is important to separate genetic alterations that really contribute to tumourigenesis (driver mutations) from those that have no effect in the generation of the tumour (passenger mutations; Stratton et al., 2009). One way of discriminating these two types of mutations is studying genes at a

single level by assessing their point mutational status, their promoter methylation status or their individual expression levels. On the other hand, SCNAs are frequent in some types of tumours. Studying how the expression of the genes located at specific genomic regions that are altered by copy number changes (or epigenomic phenomena) is really influenced by these mechanisms can represent another way for discriminating those mutations that are driver from those that are passenger. Moreover, both strategies can be considered, and the regional information can be used together with information on both the mutational and promoter methylation status at the single gene level, in a more exhaustive approach.

This thesis is contained in a larger project whose aim is the integration of genome-wide expression data, data coming from genome structural analysis, epigenetic data from DNA methylation, and a collection of point mutations from whole-exome sequencing from MPNST samples, in order to find mutated genes that are drivers of MPNST pathogenesis. In this thesis, data coming from regional information, especially at the transcriptomic level, has been used to find genes involved in the pathogenesis of NF1-associated MPNSTs.

HYPOTHESIS AND OBJECTIVES

Malignant peripheral nerve sheath tumours (MPNSTs) mainly arise from pre-existing benign plexiform neurofibromas (pNFs). While pNFs do not show gross genomic alterations, MPNSTs present a hyperploid genome with multiple and recurrent somatic copy number alterations (SCNAs). We hypothesized that these SCNAs would have an impact on gene expression in a regional manner, which can be informative when studying MPNST pathogenesis. This regional transcriptomic information could be employed for finding genes involved in the pathogenesis of MPNSTs from neurofibromatosis type 1 (NF1) patients, including some potential therapeutic targets.

The main objective of this thesis project was to characterize the MPNST genome and further identify genes and molecular mechanisms involved in the pathogenesis of MPNSTs arising in the context of NF1.

To achieve this, three specific aims were proposed:

1) To develop two qPCR assays for the detection of genomic deletions in *NF1* locus, both at constitutional and somatic levels, and for the detection of SCNAs in MPNSTs.

2) To molecularly analyze NF1-associated MPNSTs at the genomic, transcriptomic and epigenomic level, and to use the information generated at the level of genomic region for the identification and further *in vitro* functional characterization of novel genes involved in MPNST pathogenesis

3) To *in vitro* study the functional role of mitotic kinesins in MPNSTs and their use as potential therapeutic targets

MATERIALS AND METHODS

1. Human samples

All samples used in this thesis are human samples. They include different primary tissues (especially tumours), primary cell cultures, human cell lines and nucleic acid samples from these tissues and cells.

1.1. Primary tumours

Human tumours were used in this thesis for their further molecular characterization (see section 2), including dermal neurofibromas (dNFs), plexiform neurofibromas (pNFs) and malignant peripheral nerve sheath tumours (MPNSTs). Most of these samples were from neurofibromatosis type 1 (NF1) patients, which were diagnosed according to the NF1 standard diagnostic criteria (NIH, 1988). All patients gave written informed consent for the molecular studies performed.

dNFs were completely removed after minor surgery, which was carried out by either a dermatologist or a surgeon, and transported in a recipient containing Dulbecco's Modified Eagle's Medium (DMEM) medium. Surrounding skin tissue was carefully removed from dNFs and in some cases was further used for either DNA extraction or fibroblast isolation. Tumoural tissue was then chopped into small pieces. Some of them were directly frozen and preserved at -80ºC for further DNA extraction. Some other pieces were cryopreserved in freezing medium [90% fetal bovine serum (FBS), 10% dimethyl sulfoxide (DMSO)] in liquid nitrogen until they were used for SC or fibroblast isolation.

pNFs were removed after surgery performed by a surgeon, and transported in a recipient containing DMEM medium. Surrounding skin tissue was taken out and the tumoural tissue was divided in several areas, depending on the size of the tumour. Each of these pNF areas was then chopped into 1-2 mm^3 pieces. All pieces from a same area were split for preservation at -80ºC for further nucleic acid extraction, cryopreserved in freezing medium in liquid nitrogen for Schwann cell (SC) or fibroblast isolation, or fixed with 4% formaldehyde and embedded in paraffin for further histological analysis.

Primary MPNSTs were obtained from our collaborators at Hospital Universitari de Bellvitge and Cincinnati Children's Hospital Medical Center. MPNSTs were sent frozen and once arrived in the lab they were preserved at -80ºC for further DNA extraction. In some cases, DNA from MPNSTs was directly obtained from our collaborators at University of Florida and Hospital Universitari de Bellvitge.

Moreover, in some cases, blood samples from NF1 patients were also used for DNA extraction.

1.2. Primary cultures: SCs and fibroblasts

SCs were isolated from dNFs and pNFs and cultured as previously described (Serra et al., 2000). In short, neurofibromas were mechanically dissociated and incubated with 160 U/mL collagenase Type 1 (cat.no. LS004196, Worthington) and 0.8 U/mL dispase (cat.no. LS02104, Worthington) in DMEM for 16-18 hours. The obtained cell suspension was plated on 6-well plates, previously coated with 0.1 mg/mL poly-L-lysine (cat.no. P1524, Sigma) and 4 μg/mL of laminin (cat.no. 23017-015, Life technologies), and cultured with Schwann cell medium (SCM) in a cell incubator at 37ºC and 10% CO_2. SCM is composed of High Glucose DMEM with sodium pyruvate (cat.no. L0106-500, Biowest) supplemented with 10% FBS (cat.no. S181B-500, Biowest), 2mM L-Glutamine (cat.no. 25030-024, Life technologies), 0.5mM IBMX (cat.no. I7018, Sigma), 2.5 μg/mL insulin (cat.no. I4011, Sigma) and 10 nM heregulin (cat.no. 396-HB, R&D Systems). For the specific culture of $SC^{NF1-/-}$, SCM was replaced twice a week and cultured for 24 hours with SCM containing 0.5 μM forskolin (cat.no. F6886, Sigma). Confluent cultures were passaged using trypsin-EDTA (cat.no. 15400-054, Life technologies).

The purity of SC component within the culture was assessed by immunofluorescence of S100 protein, which is a cytoplasmic protein expressed in SCs (Brockes et al., 1979). Briefly, cells grown on a 24-well plate were fixed with 4% p-formaldehyde, phosphate buffered saline (PBS)-washed, permeabilized with 0.1% Triton-PBS, blocked with 10% FBS-PBS and incubated with 1:1000 the polyclonal rabbit anti-cow S100 antibody (cat.no. Z031129, Dako) in 1% FBS-PBS for 1 hour. After this, they

were washed again with 1% FBS-PBS, incubated with 1:2000 anti-rabbit IgG-AlexaFluor 568 antibody (cat.no. A11011, Life technologies) in 10% FBS-PBS for 30 minutes, and finally 1% FBS-PBS-washed and mounted with Vectashield with DAPI (cat.no. H-1200, Vector Laboratories). The multi-well cell plate was then visualized in a fluorescence-inverted microscope (Leica DMI 6000B).

In addition to SC culture, in some cases, primary cultures of fibroblasts derived from dNFs or from skin were also performed. After mechanical and enzymatic dissociation of the tissue, the obtained cell suspension was plated on 6-well plates and cultured under standard conditions (37ºC, 5% CO_2) with High Glucose DMEM with sodium pyruvate (cat.no. L0106-500, Biowest) supplemented with 10% FBS (cat.no. S181B-500, Biowest) and 2mM L-Glutamine (cat.no. 25030-024, Life technologies), referred as "supplemented DMEM" from now on. Moreover, the commercial human foreskin fibroblast CCD-1112Sk cell line (cat.no. CRL-2429™, ATCC®), used for the *in vitro* drug treatments, was also cultured under standard conditions with supplemented DMEM.

1.3. MPNST cell lines

Several MPNST cell lines were used in this thesis for different purposes. These cell lines included S462 (Frahm et al., 2004), T265 (Badache and De Vries, 1998) and S462-TY (a derivative created by passage of S462 as xenografts; all provided by Dr Nancy Ratner, Cincinnati Children's Hospital Medical Centre, Cincinnati, USA), ST88-14 (Fletcher et al., 1991) and sNF96.2 (Perrin et al., 2007; provided by Dr Thomas De Raedt, Brigham and Women's Hospital, Boston, USA), NMS-2 (Imaizumi et al., 1998; obtained from RIKEN cell bank), and 90-8 (Glover et al., 1991), and the sporadic line STS-26T (Dahlberg et al., 1993; provided by Dr Eric Legius, Catholic University Leuven, Leuven, Belgium). MPNST cells were maintained in supplemented DMEM. They were cultured under standard conditions and passaged using trypsin-EDTA (cat.no. 15400-054, Life technologies).

Among these cell lines, a G-banding staining of S462, T265 and the sporadic STS-26T was performed (**Figure 4**). These cell lines showed to be quite heterogeneous

regarding the number of chromosomes per cell and their genome was highly hyperploid (being nearly triploid or tetraploid).

Figure 4. Karyotype of the MPNST cell lines S462, T265 and STS26T. Several metaphases were analyzed and the mean number of chromosomes per cell for each cell line was calculated and was of 78 for S462, 56 for T265 and 83 for STS26T.

Moreover, DNA fingerprinting of short tandem repeats (STRs) was conducted for MPNST cell lines using the AmpFlSTR Identifiler Plus Amplification kit (cat.no. 4427368, Life technologies). **Table A.1** in Annexe 1 contains information regarding the microsatellite profile of these lines, which includes the 8 STRs used by the ATCC®.

1.4. Nucleic acid extraction

Total DNA was extracted using different methodologies depending on the sample. DNA from tissues (dNFs, pNFs, MPNSTs and skin) and MPNST cell lines was extracted with the Gentra Puregene Kit (cat.no. 158667, Qiagen). The QIAamp DNA Mini Kit (cat.no. 51304, Qiagen) was used to extract DNA from primary cell cultures (SCs and fibroblasts). For blood samples different methodologies were used: the Wizard Genomic DNA Purification Kit (cat.no. A1120, Promega), and the FlexiGene DNA Kit (cat.no. 51206, Qiagen). All extractions were performed according to the manufacturer's instructions. A NanoDrop® ND-1000 spectrophotometer (Thermo Scientific) was used to quantify DNA and to measure purity and quality. DNA integrity was assessed by gel electrophoresis. All DNA samples included in this thesis presented high purity and integrity. For the array [single nucleotide polimorphism (SNP) or methylation] experiments a fluorescence-based quantification of DNA was performed either by using the Quant-iT™ PicoGreen® dsDNA Assay (cat. no. P7589, Life technologies) or a Qubit fluorometer (Life technologies).

RNA was extracted from MPNST cell lines using Tripure Isolation Reagent (cat.no. 11667165001, Roche) and according to the manufacturer's instructions. In a summarized protocol, 500 μL of Tripure reagent were added to a well of 12-well plate containing adherent cells and the cell lysate was transferred to a tube; 100 μL of chloroform were added, mixed thoroughly and centrifuged. After centrifugation three phases were generated and upper aqueous phase was transferred to a new tube; 250 μL of isopropanol were then added, mixed and the tube was centrifuged to precipitate RNA. Precipitated RNA formed a pellet that was washed twice with 500 μL of 75% ethanol. Finally, RNA pellet was let to air dry, resuspended in RNAse-free water and incubated at 60ºC for 10 minutes. All RNA samples were stored at -80ºC. A NanoDrop® ND-1000 spectrophotometer (Thermo Scientific) was used to quantify RNA and to measure purity and quality.

2. Molecular characterization of tumours and cell lines

A set of samples comprising NF1-associated tumours and cell lines were molecularly characterized at genomic and epigenomic levels in this thesis. This characterization included different techniques, such as qPCR, SNP array and methylation array (see **Table 3** and **Figure A.1** in Annexe 1). Moreover, expression data previously generated by the NF1 Microarray Consortium from an independent set of samples (Miller et al., 2009) was also used for a transcriptomic characterization of tumours and cell lines, which included the generation of transcriptional imbalances (TIs).

2.1. qPCR

In the qPCR assay for detecting deletions in the *NF1* region (*NF1*-qPCR), a total of 59 samples were included: 14 venous blood samples previously tested by fluorescence in situ hybridization (FISH) and microsatellite markers and found to carry a constitutional deletion of *NF1* in each case (Lopez Correa et al., 1999; Steinmann et al., 2007); 16 samples from dNFs; and 5 samples from selective SC cultures derived from dNFs, previously analyzed by multiplex ligation-dependent probe amplification (MLPA), paralog ratio analysis, and SNP array and found to bear a somatic *NF1* deletion ($SC^{NF1-/-}$) in each case (Garcia-Linares et al., 2011 and data not shown). In addition, a

Set	Sample	Type	MPNST-qPCR	SNP array	methylation array
MPNSTs	MPNST-1	NF1-associated	X	X	
	MPNST-2	NF1-associated		X	X
	MPNST_A	NF1-associated	X	X	X
	MPNST_B	NF1-associated	X	X	
	MPNST_C	NF1-associated	X	X	
	MPNST_D	NF1-associated	X	X	
	MPNST_G	NF1-associated	X	X	X
	MPNST_K	NF1-associated	X	X	
	MPNST_P	NF1-associated			X
	M-23	sporadic	X		
	M-24	sporadic	X		
	M-25	sporadic	X		
	M-26	sporadic	X		
	M-27	sporadic	X		
Neuro-fibromas	pNF-1	plexiform		X	
	pNF-2	plexiform		X	
	pNF-3	plexiform		X	
	pNF-4	plexiform		X	
	pNF-5	plexiform		X	X
	pNF-6	plexiform		X	X
	pNF-7	plexiform		X	X
	pNF-8	plexiform		X	
	M-17	plexiform	X		
	M-10	dermal	X		
	M-38	dermal	X		
	M-39	dermal	X		
	M-40	dermal	X		
	M-46	dermal	X		
	M-48	dermal	X		
	M-49	dermal	X		
Control samples	M-18	MPNST-surrounding tissue	X		
	M-28	MPNST-surrounding tissue	X		
	M-29	MPNST-surrounding tissue	X		
	M-30	MPNST-surrounding tissue	X		
	M-31	MPNST-surrounding tissue	X		
	M-32	MPNST-surrounding tissue	X		
	NF-50	dNF-surrounding skin	X		
	NF-52	dNF-surrounding skin	X		
	NF-54	dNF-surrounding skin	X		
	NF-55	dNF-derived fibroblasts	X		
MPNST cell lines	S462	NF1-associated	X	X	X
	T265	NF1-associated	X	X	X
	ST-8814	NF1-associated	X	X	X
	90-8	NF1-associated		X	X
	sNF96.2	NF1-associated		X	
	S462-TY	NF1-associated	X	X	
	NMS-2	NF1-associated		X	
	STS26T	sporadic	X		
Schwann cell cultures	pNF5_SC	pNF-derived culture		X	X
	pNF6_SC	pNF-derived culture		X	X
	pNF7_SC	pNF-derived culture		X	X

Table 3. Tissue and cell samples used for the molecular characterization. Samples used for the molecular characterization including the MPNST-qPCR assay, the SNP array and the methylation array. Samples are comprised of tumours (14 MPNSTs, 9 pNFs and 7 dNFs), control tissues (9 tumour-surrounding normal tissue), 8 MPNST cell lines and primary cell cultures (3 from SCs and 1 from fibroblasts). Most of the samples for the *NF1*-qPCR are not included in this table. The *NF1*-qPCR sample set comprised 19 blood samples, 26 dNFs, 7 SC cultures, 4 skin samples and 3 fibroblast cultures. Samples NF-50, NF-52, NF-54 and NF-55 are shared by the *NF1*-qPCR and the MPNST-qPCR assays.

set of 24 control samples, each of which presenting 2 copies of the *NF1* gene was also used. These controls included 10 dNF samples, 5 blood samples, 4 skin samples, 3 fibroblast samples, and 2 $SC^{NF1+/-}$ samples.

In the qPCR assay for detecting somatic copy number alterations (SCNAs) in MPNSTs (MPNST-qPCR), a total of 35 samples were included: 7 NF1-associated MPNSTs, 5 sporadic MPNSTs, 5 MPNST cell lines (S462, T265, ST88-14, S462-TY and the sporadic STS-26T) and 8 neurofibromas (including 7 dNFs and 1 pNF). In addition, a set of 10 control samples comprising 6 MPNST-surrounding non-tumoural tissues, 3 dNF-surrounding skins and 1 dNF-derived fibroblast culture, was also used (**Table 3**).

DNA was extracted from all tumour and cell line samples as explained in section 1.4., except for 5 of the 7 NF1-associated MPNSTs, whose DNA was directly obtained from our collaborators. Primers and probes for the qPCR assay were developed with Roche Universal ProbeLibrary (UPL) technology. UPLs are hydrolysis probes of 8- to 9-nucleotide locked nucleic acid that are labeled at the 5' end with the fluorescent dye 6-carboxyfluorescein and at the 3' end with a quencher dye. The combination of the hydrolysis probe and the primer pair provided the specificity required for each particular genomic locus of interest. The design of each of the primers (desalted and purified; Sigma Life Science) was subjected to an *in silico* PCR and BLAST-like alignment tool (BLAT) search analysis to evaluate their specificity, which was later assessed experimentally by PCR and agarose gel electrophoresis before qPCR experiments were conducted. The sequences of the primers and probes used in both *NF1*-qPCR and MPNST-qPCR assays are listed in **Table 4** and **Table 5**, respectively.

qPCR experiments were performed in a Light-Cycler® 480 Real-Time PCR System with white Multiwell Plate 384 plates (Roche Diagnostics). Conditions for amplification were as follows: 95 °C for 10 min; 45 cycles of 95°C for 10 s, 60°C for 30 s, and 72°C for 1 s; and 40°C for 30 s. The linear dynamic range (LDR) and efficiency (E) of the primers were evaluated (see **Tables 4 and 5**). Each reaction in all experiments included 5 ng DNA template, 4 μL of 2X LightCycler 480 Probes Master Mix (cat.no. 04707494001, Roche Diagnostics), 0.1 μmol/L UPL probe, and 0.75 μmol/L of each primer, in a total volume of 8 μL [except for reactions for the L1 and the L1PA loci —

long interspersed nuclear elements (LINEs) — which included 0.2 μmol/L UPL probe and 1.2 μmol/L of each primer]. PCRs for each primer set and sample were performed in triplicate. Each set of PCR assays included both negative controls without template and a dilution series of a particular template for calculating the E value of the primer pair in each run. In addition, a calibrator sample of known copy number was included in triplicate in every assay.

Locus	Chromo-somal location	Name	Sequence (5' to 3')	UPL probe	Amplicon size (bp)	E	RCN 99%CI of 2 copies of the locus
MAP2K4	17p12	MAP2K4-L MAP2K4-R	cccatgaagtctccattctca ccgaagtaatccactgctgac	#4 cttcctgc	76	2.05	0.82 - 1.21
SSH2	17q11.2	SSH2-L SSH2-R	tgctttgttttgcttccttg gaatgtggccagggtgat	#4 cttcctgc	60	2.01	0.75 - 1.32
TBC1D29	17q11.2	TBC1D29-L TBC1D29-R	agccttaaaggagaagagacagc ggggacattttccctttctt	#20 ctggctgg	73	2.11	0.79 - 1.26
CRLF3	17q11.2	CRLF3-L CRLF3-R	agctgctgaagccagagaaa ctagcagacctgggcatctaa	#20 ctggctgg	86	1.95	0.84 - 1.19
RNF135	17q11.2	RNF135-L RNF135-R	ggttgaagagaaaaccctgtca aggaaagaaaggcaagaagagtt	#20 ctggctgg	81	2.06	0.81 - 1.24
NF1-5'	17q11.2	NF1-5'-L NF1-5'-R	cagagtcccctggtgagagt cctgaagaggcagttgagttg	#38 ggaagcag	60	1.99	0.85 - 1.18
NF1-C	17q11.2	NF1-C-L NF1-C-R	actctgtgtctgctttctgctaac aagagacagtgtgatactacacctgaa	#4 cttcctgc	70	1.97	0.82 - 1.22
NF1-3'	17q11.2	NF1-3'-L NF1-3'-R	ggccagggcaaaacttaaa tgtatggttccctagctccaa	#4 cttcctgc	112	1.88	0.85 - 1.18
UTP6	17q11.2	UTP6-L UTP6-R	cgccttgttgcttaaactga acctacaatcccagcccttt	#4 cttcctgc	84	1.97	0.80 - 1.25
SUZ12	17q11.2	SUZ12-L SUZ12-R	caagctccgtgaaatgcag ttcttcagttatttcttcgtttgc	#38 ggaagcag	76	1.97	0.83 - 1.20
RHOT1	17q11.2	RHOT-L RHOT-R	gcactggtctgtgtttcttcaa ccacttctgagccaagagga	#4 cttcctgc	68	1.98	0.85 - 1.18
PSMD11	17q11.2	PSMD11-L PSMD11-R	tgttactgttttgcttgaaattcct gtacacttctaaacttctcaggtcaca	#4 cttcctgc	94	1.95	0.74 - 1.34
ADARB1	21q22.3	ADARB1-L ADARB1-R	ccacacaaggacaggagagtc cagccttggaattgaattgg	#4 cttcctgc	70	2.01	n/a
L1PA	interspersed	L1PA-L L1PA-R	aaaaagtcaggaaacaacaggtg tcccaccaacagtgtaaaagtg	#55 ggagagga	71	2.00	n/a

Table 4. Primers and probes used for the *NF1*-qPCR assay. Primer and UPL probe sequences, amplicon sizes, efficiency (E) values of PCR reactions, and 99% confidence interval (CI) of the relative copy number (RCN) values indicating a normal diploid status for each interrogated locus by the *NF1*-qPCR assay.

We designed a Microsoft Excel spreadsheet to analyze qPCR data for copy number calculations. We used formulas from the qBase relative quantification framework (Hellemans et al., 2007), which are based on the Pfaffl method (Pfaffl, 2001). In brief, we averaged the 3 quantification cycle (Cq) numbers obtained from each triplicate with the second-derivative maximum method in the Light-Cycler® 480 software [as long as the difference in Cq between the replicate with the highest value and the replicate with lowest value was <0.3 for all genes and <0.2 for the *L1PA* locus (D'Haene et al.,

2010)]. We then calculated the ΔCq value for the difference between the unknown sample and the calibrator sample ($\Delta Cq = Cq_{unknown} - Cq_{calibrator}$). The relative quantity (RQ) was later calculated as: $RQ = E^{-\Delta Cq}$. We calculated the normalized relative quantity (NRQ) as: NRQ = RQ/NF, where NF is the normalization factor. The NF in turn is the geometric mean of the RQ values for the 2 selected reference loci (the *ADARB1* gene and the *L1PA* locus in the case of the *NF1*-qPCR; the *L1* and *L1PA* loci in the case of the MPNST-PCR) for the particular sample. The value for the stability parameter, *M* (Vandesompele et al., 2002), for this particular NF was previously calculated for the entire set of samples in *NF1*-qPCR and was <0.2 (M=0.168; (D'Haene et al., 2010). In the MPNST-qPCR a previous study including three single copy genes (*GLRX3*, *ACSS1* and *ADARB1*) and the repetitive elements *L1* and *L1PA* was conducted and the best combination (M=0.187) was found for a NF considering *L1* and *L1PA* (see Results, section 1.2.1).

Locus	Chromo-somal location	Name	Sequence (5' to 3')	UPL probe	Amplicon size (bp)	E	RCN 99%CI of 2 copies of the locus
AURKA	20q13.2	AURKA-L AURKA-R	ggacggttcttctggagctt gcgagacttcgtctcaaaaca	#55 ggagagga	111	2.10	0.76 - 1.32
DTL	1q32.3	DTL-L DTL-R	attgagaaagagactgagaagtagtcc aggatggtataaagtttcagactgc	#4 cttcctgc	67	2.00	0.81 - 1.24
CDCA7L	7p15.3	CDCA7L-L CDCA7L-R	atgtgacgtggggtgattc acatggcatctttcagtctacg	#4 cttcctgc	73	2.03	0.74 - 1.36
EXT1	8q24.11	EXT1-L EXT1-R	gtaccacctccaaatagcgagt ctgcagcttcagggatgc	#4 cttcctgc	63	2.00	0.73 - 1.37
EYA2	20q13.12	EYA2-L EYA2-R	tgctgtgtggactctgagtga cacctgttgacccaaactca	#4 cttcctgc	64	1.83	0.72 - 1.39
TNNI3K	1p31.1	TNNI3K-L TNNI3K-R	agtggccacagtgtagcaga ctgcagcagactccagtgat	#4 cttcctgc	63	1.82	0.74 - 1.35
ADD3	10q25.1	ADD3-L ADD3-R	aaacaaaactaggcaaaactcca tgggtgcctactgtttacca	#4 cttcctgc	88	1.86	0.76 - 1.32
STX3	11q12.1	STX3-L STX3-R	gtgcaaaaagccttctgtgat tgcattttaagtttccaagagaaga	#4 cttcctgc	78	1.78	0.75 - 1.34
OPCML	11q25	OPCML-L OPCML-R	gcccaaacaatcctactcca gggaaaccacagcacaattc	#4 cttcctgc	62	1.99	0.77 - 1.29
GLRX3	10q26.3	GLRX3-L GLRX3-R	caagtcataaagctcgacatgg accatcatgggtgtcctaaca	#4 cttcctgc	60	1.93	n/a
ACSS1	20p11.21	ACSS1-L ACSS1-R	ccctctccaccttcctcac aggacatcctgcaccatttt	#4 cttcctgc	60	2.03	n/a
ADARB1	21q22.3	ADARB1-L ADARB1-R	ccacacaaggacaggagagtc cagccttggaattgaattgg	#4 cttcctgc	70	1.75	n/a
L1	interspersed	LINE1-L LINE1-R	gcgctaaacatggaaaggaa tggtctttacaatttggcatgt	#28 ccagccgc	66	2.09	n/a
L1PA	interspersed	L1PA-L L1PA-R	aaaaagtcaggaaacaacaggtg tcccaccaacagtgtaaaagtg	#55 ggagagga	71	2.05	n/a

Table 5. Primers and probes used for the MPNST-qPCR assay. Primer and UPL probe sequences, amplicon sizes, efficiency (E) values of PCR reactions, and 99% confidence interval (CI) of the relative copy number (RCN) values indicating a normal diploid status for each interrogated locus by the MPNST-qPCR assay.

Finally, we calculated the relative copy number (RCN) as: RCN = NRQ/RF, where RF is a rescaling factor. The RF is the geometric mean of the NRQ values of a set of 24 control samples bearing 2 *NF1* copies in the case of the *NF1*-qPCR, or a set of 10 control samples with no SCNAs in the case of the MPNST-qPCR. RCN values close to 1 indicate the presence of 2 gene copies, RCN values close to 0.5 indicate a deletion, and RCN close to 1.5, 2 and 2.5 indicate 3, 4 and 5 copies of the gene, respectively. A 99% CI for the RCN values indicating 2 gene copies was calculated for each interrogated locus (see **Tables 4 and 5**).

2.2. MLPA and microsatellite multiplex PCR analysis

In parallel to the *NF1*-qPCR, we also used the MLPA technique to assess the *NF1* copy number status of both samples with *NF1* constitutional and somatic deletions. We performed MLPA reactions in duplicate with the SALSA MLPA Kit P122-C1 NF1 Area (cat.no. P081/P082, MRC-Holland) and 40 ng DNA, in accordance with the manufacturer's instructions. Once ligated and amplified, PCR fragments were separated by capillary electrophoresis (ABI 3130xl Genetic Analyzer; Applied Biosystems). Peak intensities were analyzed with Peak Scanner Software (Applied Biosystems) and normalized for peak heights, as described elsewhere (Garcia-Linares et al., 2011). For genomic regions with 2 copies in a sample, these calculations were expected to yield an RCN value of approximately 1.0. A value <0.8 was considered to indicate a deletion.

We also used microsatellite multiplex PCR analysis (MMPA) as previously developed in our laboratory (Garcia-Linares et al., 2012) to assess the *NF1* copy number status of tumour samples with *NF1* somatic deletions and to calculate the percentage of cells within the tumours with 2 *NF1* copies. This technique allows the simultaneous amplification of 16 microsatellite markers. MMPA reactions were performed in duplicate with the Multiplex PCR Kit (cat.no. 206143, Qiagen) and 50 ng DNA. Information regarding the amplification protocol, data analysis, and calculations is described elsewhere (Garcia-Linares et al., 2012).

2.3. SNP array

SNP array analysis was performed on 8 NF1-associated MPNSTs, 8 pNFs, 7 NF1-associated MPNST cell lines (S462, T265, ST-8814, 90-8, sNF96.2, S462-TY and NMS-2) and 3 pNF-derived SC cultures (**Table 3**) using Beadchip technology from Illumina, but with different chips depending on availability at the time of the analysis. In particular, all MPNSTs were analyzed using Illumina Human660WQuad chip except one that was analyzed with Illumina HumanOmni-Express v1, all pNFs and pNF-derived SC cultures were analyzed with Illumina HumanOmni1S, and MPNST cell lines were analyzed with either Illumina Human660WQuad chip or Illumina HumanOmni1S, depending on the sample. All array experiments were performed in an Illumina HIScanSQ machine in the Genomics Service from the IMPPC. Raw data was processed with Illumina Genome Studio v2009 with the Genotyping module v1.1.9 to extract B-allele frequency (BAF) and log R ratio (LRR) values for each SNP. SNP array data were analyzed using the R package ASCAT (Van Loo et al., 2012) to obtain loss of heterozygosity (LOH) and allele-specific copy number profiles from the BAF and LRR values. All samples were analyzed independently and treated as unpaired samples, using the germline genotype prediction functionality from ASCAT. In short, after loading BAF and LRR data, the germline genotype parameters were estimated and the data were segmented using the ASPCF algorithm. Next, ASCAT computed the most likely combination of copy number states, total ploidy and percentage of aberrant cells. Circular genomic plots were created using Circos (Krzywinski et al., 2009).

2.4. Methylation array

The 450k Infinium methylation array from Illumina was used to check the DNA methylation status of 4 NF1-associated MPNSTs, 3 pNFs, the NF1-associated MPNST cell lines S462, T265, ST-8814 and sNF96.2 and 3 pNF-derived SC cultures (**Table 3**).

First of all, DNA was submitted to bisulfite conversion with the EZ DNA Methylation™ Kit (cat.no. D5001, Zymo Research). This technique is based on the conversion of unmethylated cytosines into uracil. Methylated cytosines remain unchanged during bisulfite treatment, hence the DNA methylation profile can be later determined by PCR amplification and Sanger sequencing.

Bisulfite conversion of DNA was confirmed prior array experiments by Sanger sequencing the methylated Ag2c5 and unmethylated Ar3c7 Alu repeats in each sample (data not shown). Ag2c5 and Ar3c7 are Alu repetitive elements found to be methylated and unmethylated, respectively, in colorectal cancer samples (Rodriguez et al., 2008) and also in keratinocytes, fibroblasts and stem cells (Martín, 2013).

Bisulfited-converted DNA was then hybridized in an Infinium HumanMethylation450 BeadChip using an Illumina HIScanSQ machine to determine its methylation profile in the Genomics Service from the IMPPC. Data analysis was performed in R using the Bioconductor package minfi (Aryee et al., 2014). In short, methylation array data were loaded into R and after a quality control step it was normalized using the subset-quantile within array normalization (SWAN) approach (Maksimovic et al., 2012). After the normalization process, probes overlapping known SNPs were discarded and M and beta values were generated. Differential methylation was then determined for the individual probes and finally the differential methylation data were aggregated to determine the differential methylation status of gene promoters.

2.5. Generation and analysis of transcriptional imbalances

Gene expression data generated by the NF1 Microarray Consortium (Miller et al., 2009) were downloaded from the Gene Expression Omnibus repository where is available under the accession number GSE14038. Expression data were generated with the Affymetrix GeneChip Human Genome U133 Plus 2.0 Array. The analysis of the expression data was performed using R and the Bioconductor package position related data analysis (PREDA; Ferrari et al., 2011). In short, the expression data were loaded and preprocessed using the functions provided by PREDA and the custom CDF file from Brainarray v15 (Dai et al., 2005), which contains updated and more accurate positional annotation of the array probes. Data were normalized using the robust multi-array average (RMA; Irizarry et al., 2003), the raw differential gene expression statistics were computed and then smoothed using a local kernel smoothing method with adaptive local bandwidth. The extreme values identified in the smoothed statistic were evaluated using a permutation test with 100,000 permutations and those with a q-value <0.05 were deemed significant. These extreme regions were named transcriptional imbalances (TIs).

To determine if the TIs were associated with other genomic features (SCNAs, differentially methylated genes) we used the Bioconductor package regioneR (Gel et al., 2015). regioneR uses a permutation test strategy to assess the association of genomic regions and other genomic features. In short, the regions to be studied are randomly shuffled along the genome a number of times, and with each randomized region set, the value of the evaluation function is computed, creating a distribution of the evaluation function as expected by chance. Then, the original region set is evaluated and its value is compared to the random distribution, returning a P-value and a z-score. To study the association of TIs and SCNAs we defined the evaluation function as the weighted mean number of tumours presenting a genomic alteration (gain or loss) in the evaluated region, and used a complete randomization with the predefined mask as the randomization function. In the case of the differentially methylated genes, the evaluation function was the number of overlaps with hyper- or hypomethylated genes and the randomization function shuffled was the methylation status of the genes. In all cases, the randomization was performed 10,000 times.

3. *In vitro* gene expression knockdown

3.1. siRNA transfection procedures

Small interfering RNAs (siRNAs) were used for knocking down the expression of several genes in both S462 and T265 cell lines (**Figure A.1** in Annexe 1). In each transfection experiment and for each condition, a siRNA pool targeting a particular gene or a non-targeting control (NTC) siRNA construct (siGENOME SMARTpool, Dharmacon, GE Life Sciences) was introduced into cells using lipofectamine RNAiMAX (cat.no. 13778-030, Life technologies). As a mid-throughput approach has been intended in this thesis studying the effect of the expression knockdown of different genes in several tumourigenic properties of two cell lines, we selected Dharmacon siGENOME SMARTpool technology because they are composed of a mixture of 4 different siRNAs targeting a particular gene of interest in a single reagent, providing an advantage in sensitivity. Transfected cells with these reagents were used for RNA extraction and for several *in vitro* readouts, including cell viability and cell counting, cell proliferation, cell death and anchorage-independent growth.

Briefly and except for cell viability assay for the T265 cell line (see section 4.1.), 20,000 (S462) or 60,000 (T265) cells were plated for each condition in a well of a 12-well plate and incubated overnight with 400 μL of supplemented DMEM. A mixture of 0.5 μL of 20 μmol/L siRNA (20 nM final concentration) and 1 μL of lipofectamine diluted in 100 μL of opti-MEM (cat.no. 31985-062, Life technologies) was added to each well. After 24 hours of transfection, medium was replaced with 1 mL of supplemented DMEM. Only for the anchorage-independent growth assay, cells were harvested 24 hours post-transfection and used for the assay (see **Figure 5**). For RNA extraction, and the cell proliferation, cell death and cell counting *in vitro* functional assays, cells were let to grow for extra 48 hours and were harvested, 72 hours post-transfection, with trypsin-EDTA (cat.no. 15400-054, Life technologies; see **Figure 5**).

3.2. cDNA synthesis and RT-qPCR

RT-qPCR technique was used to check the gene expression knockdown after siRNA transfection in both S462 and T265 cell lines. RNA was extracted from transfected cells in each condition as explained in section 1.4. Then, 1 μg of RNA was submitted to retrotranscription (RT) using Superscript III reverse transcriptase enzyme (cat.no. 18080-044, Life technologies). Briefly, in a 0.2 mL tube, 1 μL of random hexamers (cat.no. N8080127, Life technologies), 1 μL of dNTPs mix (10mM each; cat.no. 733-1364, vWR), 4 μL of 5X First-Strand buffer (cat.no. 18080-044, Life technologies), and 2 μL of 0,1M DTT (cat.no. 18080-044, Life technologies) were mixed with 1 μg of RNA and RNAse-free water in a final volume of 20 μL. Then, 0.8 μL of the RT enzyme was added and tubes were set on a thermocycler (2720 Thermal Cycler, Applied Biosystems). Conditions for retrotranscription reaction were as follows: 25°C for 12 min, 42°C for 50 min and 70ºC for 15 min. Finally, cDNA sample was 1:10 diluted with RNAse-free water and used as a template for the qPCR experiments.

Primers and probes for the RT-qPCR assay were also developed with Roche Universal ProbeLibrary (UPL) technology. In this case, when possible, an intron spanning design was chosen, which considers both primers from the pair in different but contiguous exons, thus avoiding amplification of potential genomic DNA present in the sample. The design of each of the primers (desalted and purified; Life technologies) was

subjected to an *in silico* PCR and BLAT search analysis to evaluate their specificity, prior qPCR experiments. The sequences of the primers and probes used are listed in **Table 6**.

Gene	NCBI RefSeq	Name	Sequence (5' to 3')	UPL probe	Amplicon size (bp)	E
NUP85	NM_024844.3	NUP85-F NUP85-R	gcgtccgagcgacttcta attcacgcctggaatcaaag	#25	89	2.02
TK1	NM_003258.4	TK1-F TK1-R	gcaatgagctgcattaacctg cgagaatcacctggatctgc	#36	79	2.01
CBX2	NM_032647.3	CBX2-F CBX2-R	agccggctgagagttcct agagaggcgtgcaggaca	#4	61	1.83
CBX4	NM_003655.2	CBX4-F CBX4-R	accgctagtggtgcaggt ttgctgttgagctcgtactgat	#25	144	1.86
CBX8	NM_020649.2	CBX8-F CBX8-R	ccagcagagtggatgacaag gcctaagggcctctgtgag	#12	104	1.84
BIRC5	NM_001168.2	BIRC5-F BIRC5-R	gcccagtgtttcttctgctt gttcctctatggggtcgtca	#17	67	2.09
PLAG1	NM_002655.2	PLAG1-F PLAG1-R	agtaggcttttcgctctgctt aaagatttaggtaagcaatctgtttca	#38	72	1.84
CAD	NM_004341.3	CAD-F CAD-R	atcccagggcttcctgat ggctaccttccgagaggact	#73	111	1.96
EPHA4	NM_004438.3	EPHA4-F EPHA4-R	aacttgggtggatagcaagc tttcatccatgatactcacttcct	#12	63	1.91
BUB1	NM_004336.3	BUB1-F BUB1-R	tggattaccacagcctaaaaataa ctcttcagcatgaggcacttc	#36	109	1.90
MYBL2	NM_002466.2	MYBL2-F MYBL2-R	ctgcaagcccccagtgta ggccagttggtcagaagact	#67	102	2.00
HOXA13	NM_000522.4	HOXA13-F HOXA13-R	gaatgggaaagagaaagagacaga actggcagtctttacctttcttaaa	#55	116	1.88
LHX8	NM_001001933.1	LHX8-F LHX8-R	tcctgcaaaaggcaactttc gagggcaccttccacactaa	#55	144	2.10
CDCA8	NM_018101.2	CDCA8-F CDCA8-R	cctgacacccaggtttgact gccattccctgagatgttgt	#67	94	1.91
BCAT1	NM_001178094.1	BCAT1-F BCAT1-R	tgaagatggagaagaagaactgg tcactcctggaagaatgatgc	#25	62	1.93
CCDC8	NM_032040.3	CCDC8-F CCDC8-R	agatcaactgggcctccttt cctgatcagcctcgatgtc	#4	84	1.93
GINS2	NM_016095.2	GINS2-F GINS2-R	aacttacgaagctcctgttaaatca gaccagggtccggatttc	#8	71	1.98
KIF15	NM_020242.2	KIF15-F KIF15-R	tcattctacccaaatgcagga ttcaaggacattcaactgtgaga	#4	94	1.80
KIF18B	NM_001080443.1	KIF18B-F KIF18B-R	ggtggtgcaaggactttcttt ttacggttcccctggtc	#67	78	1.94
KIF23	NM_138555.2	KIF23-F KIF23-R	gaaccaaatgtatggaactaacaaga cacacgatcatccgcactt	#60	108	1.80
TBP	NM_003194	TBP-F TBP-R	aggaattgaggaagttgctgag cgctggaactcgtctcacta	#67	78	1.99
HMBS	NM_000190.3	HMBS-F HMBS-R	tcctgaggcacctggaag ttgtatgctatctgagccgtcta	#25	119	1.99

Table 6. Primers and probes used for the RT-qPCR experiments. Primer sequences, UPL probes, amplicon sizes and efficiency (E) values of PCR reactions by the RT-qPCR assay.

qPCR experiments were also performed in a Light-Cycler® 480 Real-Time PCR System with white Multiwell Plate 384 plates (Roche Diagnostics) with same conditions than in section 2.1. The LDR and E of the primers were also evaluated (see **Table 6**). Each reaction in all experiments included 2 μL of diluted cDNA template, 4 μL of 2X LightCycler 480 Probes Master Mix (cat.no. 04707494001, Roche Diagnostics), 0.1 μmol/L UPL probe, and 0.5 or 0.75 μmol/L of each primer (depending on the gene), in a total volume of 8 μL. PCR reactions for each primer set and sample were also performed in triplicate and each set of PCR assays included both negative controls without template. In addition, a calibrator sample was also included in triplicate in every assay.

A Microsoft Excel spreadsheet was used to analyze qPCR data for relative expression calculations. We also used formulas from the qBase relative quantification framework (Hellemans et al., 2007), which are based on the Pfaffl method (Pfaffl, 2001), as in the previous DNA-based qPCR assays (see section 2.1). We here calculated the normalized relative expression (NRE) as: NRE = RQ/NF, where RQ is the relative quantity and NF is the normalization factor (see section 2.1). In this case, the normalization factor was, for a particular sample, the geometric mean of the RQ values for the 2 selected reference genes for expression normalization. We selected *HMBS* and *TBP* genes as reference genes, as they have been described to be suitable reference genes for NF1-associated samples, such as SCs (Maertens et al., 2006a). The value for the stability parameter *M* (Vandesompele et al., 2002) for this particular NF was calculated for the entire set of MPNST cell samples and was <0.2 (D'Haene et al., 2010).

4. *In vitro* functional assays

The effect of the gene expression knockdown on several tumourigenic cellular properties was studied with a battery of functional assays (viability, proliferation and cell cycle, apoptosis and cell death, and anchorage-independent growth) in S462 and T265 cell lines (see **Figure 5** and **Figure A.1** in Annexe 1).

4.1. Cell viability analysis

Cell viability was assessed for the transfected T265 cell line using the colourimetric XTT assay (cat.no. 11465015001, Roche). XTT [2,3-Bis-(2-Methoxy-4-Nitro-5-Sulfophenyl)-2H-Tetrazolium-5-Carboxanilide] is a tetrazolium salt that, in the presence of an electron-coupling reagent, produces a water-soluble formazan salt. Tetrazolium salts are cleaved to formazan by the succinate-tetrazolium reductase system in the respiratory chain of the mitochondria. Therefore, the amount of formazan dye generated directly correlates to the number of metabolically active cells in the culture. Formazan dye can be quantified using a multi-well spectrophotometer reader.

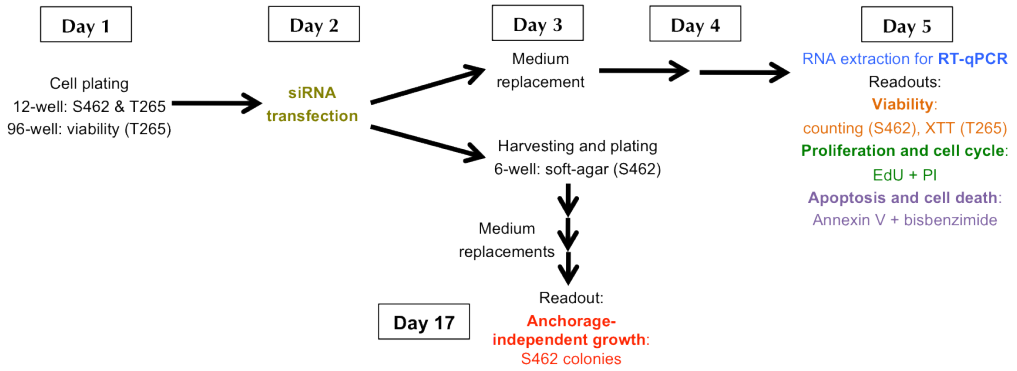

Figure 5. Experimental design of siRNA experiments and functional assays. Mid-throughput approach studying the effect of the expression knockdown by RNAi of different genes in several tumourigenic properties of S462 and T265 cell lines. Transfected cells were used for RNA extraction and for several *in vitro* readouts, including cell viability, cell proliferation and cell cycle analysis, apoptosis and total cell death and anchorage-independent growth. EdU: 5-ethynyl-2'-deoxyuridine. PI: propidium iodide.

Briefly and for each condition, 1,500 cells per well were plated in a 96-well plate and incubated overnight with 100 μL of supplemented DMEM. A mixture of siRNA pool (20 nmol/L) and lipofectamine (0.25 μL) diluted in 25 μL of opti-MEM (cat.no. 31985-062, Life technologies) was added in tetraplicate and incubated for 24 hours in standard conditions. After that, medium was replaced with 100 μL of supplemented DMEM and cells were let to grow for extra 48 hours. Moreover, 100 μL of supplemented DMEM were also added in tetraplicate in empty wells with no cells, as the blank condition. Then, 50 μL of XTT labeling mixture (XTT labeling reagent and electron-coupling reagent 50:1) were added to each well, and the plates were incubated in a cell culture incubator for 1-2 hours in standard conditions. After that, absorbances at 492 nm (A_{492})

and 690 nm (A_{690}) were measured for every well with a 96-well plate spectrophotometer reader (Spectra Max 340PC). Then, the $A_{492} – A_{690}$ value was calculated for every single well, including the blank measurement. Viability was then calculated, in arbitrary units, for a particular well as $(A_{492} – A_{690})_{well} – (A_{492} – A_{690})_{blank}$.

As the XTT results obtained for the transfected S462 cell line were inconsistent, cell viability was alternatively performed for this cell line by automated cell counting. Cells from each condition were harvested 72 hours post-transfection (see **Figure 5**) and diluted with PBS. A mixture of 10 μL of cell suspension and 10 μL of trypan blue dye (cat.no. EVS-050, Nanoentek) was added to an EVE cell counting slide (cat.no. EVS-050, Nanoentek) in duplicate. The slide was introduced into the Countess™ Automated Cell Counter (cat.no. C10227, Life technologies) and the number of cells was then calculated.

4.2. Cell proliferation and cell cycle analysis

The Click-iT® EdU Alexa Fluor® 488 Flow Cytometry Assay Kit (cat.no. C10425, Life Technologies) was used in combination with propidium iodide (PI; cat.no. P4170, Sigma) staining for the calculation of proliferating cells and cell cycle phases using the flow cytometer in both S462 and T265 cell lines. EdU (5-ethynyl-2'-deoxyuridine) is a nucleoside analogue to thymidine that is incorporated into DNA during active DNA synthesis. Detection with this technology is based on a click reaction: a copper catalyzed covalent reaction between an azide and an alkyne. In this assay, the alkyne is found in the ethynyl moiety of EdU, while the azide is coupled to an Alexa Fluor® 488 dye.

As a summarized protocol, cells were incubated with 20 μmol/L EdU for 1 hour prior trypsinization. Then, harvested cells from each condition were washed with 1% BSA-PBS, fixed with 4% p-formaldehyde, permeabilized with a saponin-based buffer, incubated for 30 min with the Click-iT EdU reaction cocktail (containing both Alexa Fluor® 488-azide and $CuSO_4$ needed for the click reaction), and then washed again. A final incubation with 15 mg/mL PI in citrate buffer for 30 min was performed. Finally, 10,000 cells per condition were analyzed with the BD LSRFortessa SORP cytometer

using the B530-A and B695-A lasers for the measurement of the Alexa Fluor® 488 dye (EdU positive cells) and PI (DNA content), respectively, in the Cytometry Service from the Institut Germans Trias i Pujol.

4.3. Cell death analysis

Apoptosis was measured for both transfected T265 and S462 cell lines using the Annexin-V-Alexa Fluor® 568 antibody (cat.no. 03703126001, Roche; cat.no. A13202, Life Technologies) by flow cytometry. This was combined with bis-benzimide dye (also known as Hoechst 33342; cat.no. B2883, Sigma) staining for the detection of late apoptotic and necrotic cells, which represents a thorough characterization of the cell death process. Annexin-V is a cytoplasmic protein with a high affinity for phosphatidylserine. In the early stages of apoptosis, there is a flip-flop translocation of phosphatidylserine from the inner layer of the cell membrane to the outer layer, thereby exposing phosphatidylserine and annexin-V at the external surface of the cell. Hence, this protein is suited to detect apoptotic cells. Because necrotic cells also expose phosphatidylserine as a result of loss of the membrane integrity, apoptotic cells must be differentiated from these necrotic cells with a concomitant use of a DNA dye, such as bisbenzimide, that allows the discrimination of necrotic cells from the apoptotic Annexin-V positive cells.

Cells from each condition were harvested and washed with PBS. Then they were incubated for 15 min with 100 μL of annexin-binding buffer (10mM HEPES, 140 mM NaCl, 2.5 mM $CaCl_2$, pH 7.4) containing Annexin-V-Alexa Fluor® 568 antibody (1:50, Roche; 1:20, Life Technologies) and 5 mg/mL bisbenzimide. Finally, 30,000 cells for each condition were analyzed with the BD LSRFortessa SORP cytometer using the G610-A and V450-A lasers for the measurement of the Alexa Fluor® 568 dye (Annexin-V positive apoptotic cells) and bisbenzimide (late apoptotic/necrotic cells), respectively, in the Cytometry Service from the Institut Germans Trias i Pujol.

4.4. Anchorage-independent growth analysis

Soft agar assay was performed on S462 cell line to assess their anchorage-independent growing properties after gene expression knockdown. T265 cell line does

not generate colonies *in vitro* with this technique. First of all, a 2X supplemented DMEM solution was prepared by mixing in sterile conditions High Glucose with L-Glutamine and sodium pyruvate DMEM powder (cat.no. 12800017, Life technologies) with 20% FBS (cat.no. S181B-500, Biowest), sodium bicarbonate (cat.no. 25080060, Life technologies) and sterile distilled water (cat.no. 1613657, Life technologies). Then, 6-well plates were prepared with bottom 1.6% agar layer [3.2% SeaPlaque Agar (cat.no. 50101, Lonza) with 2X supplemented DMEM 1:1] and allowed to solidify. After 24 hours of siRNA transfection (see section 3.1. and **Figure 5**), S462 cells from each condition were harvested and counted with the Countess™ Automated Cell Counter (cat.no. C10227, Life technologies). Then, a top agar layer was prepared by mixing the cell suspension with agarose and a total of 20,000 cells in a 0.8% agar layer were plated and allowed to solidify for each condition. Supplemented DMEM was added over the top agar layer and plates were incubated under standard conditions for two weeks, being medium replaced twice a week. Then, top medium was removed and colonies were fixed and stained with a 0.005% crystal violet in 10% formaldehyde solution for 1 hour and washed with PBS afterwards. Colonies were imaged on a microscope (Leica DMIL LED) and four photographs were taken for each condition (one per quadrant). Semi-automated colony counts were performed using an algorithm with ImageJ software (NIH).

4.5. Statistical analyses

All experiments concerning siRNA transfection experiments followed by the different functional assays were repeated at least three times. A NTC siRNA was always included in each experiment and the fold change of the specific readout (viability, proliferation, apoptosis, total cell death, number of colonies and area of colonies) of each siRNA condition versus the NTC was calculated. In cell cycle analysis, the percentage of cells in each of the three phases was calculated for each siRNA condition and the NTC. Statistical analysis was performed using SPSS software (IBM). For each biological triplicate dataset, mean and standard deviation was calculated and a non-paired Student's t-test assuming unequal variances was applied to find differences between a particular siRNA condition and the NTC. A P-value <0.05 was considered to be significant.

5. *In vitro* chemical inhibition

5.1. Drug treatment and cell viability analysis

A set of MPNST cell lines (S462, T265, ST88-14 and the sporadic STS26T), a primary SC culture, and the human foreskin fibroblast CCD-1112Sk cell line (cat.no. CRL-2429™, ATCC®) were incubated in a dose-dependent manner with the kinesin inhibitors ispinesib (cat.no. S1452, Selleckchem), GSK-923295 (cat.no. HY-10299, MedChem Express), or paprotrain (cat.no. 4813, Tocris Biosciences). These compounds selectively inhibit the kinesin proteins KIF11 (Lad et al., 2008), KIF10 (Wood et al., 2010) and KIF20A (Tcherniuk et al., 2010), respectively. Cell viability was then measured using XTT assay at three time points: 0 hours, 24 hours and 48 hours post-treatment.

Briefly, 1,000 cells (S462, 26T); 1,500 cells (T265, ST88-14 and CCD-1112Sk); or 2,500 cells (SCs) per well were plated in several 96-well plates and incubated overnight with 100 μL of supplemented DMEM. The day after, XTT assay was performed as in section 4.1. for all the conditions of 0 hours timepoint. For the rest of the conditions media was replaced with 100 μL of supplemented DMEM containing varying concentrations of ispinesib, GSK-923295 or paprotain (each concentration in tetraplicate). Then, cells were let to grow for 24 hours or 48 hours and XTT assay was perfomed in each of these timepoints as in section 4.1. So, viability measures were taken in each of the three timepoints and the log2 of fold viability was then determined versus timepoint 0 for each chemical and cell line.

5.2. IC50 determination by cell counting

The half maximal inhibitory concentration (IC_{50}) of the compounds ispinesib (cat.no. S1452, Selleckchem), GSK-923295 (cat.no. HY-10299, MedChem Express) and paprotrain (cat.no. 4813, Tocris Biosciences) was calculated by creating a dose-response curve with different concentrations of the drugs in the two MPNST cell lines S462 and T265 and the control CCD-1112Sk fibroblast cell line.

S462 (100,000 per well), T265 (150,000 per well) and fibroblasts (150,000 per well) were plated in a 6-well plate and incubated with 100 μL of supplemented DMEM. The following day media was replaced with 100 μL of supplemented DMEM containing varying concentrations of the different drugs (each concentration in triplicate). Cells were let to grow for 48 hours, trypsinized and harvested. Cells were then resuspended in PBS and counted with the Countess™ Automated Cell Counter (ref. C10227, Life technologies) as in section 4.1. Viability was calculated for each dose as the number of cells of this particular dose with respect to dose 0 (DMSO) after 48 hours of treatment.

Viability values were plotted against dose values. A non-linear regression model curve fitting was applied using the GraphPad Prism 5 software for each compound and IC_{50} values were determined.

5.3. IC50 shift assay

An IC_{50} shift assay was conducted to check if siRNA-depleted MPNST cells were more sensitive to chemical inhibition. In this assay a combination of siRNA transfection for the expression knockdown of *KIF15* (Dharmacon) and the NTC siRNA (Dharmacon), and a chemical inhibition of KIF11 protein with ispinesib (cat.no. S1452, Selleckchem) was performed in S462 cell line.

First of all, 250,000 S462 cells were plated in a 10 cm plate and incubated overnight with 5 mL of supplemented DMEM. A mixture of 6.25 μL of 20 μmol/L siRNA and 12.5 μL of lipofectamine RNAiMAX (cat.no. 13778-030, Life technologies) diluted in 1.25 mL of opti-MEM (cat.no. 31985-062, Life technologies), 20 nM siRNA final concentration, was added to each plate. After 24 hours of transfection, cells were harvested and counted. Then, 100,000 cells per well were plated on a 6-well plate and incubated with 2 mL of supplemented DMEM. The following day media was replaced with 2 mL of supplemented DMEM containing varying concentrations of ispinesib. Cells were let to grow for 48 hours, trypsinized and harvested. Cells were then resuspended in PBS and counted with the Countess™ Automated Cell Counter (ref. C10227, Life technologies) as in section 4.1. Viability was calculated for each dose as the number of cells of this particular dose with respect to dose 0 (DMSO) after 48 hours of treatment.

The IC_{50} shift assay (siRNA transfection plus ispinesib treatment) was repeated three times for each condition (NTC siRNA and siRNA targeting *KIF15*). Viability values from the three experiments were plotted against dose values. Again, a non-linear regression model curve fitting was applied using the GraphPad Prism 5 software for each compound and IC_{50} values were determined. A paired Student's t-test assuming equal variances was applied to find differences in the IC_{50} values between the two conditions. A P-value <0.05 was considered to be significant.

5.4. Immunofluorescence of anti-α tubulin

The effect of the kinesin inhibitors ispinesib and GSK-923295 in the microtubule cytoskeleton was determined by immunofluorescence of α-tubulin protein. In short, S462 and T265 cells were plated on an 8-well Labtek slide (cat.no. 94.6140.802, Sarstedt) and incubated with vehicle (DMSO), 2.5 nM ispinesib or 1 μM GSK-923295 in supplemented DMEM for 24 hours. After this incubation, cells were fixed with 4% p-formaldehyde, PBS-washed, permeabilized with 0.1% Triton-PBS, washed with 1% FBS-PBS and incubated with 1:100 of mouse anti-α tubulin-Alexa488 antibody (cat.no. 322588, Life technologies) in 10% FBS-PBS for 45 min. After this, cells were mounted with Vectashield with DAPI (cat.no. H-1200, Vector Laboratories). The Labtek slide was then visualized in a fluorescence-inverted microscope (Leica DMI 6000B) and photographs were taken.

RESULTS

1. Development of qPCR assays for the detection of copy number alterations in the context of NF1

Among the wide spectrum of constitutional mutations found in neurofibromatosis type 1 (NF1) patients, around 5% correspond to microdeletions that span *NF1* and neighbouring genes. These mutations are mostly inherited directly from the germline but sometimes they occur post-zygotically, resulting in mosaicism. In addition, it has been found that *NF1* microdeletion patients present an increased lifetime risk for the development of malignant peripheral nerve sheath tumours (MPNSTs; De Raedt et al., 2003). These tumours are characterized by presenting highly hyperploid genomes with recurrent somatic copy number alterations (SCNAs), including copy number gains and losses.

The first part of this thesis was motivated by a requirement of an easy and fast tool for the specific detection of *NF1* constitutional microdeletions, either in the context of mosaicism or not, which could be also extendable to somatic *NF1* deletions in NF1-associated tumours and other traits. Moreover, an adaptation of this tool for the detection of copy number alterations in highly aberrant genomes from malignant tumours, such as MPNSTs, was also intended. Given the high sensitivity and specificity that qPCR shows we chose this technique as our tool and we developed one probe-based qPCR assay for the detection of deletions in the *NF1* locus (*NF1*-qPCR) and another probe-based qPCR assay for the detection of SCNAs in the MPNST genome (MPNST-qPCR).

1.1. Assessment of NF1 constitutional and somatic deletions: NF1-qPCR

A first qPCR assay was designed for the detection of the four types of *NF1* constitutional microdeletions and the somatic second-hit *NF1* deletions present in NF1-associated traits, such as dermal neurofibromas (dNFs).

1.1.1. Development and validation of the qPCR assay

The qPCR assay was set up with Universal Probe Library (UPL) probes and their corresponding specific primer pairs. We chose UPL probes for our study because of their advantages of higher specificity, higher PCR efficiency (E) values, and avoidance

of primer-dimer signal that hydrolysis probes show, in contrast to fluorescent dyes such as SYBR Green. We also chose UPL probes for their flexibility of use and their reduced cost compared with DNA-sequenced hydrolysis probes.

For copy number assessment, we selected 11 genomic loci distributed along a 2.8-Mb region encompassing the *NF1* gene (**Figure 6**). To distinguish Type-1, Type-2, Type-3, and atypical *NF1* microdeletions specifically, we decided to interrogate 3 regions within the *NF1* gene (NF1-5', NF1-C, and NF1-3'), 5 loci that closely flank REP-A, REP-B, REP-C, *SUZ12*, and its pseudogene *SUZ12P1* (TBC1D29, CRLF3, RNF135, UTP6, RHOT1) and one locus within *SUZ12P1* (SUZ12P1). Two other loci located distal to the *NF1* gene (SSH2 and PSMD11) were also included. In addition, the *MAP2K4* gene, located in 17p, was selected as a control (i.e., a locus with 2 copies). Moreover, as it has been suggested (D'Haene et al., 2010), we selected two reference genes, *ADARB1* (21q22.3) and the long interspersed element (LINE) repetitive sequence *L1PA* (which is interspersed through the genome), to further normalize copy number data.

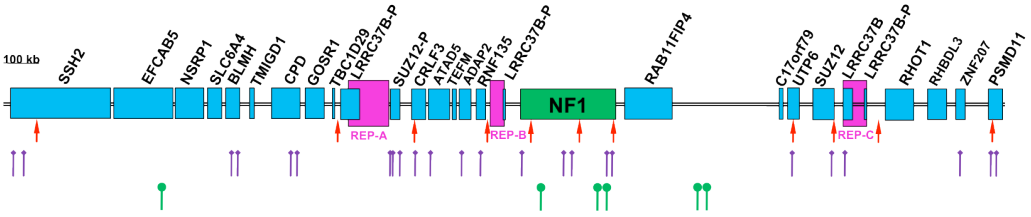

Figure 6. *NF1* region assessed with qPCR, MLPA and MMPA techniques. Schematic representation of the *NF1* region at 17q11.2. *NF1* gene is represented by a green box, protein-coding genes are represented by blue boxes, and paralogous regions REPs are represented by pink boxes. Indicated are the positions of the 11 qPCR probes (red arrows), the 24 MLPA probes ("tailed" purple circles), and the 6 microsatellites assessed by microsatellite multiplex PCR analysis (MMPA; "tailed" green circles).

Some experiments were performed to validate the qPCR assay. First, a set of 2-fold dilutions of pooled DNA samples (80 to 0.156 ng per reaction in triplicate) was used to determine the linear dynamic range (LDR) and the E value of the primers used (Hellemans et al., 2007). All designed primers showed a large LDR (at least 9 orders of magnitude) and high E values, which ranged from 1.88 to 2.11 for the analyzed loci (see **Table 4**). The qBase relative quantification framework was used for the calculations of the Relative Copy Number (RCN) values (Hellemans et al., 2007). We determined the range of the RCN values for a 2-copy status of the *NF1* gene by analyzing 24 control samples. The mean±SD Normalized Relative Quantity (NRQ) for

the 12 loci and 24 samples interrogated was 0.99±0.08. The mean calculated 99% confidence interval (CI) of RCN for the 12 loci was 0.81–1.23. An RCN value below the lower limit of the CI for a locus was considered to indicate deletion of that particular locus.

1.1.2. Detection of NF1 Type-1, Type-2 and atypical constitutional microdeletions

After validating the qPCR assay with a panel of 24 control samples, we tested the performance of the qPCR assay by using a set of 14 DNA samples previously characterized and bearing different types of constitutional deletions of the *NF1* gene: 5 Type-1 deletions, 6 Type-2 deletions, and 3 atypical deletions. No Type-3 deletion was tested. All deletions were detected with the qPCR assay (**Figure 7**). The mean±SD RCN value within the deleted loci was 0.53±0.07. Patient NF-01 beared a Type-2 microdeletion and the DNA sample from this patient showed a mean RCN value of 0.68±0.05 within the deleted loci. This result reflected the presence of mosaicism for this microdeletion, which was later confirmed in our lab by single nucleotide polimorphism (SNP) array (data not shown). Thus, when we considered all loci known to be deleted in our sample set, the qPCR assay showed 100% sensitivity and 99.2% specificity (see **Figure 7**). The *SUZ12* locus, which is essential for distinguishing a Type-1 deletion from a Type-2 deletion, showed 100% sensitivity and 96.9% specificity. All qPCR results were confirmed in a parallel analysis of these samples with the multiplex ligation-dependent probe amplification (MLPA) technique, which is a standard technique used for the assessment of DNA copy number in most genetic diagnostics laboratories (see **Figure A.2** in Annexe 1).

1.1.3. Detection of NF1 somatic deletions

We also tested the performance of the qPCR assay for detecting somatic copy number losses by using samples from tumours and cells bearing different known somatic *NF1* deletions. As mentioned above, some constitutional deletions are found in mosaicism, and some tissues present a mixture of *NF1*+/– cells (i.e. those bearing an *NF1* microdeletion) and *NF1*+/+ cells (i.e. cells with no deletion). Analogously, dNFs and

other NF1-associated traits are composed of different types of cells, containing a mixture of *NF1*–/– cells (i.e. those bearing a somatic second-hit *NF1* deletion) and *NF1*+/– cells (i.e. cells with no deletion; Serra et al., 2000). Because in both cases the cellular component bearing an *NF1* deletion is not total, we first checked the reliability of the qPCR assay for detecting deletions in these contexts that comprise cells with different genotypes.

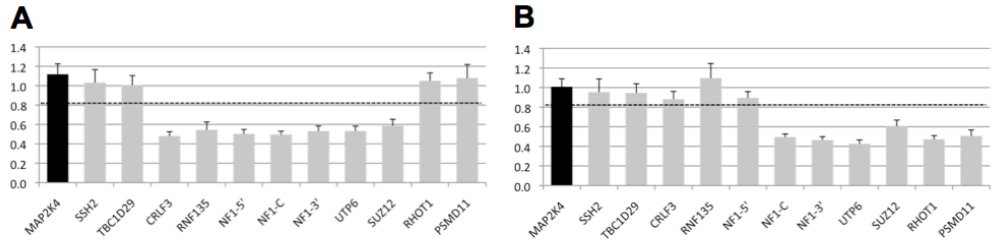

C

Sample	Deletion type	MAP2K4	SSH2	TBC1D29	R	S	CRLF3	RNF135	R	NF1-5'	NF1-C	NF1-3'	UTP6	S	SUZ12	R	RHOT1	PSMD11
NF-05	Type-1	1,12	1,03	1,01	E	U	0,48	0,54	E	0,50	0,49	0,53	0,53	U	0,59	E	1,05	1,08
NF-08	Type-1	1,16	1,08	0,95	P	Z	0,48	0,55	P	0,47	0,50	0,54	0,52	Z	0,54	P	0,96	1,10
NF-09	Type-1	1,03	0,97	1,12	-	1	0,55	0,62	-	0,51	0,48	0,54	0,56	1	0,52	-	1,02	1,17
NF-13	Type-1	0,95	1,02	0,95	A	2	0,33	0,36	B	0,47	0,47	0,51	0,45	2	0,55	C	0,98	1,08
NF-65	Type-1	1,08	1,13	0,94		P	0,58	0,46		0,57	0,60	0,57	0,59		0,48		1,12	1,11
NF-01	Type-2	1,01	0,98	1,15			0,69	0,77		0,65	0,63	0,68	0,66		0,99		0,97	1,13
NF-02	Type-2	1,12	0,98	1,14			0,54	0,60		0,54	0,53	0,42	0,56		0,96		1,05	0,95
NF-03	Type-2	1,10	0,97	0,89			0,52	0,59		0,50	0,56	0,57	0,56		0,95		0,99	1,12
NF-04	Type-2	0,98	1,23	1,11			0,46	0,44		0,49	0,54	0,52	0,45		1,08		1,05	1,10
NF-06	Type-2	1,15	0,97	1,05			0,58	0,53		0,54	0,54	0,59	0,54		1,00		1,02	1,04
NF-07	Type-2	1,01	0,99	1,04			0,51	0,59		0,51	0,48	0,55	0,53		0,98		1,00	1,05
NF-10	atypical	1,01	1,01	1,07			0,44	0,56		0,51	0,47	0,52	0,93		1,05		1,04	1,07
NF-11	atypical	0,96	1,00	0,96			0,91	1,10		1,02	0,45	0,49	0,91		1,07		0,93	1,03
NF-12	atypical	1,01	0,95	0,94			0,88	1,10		0,89	0,49	0,46	0,43		0,60		0,47	0,51

Figure 7. Characterization of *NF1* constitutional deletions by the *NF1*-qPCR assay. A, B. Relative copy number (RCN) values for the 11 loci located in the *NF1* region (grey columns) and the *MAP2K4* control locus (black bar) for a sample with a Type-1 microdeletion (A) and a sample with an atypical microdeletion (B). Dashed lines indicate the mean RCN cutoff for deletion detection. C. RCN values for the 11 loci located in the *NF1* region (from *SSH2* to *PSMD11*) and the control locus *MAP2K4*, in 14 blood samples previously diagnosed with a *NF1* constitutional deletion. Among them, 5 were classified as Type-1, 6 as Type-2 and 3 as atypical. RCN values in bold indicate a deletion. Light red-coloured rectangles show the extent of the deletion, previously identified by microsatellite analysis and FISH, and later confirmed by MLPA. A RCN similar to 0.5 indicates a deletion; a RCN around 1 indicates 2 copies of the locus.

To do so, we assessed the performance of the qPCR assay in admixtures of *NF1*-deleted and *NF1*-nondeleted DNA samples, and we set a cutoff value for the maximum percentage of *NF1*-nondeleted DNA present in a tumour (or tissue) that the qPCR assay could tolerate and still detect the presence of an *NF1* deletion. To choose this cutoff, we checked the performance of the qPCR assay with several admixtures of 2 DNA samples, one with 2 copies of *NF1* and the other with a single copy. We prepared 11 serial dilutions of NF-59 (*NF1* constitutional deletion) and NF-60 (sample with 2

copies of *NF1*) with different DNA percentages of the 2 samples in quintuplicate (i.e., 0% to 100% of the sample with 2 copies of *NF1*). For each admixture, the mean±SD of the calculated RCN for the six loci NF1-5', NF1-C, NF1-3', CRLF3, RNF135, and UTP6 were plotted against the percentage of DNA with 2 *NF1* copies present in the DNA admixture (**Figure A.3.A** in Annexe 1). To calculate the cutoff value for the percentage of cells with 2 copies of *NF1* that the qPCR assay could tolerate and still detect the presence of an *NF1* deletion, we used the mean of the lower 99% confidence limit for all loci (0.81; **Figure A.3.A** in Annexe 1). Hence, the qPCR assay detected *NF1* deletions in samples containing less than 56% of *NF1*-nondeleted DNA.

We also set a cutoff value for the MLPA technique by using the same serial DNA admixtures used for the qPCR. These samples were analyzed in duplicate, and for each admixture we plotted the mean±SD of the calculated copy number of 11 loci (from the *CRLF3* 3780 probe to the *SUZ12* 3786 probe) against the percentage of DNA with 2 copies of *NF1* present in the DNA admixture (**Figure A.3.B** in Annexe 1). We used a RCN value of 0.8 to obtain the cutoff value for the highest percentage of *NF1*-nondeleted DNA in samples at which the MLPA assay was able to detect the presence of an *NF1* deletion. This percentage was approximately 51%, similar to that of the qPCR assay.

To evaluate the ability of the qPCR assay to detect somatic deletions in dNFs and Schwann cells bearing an *NF1* somatic deletion ($SC^{NF1-/-}$ cells), we analyzed 16 DNA samples from dNFs and 5 $SC^{NF1-/-}$ samples known to bear an *NF1* somatic deletion. First, we used the microsatellite multiplex PCR analysis (MMPA) technique, previously developed in our laboratory (Garcia-Linares et al., 2012), to calculate the percentage of DNA with 2 copies of *NF1* within tumour samples (**Table A.2** in Annexe 1), as described in Garcia-Linares et al., 2012. The results with this technique also confirmed the presence of deletions in the *NF1* region in these samples (Garcia-Linares et al., 2012; see **Table A.2** in Annexe 1). The qPCR assay detected the presence of deletions in the *NF1* region in all dNF and $SC^{NF1-/-}$ samples tested that contained <56% of the *NF1*-nondeleted component (**Figure 8**). When all loci known to be deleted in this sample subset were considered, the qPCR assay showed 90.5% sensitivity and 98.9% specificity. The technique was still able to detect at least one deleted locus in the 4

tumour samples with >56% of *NF1*-nondeleted DNA, but the diagnostic sensitivity and specificity values were lower (**Figure 8**). The mean±SD RCN value within the deleted loci in $SC^{NF1-/-}$ samples was 0.62±0.11. This result pointed to the probable presence of *NF1*-nondeleted ($SC^{NF1+/-}$) cells within the SC cultures. All qPCR results for the detection of *NF1* somatic deletions in dNFs were also confirmed with the results obtained with the parallel MLPA analysis (see **Figure A.4** in Annexe 1).

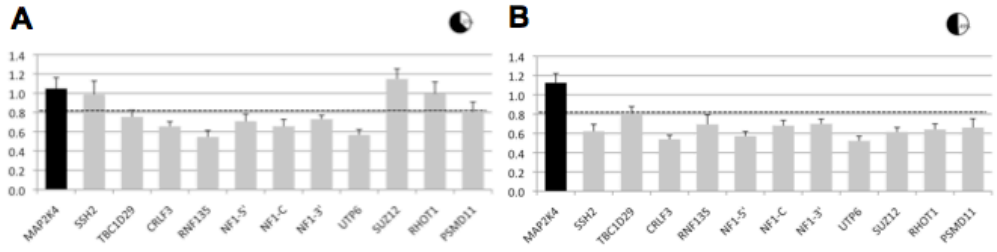

C

Sample	% normal cells	MAP2K4	SSH2	TBC1D29	R	CRLF3	RNF135	R	NF1-5'	NF1-C	NF1-3'	UTP6	R	SUZ12	R	RHOT1	PSMD11
NF-30	~0	1,04	0,75	0,89	E	0,56	0,58	E	0,51	0,62	0,55	0,65	U	0,58	E	0,58	0,65
NF-31	~0	1,11	1,04	1,12	P	0,94	0,69	P	0,59	0,64	0,62	1,02	Z	1,09	P	1,05	1,18
NF-32	~0	1,06	1,10	1,09	-	0,63	0,58	-	0,53	0,57	0,66	0,61	1	0,49	-	0,58	0,55
NF-33	~0	1,13	0,73	0,98	A	0,65	0,77	B	0,71	1,00	0,88	1,10	2	1,23	C	1,04	1,04
NF-36	~0	0,94	0,56	0,81	P	0,53	0,53		0,51	0,52	0,58	0,52		n/a		0,53	0,68
NF-19	24	1,08	1,03	1,05		0,61	0,72		0,65	0,62	0,65	0,67		0,63		1,00	1,14
NF-28	37	1,05	0,99	0,75		0,65	0,54		0,71	0,66	0,73	0,57		1,15		1,00	0,80
NF-15	42	1,12	0,65	0,88		0,61	0,73		0,60	0,66	0,71	0,64		0,85		0,90	1,02
NF-21	43	1,11	0,83	0,70		0,67	0,61		0,77	0,73	0,65	0,72		0,55		0,62	1,05
NF-18	44	1,16	0,67	0,74		0,63	0,79		0,64	0,70	0,74	0,73		0,74		0,75	0,87
NF-20	44	1,10	0,95	0,95		0,88	0,92		0,68	0,70	0,78	0,89		0,87		0,92	0,81
NF-24	44	1,15	1,08	1,00		0,97	0,81		0,69	0,67	0,72	1,03		1,02		1,00	1,16
NF-25	45	0,85	0,77	0,59		0,73	0,62		0,81	0,80	0,49	0,67		0,74		0,68	0,73
NF-63	47	1,02	0,93	0,88		0,73	0,74		0,77	0,70	0,77	0,74		1,05		0,99	0,96
NF-17	49	1,12	0,62	0,80		0,54	0,69		0,57	0,68	0,70	0,52		0,62		0,64	0,66
NF-27	52	1,10	0,82	0,78		0,77	0,88		0,79	0,71	0,83	0,72		0,90		0,75	0,87
NF-23	56	1,17	1,16	0,98		0,93	0,82		0,90	0,80	1,04	0,90		1,22		1,11	1,09
NF-16	61	0,99	0,74	0,94		0,66	0,80		0,68	0,84	0,73	0,80		0,69		0,70	0,77
NF-29	68	1,00	0,85	0,95		0,79	0,89		0,85	0,80	0,69	0,76		0,87		0,79	0,80
NF-26	71	1,04	0,87	0,72		0,85	0,95		0,93	0,86	1,04	0,84		1,15		0,90	1,02
NF-22	n/a	1,10	0,72	0,78		0,62	0,77		0,69	0,80	0,85	0,55		0,74		0,68	0,74

Figure 8. Characterization of *NF1* somatic deletions by the *NF1*-qPCR assay. A, B. RCN values are shown for the 12 interrogated loci in one sample with a somatic deletion and containing 37% of cells with 2 copies of *NF1* (A) and another sample with a somatic deletion and containing 49% of cells with 2 copies of *NF1* (B). Dashed line indicates the mean RCN cutoff for deletion detection. C. RCN values of the 11 loci located in *NF1* region and the control region located in 17p, in 16 dNFs samples and 5 SC samples previously diagnosed with a *NF1* somatic deletion. RCN values below the low value of the 99% CI of every interrogated region (deleted) are shown in bold. Light red-coloured rectangles show the extent of the deletion, previously identified by MLPA, Paralog Ratio Analysis (Garcia-Linares et al., 2011) and SNP array, and later confirmed by MMPA (Garcia-Linares et al., 2012) and MLPA. Grey rectangles show deleted loci not detected by the qPCR. A RCN similar to 0.5 indicates a deletion; a RCN around 1 indicates two copies of the locus.

So, this first probe-based developed qPCR assay, *NF1*-qPCR, has demonstrated to accurately detect different types of constitutional microdeletions in the *NF1* locus – including those occurring in mosaicism – and also *NF1* somatic second-hit deletions found in NF1 traits when the *NF1*-nondeleted component of the DNA sample analyzed is less than 56%.

1.2. Assessment of SCNAs in MPNSTs: MPNST-qPCR

As MPNSTs present hyperploid genomes with some recurrent SCNAs beyond deletions in the *NF1* gene, a second qPCR assay, similar to the one interrogating *NF1* region, was designed for the detection of copy number gains and losses in the MPNST genome.

1.2.1. LINE repetitive sequences improve the normalization of copy number data in MPNSTs

This assay was also set up with UPL probes and their corresponding specific primer pairs (**Table 5**). The qBase relative quantification framework was also used for the calculations of the RCN values (Hellemans et al., 2007).

As MPNSTs are tumours with highly altered genomes, we first studied different reference loci to identify the most suitable to be used for the normalization of target gene copy number data. Among them, we selected three single copy genes, *GLRX3* (located at 10q26.3), *ACSS1* (located at 20p11.21) and *ADARB1* (located at 21q22.3), as they were encompassed in genomic regions that seemed not to be frequently present in SCNAs from MPNSTs, according to the literature (see Introduction, section 6). Moreover, two LINE repetitive genomic sequences, the LINE1 consensus sequence, *L1*, and the *L1PA* family consensus sequence, were also chosen. These sequences are present in high number in the genome and it has been suggested that their copy number per haploid genome is similar among all human cells, either normal or tumoural, so they have been used in the qPCR technique for normalization purposes (Wang et al., 2002). We used a total of 35 samples in this MPNST-qPCR. The parameter *M* value was calculated considering all possible combinations among the five potential reference genes for all samples (Vandesompele et al., 2002). An average of the two repetitive elements, *L1* and *L1PA,* was found as the best combination (M=0.187) and was then chosen as the Normalization Factor (NF).

MPNST genomes, in addition to present several structural alterations, are also generally hyperploid. This general increased ploidy of MPNSTs should be considered

when normalizing copy number data. Although LINE repetitive sequences were found better than single copy genes for the normalization of copy number data in these hyperploid genomes, qPCR [and other methodologies such as SNP array or comparative genomic hybridisation (CGH)] calculate the copy number of a particular locus with respect to the general ploidy of the studied sample, being, therefore a relative and not an absolute quantification. This means that, for a particular amount of DNA from a hyperploid genome, some genomic gains could be underrepresented and some genomic losses could be overrepresented by these DNA-based techniques.

1.2.2. Detection of copy number gains in AURKA locus in MPNSTs as a proof of concept

After choosing the NF, we selected a specific locus for assessing its copy number status. An integrative cross-species (mice and human) transcriptome analysis identified *AURKA* as a highly overexpressed gene in primary MPNSTs and MPNST cell lines relative to neurofibromas and normal nerves (Patel et al., 2012). In this study, both *in vitro* and *in vivo* experiments evidenced that blocking AURKA may be a viable treatment for MPNSTs. In order to assess the mechanism underlying *AURKA* overexpression in MPNSTs, we determined the copy number status of the *AURKA* locus using this qPCR assay in our set of samples.

We first determined the range of RCN values for a 2-copy status of the *AURKA* gene in 10 control samples. The mean calculated 99% CI of the RCN indicating a diploid status for the *AURKA* locus was 0.76–1.32. A RCN value below the lower limit of the CI (0.76) was considered to indicate a deletion; a RCN value above the upper limit of the CI (1.32) was considered to indicate a genomic gain. Considering this, *AURKA* copy number status was assessed in neurofibromas, primary MPNSTs and MPNST cell lines samples. Among the primary MPNSTs, 7 of 12 (58%) showed three or more copies of *AURKA* locus (**Figure 9**). Most of the NF1-associated MPNSTs, 6 of 7 (86%) had *AURKA* locus amplified. Moreover, all 5 MPNST cell lines showed *AURKA* copy number gains (**Figure 9**). Only one of the neurofibroma samples showed a copy number gain, probably denoting a false positive (**Figure 9**). All 10 control samples showed a diploid status (**Figure 9**).

Moreover, to highlight the importance of selecting the most suitable NF for the normalization of copy number data in aberrant genomes (as the NF composed of the average of *L1* and *L1PA* in our set of samples), we also calculated the RCN of *AURKA* locus in these samples using single copy genes. When *L1* or *L1PA* were used as single normalizer genes, the obtained RCN results were similar to those obtained when using the NF. However, these RCN values considerably differed when *GLRX3*, *ACSS1* or *ADARB1* were used individually as normalizers (**Table A.3** in Annexe 1).

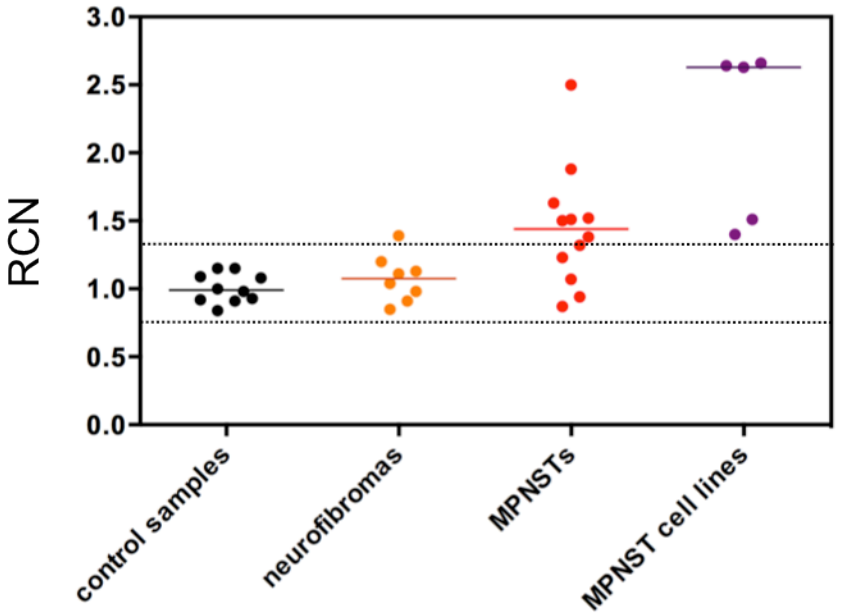

Figure 9. Copy number assessment of *AURKA* locus in MPNSTs by the MPNST-qPCR. Column scatter plot showing RCN values of *AURKA* locus in 10 control samples, 8 neurofibromas, 12 MPNSTs, and 5 MPNST cell lines. Both dashed lines show the high and the low values of the 99% CI, respectively, of RCN indicating a diploid status. Those RCN outside this 99% CI are considered to indicate a copy number change: either a genomic gain or a loss. Each line within the scatter plot indicates the median RCN value within the group.

So, this second probe-based qPCR, MPNST-qPCR has shown that using repetitive sequences improves the normalization of copy number data in altered genomes, as LINEs in MPNSTs. In addition, MPNST-qPCR has been able to detect somatic copy number gains of *AURKA* locus in MPNSTs.

2. Molecular characterization of MPNSTs and functional identification of novel genes involved in their pathogenesis

MPNSTs are rare tumours that account for 3-10% of all soft-tissue sarcomas (Katz et al., 2009). Probably due to their very low prevalence in the general population they still have not been included in scientific consortia for their genomic study unlike other tumour types. However, MPNSTs are very aggressive tumours with a poor prognosis (Brems et al., 2009) and represent the leading cause of NF1-related mortality (Evans et al., 2002).

Several studies have shown that MPNSTs present hyperploid genomes and also a recurrence of some somatic copy number gains and losses (see Introduction, section 6). The second part of this thesis was aimed to check how general this hyperploid landscape and the recurrent SCNAs were for the genome of NF1-associated MPNSTs. An analysis of MPNSTs at the genomic level was intented, with a particular focus on the genomic region, for a better understanding of MPNST pathogenesis. In addition, we also wanted to compare the genomes from MPNSTs and from benign plexiform neurofibromas (pNFs).

2.1. MPNSTs unlike pNFs are hyperploid tumours with recurrent SCNAs

A first molecular characterization of the genome of NF1-associated tumours and derived samples was conducted. SNP array analysis (for details see Materials and Methods, section 2.3) was performed to generate a global view of SCNAs in a set of samples including 8 pNFs, 8 NF1-associated MPNSTs, 7 MPNST-derived cell lines and 3 pNF-derived SC cultures (**Table 3**). SNP array data were first analyzed with different algorithms, including genoCN (Sun et al., 2009), GPHMM (Li et al., 2011) and ASCAT (Van Loo et al., 2012). We chose ASCAT for copy number data analysis because it considered both the ploidy and the fraction of non-aberrant cells present in the sample. By applying ASCAT, it was confirmed that pNFs do not present gross genomic alterations beyond deletions found in the *NF1* region in 2 of the 8 pNFs samples (**Figure 10.A**). A deletion in the *CDKN2A* locus was also detected in one pNF sample (**Figure 10.A**). All pNFs samples were also histologically studied in parallel and only the pNF sample bearing the *CDKN2A* deletion showed hypercellular regions and cellular atypia (data not shown). This pNF was histopathologically diagnosed as an

atypical neurofibroma. This finding strengthened that *CDKN2A* loss is an early event associated to atypical neurofibroma formation and considered a pre-malignant state, as it has been described (Beert et al., 2011).

MPNSTs showed, in contrast to pNFs, highly aberrant genomes with a general hyperploid landscape and some recurrent SCNAs (**Figure 10.B**). Mean ploidy value was calculated for each MPNST sample using ASCAT. The average (mean±SD) ploidy was 2.62±0.68 for the 8 primary MPNSTs, indicating that MPNSTs are globally nearly triploid, although this estimated ploidy could be underestimated due to tissue sampling. The most frequent genomic gains in our set of MPNSTs, present in at least 6 of 8 tumours (75%), were found in chromosomes 2, 7, 8, 15q and 17q22-25 (**Figure 10.B**).

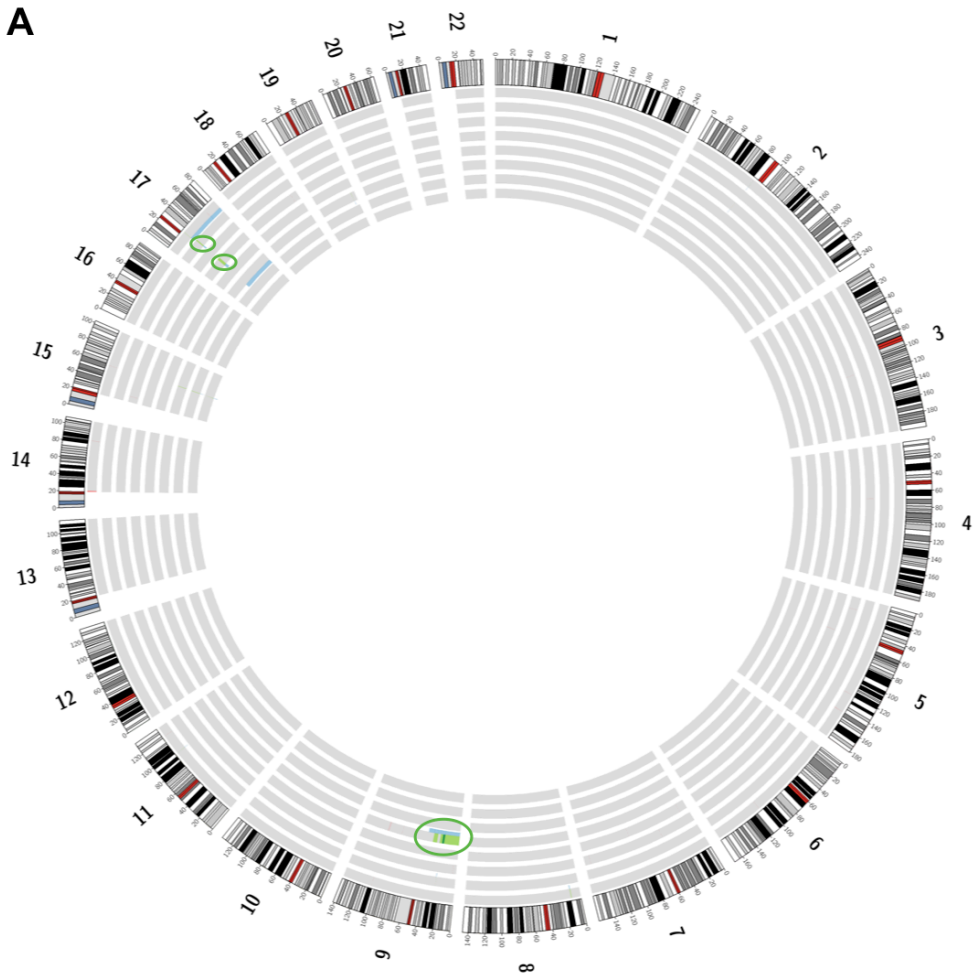

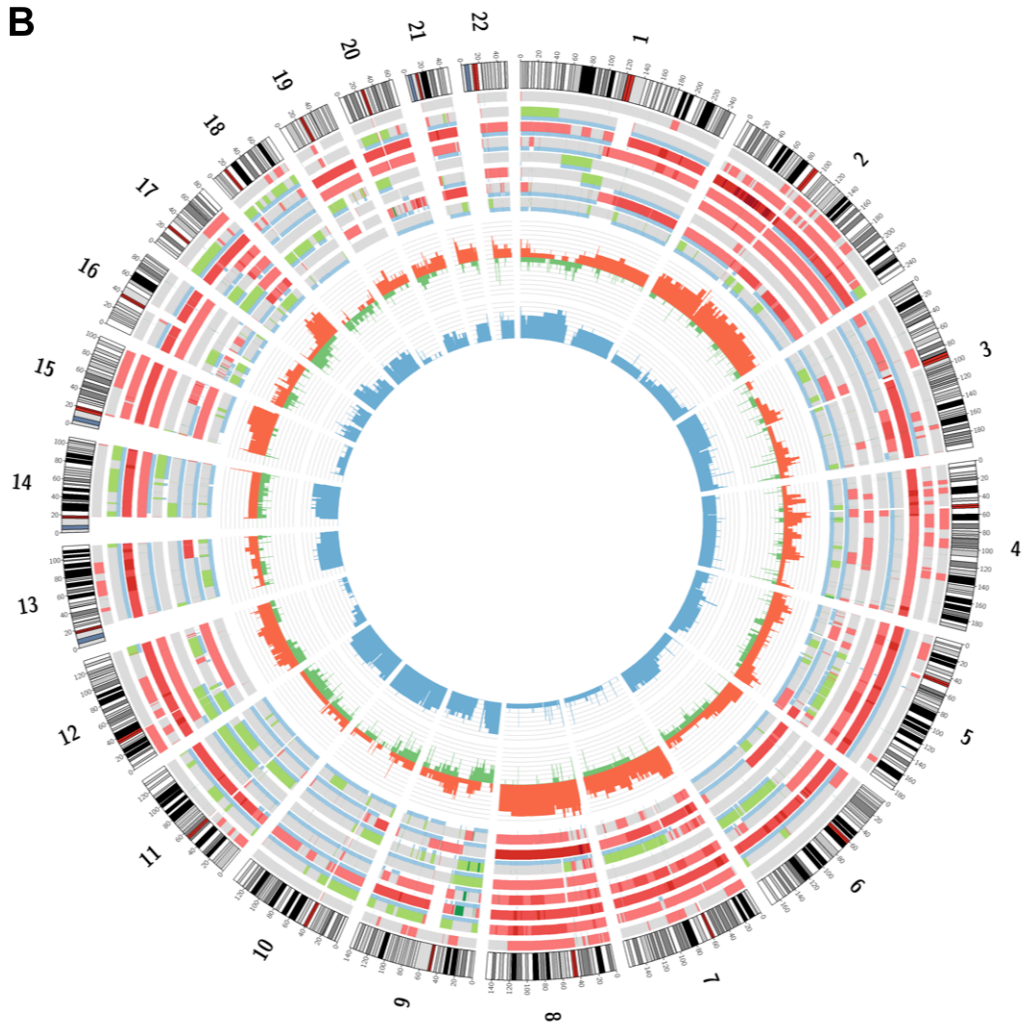

Figure 10. Circos representations showing SCNAs found in pNFs and MPNSTs. A. From outside to inside, idiograms of the 22 human autosomes with G-banding pattern are depicted. The 8 consecutive circles summarize the SCNAs obtained from SNP array data in the 8 pNFs analyzed. Only a few genomic losses, depicted in green and rounded by green circles, were found: two pNF samples showed deletions in the *NF1* locus at 17q11.2, and one pNF sample, in the *CDKN2A* locus at 9p21.3. Moreover, the loss of heterozygozity (LOH) of every sample is also depicted in blue. B. Again, from outside to inside, idiograms of the 22 human autosomes with G-banding pattern are depicted. The 8 consecutive circles summarize the SCNAs obtained from SNP array data in the 8 NF1-associated MPNSTs analyzed. Genomic gains are shown in red, and losses, in green. Colour intensity correlates with an increased copy number alteration. A global hyperploid genome was found for MPNSTs with some recurrent SCNAs. LOH of every MPNST samples is also depicted in blue. In the inner circles, the recurrence of the SCNAs (in red and green) and LOH (in blue) of all tumours is shown.

Some of the oncogenes associated to MPNSTs are located in these genomically gained regions, as *EGFR* at 7p11.2. The most frequent genomic losses, present in at least 3 of 8 tumours (37.5%), were found in 9p, 11q, 17p and 17q11.2-12 (**Figure 10.B**).

The main tumour suppressor genes (TSGs) associated to MPNSTs are located in these genomically lost regions, as is the case for *NF1* and *SUZ12* at 17q11.2, *CDKN2A* at 9p21.3 and *TP53* at 17p13.1.

MPNST cell lines also showed aberrant and highly hyperploid genomes. Mean ploidy value was also calculated for MPNST cell lines using ASCAT. The average (mean±SD) ploidy for the seven MPNST cell lines was 3.15±0.74, showing that MPNST cell lines are triploid or even nearly tetraploid, which have been confirmed by cytogenetics for S462, T265 and STS26T cell lines (see **Figure 4**). The most frequent gains in our set of MPNST cell lines, present in 6 of 7 lines (86%), were found in chromosomes 1q21, 2q32-37, 3q26.3, 4p12-13, 5q32-25, 7, 8q, 15q11-12, 17q, 19q and 20q (**Figure A.5** in Annexe 1). The most frequent losses, present in at least 3 of 7 tumours (43%), were found in 8p23.3, 9p21.3, 12p13 and 12q21 (**Figure A.5** in Annexe 1). Some of these genomically altered regions, such as 2q, 7, 8q, 9p, 15q and 17q were concurrently detected in primary MPNSTs.

Regarding SC samples, they did not show genomic alterations further than deletions found in the *NF1* region, as our group demonstrated for dNF-derived SC cultures (Garcia-Linares et al., 2011). In the set of 3 pNF-derived SC cultures, 2 of them presented loss of the *NF1* region, confirming the same genomic deletions found in the pNFs from which these SC cultures were derived.

Taken together these results show that the malignant progression of pNF to MPNST is generally associated to an increase in ploidy and the occurrence of gross genomic alterations.

2.2. Differentially expressed genes in MPNSTs vs. neurofibromas cluster in specific genomic regions: transcriptional imbalances, TIs

To study what was the impact on the transcriptome of these regional SCNAs found in the MPNST genome, microarray expression data from an independent set of samples, including 6 NF1-associated MPNSTs, 13 pNFs and 13 dNFs, was used. These data were previously generated by the NF1 Microarray Consortium (Miller et al., 2009), a

collaborative project of several research groups in NF1, where we also participated. We related the gene expression information with the location of the genes within the genome. In this way, mapping on the genome the differential gene expression between malignant and benign tumours, we identified the formation of transcriptional imbalances (TIs), regions of the genome where the mean differential expression was significatively higher (TIs of overexpression) or lower (TIs of underexpression) than expected by chance, presenting a significant abundance of over- or underexpressed genes. To do that, we used position related data analysis (PREDA; Ferrari et al., 2011), which uses an analysis based on a non-linear smoothing of the expression levels along chromosomal positions, followed by a permutation test to assess the significance of observed peaks in smoothed data. PREDA is a statistical test and as such the exact position and extent of a particular TI depends on the specific level of significance selected (**Figure A.6** in Annexe 1). When we set this level at P<0.05, we identified 36 TIs of overexpression and 28 TIs of underexpression in the MPNST genome (**Figure 11**).

Expression data from primary cell cultures and cell lines were also obtained from the NF1 Microarray Consortium (Miller et al., 2009), including 8 NF1-associated MPNST cell lines and 17 SC cultures derived from pNFs (N=6) and dNFs (N=11). When the differential expression mapped on the genome was between NF1-associated MPNST cell lines and SC cultures, TIs were also formed. In MPNST cell lines, when significance was also set at P<0.05, there were 35 TIs of overexpression and 31 TIs of underexpression (**Figures A.5** and **A.7** in Annexe 1). There was a significant overlap between the TIs identified in primary MPNSTs and those identified in cell lines (P<0.001 for TIs of overexpression and P<0.003 for TIs of underexpression). In particular, 25.4% of TIs of overexpression in primary MPNSTs were overlapping with TIs of overexpression in MPNST cell lines. This overlap was of 20.6% for TIs of underexpression (**Figure A.7** in Annexe 1).

2.2.1. TIs are significatively associated with SCNAs

To assess whether TIs found in MPNSTs were associated to SCNAs we first used the MPNST-qPCR assay to check the copy number status of a selection of genomic loci

present in TIs. In particular, we selected 4 genes present in TIs of overexpression and 4 other genes present in TIs of underexpression (**Figure 12**). In this study, we also used for the normalization of copy number data the NF considering the two repetitive elements, *L1* and *L1PA*, as in the case of *AURKA* copy number assessment.

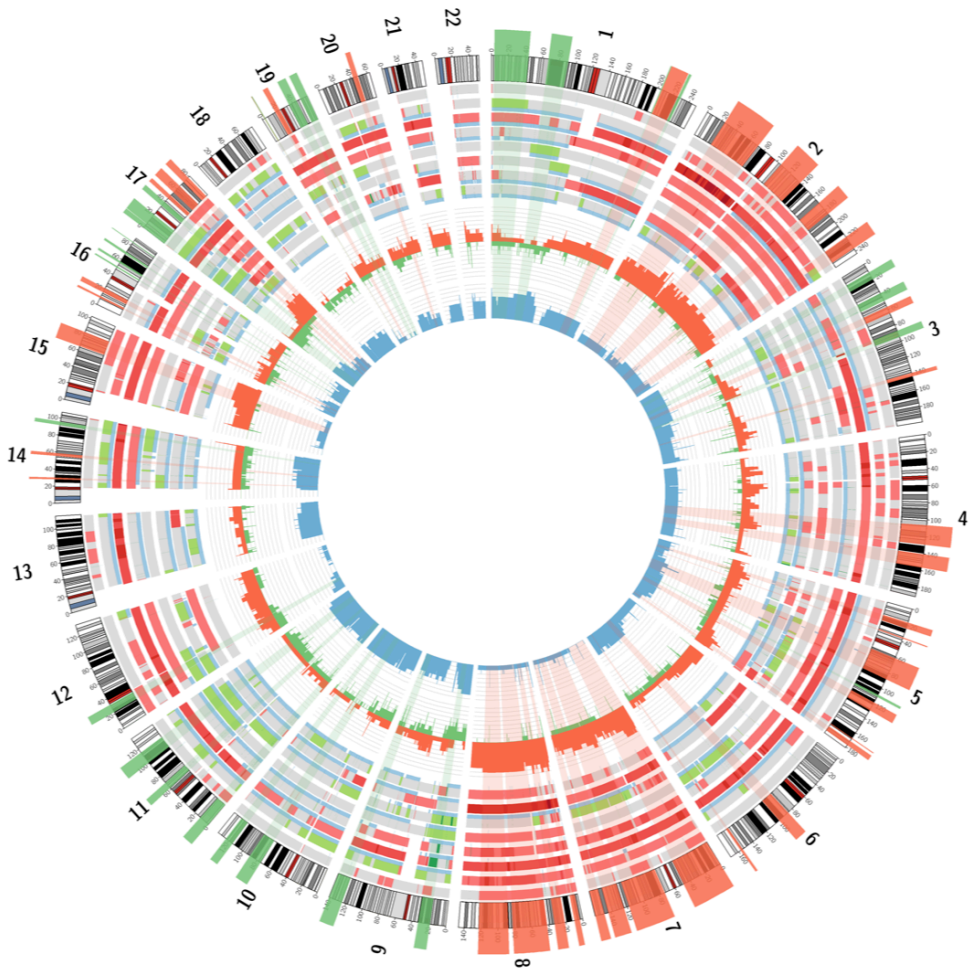

Figure 11. Circos representation showing TIs and SCNAs found in MPNSTs. From outside to inside, idiograms of the 22 human autosomes with G-banding pattern are depicted. Over these idiograms red and green boxes show TIs of overexpression and underexpression, respectively, obtained from microarray expression data. Next, the 8 consecutive circles summarize the SCNAs and LOH obtained from SNP array data in the NF1-associated MPNSTs analyzed, as in Figure 10.B. In the inner circles, the recurrence of the SCNAs (in red and green) and LOH (in blue) of all tumours is shown.

We also first determined the LDR and the E value of the primer pairs (Hellemans et al., 2007) and the range of RCN values for a 2-copy status of each of the 8 genes using the 10 control samples (see **Table 5**). The mean calculated 99% CI of RCN for these 8

loci was 0.75–1.33. As in the case of *AURKA*, a RCN value below the lower limit of the CI for a locus was considered to indicate deletion of that particular locus; and a RCN value above the upper limit of the CI for a locus was considered to indicate a gain of that particular locus.

After copy number data analysis, among the 12 primary MPNSTs and considering the 4 interrogated genes present in TIs of overexpresion (48 loci in total), 13 of 48 (27%) were genomically amplified (**Figure 12**). In the case of the 5 MPNST cell lines (20 loci in total), 7 of 20 (35%) loci were genomically gained (**Figure 12**). Among the 12 primary MPNSTs and considering the 4 interrogated genes present in TIs of underexpression (48 loci in total), 28 of 48 (58%) were genomically deleted (**Figure 12**). In the case of the 5 MPNST cell lines (20 loci in total), 5 of 20 (25%) loci were genomically lost (**Figure 12**). Almost all (98%) of the 8 interrogated genes in the 8 neurofibroma samples (64 loci in total) did not show any copy number alteration and only 1 of 64 loci showed a genomic gain (**Figure 12**). All loci in the 10 control samples (80 loci in total) showed a diploid status.

Fisher's exact test was applied to assess the association between the TIs of overexpression and the genomic gains, which was significant for both MPNSTs ($P<0.0001$) and MPNST cell lines ($P=0.008$). The association between the TIs of underexpression and the genomic losses was also significant for both MPNSTs ($P<0.0001$) and MPNST cell lines ($P=0.047$).

In order to evaluate those tumours arising in NF1 patients, we specifically assessed the association between TIs and the genomic alterations detected with the MPNST-qPCR in the subset of NF1-associated MPNSTs. Among the 7 NF1-associated MPNSTs and considering the 4 interrogated genes present in TIs of overexpression (28 loci in total), 9 of 28 (32%) were genomically gained (**Figure 12**). Considering the 4 interrogated genes present in TIs of underexpression (28 loci in total), 17 of 28 (61%) were genomically lost (**Figure 12**). In the NF1-associated MPNST sample subset, the association between TIs of overexpression and genomic gains, and the association between TIs of underexpression with genomic losses were both significant (Fisher's exact tests; $P=0.0018$ and $P<0.0001$, respectively).

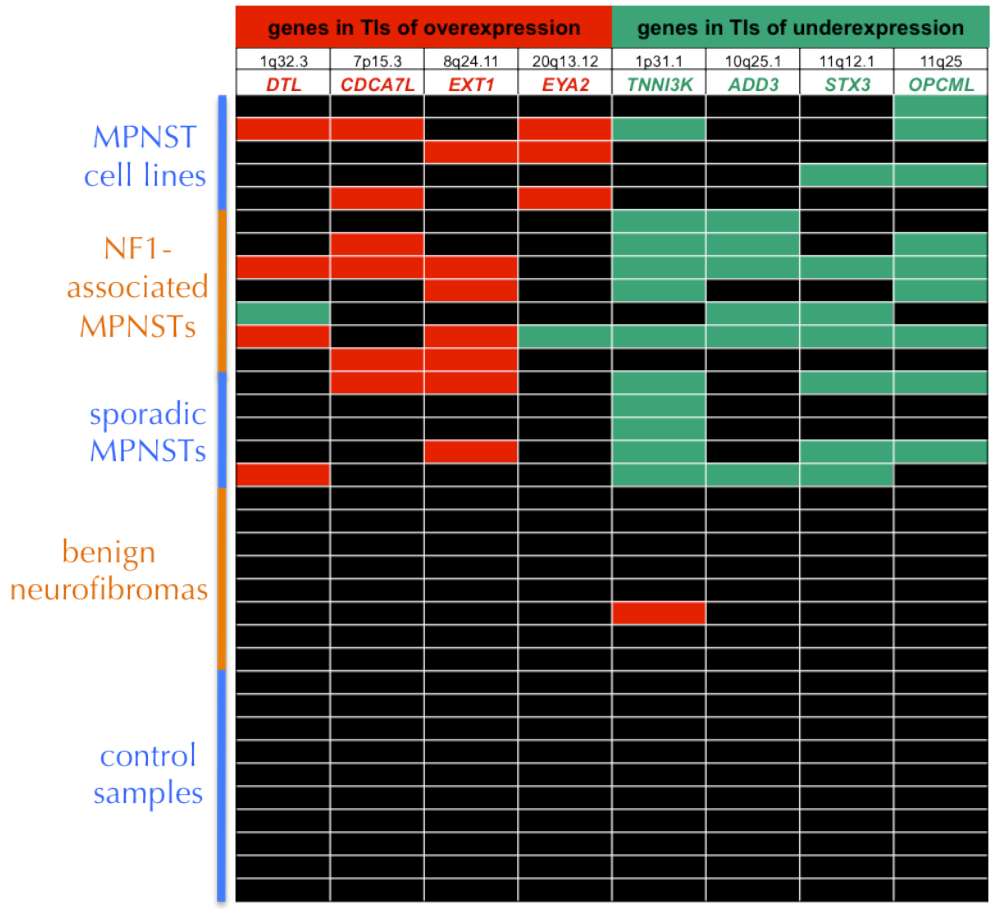

Figure 12. Association of TIs with SCNAs in MPNSTs using MPNST-qPCR results. Copy number status of the 4 loci located in TIs of overexpression (*DTL*, *CDCA7L*, *EXT1* and *EYA2*) and the 4 loci located in TIs of underexpression (*TNNI3K*, *ADD3*, *STX3* and *OPCML*) in 5 MPNST cell lines, 12 MPNSTs (7 NF1-associated and 5 sporadic), 8 neurofibromas and 10 control samples. Red boxes indicate genomic gains (i.e. those RCN values above the high value of the 99% CI of every interrogated locus) and green boxes indicate genomic losses (i.e. those RCN values below the low value of the 99% CI of every interrogated locus). Black boxes indicate two copies of the locus.

Furthermore, as the copy number of these samples was also calculated using SNP array data by applying ASCAT, we wanted to compare the copy number values obtained with the two methodologies, MPNST-qPCR assay and SNP array-ASCAT, for the 8 interrogated loci. All of the genomic gains detected by the qPCR assay were also detected as so by the SNP array (**Table 7**). However, most of the genomic losses detected by the qPCR assay were found to present 2 copies of the locus in the case of the SNP array (**Table 7**).

This discrepancy could be explained by the different way qPCR and ASCAT deal with copy number data in hyperploid genomes. While MPNST-qPCR normalizes copy number with respect to the ploidy of the sample, ASCAT algorithm estimates ploidy and considers the fraction of non-aberrant cells during normalization. Hence, although not completely accurate, ASCAT is more reliable in assessing copy number of tumours with hyperploid genomes. As suggested in section 1.2.1., these results indicate that the MPNST-qPCR assay generates some false positives of deletion events, being the number of deleted loci over-represented, and some false negatives of genomic gains, being the number of gained loci under-represented.

Sample	DTL	CDCA7L	EXT1	EYA	TNNI3K	ADD3	STX3	OPCML	PLOIDY
MPNST-1	2	**3**	**3**	2	2	2	2	2	2.4
MPNST_A	**4**	**4**	**4**	**4**	2	**4**	**4**	**4**	3.9
MPNST_B	**3**	**4**	**4**	**3**	2	2	2	2	3.0
MPNST_C	2	2	**3**	2	**1**	2	**1**	**1**	2.0
MPNST_D	2	2	2	2	2	2	2	2	2.1
MPNST_G	**4**	**4**	**5**	**3.5**	2	2	2	2	3.3
MPNST_K	2	**3**	**3**	2	2	**1**	2	2	2.2
S462	**6**	**5**	**6**	**6**	**6**	**5**	**5**	**5**	4.6
T265	**4**	**4**	**4**	**4**	2	2	**3**	2	3.1
ST-8814	**4**	**4**	**5**	**5**	**4**	**4**	**4**	**3**	4.4
S462-TY	**3**	**3**	**4**	**4**	2	2	**3**	**3**	3.2

Table 7. Comparison of copy number results from MPNST-qPCR and from SNP array. Comparison of the copy number status of 8 genomic loci present in TIs obtained by the MPNST-qPCR assay and obtained by SNP array. Red and green boxes indicate those loci detected as gained and lost, respectively, by the MPNST-qPCR assay. Numbers indicate the copy number status obtained by the analysis of SNP array data with ASCAT (genomic gains are shown in bold red; losses are shown in bold green). Moreover, the mean ploidy of every sample calculated by ASCAT is also indicated in blue.

After the analysis of the results from the MPNST-qPCR assay, we wondered if the association found with the qPCR between the 8 TIs and the 8 SCNAs was a generalized phenomenon for the MPNST genome. Then, the whole set of TIs was considered and their association with SCNAs was studied. To statistically assess the global association between TIs and SCNAs we used regioneR, an R package for the comparison of genomic regions that was being developed in parallel by our research group in collaboration with other groups from our institute (Gel et al., 2015). regioneR provided a permutation test-based framework to statistically assess the association between a set of regions and any other genomic features or annotations. In our case we tested whether TIs were associated to an increased number of SCNAs. The results of performing a permutation test with regioneR were two values: the P-value, which

indicated if the association was significant, and the z-score, which showed the strength of this association.

According to regioneR results, TIs of overexpression found in MPNSTs were significatively and strongly associated with genomic gains (P=0.0001; z-score: 4.568) (**Figure 13.A**). TIs of underexpression found in MPNSTs were also significatively associated with genomic losses (P=0.0181; z-score: 2.399) (**Figure 13.B**), but with a less extent compared to the association of TIs of overexpression with genomic gains. We hypothesized that probably this weaker association found for TIs of underexpression with genomic losses was because this association was in fact restricted to a subgroup of TIs and/or that TIs of underexpression were actually also associated with regions without copy number alterations (i.e. with a diploid status). To check this last hypothesis, regioneR was also used to assess the association of TIs of underexpression found in MPNSTs with non-gained regions (either with a diploid status or deleted). In this case, this association was found to be highly significant (P=0.0007; z-score: 2.938) (**Figure 13.C**).

In the case of MPNST cell lines, the association was also significant for their TIs of overexpression with genomic gains (P=0.0001; z-score: 4.929; **Figure A.8.A** in Annexe 1) and also for the TIs of underexpression with non-gained regions (P=0.0014; z-score: 2.797; **Figure A.8.B** in Annexe 1). TIs of underexpression were not found to be associated with genomic losses in MPNST cell lines (P=0.1682).

Taken together, both MPNST-qPCR and regioneR results showed that gene expression from MPNSTs is influenced by the genomic copy number in a regional manner. TIs of overexpression found in MPNSTs were significatively and strongly associated with genomic gains, which suggests an impact of these regional alterations on the overexpressed levels of their encompassed genes. TIs of underexpression were also significatively and strongly associated with non-gained genomic regions, suggesting that some regions are not genomically gained even in the hyperploid context of these tumours, and that may also have an influence on the expression levels of the genes included in these regions.

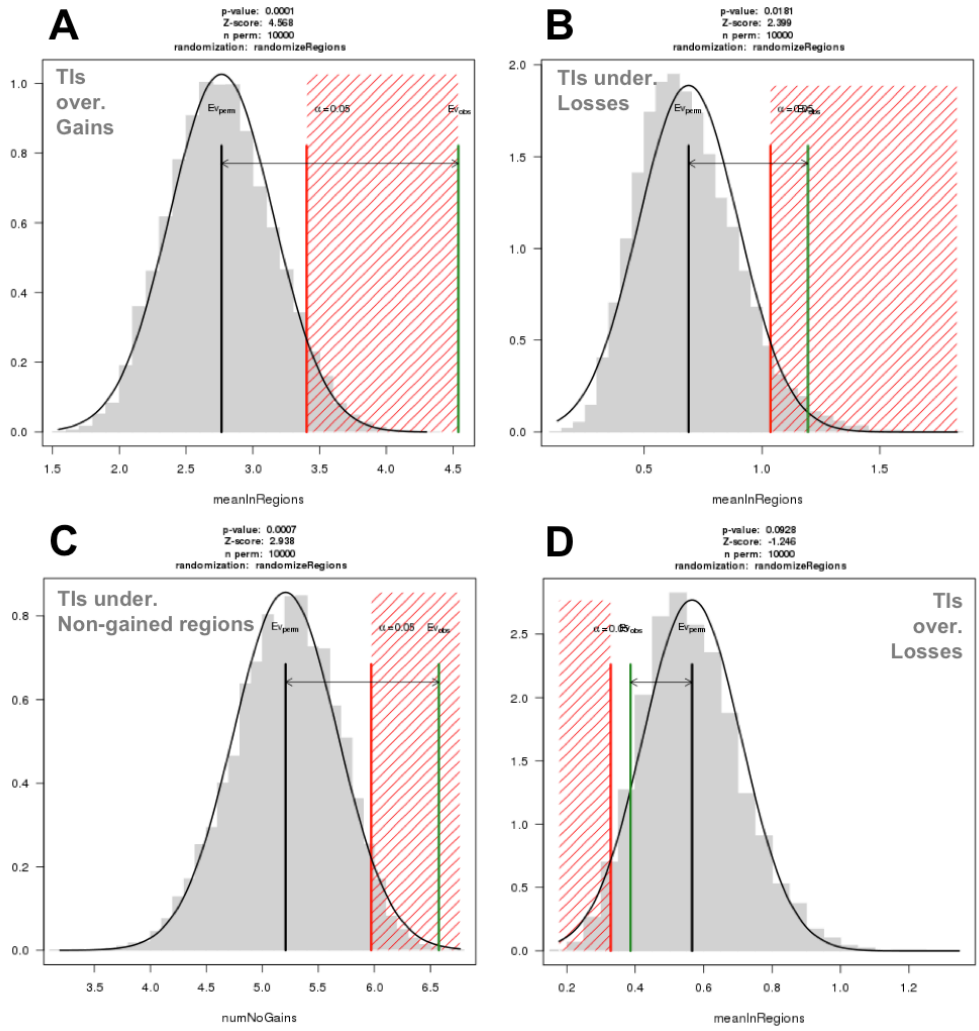

Figure 13. Global association of TIs with SCNAs in MPNSTs by regioneR. regioneR plots showing the results of permutation tests. The x-axis corresponds to the result of the evaluation function; in this case, the number of overlaps between the two sets of regions (TIs and SCNAs). The green line represents the evaluation of the original set of regions, in this case the TIs, and the grey bars and the black line represent the distribution and mean of the randomized evaluation, with the significance limit of 0.05 depicted in red. A. TIs of overexpression were significatively associated with genomic gains. B. TIs of underexpression were significatively associated with genomic losses. C. TIs of underexpression were significatively associated with non-gained genomic regions (either with a diploid status or deleted). D. TIs of overexpression were not significatively associated with genomic losses. P-values and z-scores of every association are shown.

2.2.2. TIs of underexpression are significatively enriched in hypermethylated genes

Some regional epigenomic mechanisms, such as long-range epigenetic silencing (LRES), have been described so far in several cancers. These are characterized by changes in the expression of genes placed contiguous in specific gross genomic locations by modifications in DNA methylation and chromatin remodelling. As TIs of underexpression were strongly associated with non-gained genomic regions, we wondered whether any silencing regional epigenomic mechanisms, either similar to LRES or not, were also possibly contributing to the generation of TIs of underexpression.

To obtain some evidences, we first performed a methylation array (for details see Materials and Methods, section 2.4) in 4 NF1-associated MPNSTs and 3 pNFs and analyzed the gene methylation status. The differential methylation status of genes in MPNSTs vs. pNFs was calculated (**Figure 14**). We defined a promoter as significantly hyper- or hypomethylated if it contained at least two probes with a differential methylation level and at least 80% of the differentially methylated probes within this promoter were in the same direction (either hyper- or hypomethylated). If a gene had at least one differentially methylated promoter and all its differentially methylated promoters – in the case of having multiple promoters – were concordant (all hyper- or all hypomethylated) the gene was classified as hyper- or hypomethylated.

After calculating the gene differential methylation status, we applied regioneR to check if there was an enrichment of these genes in TIs. TIs of underexpression were significatively enriched in hypermethylated genes in MPNSTs (P=0.0001; z-score: 7.478; **Figure 15.A**). Then, we wondered if this association was even stronger for those TIs of underexpression that were not coincident with genomic losses. Hence, TIs of underexpression were divided into two groups: TIs associated with genomic losses (defined as those overlapping with more genomic losses than gains: see for instance TIs in 9p and 17p in **Figure 11**) and TIs not associated with genomic losses (all TIs of underexpression not in the previous group: see for instance the larger TI in 1p and the two TIs in 19q in **Figure 11**).

Figure 14. Karyoplot showing TIs and distribution of differentially methylated genes in MPNSTs. A karyogram showing the idiograms of the 22 human autosomes with G-banding pattern is depicted. Red and green boxes represent, respectively, the TIs of overexpression and the TIs of underexpression identified in MPNSTs. A sliding window approach with a fixed window width was used to create a smoothed version of the methylation data. The orange line represents the number of hypermethylated genes divided by the total number of genes in a 3Mb window, being this window moved with a 1Mb step. The purple line represents the number of hypomethylated genes. The space between the two lines and colour-filled shows the proportion of differentially methylated genes in MPNSTs compared to pNFs: an orange area indicates a higher proportion of hypermethylated genes; a purple area indicates a higher proportion of hypomethylated genes. Finally, the grey bars below the karyogram represent the gene density using the same sliding window approach.

Both groups of TIs of underexpression were found significatively enriched in hypermethylated genes in MPNSTs (P<0.0001). However, this association was found to be stronger for those TIs not overlapping with genomic losses (z-score=6.337; **Figure 15.B**) than for TIs overlapping with deletions (z-score=3.571; **Figure 15.C**).

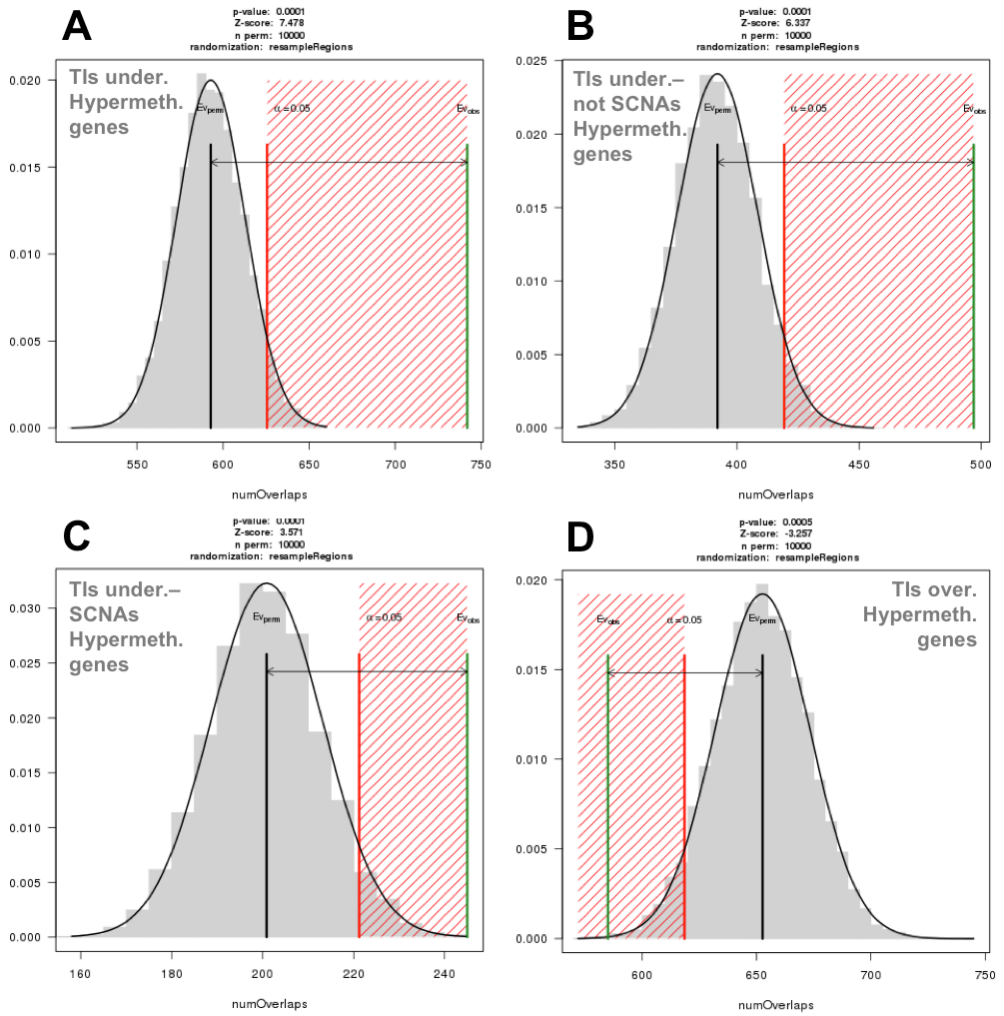

Figure 15. Global association of TIs with hypermethylated genes in MPNSTs by regioneR. regioneR plots showing the results of permutation tests. The x-axis corresponds to the result of the evaluation function; in this case, the number of overlaps between the two sets of genomic features (TIs and hypermetylated genes). The green line represents the evaluation of the original set of regions, in this case the hypermethylated genes, and the grey bars and the black line represent the distribution and mean of the randomized evaluation, with the significance limit of 0.05 depicted in red. In this case the randomization strategy was a random label shuffling. A. TIs of underexpression were significatively enriched in hypermethylated genes. B. TIs of underexpression not associated with genomic losses were significatively enriched with hypermethylated genes. C. TIs of underexpression associated with genomic losses were also enriched with hypermethylated genes, but in a weaker form than in B. D. TIs of overexpression were significatively depleted in hypermethylated genes.

Moreover, TIs of overexpression were significatively depleted in hypermetylated genes in MPNSTs (P=0.0005; z-score= –3.257; **Figure 15.D**). These TIs of overexpression were enriched, on the contrary, in hypomethylated genes (P=0.0195; z-score: 2.073; data not shown).

The differential methylation status of genes in 4 MPNST cell lines vs. 3 SC cultures was also calculated and we used the same criteria for defining a differential methylated gene than in tumours. No significant enrichment of hypermethylated genes in TIs was found with regioneR in MPNST cell lines (P=0.4087; **Figure A.8.C** in Annexe 1). Only TIs of overexpression were significatively enriched in hypomethylated genes (P=0.0024; z-score= 2.947; **Figure A.8.D** in Annexe 1).

In sum, when considering the results regarding the gene methylation status in MPNSTs, regioneR showed that TIs of underexpression found in MPNSTs are enriched in hypermethylated genes. This suggests that the global underexpression of the genes included in these TIs in MPNSTs may be influenced by, in addition to non-gained genomic regions, their hypermethylated status.

2.3. Understanding TIs: functional dissection of a specific TI

Our molecular characterization corroborated that MPNSTs contained highly altered and hyperploid genomes with recurrent SCNAs, a distinctive hallmark that differentiated MPNSTs from pNFs. At the same time, the differential expression analysis between MPNSTs and benign neurofibromas revealed the formation of TIs, regions of the genome presenting a significant abundance of over- or underexpressed genes. These TIs were strongly associated with SCNAs, especially in the case of TIs of overexpression with copy number gains. TIs of underexpression, moreover, were significatively enriched in hypermethylated genes. All this molecular characterization of MPNSTs at genomic, epigenomic and transcriptomic levels was intended for a better understanding of MPNST pathogenesis. So, we first wondered what kind of information TIs were capturing and, secondly, if TIs could help in identifying genes and molecular mechanisms involved in MPNST pathogenesis.

The recurrent SCNAs found in MPNSTs are genomic regions with a transcriptional impact in a regional manner. Hence, TIs are generated. We hypothesized that the generation of a TI is a result of a selection of a genomic (or an epigenomic) alteration because both the SCNA and the resulting TI contain at least one gene with a functional

role in tumour pathogenesis, and therefore conferring and advantage for the tumour. So, we first wondered what was the contribution to tumourigenesis of the genes located in a specific TI.

To start understanding TIs and the contribution to MPNST pathogenesis of the genes they contain, we selected as a first step a TI encompassing a gene already functionally implicated in MPNST tumourigenesis (what we call a putative driver of MPNST pathogenesis) and analyzed the function of other genes present in the same TI that were similarly expressed. We selected *BIRC5*, which is an overexpressed gene present in a TI of overexpresion in MPNSTs (**Figure 16**). *BIRC5*, also known as survivin, is an antiapoptotic and mitotic promoter gene that has been already associated to MPNST pathogenesis (Ghadimi et al., 2012b). In addition to *BIRC5*, five other overexpressed genes in MPNSTs vs. neurofibromas and present in this TI were selected for their functional study. These genes included *NUP85, TK1*, *CBX2, CBX4* and *CBX8* (**Figure 16** and **Table 8**). The three *CBX* genes are located in cluster in the genome and are components of the Polycomb Repressor Complex 1 (PRC1).

In our experimental model we studied how the loss of function of the selected overexpressed genes affected the *in vitro* tumourigenic properties of the two MPNST cell lines S462 and T265. In order to do so, a siRNA approach was designed for the expression knockdown of these genes and we set up a series of *in vitro* functional genetic approaches assessing different physiological readouts, such as cell viability, cell proliferation and cell cycle analysis, cell death and anchorage-independent growth (for details see Materials and Methods, sections 3 and 4).

We used S462 and T265 cell lines as two representative models for MPNST pathogenesis. Although both cell lines are malignant, some of their tumourigenic properties differ both *in vitro* and *in vivo,* presenting in general S462 a more aggressive phenotype than T265 cell line. The S462 cell line is nearly tetraploid (**Figure 4**), it grows fast *in vitro* with a doubling time of approximately 24 hours (data not shown), and it can also generate colonies in a soft-agar assay (see below). *In vivo*, S462 is able to engraft either subcutaneously (Demestre et al., 2013) and orthotopically (Castellsague et al., 2015) in mice, generating a MPNST histologically indistinguishable from a human

primary MPNST. The T265 cell line is nearly triploid (**Figure 4**), it grows slower than S462 with a doubling time of approximately 36 hours (data not shown) and it is not able to generate colonies *in vitro* (data not shown). Moreover, T265 cell line cannot generate MPNSTs *in vivo* in mice xenograft models.

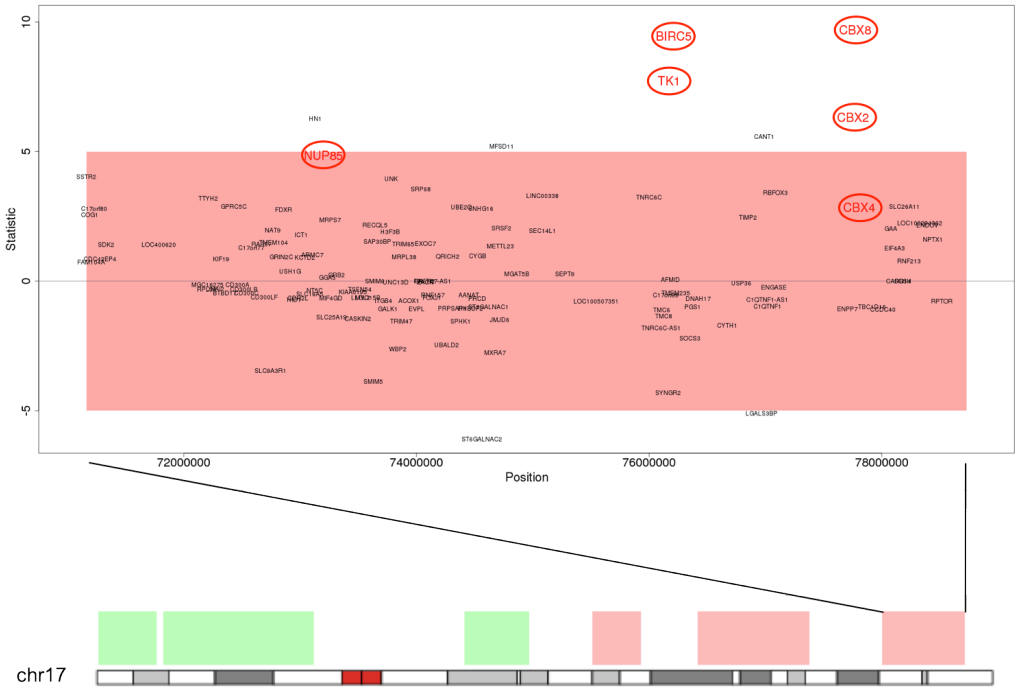

Figure 16. TI of overexpression selected for its functional dissection. Bottom part: idiogram of chromosome 17 containing 3 TIs of underexpression (green boxes) and 3 TIs of overexpression (red boxes). The more distal TI of overexpression was selected for its functional dissection. Upper part: diagram showing the TI selected for its functional dissection at 17q25.3 and the encompassed genes. Gene names are placed according to their level of significant differential expression in MPNSTs vs. neurofibromas. Selected genes for the expression knockdown and functional assays are depicted in red and rounded by red circles.

As a first step and once siRNA transfection experiments were set up, the expression knockdown of all six genes was checked by RT-qPCR after siRNA transfection in both S462 and T265 (**Figure 17.A**). The reduction of the expression by the siRNA pools was relevant for nearly all genes in both S462 and T265 cell lines, except for *CBX2*. We established criteria for the expression knockdown to select those genes to be included in the further functional genetic approaches: when the expression depletion of a siRNA pool targeting a particular gene in at least one of the two cell lines was not significant and the mean expression knockdown of this gene considering both S462 and T265 was below 50% of reduction, this particular gene was excluded from the study. That

was the case for *CBX2*, which was therefore eliminated from further analysis (**Figure 17.A**). The mean±SD expression reduction for all remaining genes, *NUP85, TK1*, *CBX4*, *CBX8* and *BIRC5*, considering the two cell lines was of 78±14% (**Figure 17.A**).

Gene	Chromo-somal location	P-value differential expression In tumours	Log2 fold change expression in tumours	Association to TI	P-value differential expression in cells	Log2 fold change expression in cells	% MPNSTs with gains / losses
NUP85	17q25.3	6.7×10^{-4}	0.95	In TI of over-expression	0.006	1.09	75 / 0
TK1	17q25.3	1.1×10^{-6}	1.52	In TI of over-expression	0.007	1.54	75 / 0
CBX2	17q25.3	2.4×10^{-5}	0.30	In TI of over-expression	0.050	0.16	75 / 0
CBX4	17q25.3	0.046	0.52	In TI of over-expression	7.83×10^{-5}	0.40	75 / 0
CBX8	17q25.3	2.0×10^{-8}	0.93	In TI of over-expression	0.005	0.02	75 / 0
BIRC5	17q25.3	3.0×10^{-8}	4.61	In TI of over-expression	0.072	1.93	75 / 0

Table 8. Genes selected for the functional dissection of a specific TI. Information on their chromosomal location, the significance (P-value) and the fold change in the differential expression in tumours (MPNSTs vs. neurofibromas) and in cells (MPNST cell lines vs. SCs), and the proportion of MPNSTs from our set showing a SCNA in their genomic location.

After analysis of all readouts from the functional genetic assays in the two cell lines analyzed, *BIRC5* expression knockdown consistently and significatively affected the *in vitro* studied tumourigenic features of both S642 and T265. When *BIRC5* expression was depleted in S462, there were strong and significant effects in all readouts: viability (96% reduction; **Figure 17.B**), proliferation (49% reduction; **Figure 18.A**), cell cycle arrest in G2-M phase (3.8-fold increase in the percentage of G2-M cells; **Figure 18.B**), apoptosis (5.8-fold increase; **Figure 19.A**), total cell death (5.2-fold increase; **Figure 19.B**), and anchorage-independent growth (96% and 99% reduction in colony number and area, respectively, **Figure 20**).

In the case of T265 cell line, there were also significant differences in all readouts analyzed: viability (36% reduction; **Figure 17.B**), proliferation (61% reduction; **Figure 18.A**), cell cycle arrest in G2-M phase (5.3-fold increase in the percentage of G2-M cells; **Figure 18.B**), apoptosis (1.9-fold increase; **Figure 19.A**), and total cell death (1.6-fold increase; **Figure 19.B**). These results confirmed the antiapoptotic effect of *BIRC5* and their requirement for the cell survival and cell cycle progression in MPNST cell lines, which have been already described (Ghadimi et al., 2012b).

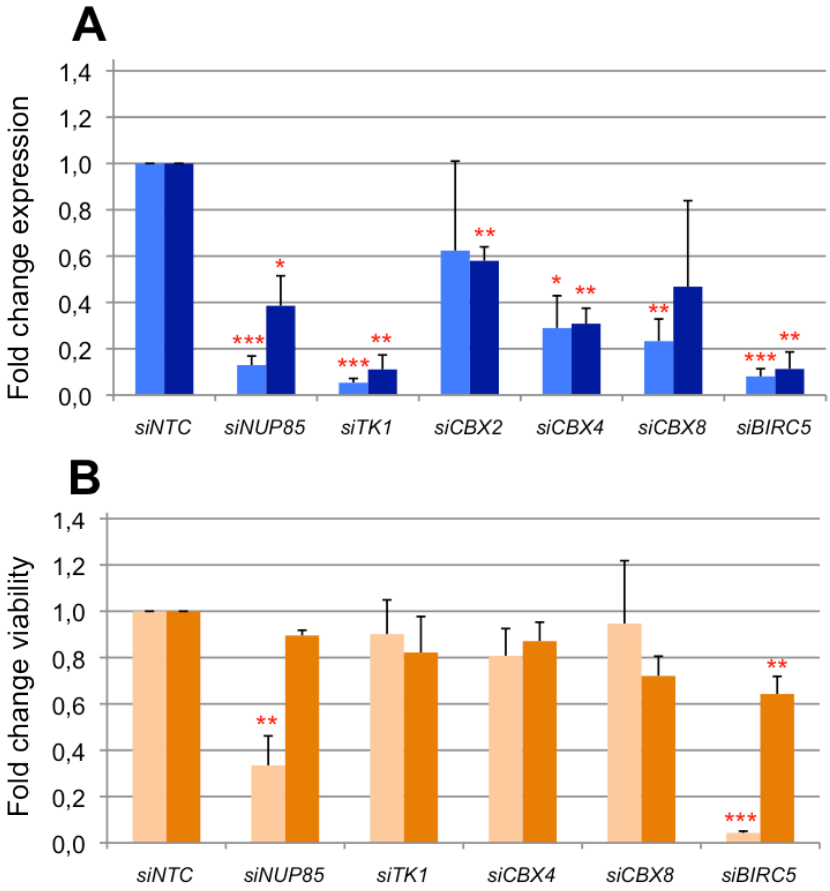

Figure 17. Expression knockdown and cell viability in S462 and T265 cell lines after depletion of overexpressed genes present in a specific TI. A. Fold change of expression knockdown in S462 (light blue) and T265 (dark blue) 72 hours post-transfection of siRNA pools targeting *NUP85, TK1, CBX2, CBX4, CBX8* or *BIRC5* genes vs. a non-targeting control siRNA (NTC). B. Fold change of cell viability in S462 (light orange) and T265 (orange) 72 hours post-transfection of siRNA pools targeting *NUP85, TK1, CBX4, CBX8* or *BIRC5* genes vs. a non-targeting control siRNA (NTC). Analysis of cell viability by cell counting in S462 and by XTT colourimetric assay in T265. All experiments in A and B were repeated three times. A T-test considering unequal variances was applied. *, $P < 0.05$; **, $P < 0.01$; ***, $P < 0.001$.

Another gene from this TI, *NUP85*, produced a mild effect in these tumourigenic properties when their expression was depleted, but this effect was lower than in the case of *BIRC5* depletion and mostly affected S462 rather than T265 cell line (**Figures 17.B, 18, 19 and 20**).

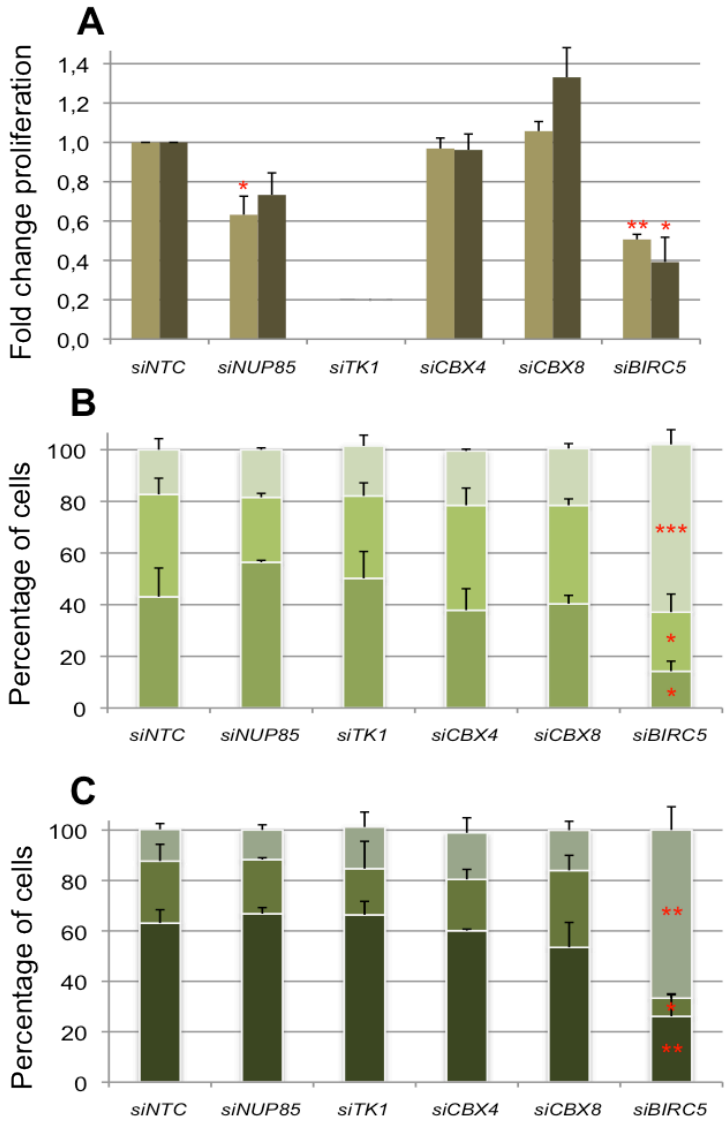

Figure 18. Cell proliferation and cell cycle analysis in S462 and T265 cell lines after expression knockdown of overexpressed genes present in a specific TI. A. Fold change of the percentage of proliferating S462 (light green) and T265 (dark green) 72 hours post-transfection of siRNA pools targeting *NUP85, CBX4, CBX8* or *BIRC5* genes vs. a non-targeting control siRNA (NTC). Analysis of EdU incorporation in 10,000 cells by flow cytometry. This assay was not valid for *TK1* knockdown. B, C. Percentages of cells in cell cycle phases G1 (bottom of column), S (middle of column) and G2 (top of column) in S462 (B) and T265 (C) 72 hours post-transfection of siRNA pools targeting *NUP85, TK1, CBX4, CBX8* or *BIRC5* genes vs. a non-targeting control siRNA (NTC). Analysis of propidium iodide staining in 10,000 cells by flow cytometry. All experiments in A, B and C were repeated three times. A T-test considering unequal variances was applied. *, $P < 0.05$; **, $P < 0.01$; ***, $P < 0.001$.

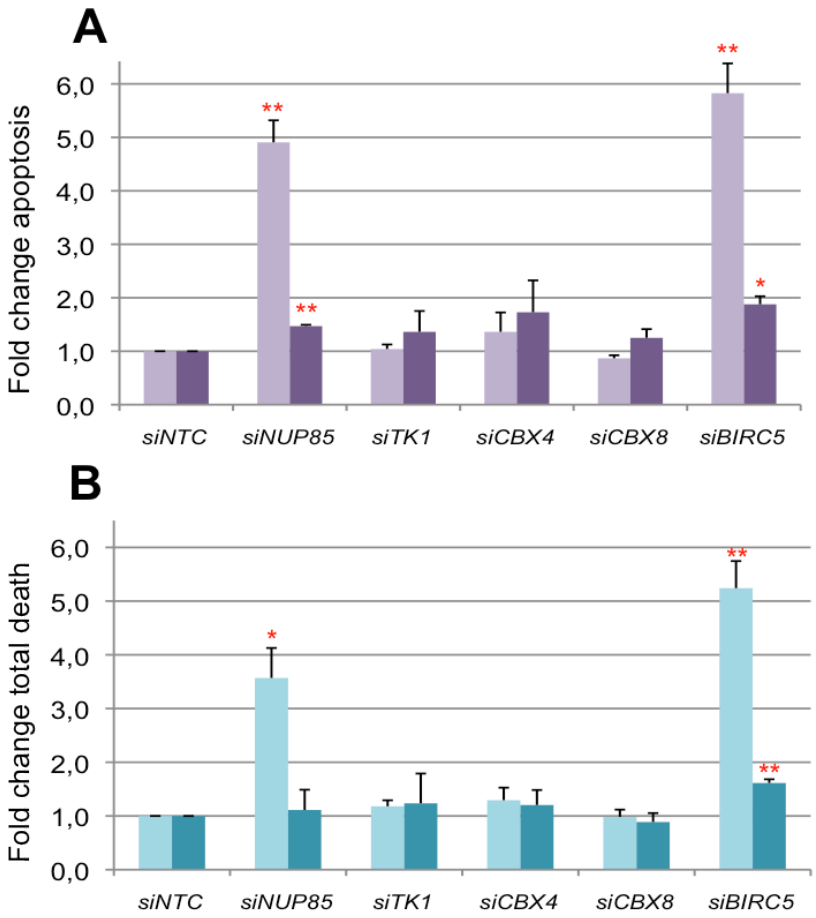

Figure 19. Apoptosis and total cell death in S462 and T265 cell lines after expression knockdown of overexpressed genes present in a specific TI. A. Fold change of the percentage of early apoptotic S462 cells (light violet) and T265 cells (dark violet) 72 hours post-transfection of siRNA pools targeting *NUP85, TK1, CBX4, CBX8* or *BIRC5* genes vs. a non-targeting control siRNA (NTC). Analysis of Annexin V staining in 30,000 cells by flow cytometry. B. Fold change of the percentage of dead S462 cells (light blue) and T265 cells (dark blue) –considering as dead cells those in late apoptotic or necrosis– 72 hours post-transfection of siRNA pools targeting *NUP85, TK1, CBX4, CBX8* or *BIRC5* genes vs. a non-targeting control siRNA (NTC). Analysis of Annexin V and bisbenzimide co-staining in 30,000 cells by flow cytometry. All experiments in A and B were repeated three times. A T-test considering unequal variances was applied. *, $P < 0.05$; **, $P < 0.01$; ***, $P < 0.001$.

The knockdown of *TK1*, *CBX4* and *CBX8* did not affect the tumourigenic properties of S462 and T265. On the contrary, *CBX8* knockdown produced an increase in both colony number and area of colonies in the soft agar assay in S462 (1.8-fold and 3.4-fold increase in colony number and area, respectively, **Figure 20**). Although more experimental data should be performed to conclude so, this result suggests that *CBX8*, rather than being oncogenic, could be acting as a TSG in S462.

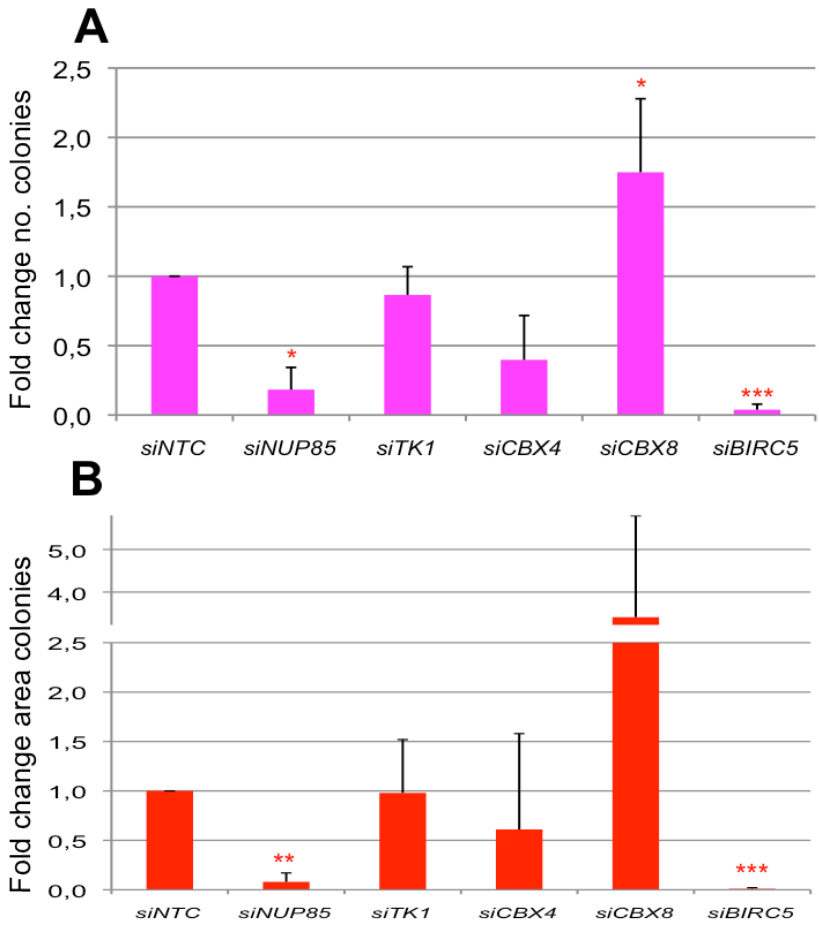

Figure 20. Anchorage-independent growth analysis in S462 cell line after expression knockdown of overexpressed genes present in a specific TI. A. Fold change of the number of colonies of S462 cells in soft agar 15 days post-transfection of siRNA pools targeting *NUP85, TK1, CBX4, CBX8* or *BIRC5* genes vs. a non-targeting control siRNA (NTC). B. Fold change of the area of colonies of S462 cells in soft agar 15 days post-transfection of siRNA pools targeting *NUP85, TK1, CBX4, CBX8* or *BIRC5* genes vs. a non-targeting control siRNA (NTC). Measurement of both number and area of colonies was performed with ImageJ software. All experiments in A and B were repeated three times (in *CBX8*, six times). A T-test considering unequal variances was applied. *, $P < 0.05$; **, $P < 0.01$; ***, $P < 0.001$.

Taken together, these results indicate that most of the studied genes in this TI, except for *BIRC5*, would not be required for the cell survival and cell cycle progression of the studied MPNST cell lines. Although our experimental model is limited (only two MPNST cell lines assessed and no *in vivo* validation performed), these results suggest that the overexpression of these genes in MPNSTs could be considered as passenger. We hypothesize that TIs would mostly capture genes differentially expressed between malignant and benign tumours that would not have a role in the pathogenesis of MPNSTs.

However, at the same time, these results also indicate that the formation of a TI would respond to the presence of one or a few genes important for MPNST pathogenesis, as is the case of *BIRC5* for this particular TI, in an analogous manner to what has been described for a SCNA (Beroukhim et al., 2010). TIs would be generated as a consequence of a selection of genomic regions containing few genes important for MPNST pathogenesis. As being gene expression closer to gene function than copy number, the information provided by TIs would be certainly relevant and could be used for both analyzing differentially expressed genes in malignant vs. benign tumours and for identifying candidate genes for MPNST pathogenesis.

2.4. Functional characterization of candidate genes for MPNST pathogenesis using information from TIs

Despite of the evidences that pointed to TIs to mainly capture passenger gene expression, we wondered whether information provided by TIs could be used for the identification of genes and mechanisms involved in MPNST pathogenesis. We focused our attention in two types of information from TIs. First, TIs were providing an impact of copy number on gene expression but, at the same time, TIs represented smaller genomic regions than the overlapped SCNAs where they were contained, thus reducing the number of genes. In addition, we also observed that many known cancer genes were present in TIs. We wondered whether some of these cancer genes could be responsible for the generation of TIs and were also drivers of MPNST pathogenesis, as a result of the selection of a particular SCNA. Second, we observed genes in TIs with an opposite differential expression than their neighbouring genes. This fact indicated that the differential expression of these genes, rather than being influenced by the mechanism that generated the TI, was mainly regulated regardless of the genomic (or the epigenomic) regional event. We hypothesized that these genes could reflect a physiological adaptation of the tumoural cell to a new altered state. This type of genes could be distributed all over the genome, being present or not in TIs. However, we were detecting these genes within TIs because their differential expression was opposed to the overall differential expression of the TI. We speculated that these genes could be representatives of pathways and molecular mechanisms where they participate. In this regard, we wondered whether this unique information,

only detected using information provided by TIs, could be useful for identifying genes and molecular mechanisms involved in MPNST pathogenesis.

2.4.1. Functional characterization of overexpressed cancer genes present in TIs of overexpression

To investigate our first hypothesis, we selected TIs of overexpression that were globally associated to copy number gains, in order to find candidate genes drivers of MPNST pathogenesis. We hypothesized that these TIs could be created as a result of the copy number gain. We considered only differentially overexpressed genes in MPNSTs versus benign tumours (dNFs and pNFs) that were included in TIs from MPNSTs, and with a described role in tumourigenesis (**Figure 21**).

We listed all the genes present in TIs of overexpression and we ranked them according to their expression levels considering both primary MPNSTs and MPNST cell lines, and their recurrence in genomic gains. We also considered, most importantly, a prior biological knowledge of their implication in cancer by using different cancer databases, as the Cancer Gene Census, and lists of putative cancer drivers of other tumour types (Tamborero et al., 2013). According to that, we selected six genes as candidate drivers of MPNST pathogenesis and also candidates for the generation of their respective TI: *PLAG1*, *CAD*, *EPHA4*, *BUB1, MYBL2* and *HOXA13* (**Table 9**).

Gene	Chromo-somal location	P-value differential expression in tumours	Log2 fold change expression in tumours	Association to TI	P-value differential expression in cells	Log2 fold change expression in cells	% MPNSTs with gains / losses
PLAG1	8q12.1	3.3×10^{-4}	3.34	In TI of over-expression	0.071	1.04	87.5 / 0
CAD	2p23.3	0.018	0.78	In TI of over-expression	0.002	1.54	50 / 0
EPHA4	2q36.1	0.002	2.15	In TI of over-expression	1.2×10^{-5}	2.42	62.5 / 0
BUB1	2q13	1.6×10^{-10}	3.34	In TI of over-expression	0.037	2.10	62.5 / 0
MYBL2	20q13.12	4.9×10^{-4}	0.80	In TI of over-expression	8.9×10^{-5}	1.82	37.5 / 0
HOXA13	7p15.2	2.7×10^{-10}	4.41	In TI of over-expression	4.4×10^{-5}	3.80	62.5 / 0

Table 9. Cancer genes selected as candidate drivers of MPNST pathogenesis. Information on their chromosomal location, the significance (P-value) and the fold change in the differential expression in tumours (MPNSTs vs. neurofibromas) and in cells (MPNST cell lines vs. SCs), and the proportion of MPNSTs from our set showing a SCNA in their genomic location.

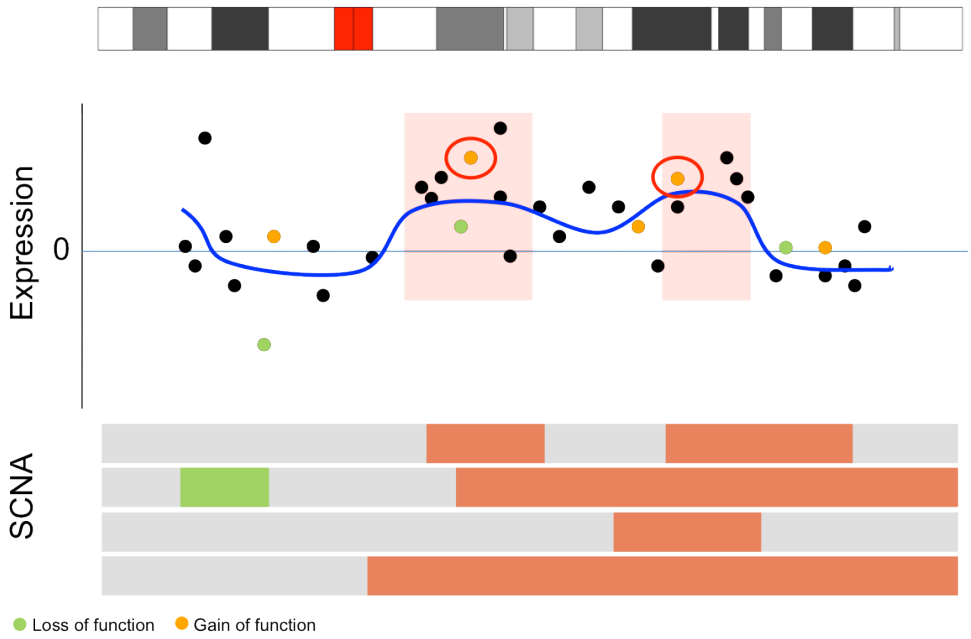

Figure 21. Diagram of the approach considering TIs of overexpression for identifying driver genes of MPNST pathogenesis. From top to bottom: a whole chromosome is depicted; red shaded areas show TIs of overexpression; blue line shows the smoothed mean differential gene expression; black dots indicate differential expression values from individual genes; red and green dots show differential expression from genes known to have a gain of function or a loss of function in cancer, respectively (circled dots represent those selected for experimental validation); somatic copy number alterations (SCNAs) are also shown as red bars indicating genomic gains and green bars indicating genomic losses.

PLAG1 is a zinc finger transcription factor that positively regulates IGF2 growth factor (Voz et al., 2000). Some studies have shown a role of PLAG1 in several tumours, being the pleomorphic adenomas of the salivary glands the most common (Kas et al., 1997).

CAD encodes the enzyme carbamoyl-phosphate synthetase 2, a protein associated with the pathway of *de novo* pyrimidine biosynthesis (Iwahana et al., 1996), which is regulated by the MAPK cascade (Graves et al., 2000), linking the processes of cell cycle and metabolism. *CAD* has been associated, among others, with breast (Zhang et al., 2013) and prostate cancer (Morin et al., 2012).

EPHA4 is a receptor tyrosine kinase that belongs to the ephrin receptor subfamily. It plays an important role in the development of the nervous system controlling different

steps of axonal guidance (Drescher et al., 1997) and in angiogenesis (Wang et al., 1998). EPHA4 has been related to several tumour types, especially to pancreatic cancer (Iiizumi et al., 2006).

BUB1 encodes a serine/threonine kinase essential for the spindle-assembly checkpoint signalling and for a correct chromosome alignment. It has a key role in the recruitment of other proteins at the kinetochore, such as the kinesin CENPE and BUB1B (Johnson et al., 2004), among others. *BUB1B* has found overexpressed in MPNSTs (Stricker et al., 2013) and *BUB1* is mutated in several cancers (reviewed in Kops et al., 2005).

MYBL2 is a member of the MYB family of transcription factors involved in the regulation of the expression of numerous genes during cell cycle progression, including *TOP2A* and *MYC*, promoting the entry into the S and M phases of the cell cycle (Joaquin and Watson, 2003). *MYBL2* is overexpressed in neuroblastoma and other tumours (reviewed in Martinez and Dimaio, 2011).

HOXA13 is a homeobox transcription factor that has been associated with acute myeloid leukemia (Fujino et al., 2002), esophageal squamous cell carcinoma (Gu et al., 2009) and hepatocellular carcinoma (Cillo et al., 2011). It has been recently also found deregulated in pancreatic cancer (Li et al., 2015) and glioma (Duan et al., 2015).

As before, their expression knockdown after siRNA transfection was first checked by RT-qPCR in both S462 and T265 and was found relevant and significant for all genes, except for *PLAG1* (**Figure 22.A**). We used the same criteria than in section 2.3 and *PLAG1* gene was then excluded from the functional genetic assays. The mean±SD expression reduction for all remaining genes, *CAD*, *EPHA4*, *BUB1, MYBL2* and *HOXA13*, considering the two cell lines was of 73±20% (**Figure 22.A**).

The results from the functional genetic approaches pointed to *MYBL2* and *CAD* to have a potential role in the *in vitro* tumourigenic features studied. When *MYBL2* expression was knocked down in S462, there were significant effects in many readouts: viability (75% reduction; **Figure 22.B**), proliferation (71% reduction; **Figure 23.A**), cell cycle arrest in G0/G1 phase (1.6-fold increase in the percentage of G0/G1

cells; **Figure 23.B**), apoptosis (2.4-fold increase; **Figure 24.A**), and total cell death (2.4-fold increase; **Figure 24.B**). In T265 cell line, some effects were also found when *MYBL2* was depleted: 34% reduction in viability (**Figure 22.B**), and 26% reduction in proliferation (**Figure 23.A**).

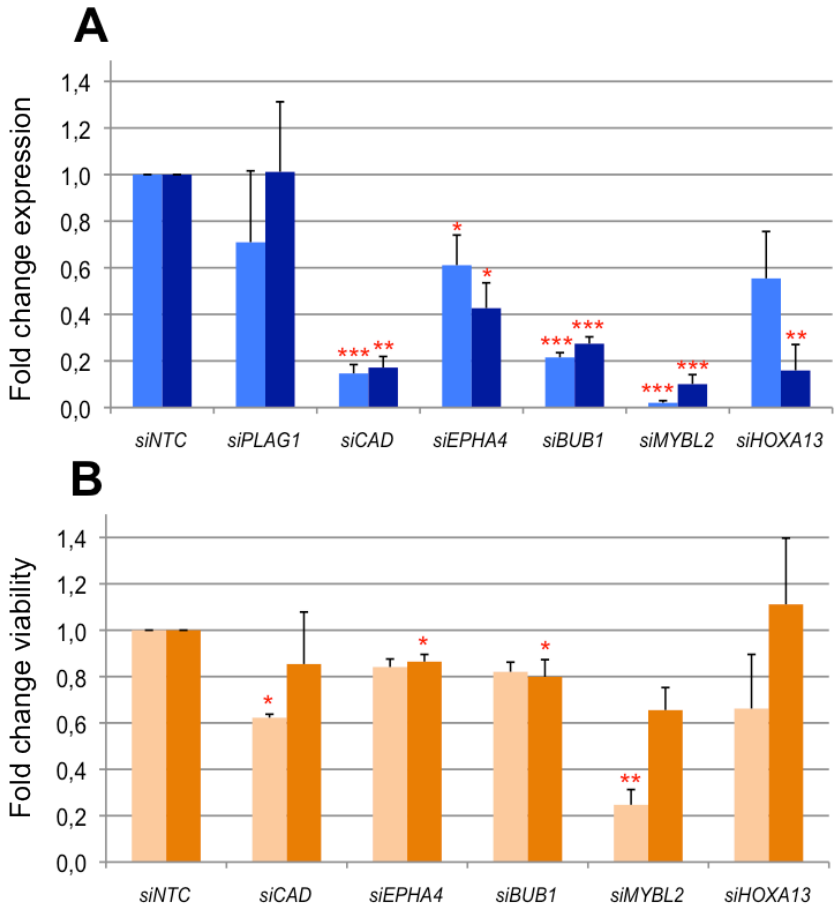

Figure 22. Expression knockdown and cell viability in S462 and T265 cell lines after depletion of cancer genes selected as candidate drivers of MPNST pathogenesis. A. Fold change of expression knockdown in S462 (light blue) and T265 (dark blue) 72 hours post-transfection of siRNA pools targeting *PLAG1*, *CAD, EPHA4, BUB1, MYBL2,* or *HOXA13* genes vs. a non-targeting control siRNA (NTC). B. Fold change of cell viability in S462 (light orange) and T265 (orange) 72 hours post-transfection of siRNA pools targeting *CAD, EPHA4, BUB1, MYBL2,* or *HOXA13* genes vs. a non-targeting control siRNA (NTC). Analysis of cell viability by cell counting in S462 and by XTT colourimetric assay in T265. All experiments in A and B were repeated three times. A T-test considering unequal variances was applied. *, $P < 0.05$; **, $P < 0.01$; ***, $P < 0.001$.

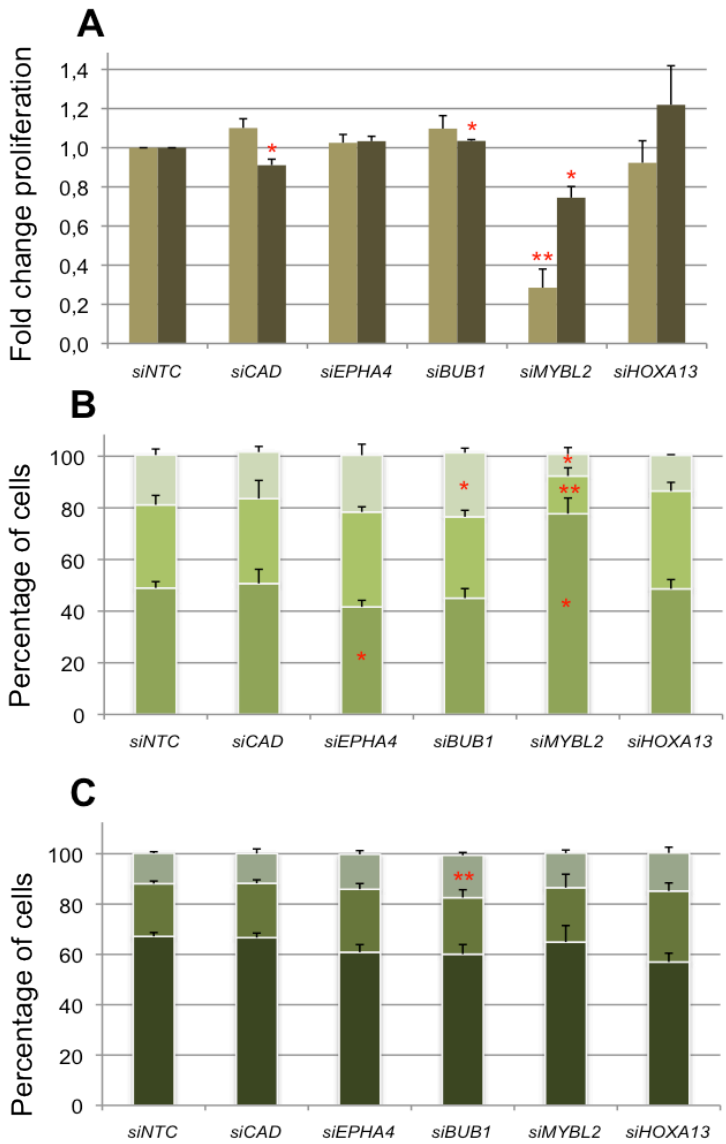

Figure 23. Cell proliferation and cell cycle analysis in S462 and T265 cell lines after expression knockdown of cancer genes selected as candidate drivers of MPNST pathogenesis. A. Fold change of the percentage of proliferating S462 (light green) and T265 (dark green) 72 hours post-transfection of siRNA pools targeting *CAD, EPHA4, BUB1, MYBL2,* or *HOXA13* genes vs. a non-targeting control siRNA (NTC). Analysis of EdU incorporation in 10,000 cells by flow cytometry. B, C. Percentages of cells in cell cycle phases G1 (bottom of column), S (middle of column) and G2 (top of column) in S462 (B) and T265 (C) 72 hours post-transfection of siRNA pools targeting *CAD, EPHA4, BUB1, MYBL2,* or *HOXA13* genes vs. a non-targeting control siRNA (NTC). Analysis of propidium iodide staining in 10,000 cells by flow cytometry. All experiments in A and B were repeated three times. A T-test considering unequal variances was applied. *, $P < 0.05$; **, $P < 0.01$; ***, $P < 0.001$.

In the case of *CAD*, when depleted in S462, there were significant effects in viability (38% reduction; **Figure 22.B**), apoptosis (1.5-fold increase; **Figure 24.A**), and anchorage-independent growth (49% reduction in colony number; **Figure 25**). No remarkable effects were found in T265 cell line when *CAD* expression was knocked down.

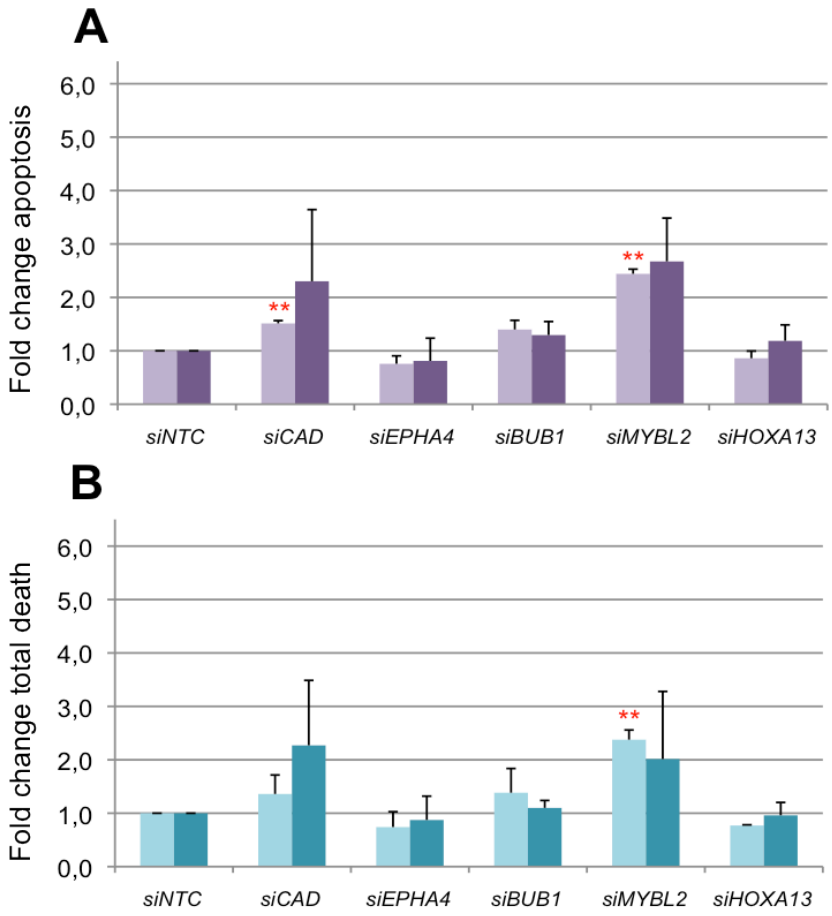

Figure 24. Apoptosis and total cell death in S462 and T265 cell lines after expression knockdown of cancer genes selected as candidate drivers of MPNST pathogenesis. A. Fold change of the percentage of early apoptotic S462 cells (light violet) and T265 cells (dark violet) 72 hours post-transfection of siRNA pools targeting *CAD, EPHA4, BUB1, MYBL2,* or *HOXA13* genes vs. a non-targeting control siRNA (NTC). Analysis of Annexin V staining in 30,000 cells by flow cytometry. B. Fold change of the percentage of dead S462 cells (light blue) and T265 cells (dark blue) –considering as dead cells those in late apoptosis or necrosis– 72 hours post-transfection of siRNA pools targeting *CAD, EPHA4, BUB1, MYBL2,* or *HOXA13* genes vs. a non-targeting control siRNA (NTC). Analysis of Annexin V and bisbenzimide co-staining in 30,000 cells by flow cytometry. All experiments in A and B were repeated three times. A T-test considering unequal variances was applied. *, P < 0.05; **, P < 0.01; ***, P < 0.001.

These results indicated that the oncogenic transcription factor *MYBL2* and, in a less extent, the enzyme *CAD* might have a role in the cell survival of the studied MPNST cell lines, especially for S462. However, these results were not as robust as the effect of *BIRC5* depletion in these cell lines, pointing that both *MYBL2* and *CAD* would contribute to MPNST pathogenesis but not having an essential role.

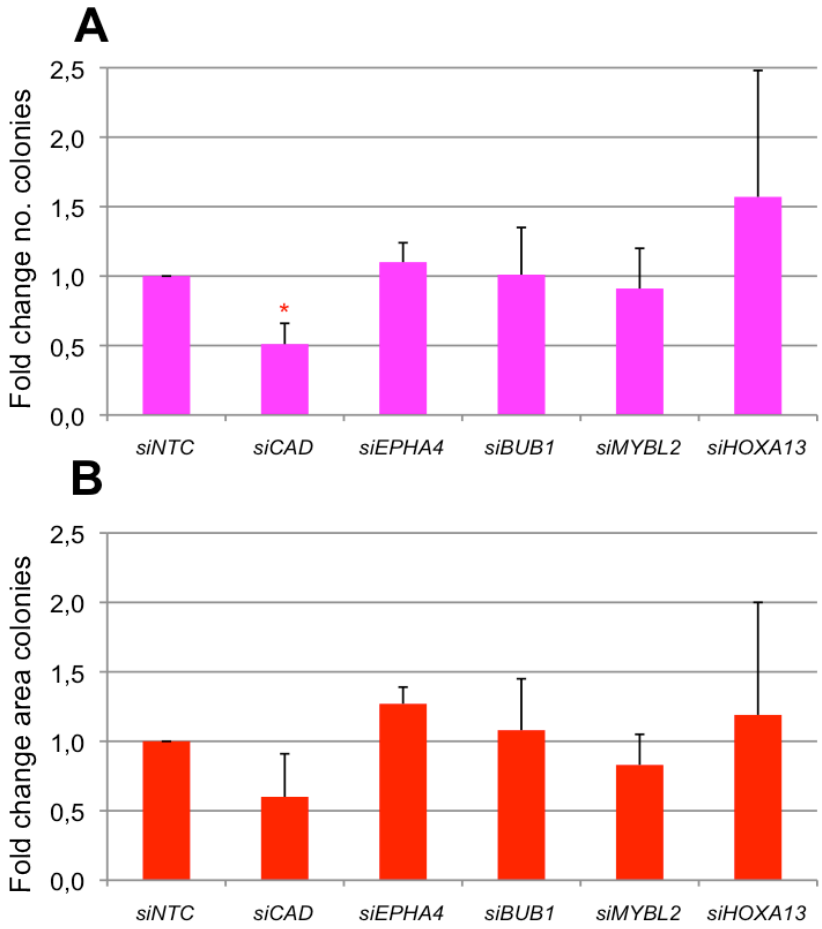

Figure 25. Anchorage-independent growth analysis in S462 cell line after expression knockdown of cancer genes selected as candidate drivers of MPNST pathogenesis. A. Fold change of the number of colonies of S462 cells in soft agar 15 days post-transfection of siRNA pools targeting *CAD, EPHA4, BUB1, MYBL2,* or *HOXA13* genes vs. a non-targeting control siRNA (NTC). B. Fold change of the area of colonies of S462 cells in soft agar 15 days post-transfection of siRNA pools targeting *CAD, EPHA4, BUB1, MYBL2,* or *HOXA13* genes vs. a non-targeting control siRNA (NTC). Measurement of both number and area of colonies was performed with ImageJ software. All experiments in A and B were repeated three times (in *CBX8*, six times). A T-test considering unequal variances was applied. *, $P < 0.05$; **, $P < 0.01$; ***, $P < 0.001$.

The expression knockdown of the other studied genes, *EPHA4*, *BUB1* and *HOXA13* did not affect the tumourigenic properties of S462 and T265, although it should be considered that the knockdown of *EPHA4* in both cell lines and *HOXA13* in S462 were not that relevant.

However, taken together, these results indicate that most of the selected and studied cancer-associated genes, would not be required for the cell survival and cell cycle progression of S462 and T265, although the limitations of our experimental model (only two cell lines and no *in vivo* experiments performed) should be considered.

The two most important factors for the selection of putative driver genes responsible for the formation of TIs of overexpression were a previous knowledge on their functional implication in tumourigenesis (or their consideration as cancer drivers) and the expression in our *in vitro* experimental model (overexpressed in MPNST cell lines). Despite all these limitations and the necessity of a further screening, a previous knowledge on cancer drivers did not provided useful information for identifying drivers of MPNST pathogenesis in TIs of overexpression.

2.4.2. Functional characterization of overexpressed genes present in or flanking TIs of underexpression

In a second step, we studied genes from TIs with an opposite differential expression than their neighbouring genes. In other words, we looked for differentially overexpressed genes in MPNSTs that were present in or flanking TIs of underexpression (**Figure 26**). We hypothesized that these genes may be mainly regulated by the physiological state of the cancerous cell regardless of the genomic (or epigenomic) regional effect. Thus, we speculated that some of these genes might be involved in molecular pathways that are required for maintaining MPNST tumoural properties.

Then, a list of all the overexpressed genes present in or flanking TIs of underexpression was generated, considering their expression levels in both primary MPNSTs and MPNST cell lines and a described functional role in tumourigenesis

according to the literature. According to that, we selected *LHX8*, *CDCA8*, *BCAT1*, *CCDC8* and *GINS2* as candidate genes (**Table 10**).

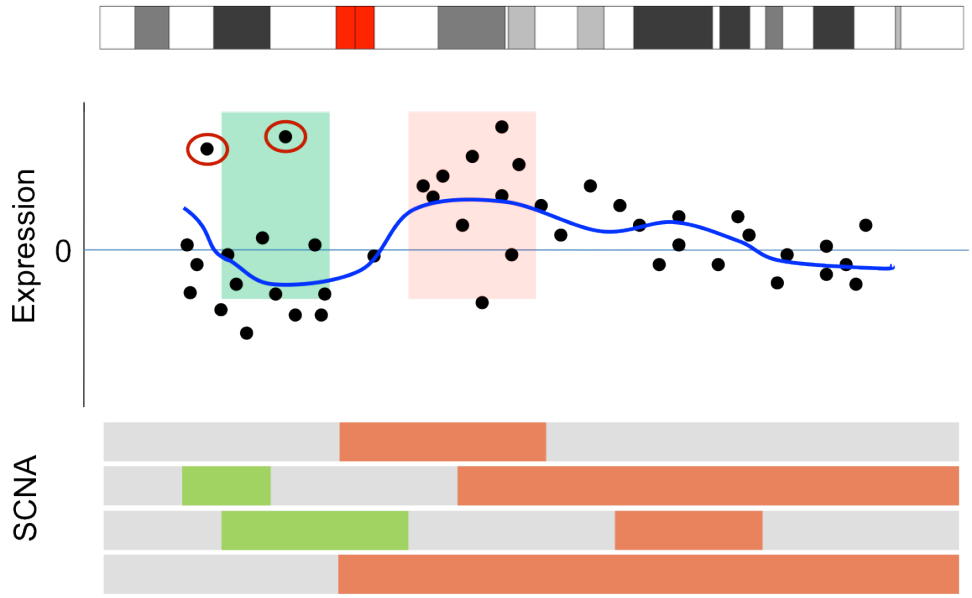

Figure 26. Diagram of the approach considering the unique information provided by TIs for identifying genes involved in MPNST pathogenesis. From top to bottom: a whole chromosome is depicted; the red shaded area show a TI of overexpression; and the green shaded area show a TI of underexpression; blue line shows the smoothed mean differential gene expression; black dots indicate differential expression values from individual genes; circled dots are those selected for experimental validation because of their differential expression is opposed to the differential expression of the neighbouring genes within the TI; somatic copy number alterations (SCNAs) are also shown as red bars indicating genomic gains and green bars indicating genomic losses.

LHX8 is a member of the LIM homeobox subfamily of transcription factors. These proteins regulate important developmental pathways in multiple tissue types (Hobert and Westphal, 2000). A role in cancer of these proteins has been suggested either acting as oncogenes or TSGs depending on the member (Wang et al., 2014a). However, little is known about their specific functions in tumourigenesis and so far no report has associated *LHX8* to cancer.

CDCA8, Cell Division Cycle Associated 8, encodes the protein borealin, a component of the chromosomal passenger complex (CPC), a heterotetramer that regulate several processes during mitotic and meiotic cell divisions (reviewed in Ruchaud et al., 2007).

CDCA8 has been associated to gastric (Chang et al., 2006), and colorectal cancer (Wang et al., 2014b).

BCAT1 encodes the enzyme Branched Chain Amino-Acid Transaminase 1 that catalyzes the reversible transamination of branched-chain alpha-keto acids to branched-chain L-amino acids (Ichihara and Koyama, 1966). It is a *MYC* target and it has been associated to nasopharyngeal (Zhou et al., 2007), urothelial (Chang et al., 2015) and ovarian carcinoma (Wang et al., 2015), and glioma (Tonjes et al., 2013).

CCDC8 encodes a coiled-coil domain-containing protein that is a core component of the 3M complex, a centrosomal complex that is required to regulate microtubule dynamics and genome integrity (Yan et al., 2014). The 3M complex inhibits CUL9, which, in turn, promotes the degradation of survivin (Li et al., 2014). So, survivin, encoded by *BIRC5*, is an indirect target of CCDC8.

Gene	Chromo-somal location	P-value differential expression in tumours	Log2 fold change expression in tumours	Association to TI	P-value differential expression in cells	Log2 fold change expression in cells	% MPNSTs with gains / losses
LHX8	1p31.1	4.1×10^{-13}	5.53	In TI of under-expression	4.9×10^{-4}	2.74	0 / 12.5
CDCA8	1p34.3	2.3×10^{-6}	2.91	In TI of under-expression	0.062	1.91	12.5 / 12.5
BCAT1	12p12.1	3.9×10^{-5}	2.02	In TI of under-expression	0.028	2.00	37.5 / 25
CCDC8	19q13.32	3.0×10^{-5}	2.18	Flanking TI of underexpression	0.006	1.54	25 / 0
GINS2	16q24.1	1.9×10^{-8}	3.00	Flanking TI of underexpression	0.072	1.61	25 / 12.5

Table 10. Genes selected because of their opposed differential expression to the TI overall differential expression. Information on their chromosomal location, the significance (P-value) and the fold change in the differential expression in tumours (MPNSTs vs. neurofibromas) and in cells (MPNST cell lines vs. SCs), and the proportion of MPNSTs from our set showing a SCNA in their genomic location.

GINS2 is a component of the GINS complex, which plays an essential role in the initiation of DNA replication (Kanemaki et al., 2003). A role of this protein in breast cancer has been suggested (Rantala et al., 2010; Zheng et al., 2014).

Again, the expression knockdown of all five genes after siRNA transfection was checked by RT-qPCR in both S462 and T265, and was found relevant and significant for all five genes (**Figure 27.A**). The mean±SD expression reduction for all genes considering the two cell lines was of 86±6% (**Figure 27.A**).

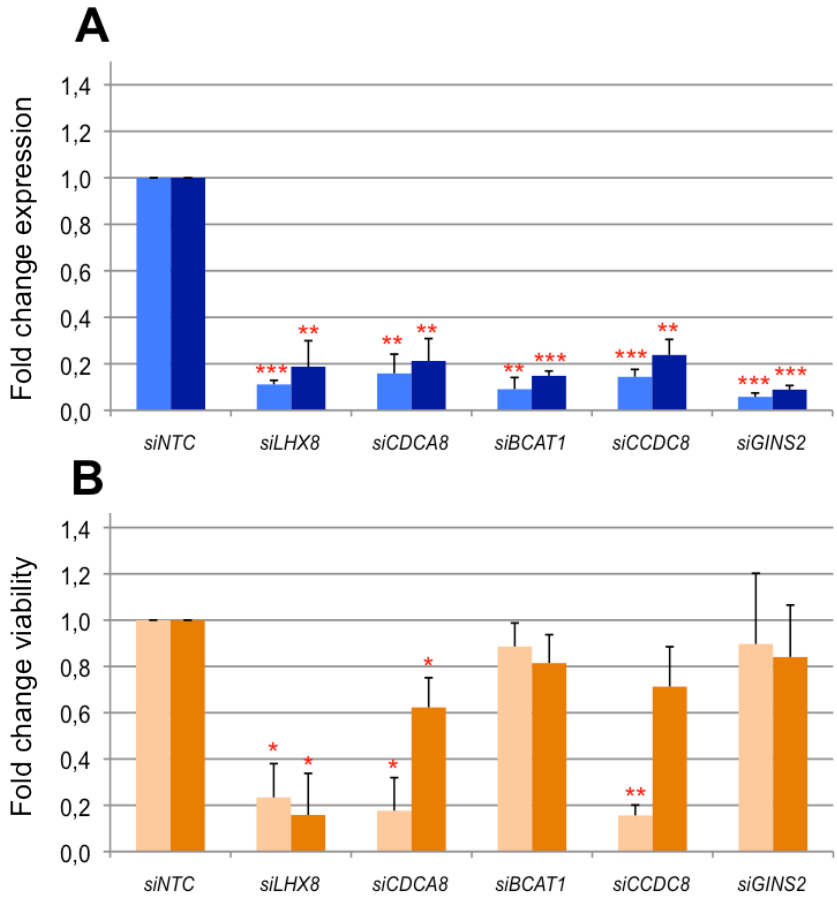

Figure 27. Expression knockdown and cell viability in S462 and T265 cell lines after depletion of genes selected because of their opposed differential expression to the TI overall differential expression. A. Fold change of expression knockdown in S462 (light blue) and T265 (dark blue) 72 hours post-transfection of siRNA pools targeting *LHX8*, *CDCA8, BCAT1, CCDC8* or *GINS2* genes vs. a non-targeting control siRNA (NTC). B. Fold change of cell viability in S462 (light orange) and T265 (orange) 72 hours post-transfection of siRNA pools targeting *LHX8*, *CDCA8, BCAT1, CCDC8* or *GINS2* genes vs. a non-targeting control siRNA (NTC). Analysis of cell viability by cell counting in S462 and by XTT colourimetric assay in T265. All experiments in A and B were repeated three times. A T-test considering unequal variances was applied. *, $P < 0.05$; **, $P < 0.01$; ***, $P < 0.001$.

The results from the functional genetic approaches, considering all readouts and cell lines, showed that the expression knockdown of *CDCA8* consistently and significatively affected the *in vitro* tumourigenic features of S462 and T265 cell lines. In S462, *CDCA8* expression depletion produced significant effects in all readouts: viability (82% reduction; **Figure 27.B**), proliferation (40% reduction; **Figure 28.A**), cell cycle arrest in G2/M phase (2.6-fold increase in the percentage of G2/M cells; **Figure 28.B**), apoptosis (3.6-fold increase; **Figure 29.A**), total cell death (3.2-fold increase; **Figure 29.B**), and

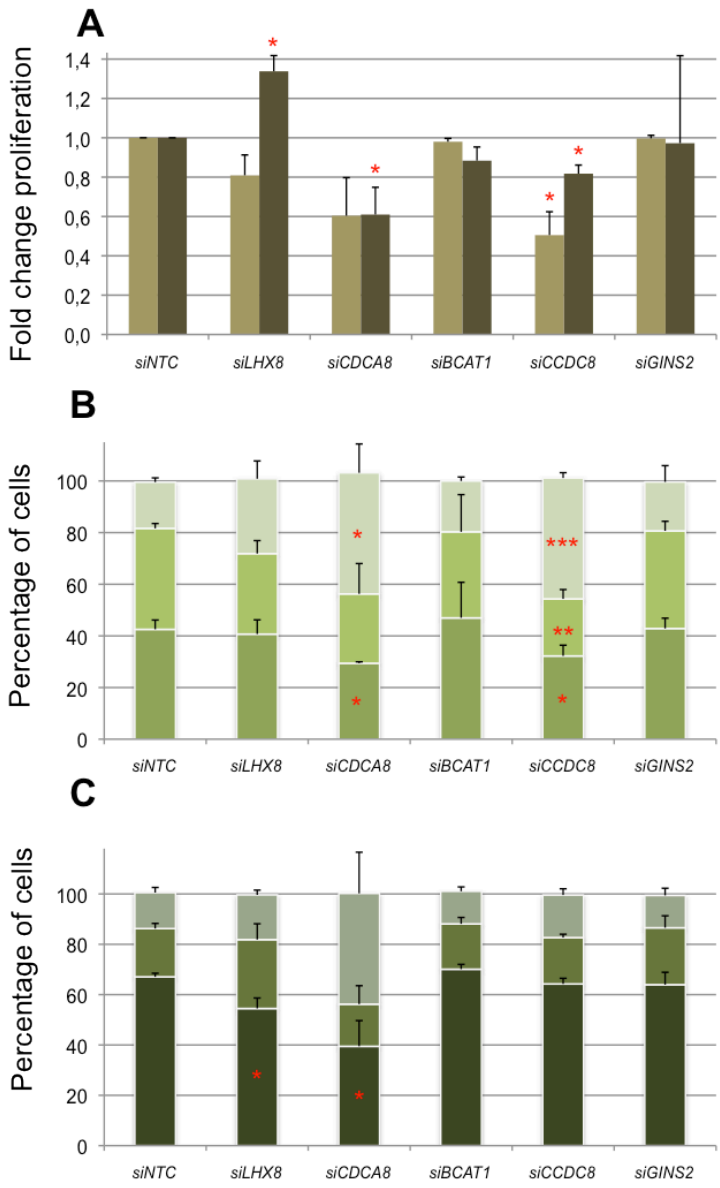

Figure 28. Cell proliferation and cell cycle analysis in S462 and T265 cell lines after expression knockdown of genes selected because of their opposed differential expression to the TI overall differential expression. A. Fold change of the percentage of proliferating S462 (light green) and T265 (dark green) 72 hours post-transfection of siRNA pools targeting *LHX8*, *CDCA8, BCAT1, CCDC8* or *GINS2* genes vs. a non-targeting control siRNA (NTC). Analysis of EdU incorporation in 10,000 cells by flow cytometry. B, C. Percentages of cells in cell cycle phases G1 (bottom of column), S (middle of column) and G2 (top of column) in S462 (B) and T265 (C) 72 hours post-transfection of siRNA pools targeting *LHX8*, *CDCA8, BCAT1, CCDC8* or *GINS2* genes vs. a non-targeting control siRNA (NTC). Analysis of propidium iodide staining in 10,000 cells by flow cytometry. All experiments in A and B were repeated three times. A T-test considering unequal variances was applied. *, $P < 0.05$; **, $P < 0.01$; ***, $P < 0.001$.

anchorage-independent growth (91% and 98% reduction in colony number and area, respectively, **Figure 30**). In the case of T265 cell line, there were also significant differences in viability (38% reduction; **Figure 27.B**), proliferation (39% reduction; **Figure 28.A**), cell cycle arrest in G2/M phase (3.1-fold increase in the percentage of G2/M cells; **Figure 28.B**) and apoptosis (2.9-fold increase; **Figure 29.A**).

These results indicated that *CDCA8* is required for the survival and cell cycle progression of these MPNST cell lines. *CDCA8* encodes borealin, a component of the CPC, together with survivin (the product of *BIRC5* gene) and two other proteins (reviewed in Ruchaud et al., 2007). Considering this, our results suggest that the CPC may have a role in MPNST pathogenesis.

Another gene from this group, *CCDC8,* when knocked down, was also found to have an effect in the tumourigenic properties studied, especially for S462. This cell line showed a 84% reduction in cell viability (**Figure 27.B**), a 49% reduction in cell proliferation (**Figure 28.A**), an arrest in G2/M phase of the cell cycle (2.6-fold increase in the percentage of G2/M cells; **Figure 28.B**), a 1.7-fold increase in total cell death (**Figure 29.B**), and a 97% and 99% reduction in colony number and area, respectively, in the soft agar assay (**Figure 30**). In T265, *CCDC8* expression depletion also produced a 29% reduction in viability (**Figure 27.B**) and an 18% reduction in proliferation (**Figure 28.A**). The centrosomal protein CCDC8 has been found to positively regulate survivin by inhibiting its negative regulator CUL9 (Li et al., 2014), linking mitosis with cell survival, which is in consistency with our results.

In the case of *LHX8*, there was a dramatic reduction in viability in both cell lines: 77% reduction in S462 (**Figure 27.B**) and 84% reduction in T265 (**Figure 27.B**). In fact, an elevated number of detached cells was observed for both lines as soon as 24 hours after *LHX8* expression knockdown. Moreover, in S462, there was 2.6-fold increase in apoptosis (**Figure 29.A**), a 2.0-fold increase in total cell death (**Figure 29.B**) and a 78% and 83% reduction in colony number (**Figure 30.A**) and area (**Figure 30.B**), respectively, in the soft agar assay, after 72 hours of siRNA transfection. In T265, there was a 1.3-fold increase in EdU incorporation (**Figure 28.A**), supported by a 1.4-fold increase in the percentage of cells in S phase (**Figure 28.B**). In this case, rather than an increase in

cell proliferation, an arrest in S phase of the cell cycle is suggested, which is consistent with the EdU incorporation increase.

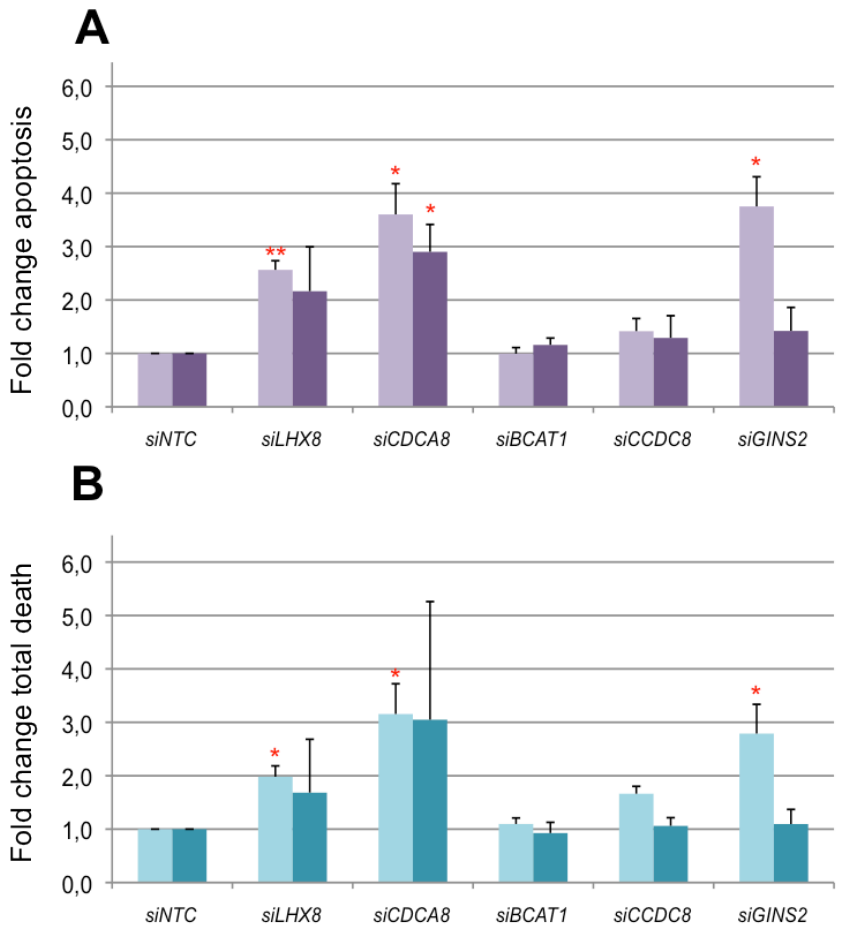

Figure 29. Apoptosis and total cell death in S462 and T265 cell lines after expression knockdown of genes selected because of their opposed differential expression to the TI overall differential expression. A. Fold change of the percentage of early apoptotic S462 cells (light violet) and T265 cells (dark violet) 72 hours post-transfection of siRNA pools targeting *LHX8*, *CDCA8, BCAT1, CCDC8* or *GINS2* genes vs. a non-targeting control siRNA (NTC). Analysis of Annexin V staining in 30,000 cells by flow cytometry. B. Fold change of the percentage of dead S462 cells (light blue) and T265 cells (dark blue) –considering as dead cells those in late apoptotic or necrosis– 72 hours post-transfection of siRNA pools targeting *LHX8*, *CDCA8, BCAT1, CCDC8* or *GINS2* genes vs. a non-targeting control siRNA (NTC). Analysis of Annexin V and bisbenzimide co-staining in 30,000 cells by flow cytometry. All experiments in A and B were repeated three times. A T-test considering unequal variances was applied. *, P < 0.05; **, P < 0.01; ***, P < 0.001.

These results showed that *LHX8* has probably different functions in S462 and in T265, but a possible role in MPNST pathogenesis is plausible as long as the cells die soon after siRNA transfection. A better characterization of these tumourigenic properties

before 72 hours post-transfection is encouraged to unravel the role of LHX8. In any case, to our knowledge, this is the first time that an essential role of *LHX8* in the cell survival of tumoural cells is demonstrated.

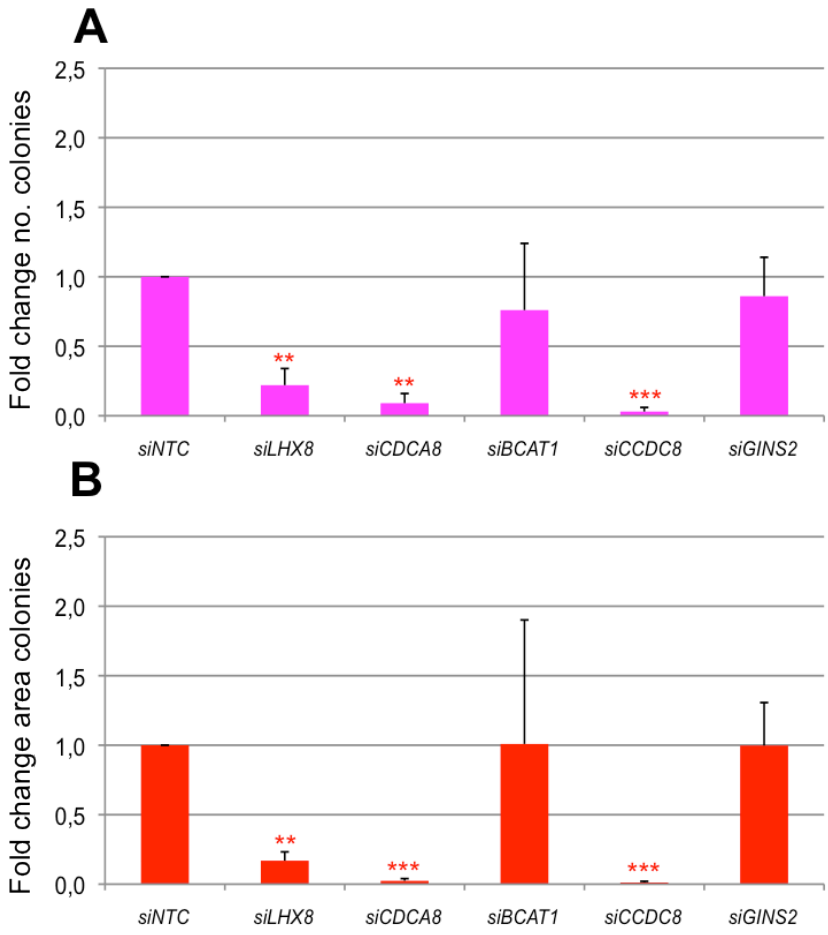

Figure 30. Anchorage-independent growth analysis in S462 cell line after expression knockdown of genes selected because of their opposed differential expression to the TI overall differential expression. A. Fold change of the number of colonies of S462 cells in soft agar 15 days post-transfection of siRNA pools targeting *LHX8*, *CDCA8, BCAT1, CCDC8* or *GINS2* genes vs. a non-targeting control siRNA (NTC). B. Fold change of the area of colonies of S462 cells in soft agar 15 days post-transfection of siRNA pools targeting *LHX8*, *CDCA8, BCAT1, CCDC8* or *GINS2* genes vs. a non-targeting control siRNA (NTC). Measurement of both number and area of colonies was performed with ImageJ software. All experiments in A and B were repeated three times (in *CBX8*, six times). A T-test considering unequal variances was applied. *, $P < 0.05$; **, $P < 0.01$; ***, $P < 0.001$.

The expression knockdown of the other two studied genes, *BCAT1* and *GINS2*, did not affect the majority of the tumourigenic properties of S462 and T265.

In sum, our results indicated that *CDCA8* is required for the cell survival and cell cycle progression of both S462 and T265. If we take into account the role of *BIRC5* in MPNSTs, we claim that the CPC could be an important player in MPNST pathogenesis. *CCDC8* also seemed to be important for maintaining the tumourigenic properties of, at least, S462 cell line. Hence, it can be suggested that *CCDC8* may have also a role in MPNST pathogenesis. Moreover, *LHX8* rapidly affected the cell survival of both S462 and T265, and despite a better characterization is needed, *LHX8* could be also involved in the pathogenesis of these tumours.

Although the limitations and constraints of our experimental model and candidate gene selection should be considered, as in previous experiments, with this approach we have identified at least two candidate genes to be involved in MPNST pathogenesis. TIs provide exclusive information on genes whose expression is mainly regulated independently from the regional genomic events observed. We suggest that these genes and the molecular pathways where they participate could help in a better understanding of MPNST pathogenesis.

3. Role of mitotic kinesins in MPNST pathogenesis: potential therapeutic targets for MPNST treatment

3.1. TIs allowed the identification of kinesin genes involved in cell division

When TIs were generated, a first evaluation of the overexpressed genes associated to TIs (either included in or flanking) was performed. In this analysis, a clear enrichment in genes from the kinesin superfamily involved in cell division was found. In particular, using data from the NF1 Microarray Consortium (Miller et al., 2009), from the 16 kinesin genes known to participate in cell division, 13 of the 15 kinesins present in the expression array were significantly overexpressed in MPNSTs compared to benign neurofibromas (**Table 11**).

Gene	Chromo-somal location	P-value differential expression in tumours	Log2 fold change expression in tumours	Association to TI	P-value differential expression in cells	Log2 fold change expression in cells	% MPNSTs with gains / losses
KIF2A	5q12.1	5.9×10^{-4}	1.15	In TI of over-expression	3.2×10^{-4}	0.66	25 / 25
KIF2B	17q22	1	0.00	Flanking TI of overexpression	1	0.00	87.5 / 12.5
KIF2C	1p34.1	4.2×10^{-8}	1.59	Flanking TI of underexpression	0.019	1.80	12.5 / 12.5
KIF4A	Xq13.1	6.8×10^{-5}	3.78	n/a	0.133	1.29	0 / n/a
KIF10	4q24	5.0×10^{-8}	3.64	Flanking TI of overexpression	0.273	1.16	25 / 0
KIF11	10q23.33	3.4×10^{-6}	4.51	Flanking TI of underexpression	0.158	1.11	0 / 12.5
KIF14	1q32.1	2.5×10^{-9}	3.34	Flanking TI of underexpression	0.058	1.60	37.5 / 0
KIF15	3p21.21	2.4×10^{-7}	2.65	In TI of under-expression	0.028	1.86	12.5 / 12.5
KIF18A	11p14.1	1.4×10^{-4}	1.35	NO	0.157	1.04	12.5 / 12.5
KIF18B	17q21.31	1.6×10^{-6}	5.91	Flanking TI of underexpression	0.054	2.30	50 / 25
KIF20A	5q31.2	9.5×10^{-9}	3.61	NO	0.281	1.40	25 / 12.5
KIF20B	10q23.31	0.019	0.99	Flanking TI of underexpression	0.500	0.43	0 / 12.5
KIF22	16p11.2	0.747	0.08	NO	0.005	0.99	37.5 / 25
KIF23	15q23	2.1×10^{-9}	3.44	In TI of over-expression	0.134	1.17	75 / 0
KIFC1	6p21.32	2.7×10^{-7}	2.56	NO	0.040	1.41	37.5 / 0

Table 11. Expression of mitotic kinesins in MPNSTs and association with TIs. Information on their chromosomal location, the significance (P-value) and the fold change of the differential expression in tumours (MPNSTs vs. neurofibromas) and in cells (MPNST cell lines vs. SCs), and the proportion of MPNSTs from our set showing a SCNA in their genomic location. In bold are those kinesins that were selected for experimental studies. n/a: not available.

Among these overexpressed kinesin genes, two of them, *KIF2A* and *KIF23* (also known as *MKLP1)* were both present in TIs of overexpression; one kinesin, *KIF15,* was in a TI of underexpression; two other members, *KIF10* (also known as *CENPE*) and *KIF18B*, were genes flanking TIs of overerexpression; and 5 genes, *KIF2C*, *KIF11* (also known as *EG5*), *KIF14*, *KIF18B* and *KIF20B* were flanking TIs of underexpression (**Table 11**). Other overexpressed mitotic kinesins in MPNSTs, including *KIF18A, KIF20A* (also known as *MKLP2*), *KIF22* and *KIFC1*, were not associated to any TI.

3.2. Selection of mitotic kinesins and study of their loss of function in MPNST cell lines

As kinesins have emerged as potential targets for cancer drug development during the last years and some clinical trials have been performed (reviewed in Rath and Kozielski, 2012), we wanted to address whether some of the kinesins identified using information from TIs were involved in MPNST pathogenesis and could represent potential therapeutic targets for MPNST treatment.

In order to do so, an experimental framework was designed to disrupt the function of a selection of kinesins involved at different stages of mitosis and cytokinesis. In particular, in addition to a gene expression knockdown using siRNA as in sections 2.3 and 2.4, a chemical inhibition using drugs was also considered. The selected kinesin members in this study included four members identified through TI analysis (*KIF23*, *KIF15*, *KIF11* and *KIF18B*) and two kinesins (KIF10, KIF11) targeted by drugs studied in clinical trials (**Figure 31**). KIF11 fulfilled both aspects. For the siRNA approach we selected *KIF15, KIF18B*, and *KIF23*, involved in prophase, prometaphase and telophase, respectively. For the chemical inhibition, we used three chemical compounds, ispinesib (Lad et al., 2008), GSK923295 (Wood et al., 2010), and paprotrain (Tcherniuk et al., 2010), to chemically inhibit the kinesins KIF11, KIF10, and KIF20A, which are also involved in prophase, prometaphase and telophase, respectively. Among these compounds, GSK923295 is in clinical phase I and ispinesib is in phase II (reviewed in Rath and Kozielski, 2012).

KIF11 is required for the separation of duplicated centrosomes during spindle formation in prophase (Blangy et al., 1995; Zhu et al., 2005) and KIF15 is required for the maintenance of the spindle (Tanenbaum et al., 2009; Vanneste et al., 2009). KIF10 participates in the microtubule–kinetochore capture during the spindle assembly checkpoint (Yen et al., 1991; Mao et al., 2005; Zhu et al., 2005). KIF18B binds to the microtubule plus end and controls the length of the microtubule (Stout et al., 2011), forming a complex with KIF2C (Tanenbaum et al., 2011). KIF20A and KIF23 are involved in telophase and are essential for cytokinesis (Nislow et al., 1992; Zhu et al., 2005).

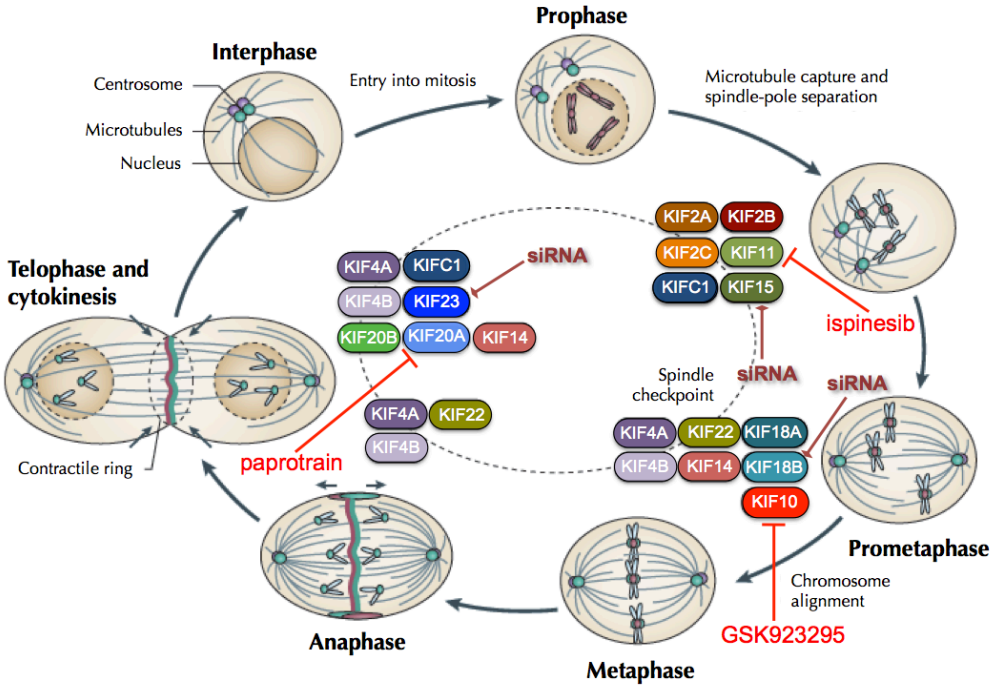

Figure 31. Mitotic kinesins and members selected for the loss of function approach. Kinesins are placed at the stages at which they have been shown to fulfil their mitotic functions. Expression of *KIF15*, *KIF18B* and *KIF23* has been knocked down with siRNA molecules. KIF15, KIF10 and KIF20A have been chemically inhibited with ispinesib, GSK923295 and paprotrain, respectively.

All of these kinesin genes, excluding *KIF18B*, have been found deregulated in some cancers. *KIF11* is overexpressed in chronic myelogenous leukaemia (Nowicki et al., 2003) and pancreatic cancer (Liu et al., 2010). Moreover, it has been shown to be essential for head and neck squamous cell carcinoma (Martens-de Kemp et al., 2013) and more recently, for glioblastoma pathogenesis (Venere et al., 2015). *KIF15* has

been associated to breast cancer (Scanlan et al., 2001). *KIF10* has been found downregulated in hepatocellular carcinoma (Liu et al., 2009) and overexpressed in some breast cancers (Agarwal et al., 2009). Finally, *KIF23* is overexpressed in glioma (Takahashi et al., 2012), and *KIF20A*, in pancreatic cancer (Imai et al., 2011).

3.3. KIF23 is required for the survival and cell cycle progression of MPNST cell lines

The same *in vitro* functional assays used in sections 2.3 and 2.4 assessing cell viability, cell proliferation, cell cycle, cell death and anchorage-independent growth, were used to evaluate the effect of the expression knockdown of *KIF15*, *KIF18B* and *KIF23* in the tumourigenic properties of S462 and T265 cell lines.

First of all, the gene expression knockdown after siRNA transfection was checked by RT-qPCR for the three selected kinesin genes in both S462 and T265. The expression reduction was relevant and significant for *KIF15* and *KIF23* genes, but not for KIF18B. Considering the same criteria than in sections 2.3 and 2.4, *KIF18B* was consequently excluded for the functional genetic assays. The mean expression reduction for *KIF15* considering the two cell lines was of 70%, and for *KIF23* was of 81% (**Figure 32.A**).

KIF23 expression knockdown produced a significant reduction in both cell viability (85% reduction; **Figure 32.B**) and proliferation (25% reduction; **Figure 33.A**) in S462 cell line after 72 hours of siRNA transfection, as well as a cell cycle arrest in G2-M phase (2.2-fold increase in the percentage of G2-M cells; **Figure 33.B**). Increases in apoptosis (2.2-fold increase) and total cell death (2.3-fold increase) were also found, although they were not significant, probably due to the high variability among the biological replicates (**Figure 34**). Moreover, *KIF23* knockdown also significantly abrogated the colony-forming capacity of S462 cell line (86% and 94% reduction in colony number and area, respectively; **Figure 35**).

Similar results were found for the T265 cell line, where nearly all readouts yielded significant differences compared to the NTC treatment: viability (42% reduction; **Figure**

32.B), proliferation (44% reduction; **Figure 33.A**), G2-M arrest (4.2-fold increase in the percentage of G2-M cells; **Figure 33.B**) and apoptosis (3.0-fold increase; **Figure 34.B**).

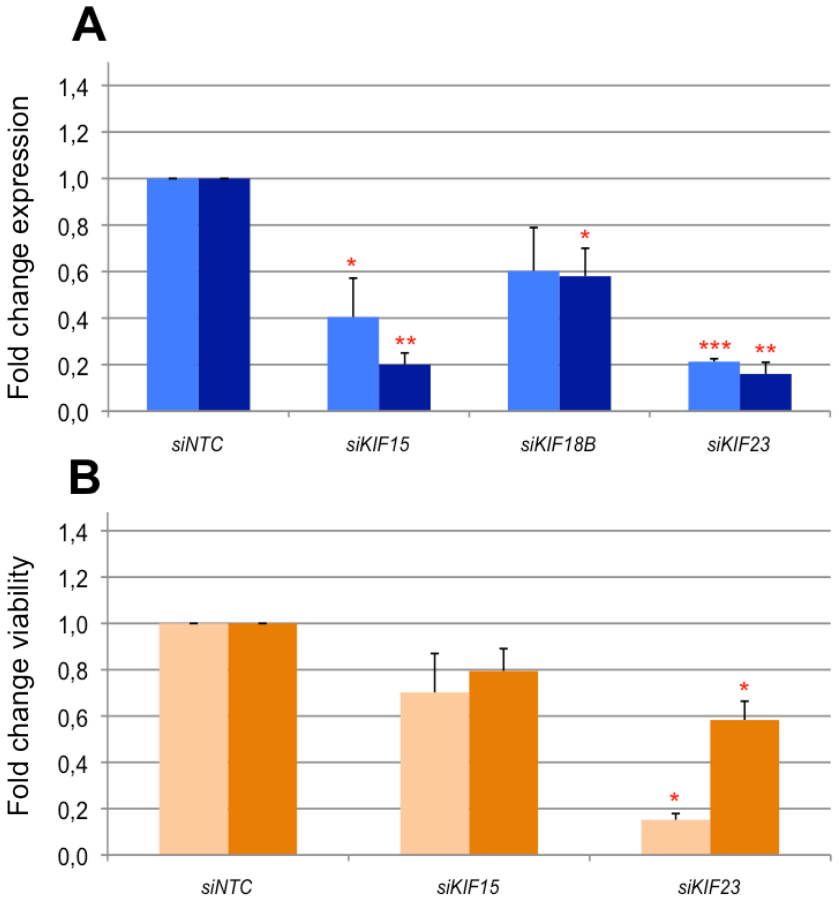

Figure 32. Expression knockdown and cell viability in S462 and T265 cell lines after depletion of kinesin genes. A. Fold change of expression knockdown in S462 (light blue) and T265 (dark blue) 72 hours post-transfection of siRNA pools targeting *KIF15*, *KIF18B* or *KIF23* genes vs. a non-targeting control siRNA (NTC). B. Fold change of cell viability in S462 (light orange) and T265 (orange) 72 hours post-transfection of siRNA pools targeting *KIF15* or *KIF23* genes vs. a non-targeting control siRNA (NTC). Analysis of cell viability by cell counting in S462 and by XTT colourimetric assay in T265. All experiments in A and B were repeated three times. A T-test considering unequal variances was applied. *, $P < 0.05$; **, $P < 0.01$; ***, $P < 0.001$.

In conjunction, these results obtained in both MPNST cell lines support a functional role of *KIF23* in the survival and the cell cycle progression of these cell lines and suggests that *KIF23* could be an important player in MPNST pathogenesis.

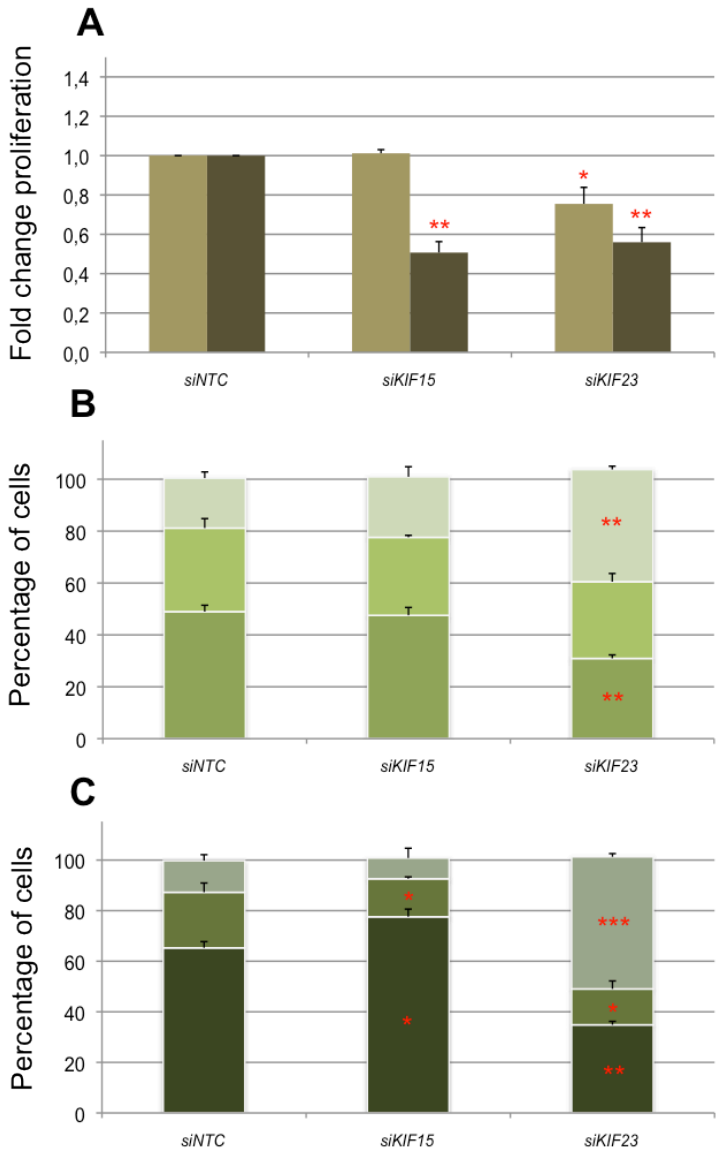

Figure 33. Cell proliferation and cell cycle analysis in S462 and T265 cell lines after expression knockdown of kinesin genes. A. Fold change of the percentage of proliferating S462 (light green) and T265 (dark green) 72 hours post-transfection of siRNA pools targeting *KIF15* or *KIF23* genes vs. a non-targeting control siRNA (NTC). Analysis of EdU incorporation in 10,000 cells by flow cytometry. B, C. Percentages of cells in cell cycle phases G1 (bottom of column), S (middle of column) and G2 (top of column) in S462 (B) and T265 (C) 72 hours post-transfection of siRNA pools targeting *KIF15* or *KIF23* genes vs. a non-targeting control siRNA (NTC). Analysis of propidium iodide staining in 10,000 cells by flow cytometry. All experiments in A and B were repeated three times. A T-test considering unequal variances was applied. *, $P < 0.05$; **, $P < 0.01$; ***, $P < 0.001$.

KIF15 expression knockdown affected most of the *in vitro* tumourigenic properties of T265, but this was not the case for S462. In T265, cell proliferation was significantly reduced in 49% (**Figure 33.A**). In this case, a significant cell cycle arrest in G0/G1 phase was detected (1.2-fold increase; **Figure 33.C**), which also produced significant increases in apoptosis (1.7-fold increase; **Figure 34.A**) and total cell death (1.3-fold increase; **Figure 34.B**).

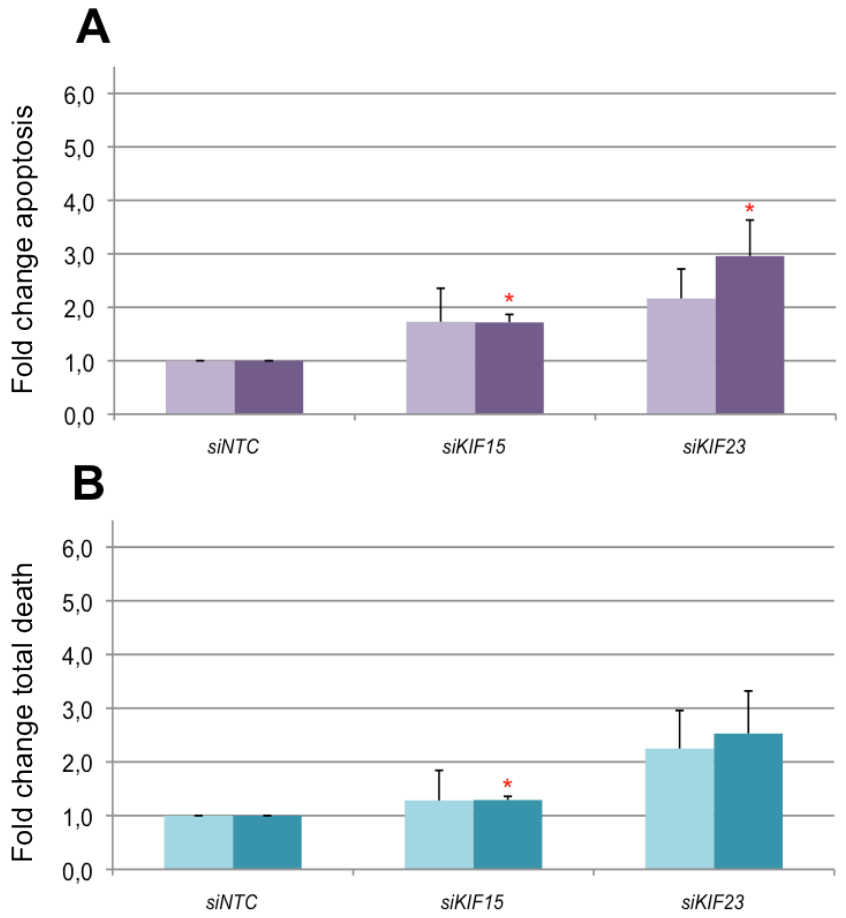

Figure 34. Apoptosis and total cell death in S462 and T265 cell lines after expression knockdown of kinesin genes. A. Fold change of the percentage of early apoptotic S462 cells (light violet) and T265 cells (dark violet) 72 hours post-transfection of siRNA pools targeting *KIF15* or *KIF23* genes vs. a non-targeting control siRNA (NTC). Analysis of Annexin V staining in 30,000 cells by flow cytometry. B. Fold change of the percentage of dead S462 cells (light blue) and T265 cells (dark blue) –considering as dead cells those in late apoptotic or necrosis– 72 hours post-transfection of siRNA pools targeting *KIF15* or *KIF23* genes vs. a non-targeting control siRNA (NTC). Analysis of Annexin V and bisbenzimide co-staining in 30,000 cells by flow cytometry. All experiments in A and B were repeated three times. A T-test considering unequal variances was applied. *, $P < 0.05$; **, $P < 0.01$; ***, $P < 0.001$.

The siRNA transfection targeting *KIF15* caused an expression reduction of 60% in S462 (**Figure 32.A**). However, this had not any remarkable effect in this cell line. According to this, a functional role of *KIF15* in the survival and the cell cycle progression of T265 cell line is suggested.

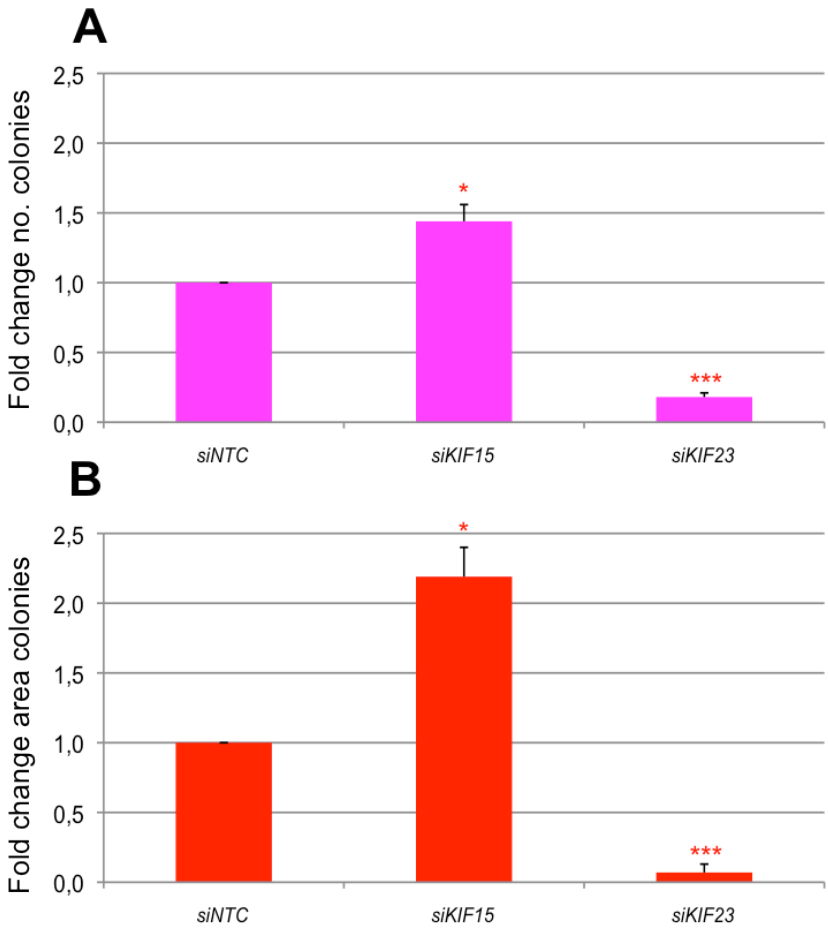

Figure 35. Anchorage-independent growth analysis in S462 cell line after expression knockdown of kinesin genes. A. Fold change of the number of colonies of S462 cells in soft agar 15 days post-transfection of siRNA pools targeting *KIF15* or *KIF23* genes vs. a non-targeting control siRNA (NTC). B. Fold change of the area of colonies of S462 cells in soft agar 15 days post-transfection of siRNA pools targeting *KIF15* or *KIF23* genes vs. a non-targeting control siRNA (NTC). Measurement of both number and area of colonies was performed with ImageJ software. All experiments in A and B were repeated three times (in *CBX8*, six times). A T-test considering unequal variances was applied. *, $P < 0.05$; **, $P < 0.01$; ***, $P < 0.001$.

3.4. Inhibition of KIF11 *and* KIF10 *with ispinesib and GSK923295, respectively, reduces cell viability in a set of MPNST cell lines*

A first screening of a chemical inhibition of the three selected kinesin proteins, KIF11, KIF10 and KIF20A was conducted using the NF1-associated MPNST cell lines T265, S462, ST-8814 and the sporadic STS26T. A primary SC culture from a benign dNF and the CCD-1112Sk human foreskin fibroblast (HFF) cell line were also used as benign and normal control cell lines. All cells were treated with vehicle (DMSO) and 4 concentrations of ispinesib, GSK923295 or paprotrain in a short time course. Cell viability was measured before treatment at 0h, after 24h, and 48h post-treatment using the XTT assay, as in sections 2.3 and 2.4 (**Figure 36**).

MPNST cell lines showed a reduction in cell viability when treated with these kinesin inhibitors, especially for ispinesib and, in a less extent, for GSK923295. In contrast, a mild effect of these drugs was found in the viability of the SC culture and the fibroblast cell line (**Figure 36**). High doses of ispinesib (40 nM and 1000 nM) were cytotoxic after 48h of treatment for all MPNST cell lines, while lower doses (0.064 nM and 1.6 nM) seemed to produce a diverse cytostatic effect among the cell lines, except for STS26T, which showed a dramatic reduction in viability. In the case of GSK923295, only the highest dose (5000 nM) was found to be cytotoxic for all MPNST cell lines and lower doses (0.32 nM, 8 nM and 200 nM) were either cytostatic or did not have a profound effect in cell viability, depending on the cell line. A mild effect of the inhibitor paprotrain was found for MPNST cell lines, which was similar in both the SC and fibroblast control cultures. Only ST-8814 and STS26T showed a remarkable reduction in viability at the highest dose (500 μM).

Taken together, these results support a functional role of KIF10 and KIF11 for the survival of MPNST cell lines and suggests that KIF10, and especially KIF11, could be involved in MPNST pathogenesis.

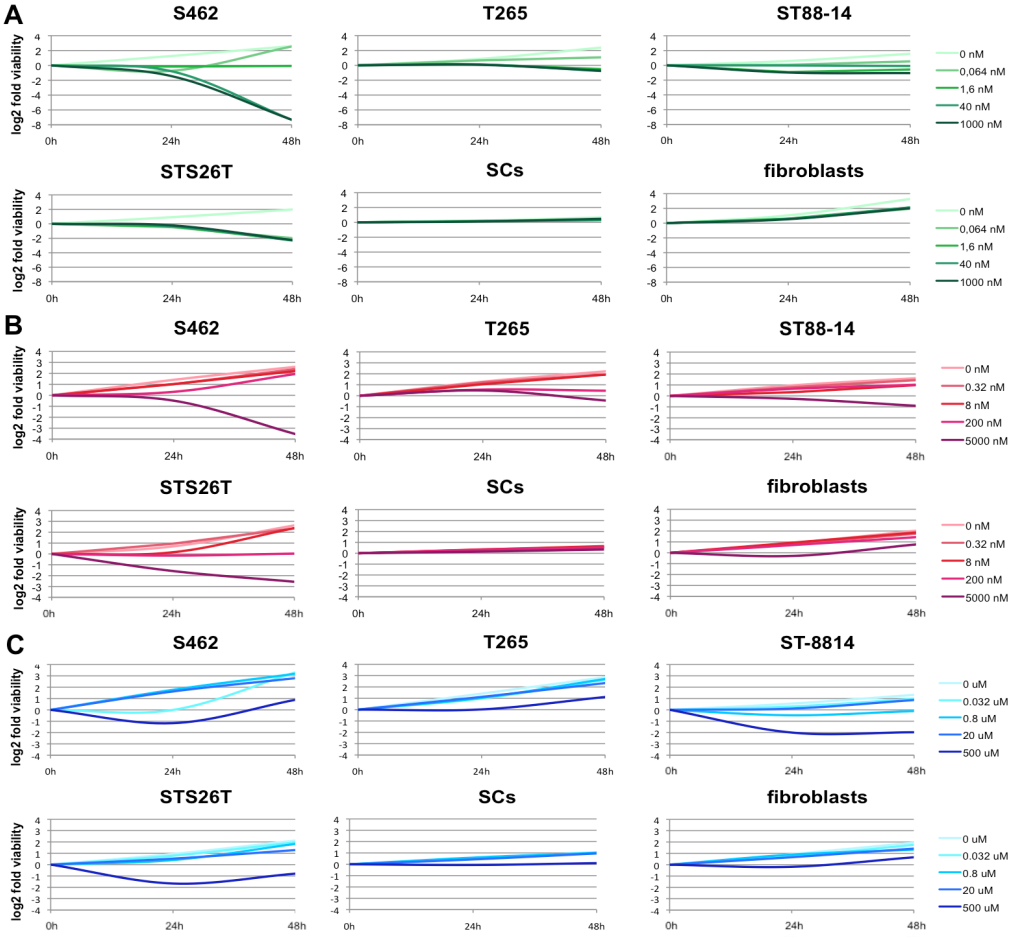

Figure 36. Effects of ispinesib, GSK923295 and paprotrain in MPNST cell lines, SCs and fibroblasts. Log2 fold viability of S462, T265, ST-8814, STS26T, a primary Schwann cell (SC) culture and the human foreskin fibroblast (HFF) cell line CCD-1112Sk at 24h and 48h versus 0h of treatment with different doses of ispinesib (A, green), GSK923295 (B, red) and paprotrain (C, blue). Analysis of cell viability by XTT colourimetric assay.

3.5. MPNST cell lines are more sensitive to ispinesib and GSK923295 than fibroblasts

To better assess the therapeutic potential of inhibiting kinesin function in MPNSTs, the sensitivity to the three kinesin inhibitors was further studied in the MPNST cell lines S462 and T265 and the control fibroblasts. Cells were again treated with vehicle (DMSO) and 4 concentrations of ispinesib, GSK923295 or paprotrain. Cell number was then calculated after 48h of treament by automated cell counting and used for

determining the half maximal inhibitory concentration (IC_{50}) for each compound and cell line. When treated with ispinesib, both S462 and T265 were more sensitive than fibroblasts, with a 4.6-fold decrease and a 7.2-fold decrease, respectively, in the IC_{50} values (**Figures 37.A** and **37.D**). Exposure to GSK923295 also showed a higher sensitivity of S462 and T265 cell lines than the HFFs, with a 1.9-fold decrease and a 1.5-fold decrease, respectively, in the IC_{50} values (**Figures 37.B** and **37.D**). Treatment with paprotrain exhibited a higher sensitivity for this drug for S462 compared to fibroblasts (6.4-fold decrease in IC_{50}), but this was not the case for T265, whose IC_{50} value was even higher than the one from the HFFs (322.7 μM vs. 223.8 μM; **Figures 37.C** and **37.D**). These results are in agreement with those generated in the previous section 3.4 from the XTT viability assay for the same drugs and cell lines.

Both experiments indicated that the MPNST cell lines S462 and T265 are more sensitive to KIF11 inhibition, and in less degree to inhibition of KIF10, than non-transformed SCs or HFFs.

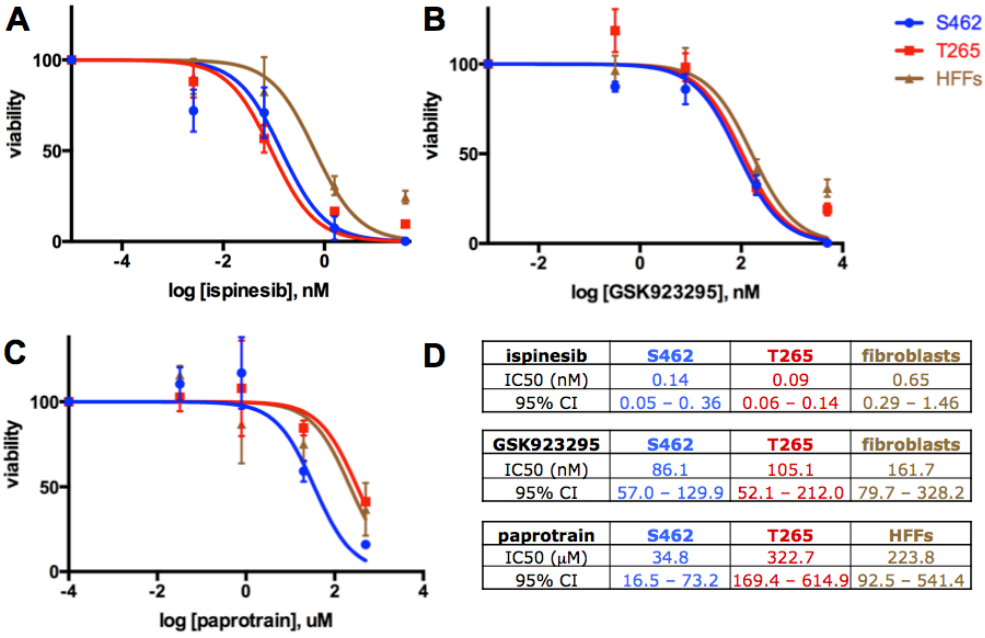

ispinesib	S462	T265	fibroblasts
IC50 (nM)	0.14	0.09	0.65
95% CI	0.05 – 0. 36	0.06 – 0.14	0.29 – 1.46

GSK923295	S462	T265	fibroblasts
IC50 (nM)	86.1	105.1	161.7
95% CI	57.0 – 129.9	52.1 – 212.0	79.7 – 328.2

paprotrain	S462	T265	HFFs
IC50 (μM)	34.8	322.7	223.8
95% CI	16.5 – 73.2	169.4 – 614.9	92.5 – 541.4

Figure 37. Viability curves and IC50 determination of kinesin inhibitors in S462, T265 and fibroblasts. A, B, C. Viability curves of the MPNST cell lines S462, T265 and the control HFFs (CCD-1112Sk cell line) after 48 hours of treatment with ispinesib (A), GSK923295 (B) or paprotrain (C). Log of several concentration points vs. the percentage of viable cells with respect to dose 0 are plotted. Analysis of cell viability by cell counting. D. IC50 values and 95% CI for each compound and cell line was calculated by applying a non-linear regression model curve fitting with the GraphPad Prism 5 software.

Both drugs ispinesib and GSK923295 inhibit the interaction between KIF11 and KIF10, respectively, with microtubules. This blockade prevents the formation of a functional bipolar mitotic spindle and the cell, consequently, dies. In order to check the phenotypic effect of these kinesin inhibitors, the mitotic spindle formation of S462 and T265 was studied by immunofluorescence of α-tubulin after 24h of treatment (**Figure 38**).

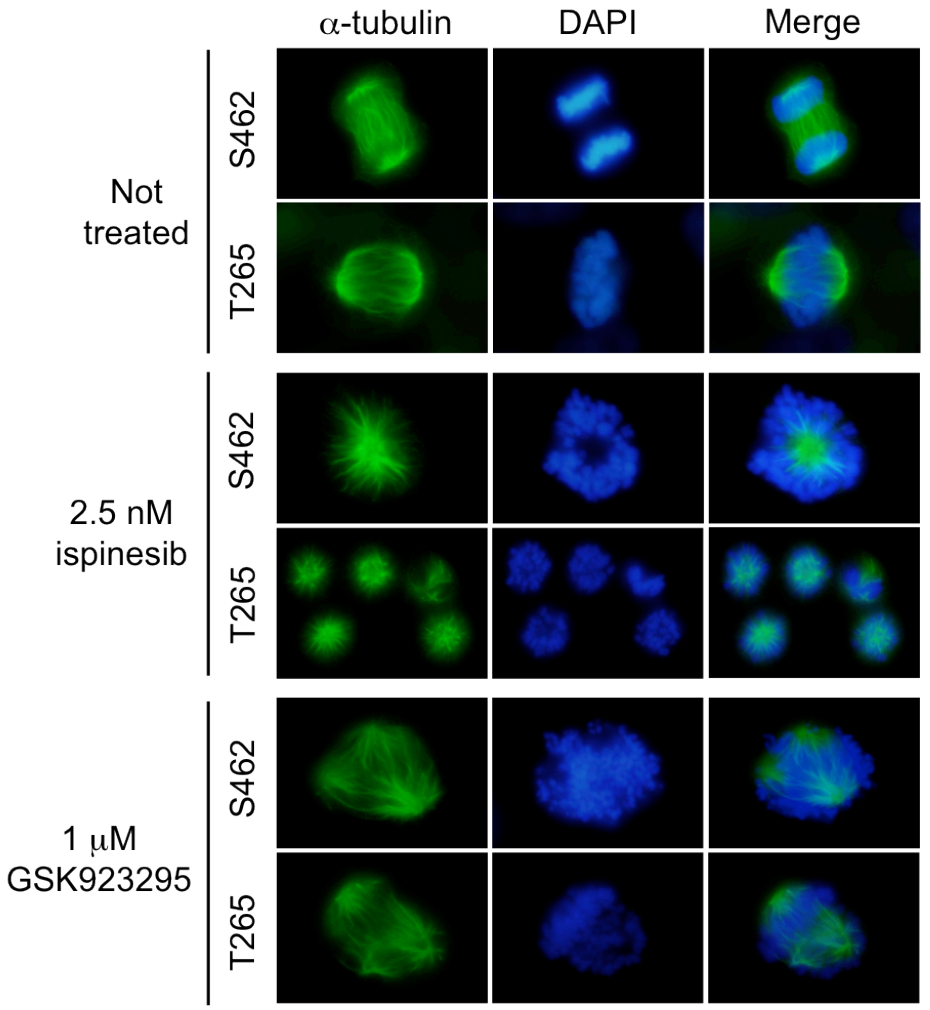

Figure 38. Effect of ispinesib and GSK923295 in the mitotic spindle of S462 and T265 cells. Immunofluorescence of the microtubular protein α-tubulin (green) 24 hours after ispinesib or GSK923295 treatment of S462 and T265 cell lines. Normal functional bipolar spindles were replaced by monopolar spindles, when treated with either ispinesib or GSK923295; or by multipolar spindle, when treated with GSK923295. Nuclei were counterstained with DAPI (blue). Images were taken in a fluorescence-inverted microscope (100x).

Inhibition of KIF11 with ispinesib replaced the functional bipolar mitotic spindles by monopolar spindles, and the alignment of chromosomes at metaphase plate was abrogated in both S462 and T265 cell lines (**Figure 38**), as described elsewhere (Walczak et al., 1998). Inhibition of KIF10 with GSK923295 also replaced the functional bipolar mitotic spindles by a combination of monopolar spindles and multipolar mitotic spindles, as it has been described when *KIF10* is depleted (Brevini et al., 2012), and several chromosomes were placed outside the spindle pole in cluster, as described (Wood et al., 2010). Moreover, both S462 and T265 also showed no alignment of chromosome at metaphase in mitosis when treated with GSK923295 (**Figure 38**).

In conjunction, these *in vitro* results obtained in both S462 and T265 cell lines suggest that KIF11 is a potential therapeutic target for the treatment of MPNST treatment, although more experimental work and an *in vivo* validation is needed to conclude so.

3.6. KIF15 expression knockdown sensitizes S462 cell line to KIF11 inhibition with ispinesib

Both KIF11 and KIF15 kinesins are crucial for a functional bipolar mitotic spindle. KIF11 is involved in the spindle formation (Blangy et al., 1995), while KIF15 participates in the spindle maintenance (Vanneste et al., 2009). However, it has been described that KIF15 can replace all essential functions of KIF11 in the creation of the bipolar spindle (Tanenbaum et al., 2009). Therefore, we wanted to address whether S462 cell line, which did not show to be affected by a *KIF15* expression knockdown, was more sensitive to KIF11 inhibition when the *KIF15* expression was previously depleted. In this experiment, *KIF15* expression knockdown was checked after ispinesib treatment (96 hours post-transfection) and resulted in a significant expression reduction of 49% (data not shown). Then, S462 cells transfected either with a siRNA pool targeting *KIF15* or a NTC were treated with vehicle (DMSO) or 5 doses of ispinesib, ranging from 1 pM to 10 nM. Cell number was calculated 48h post-treatment for IC_{50} determination, as in section 3.5. *KIF15*-depleted S462 cells were more sensitive to ispinesib treatment than cells transfected with a NTC siRNA, with a significant 2.8-fold decrease in the IC_{50} value (**Figure 39**).

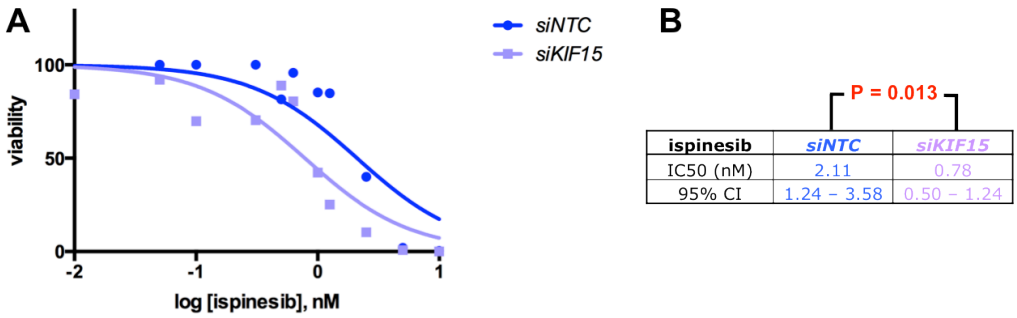

Figure 39. Viability curves and IC50 determination of ispinesib in S462 after *KIF15* expression knockdown. A. Viability curves after 48 hours of treatment with ispinesib of S462 cell line previously transfected with siRNA pools targeting *KIF15* or a non-targeting control siRNA (NTC). Log of several concentration points vs. the percentage of viable cells with respect to dose 0 are plotted. Analysis of cell viability by cell counting. B. IC50 values and 95% CI for ispinesib in *KIF15*-depleted S462 cells and *KIF15*-non depleted S462 cells were calculated by applying a non-linear regression model curve fitting with the GraphPad Prism 5 software. The experimental combination of siRNA transfection plus ispinesib treatment was repeated three times. A paired T-test was applied.

These results show that although *KIF15* expression knockdown does not have an apparent effect in the survival and cell cycle progression of S462, unlike in T265 cell line, *KIF15* depletion conferred S462 to be more sensitive to KIF11 inhibition than when the expression of *KIF15* was not depleted.

In conjunction, these results support a functional role of KIF11 and KIF15 in the survival and the cell cycle progression of MPNST cell lines, and suggest that KIF11 and KIF15 could be also important players in MPNST pathogenesis. Again, although *in vivo* experimental support is required, KIF11 and KIF15 are proposed as potential therapeutic targets for MPNST treatment.

DISCUSSION

1. A novel application of qPCR technique for DNA copy number assessment in the context of NF1

Different techniques, including fluorescence in situ hybridization (FISH), multiplex ligation-dependent probe amplification (MLPA), and array comparative genomic hybridization (aCGH), are currently being used to assess the presence of microdeletions involving the *NF1* locus. More recently, our group and others have proposed next-generation sequencing (NGS) not only for detecting *NF1* point mutations but also deletions of *NF1* exons or the entire *NF1* locus (Pasmant et al., 2015; Castellanos, manuscript in preparation).

qPCR has already been used to assess the copy number status of the *NF1* gene at the constitutional level: a qPCR approach has been developed to validate deletions involving specific exons within the *NF1* gene, previously detected by MLPA (De Luca et al., 2004); and a sequence-tagged site qPCR has been designed to locate the deletion end points of a 7.6-Mb *NF1* constitutional deletion from a neurofibromatosis type 1 (NF1) patient (Pasmant et al., 2008). At the somatic level, a cohort of acute myeloid leukaemia patients has been screened for *NF1* somatic deletions using qPCR (Boudry-Labis et al., 2013), and qPCR has been also used, moreover, to detect low percentages of somatic *NF1* point mutations in cultured Schwann cells (SCs; Maertens et al., 2006b). However, no probe-based qPCR assay has been developed so far to detect and distinguish between the four different types of *NF1* constitutional microdeletions in NF1 patients or to check for *NF1* somatic second-hit deletions in neurofibromas and other NF1 traits.

In addition, some NF1 research groups, including our group, have tried to characterize the copy number of the genome of NF1-associated tumours [dermal neurofibromas (dNFs), plexiform neurofibromas (pNFs) and malignant peripheral nerve sheath tumours (MPNSTs)] and derived samples [Schwann cells (SCs), MPNST cell lines] using several methodologies, such as CGH (Mechtersheimer et al., 1999; Schmidt et al., 2000; Fang et al., 2009), cytogenetic karyotyping (Wallace et al., 2000; Mertens et al., 2000), array CGH (Mantripragada et al., 2008; Beert et al., 2011), and single nucleotide polimorphism (SNP) array (Garcia-Linares et al., 2011; Upadhyaya et al.,

2012; Lee et al., 2014). In MPNSTs, the qPCR technique has been used for validating some somatic copy number alterations (SCNAs) found by array CGH (Mantripragada et al., 2008; Upadhyaya et al., 2012). Nevertheless, qPCR has not been used to prospectively analyze SCNAs in the MPNST genome.

We believed that, given the advantages of the qPCR technique, it was a suitable technique to be used for the characterization of the copy number status of samples in the context of NF1. In this regard, two qPCR assays were developed in this thesis: *NF1*-qPCR, a novel probe-based qPCR assay that detects both *NF1* constitutional and somatic deletions; and another similar qPCR assay, MPNST-qPCR, that detects copy number alterations in the MPNST genome.

qPCR is a reliable technique for the quantification of DNA copy number

qPCR is a highly analytically sensitive, specific, and precise technique that has several advantages over other methodologies. It is cheap and fast. Determining the copy number status of different loci in several samples can be performed in just three hours, including plate preparation, PCR amplification, and data analysis. Detecting copy number changes in samples of DNA extracted with different methodologies and kits or from different tissues and tumours can be challenging for many techniques, such as MLPA. Quantitative PCR, however, is very robust with respect to DNA quality, thereby permitting the screening and comparison of DNA samples from different sources.

Both *NF1*-qPCR and MPNST-qPCR assays require small amounts of DNA: each reaction can be performed in just 8 μL, and only 15 ng per interrogated locus is required. Five nanograms of DNA per PCR reaction have been used, although smaller DNA quantities may be analyzed.

qPCR reactions were highly efficient with large linear dynamic ranges. Moreover, to increase specificity and minimize the false-positive rate, we applied a stringent confidence interval (CI) of 99% to assess for the absence of a copy number change.

In addition, these assays fulfil most of the essential aspects of the MIQE (minimum information for publication of quantitative real-time PCR experiments) guidelines. MIQE

is a set of guidelines that describe the minimum information necessary for evaluating qPCR experiments, allowing more reliable and unequivocal interpretation of qPCR results (Bustin et al., 2009). Our adherence to these criteria strengthens the reliability of the developed qPCR assays and the results obtained. All the information regarding the development, validation and performance of the *NF1*-qPCR assay has been published in *Clinical Chemistry* journal (Terribas et al., 2013; see Annexe 2).

The NF1-qPCR assay accurately detects NF1 constitutional deletions

Most of the *NF1* constitutional microdeletions are directly inherited from the parental germline. When this happens, all cells from the body present one copy of the *NF1* gene deleted. The *NF1*-qPCR assay was used in these cases and enabled the detection of the *NF1* constitutional microdeletions in thirteen blood samples from NF1 patients, including Type-1, Type-2 and atypical microdeletions. The sensitivity and specificity of the assay were near or at 100% when all of the interrogated loci were considered.

The reliable design of the *NF1*-qPCR assay, along with the specific locations of the eleven interrogated loci within the *NF1* region, allow an accurate detection of Type-1, Type-2, and atypical *NF1* microdeletions and are suitable for detecting the rare Type-3 microdeletions. The assay could be expanded, if required, to incorporate more loci for copy number assessment.

The NF1-qPCR assay accurately detects NF1 deletions that occur somatically or in mosaicism

When *NF1* constitutional microdeletions are not inherited directly from the germline and occur post-zygotically, these deletions are present in mosaicism. In these cases not all cells of the body bear the deletion. This is particularly important for Type-2 microdeletions, which are generated by somatic mitotic recombination and can be transmitted to the offspring (Petek et al., 2003). Moreover, *NF1* somatic second-hit deletions are found in ~10% of dNFs (Garcia-Linares et al., 2011), and in a similar manner, not every cell from the dNF presents a deletion of the *NF1* gene.

Because in both cases the *NF1*-deleted cellular component is not total, we wanted to also apply the *NF1*-qPCR assay for detecting *NF1* deletions in these contexts. Thus, the performance of the qPCR assay in admixtures of *NF1*-deleted and *NF1*-nondeleted DNA samples was studied.

The *NF1*-qPCR assay enabled the detection of a Type-2 microdeletion in the context of mosaicism in one blood sample, and somatic deletions in twenty-one samples, including dNFs and SCs, which contained less than 56% of *NF1*-nondeleted cells. Considering somatic deletions, the specificity of the assay was close to 100%. The sensitivity was around 90% because there were some false negative results: the qPCR assay detected in some dNFs two copies for a few loci that were, in fact, deleted. However, the presence of a deletion event in these dNF samples was considered because most of the deleted loci within the 2.8-Mb *NF1* region in that samples were detected as single copies.

In conclusion, the NF1-qPCR assay allows an accurate identification of *NF1* deletions in constitutional samples, and other NF1 traits that require the double inactivation of the *NF1* gene, when the deletion is present in at least 44% of the tissue sample. This qPCR assay is ready to be incorporated into a genetic-testing setting as a useful diagnostic tool, either as a first screening step or as a validation technique for *NF1* microdeletions (approximately 5% of NF1 cases) and also for the detection of somatic deletions in NF1 traits, such as dNFs, pNFs or café-au-lait macules (CALMs).

The MPNST-qPCR assay is a reliable tool to detect SCNAs in the MPNST genome

Similarly to the fact that not all the cells from a dNF or other NF1 traits are bearing the *NF1* somatic deletion, when detecting SCNAs in MPNST samples, not all the cells present in the tumour are genomically altered. This is particularly important during tumour sampling, where some normal diploid cells from surrounding tissue can be also removed together with the tumoural ones. In addition, some stromal cells from the tumour are also diploid. Moreover, and most importantly, MPNST genomes are hyperploid and present several chromosomal alterations, with many genomic gains

and also some losses. Hence, the detection of copy number changes in these tumours by qPCR can be challenging if all these factors are considered, as it is for other DNA-based techniques.

Requirement for a thorough normalization of copy number data, especially in genomically altered tumours

Inappropriate normalization of expression data in RT-qPCR experiments has been thoroughly discussed during the last years, claiming that reference gene validation is essential to ensure accurate and reliable gene expression results (Vandesompele et al., 2002; Nolan et al., 2006; Bustin et al., 2009; Jacob et al., 2013; Hellemans and Vandesompele, 2014). However this concern has barely been applied for the normalization of DNA copy number data from qPCR experiments in highly aneuploid genomes presenting copy number alterations. For instance, two studies using qPCR for validating SCNAs found in MPNSTs by aCGH have been published so far (Mantripragada et al., 2008; Upadhyaya et al., 2012), but information on the normalization process was insufficient or inexistent.

Some expressed repetitive elements, such as expressed Alu repeats, have been recently shown to improve normalization of expression data when using RT-qPCR in tumours (Rihani et al., 2013) and other samples (Marullo et al., 2010; Vossaert et al., 2013; Vanhauwaert et al., 2014). Other repetitive sequences, long interspersed nuclear elements (LINEs), present in high number in the genome, have been used for normalization of DNA copy number data in two studies comparing qPCR with digital karyotyping for the assessment of copy number alterations in cancer cell lines (Wang et al., 2002; Wang et al., 2004). In these studies it was suggested that the copy number values per haploid genome of these repetitive element are similar among all human cells, either normal or tumoural.

Hence, in the development of the MPNST-qPCR assay, the average of the relative quantities (RQ) of the two LINE repetitive genomic sequences, the LINE1 consensus sequence, *L1*, and the family consensus sequence, *L1PA*, were found to be the most suitable normalization factor (NF) for the normalization of copy number data. We demonstrated that the utilization of repetitive sequences as reference genes in

samples with aberrant genomes, as our set of MPNSTs, was more precise than using single genes, according to the value obtained from the gene stability *M* (Vandesompele et al., 2002). The only combination that yielded an *M* value below 0.2, as it has been proposed for DNA copy number (D'Haene et al., 2010), was the combination of the two LINE sequences. Moreover, when single genes are used for normalization purposes, misleading results can be generated, as we showed for *AURKA* copy number in MPNST samples (see **Table A.3**). In this regard, we also encourage the use of multiple loci for DNA copy number normalization in aneuploid genomes, as suggested by others (Rosenberg et al., 1997; Fang et al., 2011).

Limitations of copy number assessment in hyperploid genomes by qPCR and other DNA-based techniques

Some limitations of qPCR, shared by other methodologies for DNA copy number assessment – such as SNP array or CGH – should be considered when dealing with DNA samples coming from hyperploid genomes, as for MPNSTs. These DNA-based techniques calculate the copy number of a particular locus with respect to the general ploidy of the studied sample. Since the mean ploidy of a sample is generally assumed to be diploid (2N), there is a bias when determining the copy number status of a particular locus of the sample. This effect can be partially overcome by applying some algorithms that compensate for the ploidy of the sample, like ASCAT for the analysis of SNP array data (Van Loo et al., 2012), although this cannot be completely controlled. So, for a particular amount of DNA from a hyperploid genome, some genomic gains would not be detected and some genomic losses would be detected as so being not real deletions. In other words, in samples with hyperploid genomes the MPNST-qPCR can generate both false negative results of genomic gain events and false positive results of deletion events (see **Table 7**).

Consequently, when normalizing copy number data in hyperploid tumours using qPCR, CGH or SNP array techniques, this bias should be taken into account, and either use the correct algorithm to correct for the ploidy or be aware of this bias when interpreting copy number results. This drawback could be overcome if working with a particular and precise number of cells instead of a given DNA quantity. However, when working with

tumours and other tissues this can be challenging, as the number of cells present in a particular amount of tissue can differ among tissue types. Moreover, some tumours can also show tumour heterogeneity and a proportion of normal cells with a diploid genome.

Copy number gains and losses in MPNSTs are detected by the MPNST-qPCR assay

Despite of these limitations, the design of the MPNST-qPCR assay allowed the detection of copy number gains of the *AURKA* locus in our set of MPNSTs and derived cell lines, and an association with the high *AURKA* expression values found in an independent set of MPNST samples was suggested (Patel et al., 2012). Moreover, this qPCR assay also permitted to find a significant association between four TIs of overexpression with genomic gains, and between four TIs of underexpression with genomic losses in our set of MPNSTs. These results were later confirmed for the global sets of TIs and SCNAs by the regioneR tool.

2. Transcriptional imbalances: how they are generated and what information they contain

Using genomic regional information as part of our integrative biology approach

In our research group we are interested in finding genes and molecular mechanisms driving the development, progression and maintenance of MPNSTs. In order to do so, an integrative biology approach has been conceived considering both information at the single gene level and regional genomic information. This approach includes a thorough characterization of a set of MPNSTs and derived samples including genome-wide expression data, data coming from genomic structural analysis, epigenetic data from DNA methylation, and a collection of point mutations from whole-exome sequencing.

So far, among the mutational spectrum of the known drivers of MPNST pathogenesis, somatic point mutations have only been found in some tumour suppressor genes (TSGs), such as *NF1*, *TP53*, *SUZ12* and *EED* (see Introduction, sections 6.1 and 6.2). These genes are also frequently deleted and other drivers – such as the TSG *CDKN2A* and oncogenes from the EGFR family receptors – are mainly mutated by genomic alterations rather than point mutations (see Introduction, section 6.1).

As part of our integrative biology approach, a whole-exome sequencing analysis is also being performed in order to check the mutational status of the known MPNST drivers and especially for the identification of possible novel drivers of MPNST pathogenesis. However, in this thesis, the gene point mutational status has not still considered and a first focus on regional genomic information, especially at the transcriptomic level, has been intended following two premises: the distinctive hallmark that differentiated pNFs from MPNSTs is that MPNSTs contained highly altered and hyperploid genomes with recurrent SCNAs, and gene expression is closer to gene function that genomic copy number. The use of this regional information for the identification of novel candidate genes for the pathogenesis of NF1-associated MPNSTs is proposed.

Confirmation of CDKN2A loss as an early event in MPNST tumourigenesis

The molecular characterization of the genome of our set of pNFs has confirmed that *CDKN2A* genomic loss is an early event in the progression of pNF to MPNST. One of the eight pNFs analyzed, diagnosed as an atypical pNF, showed an homozygous loss of this locus, as it has been described in an elegant study demonstrating that *CDKN2A* loss is an early event in the malignant progression of atypical pNF to MPNST (Beert et al., 2011). Moreover, *CDKN2A* locus is also deleted in five of the eight MPNSTs analyzed by SNP array.

Confirmation of a hyperploid genome and recurrent SCNAs in MPNSTs

All the studies published so far using DNA-based methodologies for the analysis of the genome of NF1-associated tumours have evidenced that, in general, both dNFs and

pNFs do not present recurrent structural aberrations in their genome, beyond those found in 17q11.2 region due to *NF1* double inactivation (Mantripragada et al., 2008; Garcia-Linares et al., 2011; Beert et al., 2011). However, MPNSTs present a high degree of genomic instability and frequently altered genomic regions have been identified in these tumours (see Introduction, section 6).

MPNSTs are very aggressive soft-tissue sarcomas. There are three types of sarcomas according to the degree of genomic stability: translocation-associated sarcomas with few copy number alterations, an intermediate category characterized by few but highly recurrent amplifications, and a group with highly complex genomes (Taylor et al., 2011). MPNSTs seem to fall in this last category, as they are highly hyperploid tumours characterized by the occurrence of many chromosomal aberrations.

The molecular characterization of the genome of our set of NF1-associated MPNSTs has confirmed this hyperploid genome, being globally nearly triploid. In addition, the recurrence of some SCNAs has also been corroborated: the most frequent genomic gains were found in chromosomes 2, 7, 8, 15q and 17q22-25, as it has also described elsewere (see **Table 12**), and the most frequent genomic losses were present in 9p, 11q, 17p and 17q11.2-12, which it has also been previously found (see **Table 12**).

No. of MPNSTs	Method-ology	Genomic gains	Genomic losses	Reference
8	CGH	**2p22-p23**, **7p, 7q31-qter, 8q13-qter**, 9p, 9q22-q33, 12p, 12q12-q23, **15q, 17q22-qter**	1p, 9q12-q21, 13q21-q22, **17p**	Schmidt et al., 1999
6	CGH	1q, 5p, **7**, **17q21-25**	1p22p31, **11q14-22**, 13q21-22, 18q	Mechtersheimer et al., 1999
14	CGH	**7, 8q, 15q** and **17q**	**17p**	Schmidt et al., 2000
7	aCGH	1q, **8p**, 9q and **17q**	**9p22.3-p21.2**, 11p13, **11q**, 14q21.3-q23.3	Kresse et al., 2008
24	aCGH	1q25, 3p26, 3q13, 5p12, 5q, 6, **7**, **8q22-q24**, 14q22, and **17q21-q25**	1p, **9p21.3**, 10q25, **11q22-23**, **17q11** and 20p12.2	Mantripragada et al., 2009
23	aCGH	4, **7**, 8q, 12, **15**, **17q**	1p, 4q, **9p**, 10, **11,** 13, **17p**, 18, 22	Beert et al., 2011
15	SNP array	**2p**, 5p, **7**, **8q**, **15q**, **17q**, 18q	1p, 10q, **11q**, **17q11.2-12**, 18	Upadhyaya et al., 2012
8	**SNP array**	**2, 7, 8, 15q, 17q22-25**	**9p, 11q, 17p, 17q11.2-12**	**this thesis**

Table 12. Recurrent SCNAs found in NF1-associated MPNSTs. Information on the main SCNAs found in MPNST samples from NF1 patients (a total of 105 samples from 8 independent studies) by CGH, aCGH or SNP array, including those SCNAs found in our set of NF1-associated MPNSTs by SNP array (last row in bold). Gained and lost genomic regions from the other 7 studies that were coincident with the SCNAs found in our set of MPNSTs are highlighted in bold.

Moreover, some of the SCNAs we found in the MPNST cell lines, such as the genomic gains in 17q and the copy number losses in 9p and 12q, have also been described (Fang et al., 2009).

Global gene expression from MPNSTs is influenced by the genomic copy number in a regional manner: generation of transcriptional imbalances

An association between SCNAs and the expression changes of the genes encompassed in these altered regions has been described in different cancer types, although the number of these studies is limited (see Introduction, section 8). This direct relationship between DNA copy number changes and gene expression has allowed the identification of cancer driver genes in SCNAs and also expression signatures that have been correlated with these altered regions (Akavia et al., 2010; Huang et al., 2012). In this regard, several integrative methodologies of SCNAs and gene expression data have been developed (reviewed in Huang et al., 2012).

In NF1 research, these studies have been restricted to individual genes and copy number alterations of some known drivers of MPNST pathogenesis have been associated with changes in the expression levels of these single genes in the MPNST genome, such as in *CDKN2A* (Berner et al., 1999; Nielsen et al., 1999; Perrone et al., 2003; Tajima and Koda, 2015), *EGFR* (Holtkamp et al., 2008; Tabone-Eglinger et al., 2008; Perrone et al., 2009; Du et al., 2013), *PDGFRA* (Holtkamp et al., 2006; Perrone et al., 2009; Zietsch et al., 2010), *IGF1R* (Yang et al., 2011), and other receptor tyrosine kinases (RTKs; reviewed in Katz et al., 2009). Moreover, some recently described candidate drivers can also be included, such as *BIRC5* (Storlazzi et al., 2006; Kresse et al., 2008; Ghadimi et al., 2012b; Alaggio et al., 2013; Kolberg et al., 2015), *AURKA* (Patel et al., 2012; Mohan et al., 2013) and *TOP2A* (Skotheim et al., 2003; Kresse et al., 2008; Kolberg et al., 2015). In addition, comparative transcriptomic analyses using MPNSTs, MPNST cell lines, benign neurofibromas and derived SCs have been performed and some candidate driver genes of MPNST tumourigenesis have also been proposed, such as *TWIST1* (Miller et al., 2006), *SOX9* (Miller et al., 2009), *EYA4* (Miller et al., 2010), *miR-34a* (Subramanian et al., 2010), *AURKA* (Patel et al., 2012), *MEK* (Jessen et al., 2013) and *MAF* (Brundage et al., 2014).

In this thesis, we describe for the first time that global gene expression from MPNSTs is influenced by DNA copy number changes in a regional manner. Genomic copy number data were generated from a set of NF1-associated MPNSTs and derived cell lines and some SCNAs were identified with the analysis of SNP array experiments with ASCAT. Moreover, the differential expression from MPNSTs vs. neurofibromas in an independent set of samples was used to identify regions of the MPNST genome, known as transcriptional imbalances (TIs), where the mean differential expression was significatively higher or lower than expected by chance, presenting a significant abundance of over- or underexpressed genes in MPNSTs compared to their expression in benign tumours (pNFs and dNFs). TIs were also identified in MPNST cell lines using differential expression from another independent set of MPNST cell lines and primary neurofibroma-derived SC cultures. The use of the regioneR tool with SNP array results, and in a less extent, the analysis of MPNST-qPCR results, showed a significant association of TIs and SCNAs in MPNSTs, especially for TIs of overexpression and copy number gains. These results are robust, as long as two independent sets of samples (DNA copy number assessment from our set of tumours and differential expression analysis from samples of the NF1 Microarray Consortium; Miller et al., 2009) were used for determining the association of TIs with SCNAs.

Considering the results obtained with regioneR, we propose that during the process of MPNST tumourigenesis, the formation of TIs of overexpression could be explained by the selection of regions of the MPNST genome exhibiting recurrent copy number gains; whereas the formation of TIs of underexpression could be in turn explained by a combination of a selection of regions that, within the hyperploid MPNST genome, are either maintained as not changed or lost in terms of copy number.

Regional epigenomic silencing could be contributing to the generation of TIs of underexpression

We also studied the differentially methylated genes between MPNSTs and benign neurofibromas in a regional manner: the main results from regioneR analysis indicated a significant enrichment of differentially hypermethylated genes in TIs of underexpression in MPNSTs. Moreover, this association was found to be stronger for

those hypermethylated genes present in TIs not overlapping with copy number losses. This result suggests the possibility that TIs of underexpression could be associated with different phenomena, either with copy number losses or with regions with no change in copy number and enriched in epigenetic modifications, generating a regional genomic silencing.

Different possibilities could explain this possible regional epigenetic silencing associated to TIs of underexpression. It has been shown that some epigenomic mechanisms, such as long-range epigenetic silencing (LRES), could be the underlying cause of the inactivation of the gene expression of a large genomic region (Frigola et al., 2006; Coolen et al., 2010). In this regard, we have also performed ChIP-on-chip experiments to check the global levels of the three LRES-associated histone marks H3K27me3, H3K9me2 and H3K9ac in the two MPNST cell lines S462 and T265. We are currently analyzing these results and planning to check, by using regioneR, whether there is an association of TIs from MPNST cell lines with these histone marks in a regional manner.

Another possibility would be that these regions enriched in hypermethylated genes reflect the epigenetic status of the cell originating an MPNST. The cell-of-origin of an pNF is still an open debate (Buchstaller et al, 2012). However, experiments in genetically engineered mice (GEM) models point to a SC precursor in the lineage from neural crest to committed SC (Chen et al., 2014). MPNSTs could represent a clonal expansion of these progenitor cells, only present in a low percentage in pNFs, which retain some stem cell properties, including those epigenetic mechanisms involved in self-renewal and cell identity. In this regard, TIs of underexpression enriched in hypermethylated genes could also be interpreted as signatures of cancer stemness at an epigenetic level, as it has been shown for other tumour types (reviewed in Hernandez-Vargas et al., 2009).

Whether our results are compatible with LRES, epigenetic signatures of cancer stemness, or probably with a combination of both, needs to be better experimentally addressed to conclude so.

TIs mainly represent signatures of passenger gene expression

After showing the association of TIs with SCNAs in MPNSTs, we wanted to focus on understanding what a TI was and what kind of information was capturing. We wondered if all the differential expression contained in TIs was relevant to MPNST pathogenesis. To answer this question we selected a TI encompassing a described candidate driver of MPNST pathogenesis, *BIRC5*, and functionally dissected this TI by studying other overexpressed genes within this TI.

The RNAi functional *in vitro* genetic approach together with the physiological readouts studying the viability, proliferation, death and anchorage-independent growth of the MPNST cell lines S462 and T265 confirmed *BIRC5* as a gene involved in MPNST pathogenesis (Ghadimi et al., 2012b). In contrast, this genetic approach showed that the other studied genes present in the same TI (i.e. *NUP85*, *TK1*, *CBX4* and *CBX8*) had not a remarkable effect in the assessed tumourigenic properties of these cell lines, when their expression was depleted. At least, when any of these genes was depleted and considering all readouts in both cell lines, their tumourigenic properties were not as compromised as when *BIRC5* was knocked down. So, although these genes are also differentially overexpressed in MPNSTs compared to benign neurofibromas and present in genomically gained regions, they seem not to be essential for the studied MPNST cell lines.

According to these results, the overexpression of these four studied genes *NUP85*, *TK1*, *CBX4* and *CBX8* would be passenger regarding MPNST pathogenesis, unlike *BIRC5* overexpression, which seems to be driver. Although only one TI has been functionally dissected to conclude so, we suggest that TIs found in MPNSTs would capture expression changes produced mainly by genomic copy number alterations (and maybe by regional epigenomic mechanisms) affecting large regions of the genome. Our hypothesis is that these regions include the gene (or genes) that are responsible for the acquisition of tumourigenic properties as long as they undergo a gain or a loss of function caused by the copy number alteration. However, these selected genes may represent a minority in these genomic regions and most of the other neighbouring genes within the region would also change in expression because of the regional change but without a major functional implication. In consequence,

analogously to the fact that not all genes present in SCNAs are important for the pathogenesis of a tumour type (Beroukhim et al., 2010), TIs would mainly represent signatures of passenger gene expression containing only a few genes relevant for MPNST pathogenesis, as it has been suggested in a similar way for head and neck squamous cell carcinoma (Masayesva et al., 2004) and colorectal cancer (Tsafrir et al., 2006). We also highlight that when studying differential expression in tumours with genomes governed by large SCNAs, a consideration of these regional effects can help in a better selection and interpretation of this expression in the context of tumoural pathogenesis.

Genomic alterations with a regional impact on gene expression: an easy way to identify candidate drivers of MPNST pathogenesis?

According to our hypothesis, most of the gene expression contained in TIs would be passenger and not related to tumour pathogenesis, and only one or a few genes within TIs would be relevant to MPNST pathogenesis.

Thus, TIs would represent a transcriptional impact produced by genomic (or epigenomic) phenomena in a regional manner. Despite of the fact that only one or few genes within each of these regions may have an important effect in MPNST pathogenesis, we believe that TIs can help in the identification of these genes, as TIs reduce the size of the altered genomic region (**Figure 40**).

In this regard, if we consider the genomic location of candidate driver genes that have already been functionally involved in MPNST pathogenesis, most of the TSGs – such as *CDKN2A*, *TP53*, and *PTEN* – are present in TIs of underexpression associated to genomic copy number losses in MPNSTs (**Figure 40**). In the case of the candidate oncogenes that have also showed a role in MPNST pathogenesis, including RTKs, their ligands and others, the majority are associated to genomic gains, being also some of them present in TIs of overexpression, such as *MET*, *NRG1* or *CXCR4*. Other candidate oncogenes are in TIs of underexpression, such as *ERBB2* or *TOP2A* (**Figure 40**).

Figure 40. Karyoplot showing TIs and SCNAs found in MPNSTs and the genomic location of genes with a described role in MPNST pathogenesis. A karyogram showing the idiograms of the 22 human autosomes with G-banding pattern is depicted. Above the chromosomes: red and green boxes represent, respectively, the TIs of overexpression and the TIs of underexpression identified in MPNSTs. Below the chromosomes: the red line represents the number of MPNSTs from our set with genomic gains at that locus; the green line represents the proportion of MPNSTs with genomic losses at that locus. The space between the two lines and colour-filled shows the number of tumours with a SCNA at that locus: a red area indicates a higher proportion of genomic gains; a green area indicates a higher proportion of genomic losses. Green names are the candidate driver TSGs with a described functional role in MPNST pathogenesis, which are placed at their location in the genome: most of them are present in TIs of underexpresssion. Red names are the candidate oncogenes with a described functional role in MPNST pathogenesis, which are placed at their location in the genome: some of them are present in TIs.

When considering TIs for the identification of candidate drivers of MPNST pathogenesis (**Figure 21**), a previous knowledge of cancer genes, putative drivers of other tumour types, together with the overexpression status of these genes in MPNST

cell lines were the two major constraints when selecting candidates within TIs of overexpression. After gene selection, the effect of the expression knockdown of the cancer-associated genes *CAD*, *EPHA4*, *BUB1, MYBL2* and *HOXA13* in the tumourigenic properties of S462 and T265 cell lines was studied.

Among these genes, only the transcription factor MYBL2 and the enzyme CAD showed to have a role in the cell survival and cell cycle progression of the studied MPNST cell lines, suggesting that they could be also contributing to MPNST pathogenesis. However, as these results were not as consistent as the effect of *BIRC5* depletion in these cell lines, we point to *MYBL2* and *CAD* not to be candidate drivers of MPNST pathogenesis.

Although the number of genes analyzed is low and our experimental model is limited (as discussed below), our results indicate that previous knowledge of cancer genes associated to other tumour types seem not to provide valuable information for the identification of driver genes within TIs. If we assume that TIs of overexpression must contain at least one driver that can be functionally identified with the tumourigenic properties studied in S462 and T265 cell lines, a previous information on known drivers of other cancers have not helped in the identification of drivers of MPNST pathogenesis and, consequently, other genes present in these TIs may be the true drivers. So, considering the information of being a driver cancer gene contained in a TI would not be that useful when identifying candidate driver genes of MPNST pathogenesis.

TIs capture unique information that helps to identify genes and molecular mechanisms involved in MPNST pathogenesis

When we observed what was the differential expression of the genes within TIs or the genes placed contiguously to TI boundaries, we identified some genes whose differential expression was in an opposite direction than the differential expression of most of their neighbouring genes (i.e. we found differentially overexpressed genes in or flanking TIs of underexpression and differentially underexpressed genes in or flanking TIs of overexpression; **Figure 26**).

These are genes whose expression would be regulated independently from the regional genomic alteration, so as many other genes located along the MPNST genome. We hypothesized that their expression could be related to a physiological adaptation of the tumoural cell to a new altered state. This kind of genes could be distributed all over the genome. However, TIs are able to trap some of these genes, thus providing this unique information. We believed they could be considered as representatives of pathways and molecular mechanisms where they participate and we wondered if they were involved in MPNST pathogenesis. Since the expression of these genes would be mainly regulated by the physiological state of the tumour cell and independently from SCNAs, they would not be genes driving MPNST tumourigenesis but they could be in part participating somewhat in pathways and molecular mechanisms relevant for MPNST pathogenesis. Hence, some of them may represent candidates for MPNST pathogenesis.

Considering this unique information provided by TIs for the identification of candidate genes involved in MPNST pathogenesis, we first performed a selection of candidate genes that fulfilled to be overexpressed within or flanking TIs of underexpression and to be also overexpressed in MPNST cell lines. Secondly, we studied the effect of the expression knockdown of the selected candidates, *LHX8*, *CDCA8*, *BCAT1*, *CCDC8* and *GINS2* in the tumourigenic properties of S462 and T265 cell lines.

Among the studied genes, two of them, *CDCA8* and *CCDC8*, are both related to *BIRC5*: CDCA8 as a partner of BIRC5 forming the chromosomal passenger complex (CPC), and CCDC8 as an indirect activator of BIRC5 function. These two genes showed to be required for cell survival and cell cycle progression in MPNST cell lines, indicating a possible contribution to MPNST pathogenesis. A possible contribution of *LHX8* is also suggested according to our results. LIM homeobox member LHX8 has not been related to cancer so far (Wang et al., 2014a), so in this thesis some preliminary data on a potential tumourigenic role for *LHX8* have been shown. Although the number of genes analyzed was again low and our experimental constraints must be considered (see below), with this approach we have identified at least two genes as candidates for MPNST pathogenesis. This suggests that the use of the differential gene expression status together with the unique information provided by TIs was helpful when identifying genes candidates for MPNST pathogenesis.

Limitations of our experimental approach when identifying candidate drivers of MPNST pathogenesis

Our experimental framework presented some limitations that must be considered for an appropriate interpretation of the results. First, only *in vitro* experiments with two MPNST cell lines were performed. Information on protein levels from primary MPNST samples and an *in vivo* validation in mice models of the discovered candidate genes are mandatory before reaching conclusions on their real implication in MPNST pathogenesis. Secondly, both S462 and T265 cell lines are two *in vitro* representative models of MPNSTs but some of their tumourigenic properties could have been acquired during their establishment or as a result of their consecutive passages in cell culture over time, providing some experimental noise. Third, the several physiological readouts studied on these cell lines included important tumourigenic properties, which can be globally integrated as the study of the cell survival as a surrogate of the tumour maintenance. However, other readouts, such as cell migration or invasion, which would be related to the metastasic properties of MPNSTs, were not studied. Lastly, only overexpressed genes in MPNSTs associated to TIs have been considered and their loss-of-function has been studied. For a global picture on how informative TIs can be when searching drivers of MPNST pathogenesis, underexpressed genes in MPNSTs should also been studied using gain-of-function approaches. Hence, all the results generated from this candidate search approach should be contemplated as a first round of screening and, consequently, a further experimental characterization of these genes would be needed to describe them as true drivers of MPNST pathogenesis.

These experimental limitations have leaded us to reconsider what is needed for characterizing the funtion of a gene in order to determine that it is really involved in MPNST pathogenesis. Cancer driver genes are defined as those genes carrying mutations that are causally implicated in oncogenesis, conferring a growth advantage and being positively selected during tumourigenesis (Stratton et al., 2009). In our understanding, the genes that are drivers of MPNST pathogenesis are those that are mutated by genetic or epigenetic alterations and are required for the development of an MPNST from a preexisting pNF (in the case of NF1-associated MPNSTs), the maintenance of their tumourigenic properties (survival, proliferation, apoptosis

avoidance, anchorage-independent growth) or the acquisition of metastatic properties (migration, invasion and colonization of distant organs). Hence, a mutation in a driver gene is essential for one of these stages of tumour progression to occur but not necessarily for the others.

We believe that the tumourigenic properties of a particular tumour are composed by genetic and epigenetic alterations (including SCNAs, point mutations, hypermethylation of gene promoters, etc), which represent driver mutations, but also by changes in the cell physiology arising by an adaptation to the new tumoural state. These two components are tangled and it is a challenging task to distinguish between genes that drive the development, maintenance and acquisition of metastatic properties of a malignant tumour and those genes that are essential (althought not being mutated in the genome) for the maintenance of these tumourigenic properties. We have particularly focused on searching genes that are involved in MPNST maintenance (including driver genes and other genes that are required), as we have assessed *in vitro* the role of a list of candidate genes in cell viability, proliferation, death and anchorage-independent growth. To elucidate whether these genes are also involved in MPNST development or not, requires a different experimental approach.

A working model of MPNST pathogenesis

Taken together the results generated in this thesis, we propose a model of MPNST pathogenesis. In this model, a pNF would be generated when a SC precursor from a nerve from an NF1 patient would acquire a second-hit *NF1* somatic mutation (**Figure 41**), as it has been described in mice models (Chen et al., 2014). These pNF benign cells would then acquire a loss of *CDKN2A* locus (and probably also other mutations), which lead to the development of an atypical pNF containing bigger and hyperchromatic pre-malignant cells (**Figure 41**), as reported (Beert et al., 2011). The SCNA analysis of our set of pNFs is in consistency with this finding, as one of the pNF samples presented a homozygous deletion in *CDKN2A*. These pre-malignant cells would then undergo a hyperploidization of their genome and the occurrence of several SCNAs, such as gains in chromosomes 2, 7, 8, 15q, 17q22-25 and genomic losses in 9p, 11q, 17p, 17q11.2-12, as found in our set of MPNSTs. These SCNAs would have

an impact on gene expression in a regional manner and TIs would be generated. These TIs would contain, among a major passenger gene expression, some of the genes that drive the development of an MPNST (**Figure 41**), although some other drivers of MPNST tumourigenesis may also not be associated to TIs. Malignant cells from MPNSTs would then adapt to the new altered state, which could imply transcriptional regulation of other genes and molecular mechanisms required for the maintenance of the tumour. Some of these genes and molecular mechanisms could be detected by analyzing the unique information captured by TIs, that is those genes whose differential expression is in an opposite direction than the differential expression of most of their neighbouring genes within the TI (**Figure 41**).

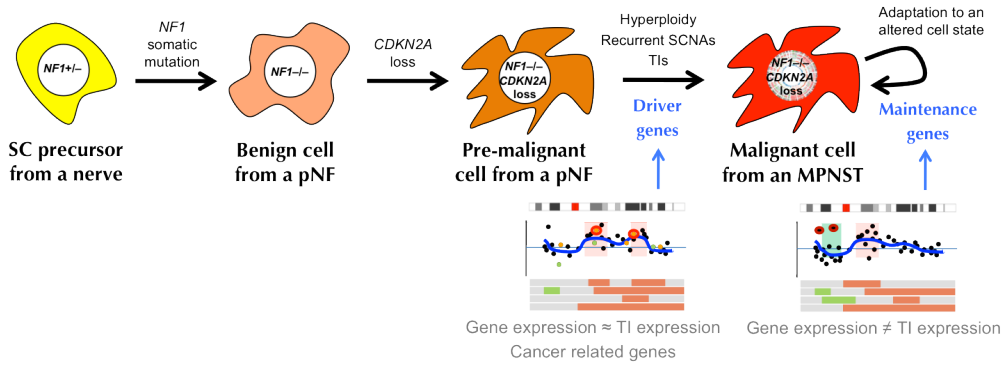

Figure 41. Working model of MPNST pathogenesis including the results generated in this thesis. A working model of MPNST pathogenesis is proposed considering TIs for the identification of genes drivers of MPNST pathogenesis and for the identification of genes that are required for their tumoural maintenance.

From genes to molecular mechanisms: the chromosome passenger complex as an important player in MPNST pathogenesis

Considering all genes studied in the RNAi functional *in vitro* genetic approach together with the physiological readouts studying the viability, proliferation, death and anchorage-independent growth of the MPNST cell lines S462 and T265, only two genes consistently affected all the tumourigenic properties studied in both cell lines, when their expression was depleted: *BIRC5* and *CDCA8*. Hence, in addition to *BIRC5*, the *CDCA8* gene was also found to be required for the survival and cell cycle progression of MPNST cell lines, being therefore its functional role in MPNST pathogenesis also plausible.

Borealin, encoded by the *CDCA8* gene forms, together with survivin (*BIRC5*), aurora-B-kinase (*AURKB*) and the protein encoded by *INCENP*, an heterotetramer known as CPC. The CPC is an essential coordinator of several cellular processes that are necessary for a proper cell division, such as the regulation of the kinetochore–microtubule attachment during the spindle assembly checkpoint, and the spindle disassembly during cytokinesis (reviewed in Ruchaud et al., 2007). We propose the CPC as an important player in the pathogenesis of MPNSTs. Thus, it can be explored if other CPC members, such as borealin, could also be viable targets for MPNST treatment, as it has been proposed for survivin (Ghadimi et al., 2012b).

MPNSTs can be classified as aneuploid tumours with a heterogeneous karyotype and a general hyperploid landscape. Polyploidy or aneuploidy can result in chromosome instability, a condition that is highly prevalent in different forms of cancers. Overexpression of CPC proteins, such as AURKB or survivin, is a hallmark of various cancers and it has been demonstrated that inducing stable forms of CPC proteins, such as AURKB, can promote tetraploidy or aneuploidy, suggesting a functional role of CPC in chromosome instability (reviewed in Nguyen and Ravid, 2006). However, whether aneuploidy and chromosome instability may be caused by deregulation of the CPC remain unknown and still a subject of debate (Nguyen and Ravid, 2006). According to our results, a possible role of the CPC in the generation and/or the maintenance of the hyperploid MPNST genome are suggested.

In addition, during mitosis, the CPC regulate the function of, among others, some kinesin proteins (reviewed in Carmena et al., 2012). Kinesin genes have also been identified when using information from TIs. We also suggest that some members may have a role in MPNST pathogenesis and are proposed as potential therapeutic targets for MPNST treatment, which is discussed below.

3. Kinesins are potential therapeutic targets for the treatment of MPNSTs

The mitotic spindle as a validated target in cancer chemotherapy

Several anti-mitotic drugs are being used, either as single agents or in combination with other compounds, for the treatment of certain types of cancers. These agents

target tubulin, the microtubular protein that is essential for a functional mitotic spindle (Jordan and Wilson, 2004). During cell division, condensed chromosomes, microtubules and hundreds of microtubule-associated proteins comprise the spindle apparatus, the machinery that separates chromosome between daughter cells. Among the main anti-proliferative compounds targeting microtubules there are the taxanes (such as paclitaxel and docetaxel), the vinca alkaloids (such as vincristine and vinblastine), and the epothilones. However, microtubules are also essential for the neuronal transport and the use of these compounds can develop peripheral neuropathy or cumulative neurotoxicity (Cavaletti and Marmiroli, 2010). Moreover, resistance to these spindle poisons has also been described (Kavallaris, 2010).

To bypass these problems, several other mitotic spindle proteins have been identified as potential anticancer targets, including PLK1 (Strebhardt and Ullrich, 2006); AURKA (Dar et al., 2010), which has also been proposed as a target for the treatment of MPNSTs (Patel et al., 2012; Mohan et al., 2013); the CPC component AURKB (Dar et al., 2010); and some cyclin dependent kinase proteins (Malumbres and Barbacid, 2009), including CDK4, which has also been recently suggested as a potential target for MPNSTs (Perez et al., 2015). Among these alternative mitotic spindle proteins, kinesins, an important family of proteins of molecular motors that are essential for mitosis, has also emerged as potential antitumoural targets (Wood et al., 2001). There are sixteen kinesin members with described roles at different stages of mitosis and cytokinesis, and some members, such as KIF11 and KIF10, have been associated with cancer (reviewed in Rath and Kozielski, 2012).

Hence, several compounds targeting KIF11 have been developed, showing some of them anti-tumour activity in several cancer types and being studied in several clinical trials (reviewed in Rath and Kozielski, 2012). Among them, ispinesib, although it has not shown promising results when administered as a monotherapy in some clinical trials (Lee et al., 2008a; Tang et al., 2008; Knox et al., 2008), it has enhanced the antitumoural effect of other drugs in pre-clinical models of breast cancer (Purcell et al., 2010). In another clinical trial, filanesib (also known as ARRY-520) stabilized tumour growth (LoRusso et al., 2015). Another KIF11 inhibitor, SB-743921, has also recently shown promising results in patients with relapsed or refractory lymphoma (O'Connor et al., 2015). Finally, litronesib (also known as LY2523355), another novel KIF11 inhibitor,

has also demonstrated a strong antitumoural activity in tumour xenograft models (Ye et al., 2015).

The results from the last part of this thesis provide some evidences of a potential role of kinesins in MPNST pathogenesis and tempt to further explore some members of this family as molecular targets for the treatment of these tumours.

Transcriptional imbalances allowed the identification of kinesins as candidate drivers of MPNST pathogenesis

When analyzing genes associated with TIs, among the significatively overexpressed genes, we identified a clear enrichment of genes from the kinesin superfamily involved in cell division. From the thirteen out of fifteen kinesin genes found overexpressed in MPNST vs. neurofibromas in the expression microarray, two of them were in TIs of overexpression and six others were overexpressed kinesins included in or flanking TIs of undexpression. Hence, we decided to explore whether the molecular functions driven by kinesins were involved in MPNST pathogenesis. In order to do so, some kinesins were selected, and we performed an experimental approach combining the previous RNAi functional *in vitro* genetic assays for *KIF15* and *KIF23* genes with a chemical inhibition of KIF10, KIF11 and KIF20A proteins.

KIF11, KIF15 and KIF23 may be involved in MPNST pathogenesis

In our data set, *KIF23* is overexpressed in a TI of overexpression, *KIF15* is overexpressed in a TI of underexpression and *KIF11* is overexpressed flanking a TI of underexpression. The performed RNAi approach showed that *KIF23* is required for the survival and cell cycle progression of both S462 and T265 and *KIF15*, for the survival and cell cycle progression of T265 cell line. The chemical inhibition of the kinesin proteins showed a general reduction in cell viability of a set of MPNST cell lines when inhibiting KIF11, and, in a less extent, when inhibiting KIF10. These results strengthen that using information from TIs can help to identify genes and molecular mechanisms involved in MPNST pathogenesis. Again, despite the limitations of our model should be considered, we claim *KIF23* as an important player in the pathogenesis of MPNSTs.

Moreover the TI where *KIF23* is located could be possibly generated as a result of a selection of a genomic copy gain in MPNSTs, in a similar way than *BIRC5* gene. *KIF15*, and especially *KIF11*, would also have an important role in MPNST pathogenesis and their expression could be regulated regardless of the generation of the TI, similarly to *CDCA8* gene.

Studying KIF11 as a potential therapeutic target for MPNSTs

The last results of this thesis demonstrated that treating S462 and T265 cell lines with the KIF10 inhibitor GSK923295, and most importantly, with the KIF11 inhibitor ispinesib, were more effective reducing their viability than in a control fibroblast cell line. According to the calculated half maximal inhibitory concentration (IC_{50}) values, MPNST cell lines globally showed an average IC_{50} value around six times lower than fibroblasts for the KIF11 inhibitor. This *in vitro* therapeutic window found for ispinesib encourages the performance of further experiments to assess tumour growth in *in vivo* mice models treated with ispinesib or other KIF11 inhibitors. With this in mind, KIF11 is proposed as a novel potential therapeutic target for the treatment of MPNSTs (**Figure 42)**. KIF11 could be targeted in combination to other targets, such as MEK, which has shown to be a promising therapeutic target in several pre-clinical models for MPNST treatment, especially when combined with other targets (see **Table 2**).

In addition, whereas the expression knockdown of *KIF15* in S462 cell line seemed not have a remarkable effect in their tumourigenic properties, an increased sensitivity to KIF11 inhibition with ispinesib was found for S462 when *KIF15* expression was previously depleted. As KIF15 has been described to replace all essential functions of KIF11 in the creation of the bipolar spindle *in vitro* (Tanenbaum et al., 2009) and there are not specific KIF15 inhibitors so far, we also propose to better experimentally address both the *in vitro* and *in vivo* effects of inhibiting KIF11 in a *KIF15*-deficient cellular background, as another potential therapeutic approach for MPNSTs. The design of a combined treatment aiming to bypass a potential KIF15-dependent resistance to KIF11 inhibitors is also under consideration. In this regard, a combined therapy targeting AURKA and KIF11 has recently proved to overcome *in vitro* a KIF15-dependent resistance to the KIF11 inhibitor SB743921 (Ma et al., 2014).

During the last decade several targets have been proposed for the treatment of MPNSTs. These targets participate in various molecular mechanisms, including neurofibromin-associated signalling pathways, angiogenesis, apoptosis, epigenetics and mitosis (reviewed in Farid et al., 2014; **Figure 42**). In this thesis, throughout the information provided by TIs, we have identified two important players of mitosis as candidates of MPNST pathogenesis: the CPC and mitotic kinesins. Moreover, the kinesin KIF11, also known as EG5, is proposed as a potential therapeutic target for MPNSTs.

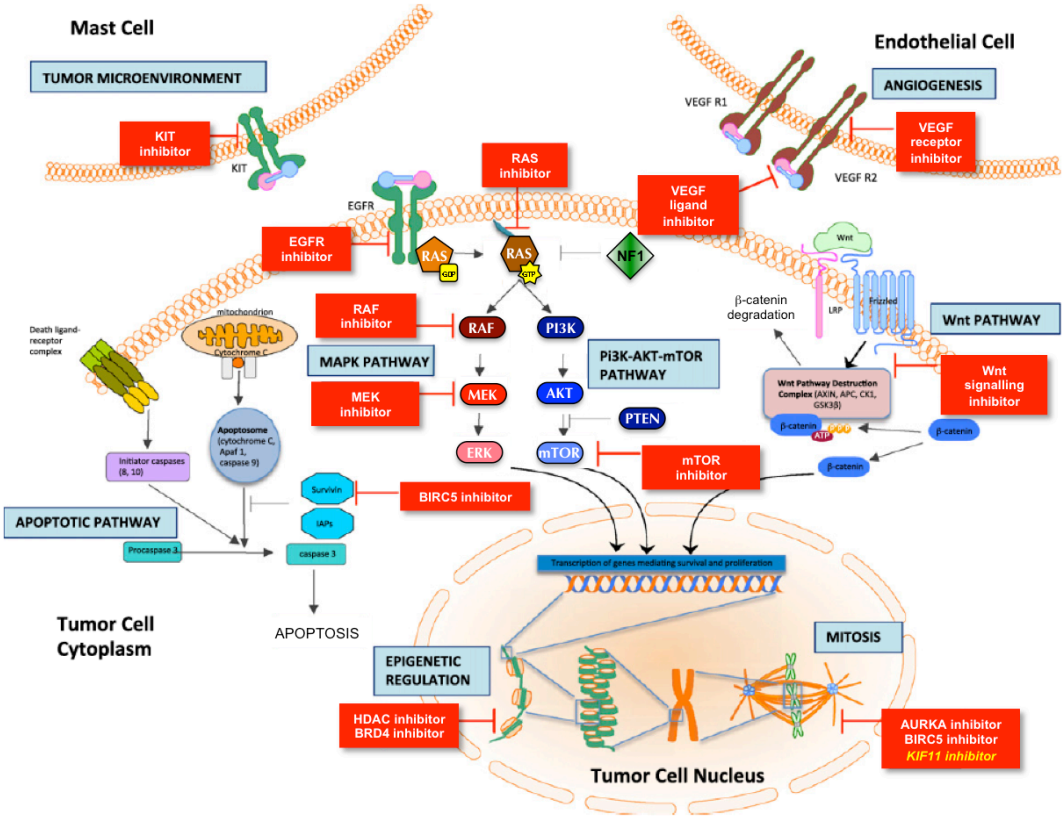

Figure 42. Pathways and potential targets for the treatment of MPNSTs. Pathways involved in MPNST pathogenesis, including proliferation, survival, angiogenesis, interaction with tumour microenvironment, epigenetic regulation and mitosis. The main inhibitors of these pathways are also shown. Inhibition of KIF11 in mitosis is suggested as a novel potential therapeutic target.

CONCLUSIONS

The main conclusions of this thesis are:

- A probe-based qPCR assay has been developed and validated for an accurate detection of constitutional microdeletions in the *NF1* locus – including those occurring in mosaicism – and for *NF1* somatic deletions found in NF1 traits.

- A second probe-based qPCR has been designed to detect somatic copy number alterations in MPNSTs. The use of repetitive sequences improves the normalization of copy number data in altered genomes, as LINEs in MPNSTs.

- A loss of the *CDKN2A* locus has been confirmed as an early event of pNF progression to MPNST.

- A hyperploid genome with recurrent SCNAs has been confirmed for MPNSTs, with the most recurrent gains in chromosomes 2, 7, 8, 15q and 17q22-25, and losses in 9p, 11q and 17p and 17q11.2-12.

- Regions of the MPNST genome with a significant abundance of over- or underexpressed genes, known as transcriptional imbalances (TIs), have been identified.

- Genomic copy number – especially genomic gains – influence global gene expression from MPNSTs in a regional manner: the generation of TIs in MPNSTs can be explained as a result of a selection of genomically altered regions.

- TIs of underexpression are, in addition, significatively enriched in hypermethylated genes and thus could also be influenced by a regional epigenomic silencing.

- TIs would include some drivers of MPNST pathogenesis but they would mainly capture signatures of passenger gene expression containing only a few genes relevant to tumour biology.

- The use of exclusive information provided by TIs facilitates the identification of candidate genes and molecular mechanisms involved in MPNST pathogenesis.

- Borealin, encoded by the *CDCA8* gene, and the chromosomal passenger complex are suggested to be involved in MPNST pathogenesis.

- Some mitotic kinesins, such as KIF11, KIF15 and KIF23, are also proposed as important players in MPNST pathogenesis.

- KIF11 represents a novel potential therapeutic target for the treatment of MPNSTs.

BIBLIOGRAPHY

A

Agarwal, R., Gonzalez-Angulo, A. M., Myhre, S., Carey, M., Lee, J. S., Overgaard, J., Alsner, J., Stemke-Hale, K., Lluch, A., Neve, R. M.*, et al.* (2009). Integrative analysis of cyclin protein levels identifies cyclin b1 as a classifier and predictor of outcomes in breast cancer. Clin Cancer Res *15*, 3654-3662.

Akavia, U. D., Litvin, O., Kim, J., Sanchez-Garcia, F., Kotliar, D., Causton, H. C., Pochanard, P., Mozes, E., Garraway, L. A., and Pe'er, D. (2010). An integrated approach to uncover drivers of cancer. Cell *143*, 1005-1017.

Alaggio, R., Turrini, R., Boldrin, D., Merlo, A., Gambini, C., Ferrari, A., Dall'igna, P., Coffin, C. M., Martines, A., Bonaldi, L.*, et al.* (2013). Survivin expression and prognostic significance in pediatric malignant peripheral nerve sheath tumors (MPNST). PLoS One *8*, e80456.

Albritton, K., Rankin, C., Coffin, C., Ratner, N., Budd, G., Schuetze, S., Randall, R., Declue, J., Borden, E. (2006) Phase II study of erlotinib in metastatic or unresectable malignant peripheral nerve sheath tumors (MPNST) J Clin Oncol 24, 9518

Andersen, L. B., Ballester, R., Marchuk, D. A., Chang, E., Gutmann, D. H., Saulino, A. M., Camonis, J., Wigler, M., and Collins, F. S. (1993). A conserved alternative splice in the von Recklinghausen neurofibromatosis (NF1) gene produces two neurofibromin isoforms, both of which have GTPase-activating protein activity. Mol Cell Biol *13*, 487-495.

Aravind, L., Neuwald, A. F., and Ponting, C. P. (1999). Sec14p-like domains in NF1 and Dbl-like proteins indicate lipid regulation of Ras and Rho signaling. Curr Biol *9*, R195-197.

Aryee, M. J., Jaffe, A. E., Corrada-Bravo, H., Ladd-Acosta, C., Feinberg, A. P., Hansen, K. D., and Irizarry, R. A. (2014). Minfi: a flexible and comprehensive Bioconductor package for the analysis of Infinium DNA methylation microarrays. Bioinformatics *30*, 1363-1369.

B

Badache, A., and De Vries, G. H. (1998). Neurofibrosarcoma-derived Schwann cells overexpress platelet-derived growth factor (PDGF) receptors and are induced to proliferate by PDGF BB. J Cell Physiol *177*, 334-342.

Ballester, R., Marchuk, D., Boguski, M., Saulino, A., Letcher, R., Wigler, M., and Collins, F. (1990). The NF1 locus encodes a protein functionally related to mammalian GAP and yeast IRA proteins. Cell *63*, 851-859.

Barker, D., Wright, E., Nguyen, K., Cannon, L., Fain, P., Goldgar, D., Bishop, D. T., Carey, J., Baty, B., Kivlin, J., and et al. (1987). Gene for von Recklinghausen neurofibromatosis is in the pericentromeric region of chromosome 17. Science *236*, 1100-1102.

Barretina, J., Taylor, B. S., Banerji, S., Ramos, A. H., Lagos-Quintana, M., Decarolis, P. L., Shah, K., Socci, N. D., Weir, B. A., Ho, A.*, et al.* (2010). Subtype-specific genomic alterations define new targets for soft-tissue sarcoma therapy. Nat Genet *42*, 715-721.

Basu, T. N., Gutmann, D. H., Fletcher, J. A., Glover, T. W., Collins, F. S., and Downward, J. (1992). Aberrant regulation of ras proteins in malignant tumour cells from type 1 neurofibromatosis patients. Nature *356*, 713-715.

Beert, E., Brems, H., Daniels, B., De Wever, I., Van Calenbergh, F., Schoenaers, J., Debiec-Rychter, M., Gevaert, O., De Raedt, T., Van Den Bruel, A.*, et al.* (2011). Atypical neurofibromas in neurofibromatosis type 1 are premalignant tumors. Genes Chromosomes Cancer *50*, 1021-1032.

Bengesser, K., Cooper, D. N., Steinmann, K., Kluwe, L., Chuzhanova, N. A., Wimmer, K., Tatagiba, M., Tinschert, S., Mautner, V. F., and Kehrer-Sawatzki, H. (2010). A novel third type of recurrent NF1 microdeletion mediated by nonallelic homologous recombination between LRRC37B-containing low-copy repeats in 17q11.2. Hum Mutat *31*, 742-751.

Bergamaschi, A., Kim, Y. H., Wang, P., Sorlie, T., Hernandez-Boussard, T., Lonning, P. E., Tibshirani, R., Borresen-Dale, A. L., and Pollack, J. R. (2006). Distinct patterns of DNA copy number alteration are associated with different clinicopathological features and gene-expression subtypes of breast cancer. Genes Chromosomes Cancer *45*, 1033-1040.

Bernards, A., Snijders, A. J., Hannigan, G. E., Murthy, A. E., and Gusella, J. F. (1993). Mouse neurofibromatosis type 1 cDNA sequence reveals high degree of conservation of both coding and non-coding mRNA segments. Hum Mol Genet *2*, 645-650.

Berner, J. M., Sorlie, T., Mertens, F., Henriksen, J., Saeter, G., Mandahl, N., Brogger, A., Myklebost, O., and Lothe, R. A. (1999). Chromosome band 9p21 is frequently altered in malignant peripheral nerve sheath tumors: studies of CDKN2A and other genes of the pRB pathway. Genes Chromosomes Cancer *26*, 151-160.

Beroukhim, R., Mermel, C. H., Porter, D., Wei, G., Raychaudhuri, S., Donovan, J., Barretina, J., Boehm, J. S., Dobson, J., Urashima, M.*, et al.* (2010). The landscape of somatic copy-number alteration across human cancers. Nature *463*, 899-905.

Bert, S. A., Robinson, M. D., Strbenac, D., Statham, A. L., Song, J. Z., Hulf, T., Sutherland, R. L., Coolen, M. W., Stirzaker, C., and Clark, S. J. (2013). Regional activation of the cancer genome by long-range epigenetic remodeling. Cancer Cell *23*, 9-22.

Bhola, P., Banerjee, S., Mukherjee, J., Balasubramanium, A., Arun, V., Karim, Z., Burrell, K., Croul, S., Gutmann, D. H., and Guha, A. (2010). Preclinical in vivo evaluation of rapamycin in human malignant peripheral nerve sheath explant xenograft. Int J Cancer *126*, 563-571.

Birindelli, S., Perrone, F., Oggionni, M., Lavarino, C., Pasini, B., Vergani, B., Ranzani, G. N., Pierotti, M. A., and Pilotti, S. (2001). Rb and TP53 pathway alterations in sporadic and NF1-related malignant peripheral nerve sheath tumors. Lab Invest *81*, 833-844.

Blangy, A., Lane, H. A., d'Herin, P., Harper, M., Kress, M., and Nigg, E. A. (1995). Phosphorylation by p34cdc2 regulates spindle association of human Eg5, a kinesin-related motor essential for bipolar spindle formation in vivo. Cell *83*, 1159-1169.

Bollag, G., and McCormick, F. (1991). Differential regulation of rasGAP and neurofibromatosis gene product activities. Nature *351*, 576-579.

Bollag, G., McCormick, F., and Clark, R. (1993). Characterization of full-length neurofibromin: tubulin inhibits Ras GAP activity. EMBO J *12*, 1923-1927.

Bottillo, I., Ahlquist, T., Brekke, H., Danielsen, S. A., van den Berg, E., Mertens, F., Lothe, R. A., and Dallapiccola, B. (2009). Germline and somatic NF1 mutations in sporadic and NF1-associated malignant peripheral nerve sheath tumours. J Pathol *217*, 693-701.

Boudry-Labis, E., Roche-Lestienne, C., Nibourel, O., Boissel, N., Terre, C., Perot, C., Eclache, V., Gachard, N., Tigaud, I., Plessis, G.*, et al.* (2013). Neurofibromatosis-1 gene deletions and mutations in de novo adult acute myeloid leukemia. Am J Hematol *88*, 306-311.

Bradtmoller, M., Hartmann, C., Zietsch, J., Jaschke, S., Mautner, V. F., Kurtz, A., Park, S. J., Baier, M., Harder, A., Reuss, D.*, et al.* (2012). Impaired Pten expression in human malignant peripheral nerve sheath tumours. PLoS One *7*, e47595.

Brems, H., Beert, E., de Ravel, T., and Legius, E. (2009). Mechanisms in the pathogenesis of malignant tumours in neurofibromatosis type 1. Lancet Oncol *10*, 508-515.

Brevini, T. A., Pennarossa, G., Maffei, S., Tettamanti, G., Vanelli, A., Isaac, S., Eden, A., Ledda, S., de Eguileor, M., and Gandolfi, F. (2012). Centrosome amplification and chromosomal instability in human and animal parthenogenetic cell lines. Stem Cell Rev *8*, 1076-1087.

Brockes, J. P., Fields, K. L., and Raff, M. C. (1979). Studies on cultured rat Schwann cells. I. Establishment of purified populations from cultures of peripheral nerve. Brain Res *165*, 105-118.

Brosius, S. N., Turk, A. N., Byer, S. J., Brossier, N. M., Kohli, L., Whitmire, A., Mikhail, F. M., Roth, K. A., and Carroll, S. L. (2014). Neuregulin-1 overexpression and Trp53 haploinsufficiency cooperatively promote de novo malignant peripheral nerve sheath tumor pathogenesis. Acta Neuropathol *127*, 573-591.

Brundage, M. E., Tandon, P., Eaves, D. W., Williams, J. P., Miller, S. J., Hennigan, R. H., Jegga, A., Cripe, T. P., and Ratner, N. (2014). MAF mediates crosstalk between Ras-MAPK and mTOR signaling in NF1. Oncogene *33*, 5626-5636.

Buchstaller, J., Clapp, D. W., Parada, L. F., Zhu, Y. (2012). Cell of Origin and the Contribution of Microenvironment in NF1 Tumorigenesis and Therapeutic Implications. In: Upadhyaya, M., Cooper, D., eds. Berlin Heidelberg: Springer-Verlag (Neurofibromatosis Type 1 Molecular and Cellular Biology; vol. 36, p. 549–568)

Bustin, S. A., Benes, V., Garson, J. A., Hellemans, J., Huggett, J., Kubista, M., Mueller, R., Nolan, T., Pfaffl, M. W., Shipley, G. L.*, et al.* (2009). The MIQE guidelines: minimum information for publication of quantitative real-time PCR experiments. Clin Chem *55*, 611-622.

Byer, S. J., Brossier, N. M., Peavler, L. T., Eckert, J. M., Watkins, S., Roth, K. A., Carroll, S. L. (2013). Malignant peripheral nerve sheath tumor invasion requires aberrantly expressed EGF receptors and is variably enhanced by multiple EGF family ligands. J Neuropathol Exp Neurol *72*, 219-233

C

Carmena, M., Wheelock, M., Funabiki, H., and Earnshaw, W. C. (2012). The chromosomal passenger complex (CPC): from easy rider to the godfather of mitosis. Nat Rev Mol Cell Biol *13*, 789-803.

Castellanos, E., *et al*. Comprehensive panel-based genetic diagnostic testing for hereditary cancer: extending mutation identification. Manuscript in preparation.

Castellsague, J., Gel, B., Fernandez-Rodriguez, J., Llatjos, R., Blanco, I., Benavente, Y., Perez-Sidelnikova, D., Garcia-Del Muro, J., Vinals, J. M., Vidal, A.*, et al.* (2015). Comprehensive establishment and characterization of orthoxenograft mouse models of malignant peripheral nerve sheath tumors for personalized medicine. EMBO Mol Med *7*, 608-627.

Cavaletti, G., and Marmiroli, P. (2010). Chemotherapy-induced peripheral neurotoxicity. Nat Rev Neurol *6*, 657-666.

Cawthon, R. M., Andersen, L. B., Buchberg, A. M., Xu, G. F., O'Connell, P., Viskochil, D., Weiss, R. B., Wallace, M. R., Marchuk, D. A., Culver, M., and et al. (1991). cDNA sequence and genomic structure of EV12B, a gene lying within an intron of the neurofibromatosis type 1 gene. Genomics *9*, 446-460.

Cawthon, R. M., O'Connell, P., Buchberg, A. M., Viskochil, D., Weiss, R. B., Culver, M., Stevens, J., Jenkins, N. A., Copeland, N. G., and White, R. (1990a). Identification and characterization of transcripts from the neurofibromatosis 1 region: the sequence and genomic structure of EVI2 and mapping of other transcripts. Genomics *7*, 555-565.

Cawthon, R. M., Weiss, R., Xu, G. F., Viskochil, D., Culver, M., Stevens, J., Robertson, M., Dunn, D., Gesteland, R., O'Connell, P., and et al. (1990b). A major segment of the neurofibromatosis type 1 gene: cDNA sequence, genomic structure, and point mutations. Cell *62*, 193-201.

Chang, I. W., Wu, W. J., Wang, Y. H., Wu, T. F., Liang, P. I., He, H. L., Yeh, B. W., and Li, C. F. (2015). BCAT1 overexpression is an indicator of poor prognosis in patients with urothelial carcinomas of the upper urinary tract and urinary bladder. Histopathology.

Chang, J. L., Chen, T. H., Wang, C. F., Chiang, Y. H., Huang, Y. L., Wong, F. H., Chou, C. K., and Chen, C. M. (2006). Borealin/Dasra B is a cell cycle-regulated chromosomal passenger protein and its nuclear accumulation is linked to poor prognosis for human gastric cancer. Exp Cell Res *312*, 962-973.

Chaudhary, J., and Schmidt, M. (2006). The impact of genomic alterations on the transcriptome: a prostate cancer cell line case study. Chromosome Res *14*, 567-586.

Chen, Z., Liu, C., Patel, A. J., Liao, C. P., Wang, Y., and Le, L. Q. (2014). Cells of origin in the embryonic nerve roots for NF1-associated plexiform neurofibroma. Cancer Cell *26*, 695-706.

Chugh, R., Wathen, J. K., Maki, R. G., Benjamin, R. S., Patel, S. R., Meyers, P. A., Priebat, D. A., Reinke, D. K., Thomas, D. G., Keohan, M. L.*, et al.* (2009). Phase II multicenter trial of imatinib in 10 histologic subtypes of sarcoma using a bayesian hierarchical statistical model. J Clin Oncol *27*, 3148-3153.

Cichowski, K., and Jacks, T. (2001). NF1 tumor suppressor gene function: narrowing the GAP. Cell *104*, 593-604.

Cichowski, K., Santiago, S., Jardim, M., Johnson, B. W., and Jacks, T. (2003). Dynamic regulation of the Ras pathway via proteolysis of the NF1 tumor suppressor. Genes Dev *17*, 449-454.

Cichowski, K., Shih, T. S., Schmitt, E., Santiago, S., Reilly, K., McLaughlin, M. E., Bronson, R. T., and Jacks, T. (1999). Mouse models of tumor development in neurofibromatosis type 1. Science *286*, 2172-2176.

Cillo, C., Schiavo, G., Cantile, M., Bihl, M. P., Sorrentino, P., Carafa, V., M, D. A., Roncalli, M., Sansano, S., Vecchione, R.*, et al.* (2011). The HOX gene network in hepatocellular carcinoma. Int J Cancer *129*, 2577-2587.

Colman, S. D., Williams, C. A., and Wallace, M. R. (1995). Benign neurofibromas in type 1 neurofibromatosis (NF1) show somatic deletions of the NF1 gene. Nat Genet *11*, 90-92.

Coolen, M. W., Stirzaker, C., Song, J. Z., Statham, A. L., Kassir, Z., Moreno, C. S., Young, A. N., Varma, V., Speed, T. P., Cowley, M.*, et al.* (2010). Consolidation of the cancer genome into domains of repressive chromatin by long-range epigenetic silencing (LRES) reduces transcriptional plasticity. Nat Cell Biol *12*, 235-246.

Cummings, L. M., Trent, J. M., and Marchuk, D. A. (1996). Identification and mapping of type 1 neurofibromatosis (NF1) homologous loci. Cytogenet Cell Genet *73*, 334-340.

D

D'Angelo, I., Welti, S., Bonneau, F., and Scheffzek, K. (2006). A novel bipartite phospholipid-binding module in the neurofibromatosis type 1 protein. EMBO Rep *7*, 174-179.

D'Haene, B., Vandesompele, J., and Hellemans, J. (2010). Accurate and objective copy number profiling using real-time quantitative PCR. Methods *50*, 262-270.

Dahlberg, W. K., Little, J. B., Fletcher, J. A., Suit, H. D., and Okunieff, P. (1993). Radiosensitivity in vitro of human soft tissue sarcoma cell lines and skin fibroblasts derived from the same patients. Int J Radiat Biol *63*, 191-198.

Dai, M., Wang, P., Boyd, A. D., Kostov, G., Athey, B., Jones, E. G., Bunney, W. E., Myers, R. M., Speed, T. P., Akil, H.*, et al.* (2005). Evolving gene/transcript definitions significantly alter the interpretation of GeneChip data. Nucleic Acids Res *33*, e175.

Dallosso, A. R., Hancock, A. L., Szemes, M., Moorwood, K., Chilukamarri, L., Tsai, H. H., Sarkar, A., Barasch, J., Vuononvirta, R., Jones, C.*, et al.* (2009). Frequent long-range epigenetic silencing of protocadherin gene clusters on chromosome 5q31 in Wilms' tumor. PLoS Genet *5*, e1000745.

Danglot, G., Regnier, V., Fauvet, D., Vassal, G., Kujas, M., and Bernheim, A. (1995). Neurofibromatosis 1 (NF1) mRNAs expressed in the central nervous system are differentially spliced in the 5' part of the gene. Hum Mol Genet *4*, 915-920.

Danielsen, S. A., Lind, G. E., Kolberg, M., Holand, M., Bjerkehagen, B., Sundby Hall, K., van den Berg, E., Mertens, F., Smeland, S., Picci, P., and Lothe, R. A. (2015). Methylated RASSF1A in malignant peripheral nerve sheath tumors identifies neurofibromatosis type 1 patients with inferior prognosis. Neuro Oncol *17*, 63-69.

Dar, A. A., Goff, L. W., Majid, S., Berlin, J., and El-Rifai, W. (2010). Aurora kinase inhibitors--rising stars in cancer therapeutics? Mol Cancer Ther *9*, 268-278.

Daschner, K., Assum, G., Eisenbarth, I., Krone, W., Hoffmeyer, S., Wortmann, S., Heymer, B., and Kehrer-Sawatzki, H. (1997). Clonal origin of tumor cells in a plexiform neurofibroma with LOH in NF1 intron 38 and in dermal neurofibromas without LOH of the NF1 gene. Biochem Biophys Res Commun *234*, 346-350.

Daston, M. M., Scrable, H., Nordlund, M., Sturbaum, A. K., Nissen, L. M., and Ratner, N. (1992). The protein product of the neurofibromatosis type 1 gene is expressed at highest abundance in neurons, Schwann cells, and oligodendrocytes. Neuron *8*, 415-428.

De Luca, A., Bernardini, L., Ceccarini, C., Sinibaldi, L., Novelli, A., Giustini, S., Daniele, I., Calvieri, S., and Mingarelli, R. (2004). Fluorescence in situ hybridization analysis of allelic losses involving the long arm of chromosome 17 in NF1-associated neurofibromas. Cancer Genet Cytogenet *150*, 168-172.

De Raedt, T., Beert, E., Pasmant, E., Luscan, A., Brems, H., Ortonne, N., Helin, K., Hornick, J. L., Mautner, V., Kehrer-Sawatzki, H.*, et al.* (2014). PRC2 loss amplifies Ras-driven transcription and confers sensitivity to BRD4-based therapies. Nature *514*, 247-251.

De Raedt, T., Brems, H., Wolkenstein, P., Vidaud, D., Pilotti, S., Perrone, F., Mautner, V., Frahm, S., Sciot, R., and Legius, E. (2003). Elevated risk for MPNST in NF1 microdeletion patients. Am J Hum Genet *72*, 1288-1292.

De Raedt, T., Maertens, O., Chmara, M., Brems, H., Heyns, I., Sciot, R., Majounie, E., Upadhyaya, M., De Schepper, S., Speleman, F.*, et al.* (2006). Somatic loss of wild type NF1 allele in neurofibromas: Comparison of NF1 microdeletion and non-microdeletion patients. Genes Chromosomes Cancer *45*, 893-904.

De Raedt, T., Maertens, O., Serra, E., and Legius, E. (2008). Somatic NF1 Mutations in Tumors and Other Tissues. In: Kaufmann D, ed. Neurofibromatoses. Basel: Karger (Monographs in human genetics; vol. 16, p.143–153).

De Raedt, T., Walton, Z., Yecies, J. L., Li, D., Chen, Y., Malone, C. F., Maertens, O., Jeong, S. M., Bronson, R. T., Lebleu, V.*, et al.* (2011). Exploiting cancer cell vulnerabilities to develop a combination therapy for ras-driven tumors. Cancer Cell *20*, 400-413.

De Schepper, S., Maertens, O., Callens, T., Naeyaert, J. M., Lambert, J., and Messiaen, L. (2008). Somatic mutation analysis in NF1 cafe au lait spots reveals two NF1 hits in the melanocytes. J Invest Dermatol *128*, 1050-1053.

de Tayrac, M., Etcheverry, A., Aubry, M., Saikali, S., Hamlat, A., Quillien, V., Le Treut, A., Galibert, M. D., and Mosser, J. (2009). Integrative genome-wide analysis reveals a robust genomic glioblastoma signature associated with copy number driving changes in gene expression. Genes Chromosomes Cancer *48*, 55-68.

DeBella, K., Szudek, J., and Friedman, J. M. (2000). Use of the national institutes of health criteria for diagnosis of neurofibromatosis 1 in children. Pediatrics *105*, 608-614.

DeClue, J. E., Cohen, B. D., and Lowy, D. R. (1991). Identification and characterization of the neurofibromatosis type 1 protein product. Proc Natl Acad Sci U S A *88*, 9914-9918.

DeClue, J. E., Papageorge, A. G., Fletcher, J. A., Diehl, S. R., Ratner, N., Vass, W. C., and Lowy, D. R. (1992). Abnormal regulation of mammalian p21ras contributes to malignant tumor growth in von Recklinghausen (type 1) neurofibromatosis. Cell *69*, 265-273.

Demestre, M., Terzi, M. Y., Mautner, V., Vajkoczy, P., Kurtz, A., and Pina, A. L. (2013). Effects of pigment epithelium derived factor (PEDF) on malignant peripheral nerve sheath tumours (MPNSTs). J Neurooncol *115*, 391-399.

Dorschner, M. O., Sybert, V. P., Weaver, M., Pletcher, B. A., and Stephens, K. (2000). NF1 microdeletion breakpoints are clustered at flanking repetitive sequences. Hum Mol Genet *9*, 35-46.

Drescher, U., Bonhoeffer, F., and Muller, B. K. (1997). The Eph family in retinal axon guidance. Curr Opin Neurobiol *7*, 75-80.

Du, X., Yang, J., Ylipaa, A., and Zhu, Z. (2013). Genomic amplification and high expression of EGFR are key targetable oncogenic events in malignant peripheral nerve sheath tumor. J Hematol Oncol *6*, 93.

Duan, R., Han, L., Wang, Q., Wei, J., Chen, L., Zhang, J., Kang, C., and Wang, L. (2015). HOXA13 is a potential GBM diagnostic marker and promotes glioma invasion by activating the Wnt and TGF-beta pathways. Oncotarget *6*, 27778-27793.

Ducatman, B. S., Scheithauer, B. W., Piepgras, D. G., Reiman, H. M., and Ilstrup, D. M. (1986). Malignant peripheral nerve sheath tumors. A clinicopathologic study of 120 cases. Cancer *57*, 2006-2021.

Dugoff, L., and Sujansky, E. (1996). Neurofibromatosis type 1 and pregnancy. Am J Med Genet *66*, 7-10.

E

Easton, D. F., Ponder, M. A., Huson, S. M., and Ponder, B. A. (1993). An analysis of variation in expression of neurofibromatosis (NF) type 1 (NF1): evidence for modifying genes. Am J Hum Genet *53*, 305-313.

Eckert, J. M., Byer, S. J., Clodfelder-Miller, B. J., and Carroll, S. L. (2009). Neuregulin-1 beta and neuregulin-1 alpha differentially affect the migration and invasion of malignant peripheral nerve sheath tumor cells. Glia *57*, 1501-1520.

Evans, D. G., Baser, M. E., McGaughran, J., Sharif, S., Howard, E., and Moran, A. (2002). Malignant peripheral nerve sheath tumours in neurofibromatosis 1. J Med Genet *39*, 311-314.

F

Fang, N., Di Pasquale, F., Beckmann, C., Deutsch, U., Missel, A. (2011). A novel reference assay for reliable qPCR-based CNV quantification, Sample & Assay Technologies, QIAGEN GmbH, Hilden, Germany

Fang, Y., Elahi, A., Denley, R. C., Rao, P. H., Brennan, M. F., and Jhanwar, S. C. (2009). Molecular characterization of permanent cell lines from primary, metastatic and recurrent malignant peripheral nerve sheath tumors (MPNST) with underlying neurofibromatosis-1. Anticancer Res *29*, 1255-1262.

Farid, M., Demicco, E. G., Garcia, R., Ahn, L., Merola, P. R., Cioffi, A., and Maki, R. G. (2014). Malignant peripheral nerve sheath tumors. Oncologist *19*, 193-201.

Feber, A., Wilson, G. A., Zhang, L., Presneau, N., Idowu, B., Down, T. A., Rakyan, V. K., Noon, L. A., Lloyd, A. C., Stupka, E., *et al.* (2011). Comparative methylome analysis of benign and malignant peripheral nerve sheath tumors. Genome Res *21*, 515-524.

Ferner, R. E. (2007). Neurofibromatosis 1. Eur J Hum Genet *15*, 131-138.

Ferner, R. E., Golding, J. F., Smith, M., Calonje, E., Jan, W., Sanjayanathan, V., and O'Doherty, M. (2008). [18F]2-fluoro-2-deoxy-D-glucose positron emission tomography (FDG PET) as a diagnostic tool for neurofibromatosis 1 (NF1) associated malignant peripheral nerve sheath tumours (MPNSTs): a long-term clinical study. Ann Oncol *19*, 390-394.

Ferrari, F., Solari, A., Battaglia, C., and Bicciato, S. (2011). PREDA: an R-package to identify regional variations in genomic data. Bioinformatics *27*, 2446-2447.

Fishbein, L., Eady, B., Sanek, N., Muir, D., and Wallace, M. R. (2005). Analysis of somatic NF1 promoter methylation in plexiform neurofibromas and Schwann cells. Cancer Genet Cytogenet *157*, 181-186.

Fletcher, J. A., Kozakewich, H. P., Hoffer, F. A., Lage, J. M., Weidner, N., Tepper, R., Pinkus, G. S., Morton, C. C., and Corson, J. M. (1991). Diagnostic relevance of clonal cytogenetic aberrations in malignant soft-tissue tumors. N Engl J Med *324*, 436-442.

Frahm, S., Mautner, V. F., Brems, H., Legius, E., Debiec-Rychter, M., Friedrich, R. E., Knofel, W. T., Peiper, M., and Kluwe, L. (2004). Genetic and phenotypic characterization of tumor cells derived from malignant peripheral nerve sheath tumors of neurofibromatosis type 1 patients. Neurobiol Dis *16*, 85-91.

Friedman, J. M. (1999). Epidemiology of neurofibromatosis type 1. Am J Med Genet *89*, 1-6.

Friedrich, R. E., Hartmann, M., and Mautner, V. F. (2007). Malignant peripheral nerve sheath tumors (MPNST) in NF1-affected children. Anticancer Res *27*, 1957-1960.

Frigola, J., Song, J., Stirzaker, C., Hinshelwood, R. A., Peinado, M. A., and Clark, S. J. (2006). Epigenetic remodeling in colorectal cancer results in coordinate gene suppression across an entire chromosome band. Nat Genet *38*, 540-549.

Fujino, T., Suzuki, A., Ito, Y., Ohyashiki, K., Hatano, Y., Miura, I., and Nakamura, T. (2002). Single-translocation and double-chimeric transcripts: detection of NUP98-HOXA9 in myeloid leukemias with HOXA11 or HOXA13 breaks of the chromosomal translocation t(7;11)(p15;p15). Blood *99*, 1428-1433.

G

Garcia-Linares, C., Fernandez-Rodriguez, J., Terribas, E., Mercade, J., Pros, E., Benito, L., Benavente, Y., Capella, G., Ravella, A., Blanco, I.*, et al.* (2011). Dissecting loss of heterozygosity (LOH) in neurofibromatosis type 1-associated neurofibromas: Importance of copy neutral LOH. Hum Mutat *32*, 78-90.

Garcia-Linares, C., Mercade, J., Gel, B., Biayna, J., Terribas, E., Lazaro, C., and Serra, E. (2012). Applying microsatellite multiplex PCR analysis (MMPA) for determining allele copy-number status and percentage of normal cells within tumors. PLoS One *7*, e42682.

Gasparini, P., Grifa, A., Origone, P., Coviello, D., Antonacci, R., and Rocchi, M. (1993). Detection of a neurofibromatosis type I (NF1) homologous sequence by PCR: implications for the diagnosis and screening of genetic diseases. Mol Cell Probes *7*, 415-418.

Geiger, T., Cox, J., and Mann, M. (2010). Proteomic changes resulting from gene copy number variations in cancer cells. PLoS Genet *6*, e1001090.

Gel, B., Diez-Villanueva, A., Serra, E., Buschbeck, M., Peinado, M. A., and Malinverni, R. (2015). regioneR: an R/Bioconductor package for the association analysis of genomic regions based on permutation tests. Bioinformatics.

Ghadimi, M. P., Lopez, G., Torres, K. E., Belousov, R., Young, E. D., Liu, J., Brewer, K. J., Hoffman, A., Lusby, K., Lazar, A. J.*, et al.* (2012a). Targeting the PI3K/mTOR axis, alone and in combination with autophagy blockade, for the treatment of malignant peripheral nerve sheath tumors. Mol Cancer Ther *11*, 1758-1769.

Ghadimi, M. P., Young, E. D., Belousov, R., Zhang, Y., Lopez, G., Lusby, K., Kivlin, C., Demicco, E. G., Creighton, C. J., Lazar, A. J.*, et al.* (2012b). Survivin is a viable target for the treatment of malignant peripheral nerve sheath tumors. Clin Cancer Res *18*, 2545-2557.

Glover, T. W., Stein, C. K., Legius, E., Andersen, L. B., Brereton, A., and Johnson, S. (1991). Molecular and cytogenetic analysis of tumors in von Recklinghausen neurofibromatosis. Genes Chromosomes Cancer *3*, 62-70.

Gong, M., Ma, J., Li, M., Zhou, M., Hock, J. M., and Yu, X. (2012). MicroRNA-204 critically regulates carcinogenesis in malignant peripheral nerve sheath tumors. Neuro Oncol *14*, 1007-1017.

Graves, L. M., Guy, H. I., Kozlowski, P., Huang, M., Lazarowski, E., Pope, R. M., Collins, M. A., Dahlstrand, E. N., Earp, H. S., 3rd, and Evans, D. R. (2000). Regulation of carbamoyl phosphate synthetase by MAP kinase. Nature *403*, 328-332.

Gregory, P. E., Gutmann, D. H., Mitchell, A., Park, S., Boguski, M., Jacks, T., Wood, D. L., Jove, R., and Collins, F. S. (1993). Neurofibromatosis type 1 gene product (neurofibromin) associates with microtubules. Somat Cell Mol Genet *19*, 265-274.

Gu, Z. D., Shen, L. Y., Wang, H., Chen, X. M., Li, Y., Ning, T., and Chen, K. N. (2009). HOXA13 promotes cancer cell growth and predicts poor survival of patients with esophageal squamous cell carcinoma. Cancer Res *69*, 4969-4973.

Guha, A., Lau, N., Huvar, I., Gutmann, D., Provias, J., Pawson, T., and Boss, G. (1996). Ras-GTP levels are elevated in human NF1 peripheral nerve tumors. Oncogene *12*, 507-513.

Guo, H. F., The, I., Hannan, F., Bernards, A., and Zhong, Y. (1997). Requirement of Drosophila NF1 for activation of adenylyl cyclase by PACAP38-like neuropeptides. Science *276*, 795-798.

Gutman, D. H., Andersen, L. B., Cole, J. L., Swaroop, M., and Collins, F. S. (1993). An alternatively-spliced mRNA in the carboxy terminus of the neurofibromatosis type 1 (NF1) gene is expressed in muscle. Hum Mol Genet *2*, 989-992.

Gutmann, D. H., Wood, D. L., and Collins, F. S. (1991). Identification of the neurofibromatosis type 1 gene product. Proc Natl Acad Sci U S A *88*, 9658-9662.

Gutmann, D. H., Wu, Y. L., Hedrick, N. M., Zhu, Y., Guha, A., and Parada, L. F. (2001). Heterozygosity for the neurofibromatosis 1 (NF1) tumor suppressor results in abnormalities in cell attachment, spreading and motility in astrocytes. Hum Mol Genet *10*, 3009-3016.

H

Hadfield, K. D., Newman, W. G., Bowers, N. L., Wallace, A., Bolger, C., Colley, A., McCann, E., Trump, D., Prescott, T., and Evans, D. G. (2008). Molecular characterisation of SMARCB1 and NF2 in familial and sporadic schwannomatosis. J Med Genet *45*, 332-339.

Hajra, A., Martin-Gallardo, A., Tarle, S. A., Freedman, M., Wilson-Gunn, S., Bernards, A., and Collins, F. S. (1994). DNA sequences in the promoter region of the NF1 gene are highly conserved between human and mouse. Genomics *21*, 649-652.

Hakimi, M. A., Speicher, D. W., and Shiekhattar, R. (2002). The motor protein kinesin-1 links neurofibromin and merlin in a common cellular pathway of neurofibromatosis. J Biol Chem *277*, 36909-36912.

Hamad, N. M., Elconin, J. H., Karnoub, A. E., Bai, W., Rich, J. N., Abraham, R. T., Der, C. J., and Counter, C. M. (2002). Distinct requirements for Ras oncogenesis in human versus mouse cells. Genes Dev *16*, 2045-2057.

Hanahan, D., and Weinberg, R. A. (2000). The hallmarks of cancer. Cell *100*, 57-70.

Hanahan, D., and Weinberg, R. A. (2011). Hallmarks of cancer: the next generation. Cell *144*, 646-674.

Harder, A., Rosche, M., Reuss, D. E., Holtkamp, N., Uhlmann, K., Friedrich, R., Mautner, V. F., and von Deimling, A. (2004). Methylation analysis of the neurofibromatosis type 1 (NF1) promoter in peripheral nerve sheath tumours. Eur J Cancer *40*, 2820-2828.

Hattermann, K., Li, G., Hugo, H. H., Mentlein, R., Mehdorn, H. M., and Held-Feindt, J. (2013). Expression of the chemokines CXCL12 and CX3CL1 and their receptors in human nerve sheath tumors. Histol Histopathol *28*, 1337-1349.

Hellemans, J., Mortier, G., De Paepe, A., Speleman, F., and Vandesompele, J. (2007). qBase relative quantification framework and software for management and automated analysis of real-time quantitative PCR data. Genome Biol *8*, R19.

Hellemans, J., and Vandesompele, J. (2014). Selection of reliable reference genes for RT-qPCR analysis. Methods Mol Biol *1160*, 19-26.

Hernandez-Vargas, H., Sincic, N., Ouzounova, M., and Herceg, Z. (2009). Epigenetic signatures in stem cells and cancer stem cells. Epigenomics *1*, 261-280.

Hirokawa, N., Niwa, S., and Tanaka, Y. (2010). Molecular motors in neurons: transport mechanisms and roles in brain function, development, and disease. Neuron *68*, 610-638.

Hirokawa, N., Noda, Y., Tanaka, Y., and Niwa, S. (2009). Kinesin superfamily motor proteins and intracellular transport. Nat Rev Mol Cell Biol *10*, 682-696.

Hobert, O., and Westphal, H. (2000). Functions of LIM-homeobox genes. Trends Genet *16*, 75-83.

Holtkamp, N., Atallah, I., Okuducu, A. F., Mucha, J., Hartmann, C., Mautner, V. F., Friedrich, R. E., Mawrin, C., and von Deimling, A. (2007). MMP-13 and p53 in the progression of malignant peripheral nerve sheath tumors. Neoplasia *9*, 671-677.

Holtkamp, N., Malzer, E., Zietsch, J., Okuducu, A. F., Mucha, J., Mawrin, C., Mautner, V. F., Schildhaus, H. U., and von Deimling, A. (2008). EGFR and erbB2 in malignant peripheral nerve sheath tumors and implications for targeted therapy. Neuro Oncol *10*, 946-957.

Holtkamp, N., Okuducu, A. F., Mucha, J., Afanasieva, A., Hartmann, C., Atallah, I., Estevez-Schwarz, L., Mawrin, C., Friedrich, R. E., Mautner, V. F., and von Deimling, A. (2006). Mutation and expression of PDGFRA and KIT in malignant peripheral nerve sheath tumors, and its implications for imatinib sensitivity. Carcinogenesis *27*, 664-671.

Horan, M. P., Cooper, D. N., and Upadhyaya, M. (2000). Hypermethylation of the neurofibromatosis type 1 (NF1) gene promoter is not a common event in the inactivation of the NF1 gene in NF1-specific tumours. Hum Genet *107*, 33-39.

Hsiao, M. C., Piotrowski, A., Callens, T., Fu, C., Wimmer, K., Claes, K. B., and Messiaen, L. (2015). Decoding NF1 Intragenic Copy-Number Variations. Am J Hum Genet *97*, 238-249.

Hsu, P. Y., Hsu, H. K., Singer, G. A., Yan, P. S., Rodriguez, B. A., Liu, J. C., Weng, Y. I., Deatherage, D. E., Chen, Z., Pereira, J. S.*, et al.* (2010). Estrogen-mediated epigenetic repression of large chromosomal regions through DNA looping. Genome Res *20*, 733-744.

Hsueh, Y. P., Roberts, A. M., Volta, M., Sheng, M., and Roberts, R. G. (2001). Bipartite interaction between neurofibromatosis type I protein (neurofibromin) and syndecan transmembrane heparan sulfate proteoglycans. J Neurosci *21*, 3764-3770.

Huang, N., Shah, P. K., and Li, C. (2012). Lessons from a decade of integrating cancer copy number alterations with gene expression profiles. Brief Bioinform *13*, 305-316.

Hulsebos, T. J., Plomp, A. S., Wolterman, R. A., Robanus-Maandag, E. C., Baas, F., and Wesseling, P. (2007). Germline mutation of INI1/SMARCB1 in familial schwannomatosis. Am J Hum Genet *80*, 805-810.

Huson, S. M., Compston, D. A., Clark, P., and Harper, P. S. (1989). A genetic study of von Recklinghausen neurofibromatosis in south east Wales. I. Prevalence, fitness, mutation rate, and effect of parental transmission on severity. J Med Genet *26*, 704-711.

Huson, S. M., Harper, P. S., and Compston, D. A. (1988). Von Recklinghausen neurofibromatosis. A clinical and population study in south-east Wales. Brain *111 (Pt 6)*, 1355-1381.

Hyman, E., Kauraniemi, P., Hautaniemi, S., Wolf, M., Mousses, S., Rozenblum, E., Ringner, M., Sauter, G., Monni, O., Elkahloun, A.*, et al.* (2002). Impact of DNA amplification on gene expression patterns in breast cancer. Cancer Res *62*, 6240-6245.

I

Ichihara, A., and Koyama, E. (1966). Transaminase of branched chain amino acids. I. Branched chain amino acids-alpha-ketoglutarate transaminase. J Biochem *59*, 160-169.

Iizumi, M., Hosokawa, M., Takehara, A., Chung, S., Nakamura, T., Katagiri, T., Eguchi, H., Ohigashi, H., Ishikawa, O., Nakamura, Y., and Nakagawa, H. (2006). EphA4 receptor, overexpressed in pancreatic ductal adenocarcinoma, promotes cancer cell growth. Cancer Sci *97*, 1211-1216.

Imai, K., Hirata, S., Irie, A., Senju, S., Ikuta, Y., Yokomine, K., Harao, M., Inoue, M., Tomita, Y., Tsunoda, T.*, et al.* (2011). Identification of HLA-A2-restricted CTL epitopes of a novel tumour-associated antigen, KIF20A, overexpressed in pancreatic cancer. Br J Cancer *104*, 300-307.

Imaizumi, S., Motoyama, T., Ogose, A., Hotta, T., and Takahashi, H. E. (1998). Characterization and chemosensitivity of two human malignant peripheral nerve sheath tumour cell lines derived from a patient with neurofibromatosis type 1. Virchows Arch *433*, 435-441.

Irizarry, R. A., Hobbs, B., Collin, F., Beazer-Barclay, Y. D., Antonellis, K. J., Scherf, U., and Speed, T. P. (2003). Exploration, normalization, and summaries of high density oligonucleotide array probe level data. Biostatistics *4*, 249-264.

Itani, S., Kunisada, T., Morimoto, Y., Yoshida, A., Sasaki, T., Ito, S., Ouchida, M., Sugihara, S., Shimizu, K., and Ozaki, T. (2012). MicroRNA-21 correlates with tumorigenesis in malignant peripheral nerve sheath tumor (MPNST) via programmed cell death protein 4 (PDCD4). J Cancer Res Clin Oncol *138*, 1501-1509.

Iwahana, H., Fujimura, M., Ii, S., Kondo, M., Moritani, M., Takahashi, Y., Yamaoka, T., Yoshimoto, K., and Itakura, M. (1996). Molecular cloning of a human cDNA encoding a trifunctional enzyme of carbamoyl-phosphate synthetase-aspartate transcarbamoylase-dihydroorotase in de Novo pyrimidine synthesis. Biochem Biophys Res Commun *219*, 249-255.

Izawa, I., Tamaki, N., and Saya, H. (1996). Phosphorylation of neurofibromatosis type 1 gene product (neurofibromin) by cAMP-dependent protein kinase. FEBS Lett *382*, 53-59.

J

Jacob, F., Guertler, R., Naim, S., Nixdorf, S., Fedier, A., Hacker, N. F., and Heinzelmann-Schwarz, V. (2013). Careful selection of reference genes is required for reliable performance of RT-qPCR in human normal and cancer cell lines. PLoS One *8*, e59180.

Jarvinen, A. K., Autio, R., Haapa-Paananen, S., Wolf, M., Saarela, M., Grenman, R., Leivo, I., Kallioniemi, O., Makitie, A. A., and Monni, O. (2006). Identification of target genes in laryngeal squamous cell carcinoma by high-resolution copy number and gene expression microarray analyses. Oncogene *25*, 6997-7008.

Jenne, D. E., Tinschert, S., Reimann, H., Lasinger, W., Thiel, G., Hameister, H., and Kehrer-Sawatzki, H. (2001). Molecular characterization and gene content of breakpoint boundaries in patients with neurofibromatosis type 1 with 17q11.2 microdeletions. Am J Hum Genet *69*, 516-527.

Jessen, W. J., Miller, S. J., Jousma, E., Wu, J., Rizvi, T. A., Brundage, M. E., Eaves, D., Widemann, B., Kim, M. O., Dombi, E*., et al.* (2013). MEK inhibition exhibits efficacy in human and mouse neurofibromatosis tumors. J Clin Invest *123*, 340-347.

Jhanwar, S. C., Chen, Q., Li, F. P., Brennan, M. F., and Woodruff, J. M. (1994). Cytogenetic analysis of soft tissue sarcomas. Recurrent chromosome abnormalities in malignant peripheral nerve sheath tumors (MPNST). Cancer Genet Cytogenet *78*, 138-144.

Joaquin, M., and Watson, R. J. (2003). Cell cycle regulation by the B-Myb transcription factor. Cell Mol Life Sci *60*, 2389-2401.

Johannessen, C. M., Johnson, B. W., Williams, S. M., Chan, A. W., Reczek, E. E., Lynch, R. C., Rioth, M. J., McClatchey, A., Ryeom, S., and Cichowski, K. (2008). TORC1 is essential for NF1-associated malignancies. Curr Biol *18*, 56-62.

John, A. M., Ruggieri, M., Ferner, R., and Upadhyaya, M. (2000). A search for evidence of somatic mutations in the NF1 gene. J Med Genet *37*, 44-49.

Johnson, M. D., Kamso-Pratt, J., Federspiel, C. F., and Whetsell, W. O., Jr. (1989). Mast cell and lymphoreticular infiltrates in neurofibromas. Comparison with nerve sheath tumors. Arch Pathol Lab Med *113*, 1263-1270.

Johnson, V. L., Scott, M. I., Holt, S. V., Hussein, D., and Taylor, S. S. (2004). Bub1 is required for kinetochore localization of BubR1, Cenp-E, Cenp-F and Mad2, and chromosome congression. J Cell Sci *117*, 1577-1589.

Jordan, M. A., and Wilson, L. (2004). Microtubules as a target for anticancer drugs. Nat Rev Cancer *4*, 253-265.

Joseph, N. M., Mosher, J. T., Buchstaller, J., Snider, P., McKeever, P. E., Lim, M., Conway, S. J., Parada, L. F., Zhu, Y., and Morrison, S. J. (2008). The loss of Nf1 transiently promotes self-renewal but not tumorigenesis by neural crest stem cells. Cancer Cell *13*, 129-140.

Jouhilahti, E. M., Peltonen, S., Callens, T., Jokinen, E., Heape, A. M., Messiaen, L., and Peltonen, J. (2011). The development of cutaneous neurofibromas. Am J Pathol *178*, 500-505.

K

Kanemaki, M., Sanchez-Diaz, A., Gambus, A., and Labib, K. (2003). Functional proteomic identification of DNA replication proteins by induced proteolysis in vivo. Nature *423*, 720-724.

Kang, J. Y., Song, S. H., Yun, J., Jeon, M. S., Cha, Y., Lee, S. H., Kim, H. P., Jeong, E. G., Han, S. W., Cho, N. Y*., et al.* (2015). Identification of long-range epigenetic silencing on chromosome 15q25 and its clinical implication in gastric cancer. Am J Pathol *185*, 666-678.

Kas, K., Voz, M. L., Roijer, E., Astrom, A. K., Meyen, E., Stenman, G., and Van de Ven, W. J. (1997). Promoter swapping between the genes for a novel zinc finger protein and beta-catenin in pleiomorphic adenomas with t(3;8)(p21;q12) translocations. Nat Genet *15*, 170-174.

Katz, D., Lazar, A., and Lev, D. (2009). Malignant peripheral nerve sheath tumour (MPNST): the clinical implications of cellular signalling pathways. Expert Rev Mol Med *11*, e30.

Kaufmann, D., Muller, R., Kenner, O., Leistner, W., Hein, C., Vogel, W., and Bartelt, B. (2002). The N-terminal splice product NF1-10a-2 of the NF1 gene codes for a transmembrane segment. Biochem Biophys Res Commun *294*, 496-503.

Kavallaris, M. (2010). Microtubules and resistance to tubulin-binding agents. Nat Rev Cancer *10*, 194-204.

Kawachi, Y., Xu, X., Ichikawa, E., Imakado, S., and Otsuka, F. (2003). Expression of angiogenic factors in neurofibromas. Exp Dermatol *12*, 412-417.

Kayes, L. M., Burke, W., Riccardi, V. M., Bennett, R., Ehrlich, P., Rubenstein, A., and Stephens, K. (1994). Deletions spanning the neurofibromatosis 1 gene: identification and phenotype of five patients. Am J Hum Genet *54*, 424-436.

Kazmi, S. J., Byer, S. J., Eckert, J. M., Turk, A. N., Huijbregts, R. P., Brossier, N. M., Grizzle, W. E., Mikhail, F. M., Roth, K. A., and Carroll, S. L. (2013). Transgenic mice overexpressing neuregulin-1 model neurofibroma-malignant peripheral nerve sheath tumor progression and implicate specific chromosomal copy number variations in tumorigenesis. Am J Pathol *182*, 646-667.

Kehrer-Sawatzki, H., and Cooper, D. N. (2008). Mosaicism in sporadic neurofibromatosis type 1: variations on a theme common to other hereditary cancer syndromes? J Med Genet *45*, 622-631.

Kehrer-Sawatzki, H., Schwickardt, T., Assum, G., Rocchi, M., and Krone, W. (1997). A third neurofibromatosis type 1 (NF1) pseudogene at chromosome 15q11.2. Hum Genet *100*, 595-600.

Keng, V. W., Rahrmann, E. P., Watson, A. L., Tschida, B. R., Moertel, C. L., Jessen, W. J., Rizvi, T. A., Collins, M. H., Ratner, N., and Largaespada, D. A. (2012a). PTEN and NF1 inactivation in Schwann cells produces a severe phenotype in the peripheral nervous system that promotes the development and malignant progression of peripheral nerve sheath tumors. Cancer Res *72*, 3405-3413.

Keng, V. W., Watson, A. L., Rahrmann, E. P., Li, H., Tschida, B. R., Moriarity, B. S., Choi, K., Rizvi, T. A., Collins, M. H., Wallace, M. R*., et al.* (2012b). Conditional Inactivation of Pten with EGFR Overexpression in Schwann Cells Models Sporadic MPNST. Sarcoma *2012*, 620834.

Kinzler, K. W., and Vogelstein, B. (1996). Lessons from hereditary colorectal cancer. Cell *87*, 159-170.

Kluwe, L., Friedrich, R., and Mautner, V. F. (1999a). Loss of NF1 allele in Schwann cells but not in fibroblasts derived from an NF1-associated neurofibroma. Genes Chromosomes Cancer *24*, 283-285.

Kluwe, L., Friedrich, R. E., and Mautner, V. F. (1999b). Allelic loss of the NF1 gene in NF1-associated plexiform neurofibromas. Cancer Genet Cytogenet *113*, 65-69.

Knox, J. J., Gill, S., Synold, T. W., Biagi, J. J., Major, P., Feld, R., Cripps, C., Wainman, N., Eisenhauer, E., and Seymour, L. (2008). A phase II and pharmacokinetic study of SB-715992, in patients with metastatic hepatocellular carcinoma: a study of the National Cancer Institute of Canada Clinical Trials Group (NCIC CTG IND.168). Invest New Drugs *26*, 265-272.

Knudson, A. G., Jr. (1971). Mutation and cancer: statistical study of retinoblastoma. Proc Natl Acad Sci U S A *68*, 820-823.

Koivunen, J., Yla-Outinen, H., Korkiamaki, T., Karvonen, S. L., Poyhonen, M., Laato, M., Karvonen, J., Peltonen, S., and Peltonen, J. (2000). New function for NF1 tumor suppressor. J Invest Dermatol *114*, 473-479.

Kolberg, M., Holand, M., Lind, G. E., Agesen, T. H., Skotheim, R. I., Hall, K. S., Mandahl, N., Smeland, S., Mertens, F., Davidson, B., and Lothe, R. A. (2015). Protein expression of BIRC5, TK1, and TOP2A in malignant peripheral nerve sheath tumours--A prognostic test after surgical resection. Mol Oncol *9*, 1129-1139.

Kops, G. J., Weaver, B. A., and Cleveland, D. W. (2005). On the road to cancer: aneuploidy and the mitotic checkpoint. Nat Rev Cancer *5*, 773-785.

Kourea, H. P., Orlow, I., Scheithauer, B. W., Cordon-Cardo, C., and Woodruff, J. M. (1999). Deletions of the INK4A gene occur in malignant peripheral nerve sheath tumors but not in neurofibromas. Am J Pathol *155*, 1855-1860.

Kresse, S. H., Skarn, M., Ohnstad, H. O., Namlos, H. M., Bjerkehagen, B., Myklebost, O., and Meza-Zepeda, L. A. (2008). DNA copy number changes in high-grade malignant peripheral nerve sheath tumors by array CGH. Mol Cancer *7*, 48.

Krone, W., Jirikowski, G., Muhleck, O., Kling, H., and Gall, H. (1983). Cell culture studies on neurofibromatosis (von Recklinghausen). II. Occurrence of glial cells in primary cultures of peripheral neurofibromas. Hum Genet *63*, 247-251.

Krzywinski, M., Schein, J., Birol, I., Connors, J., Gascoyne, R., Horsman, D., Jones, S. J., and Marra, M. A. (2009). Circos: an information aesthetic for comparative genomics. Genome Res *19*, 1639-1645.

L

Lad, L., Luo, L., Carson, J. D., Wood, K. W., Hartman, J. J., Copeland, R. A., and Sakowicz, R. (2008). Mechanism of inhibition of human KSP by ispinesib. Biochemistry *47*, 3576-3585.

Lawrence, C. J., Dawe, R. K., Christie, K. R., Cleveland, D. W., Dawson, S. C., Endow, S. A., Goldstein, L. S., Goodson, H. V., Hirokawa, N., Howard, J.*, et al.* (2004). A standardized kinesin nomenclature. J Cell Biol *167*, 19-22.

Laycock-van Spyk, S., Thomas, N., Cooper, D. N., and Upadhyaya, M. (2011). Neurofibromatosis type 1-associated tumours: their somatic mutational spectrum and pathogenesis. Hum Genomics *5*, 623-690.

Le, L. Q., Shipman, T., Burns, D. K., and Parada, L. F. (2009). Cell of origin and microenvironment contribution for NF1-associated dermal neurofibromas. Cell Stem Cell *4*, 453-463.

Lee, C. W., Belanger, K., Rao, S. C., Petrella, T. M., Tozer, R. G., Wood, L., Savage, K. J., Eisenhauer, E. A., Synold, T. W., Wainman, N., and Seymour, L. (2008a). A phase II study of ispinesib (SB-715992) in patients with metastatic or recurrent malignant melanoma: a National Cancer Institute of Canada Clinical Trials Group trial. Invest New Drugs *26*, 249-255.

Lee, H., Kong, S. W., and Park, P. J. (2008b). Integrative analysis reveals the direct and indirect interactions between DNA copy number aberrations and gene expression changes. Bioinformatics *24*, 889-896.

Lee, W., Teckie, S., Wiesner, T., Ran, L., Prieto Granada, C. N., Lin, M., Zhu, S., Cao, Z., Liang, Y., Sboner, A.*, et al.* (2014). PRC2 is recurrently inactivated through EED or SUZ12 loss in malignant peripheral nerve sheath tumors. Nat Genet *46*, 1227-1232.

Legius, E., Dierick, H., Wu, R., Hall, B. K., Marynen, P., Cassiman, J. J., and Glover, T. W. (1994). TP53 mutations are frequent in malignant NF1 tumors. Genes Chromosomes Cancer *10*, 250-255.

Legius, E., Marchuk, D. A., Collins, F. S., and Glover, T. W. (1993). Somatic deletion of the neurofibromatosis type 1 gene in a neurofibrosarcoma supports a tumour suppressor gene hypothesis. Nat Genet *3*, 122-126.

Legius, E., Marchuk, D. A., Hall, B. K., Andersen, L. B., Wallace, M. R., Collins, F. S., and Glover, T. W. (1992). NF1-related locus on chromosome 15. Genomics *13*, 1316-1318.

Leppig, K. A., Kaplan, P., Viskochil, D., Weaver, M., Ortenberg, J., and Stephens, K. (1997). Familial neurofibromatosis 1 microdeletions: cosegregation with distinct facial phenotype and early onset of cutaneous neurofibromata. Am J Med Genet *73*, 197-204.

Levy, P., Vidaud, D., Leroy, K., Laurendeau, I., Wechsler, J., Bolasco, G., Parfait, B., Wolkenstein, P., Vidaud, M., and Bieche, I. (2004). Molecular profiling of malignant peripheral nerve sheath tumors associated with neurofibromatosis type 1, based on large-scale real-time RT-PCR. Mol Cancer *3*, 20.

Li, A., Liu, Z., Lezon-Geyda, K., Sarkar, S., Lannin, D., Schulz, V., Krop, I., Winer, E., Harris, L., and Tuck, D. (2011). GPHMM: an integrated hidden Markov model for identification of copy number alteration and loss of heterozygosity in complex tumor samples using whole genome SNP arrays. Nucleic Acids Res *39*, 4928-4941.

Li, C., Cheng, Y., Gutmann, D. A., and Mangoura, D. (2001). Differential localization of the neurofibromatosis 1 (NF1) gene product, neurofibromin, with the F-actin or microtubule cytoskeleton during differentiation of telencephalic neurons. Brain Res Dev Brain Res *130*, 231-248.

Li, Z., Pei, X. H., Yan, J., Yan, F., Cappell, K. M., Whitehurst, A. W., and Xiong, Y. (2014). CUL9 mediates the functions of the 3M complex and ubiquitylates survivin to maintain genome integrity. Mol Cell *54*, 805-819.

Li, Z., Zhao, X., Zhou, Y., Liu, Y., Zhou, Q., Ye, H., Wang, Y., Zeng, J., Song, Y., Gao, W*., et al.* (2015). The long non-coding RNA HOTTIP promotes progression and gemcitabine resistance by regulating HOXA13 in pancreatic cancer. J Transl Med *13*, 84.

Liu, M., Wang, X., Yang, Y., Li, D., Ren, H., Zhu, Q., Chen, Q., Han, S., Hao, J., and Zhou, J. (2010). Ectopic expression of the microtubule-dependent motor protein Eg5 promotes pancreatic tumourigenesis. J Pathol *221*, 221-228.

Liu, Z., Ling, K., Wu, X., Cao, J., Liu, B., Li, S., Si, Q., Cai, Y., Yan, C., Zhang, Y., and Weng, Y. (2009). Reduced expression of cenp-e in human hepatocellular carcinoma. J Exp Clin Cancer Res *28*, 156.

Loo, L. W., Tiirikainen, M., Cheng, I., Lum-Jones, A., Seifried, A., Church, J. M., Gryfe, R., Weisenberger, D. J., Lindor, N. M., Gallinger, S*., et al.* (2013). Integrated analysis of genome-wide copy number alterations and gene expression in microsatellite stable, CpG island methylator phenotype-negative colon cancer. Genes Chromosomes Cancer *52*, 450-466.

Lopez Correa, C., Brems, H., Lazaro, C., Estivill, X., Clementi, M., Mason, S., Rutkowski, J. L., Marynen, P., and Legius, E. (1999). Molecular studies in 20 submicroscopic neurofibromatosis type 1 gene deletions. Hum Mutat *14*, 387-393.

Lopez Correa, C., Brems, H., Lazaro, C., Marynen, P., and Legius, E. (2000). Unequal meiotic crossover: a frequent cause of NF1 microdeletions. Am J Hum Genet *66*, 1969-1974.

Lopez, G., Bill, K. L., Bid, H. K., Braggio, D., Constantino, D., Prudner, B., Zewdu, A., Batte, K., Lev, D., and Pollock, R. E. (2015). HDAC8, A Potential Therapeutic Target for the Treatment of Malignant Peripheral Nerve Sheath Tumors (MPNST). PLoS One *10*, e0133302.

Lopez, G., Torres, K., Liu, J., Hernandez, B., Young, E., Belousov, R., Bolshakov, S., Lazar, A. J., Slopis, J. M., McCutcheon, I. E*., et al.* (2011). Autophagic survival in resistance to histone deacetylase inhibitors: novel strategies to treat malignant peripheral nerve sheath tumors. Cancer Res *71*, 185-196.

LoRusso, P. M., Goncalves, P. H., Casetta, L., Carter, J. A., Litwiler, K., Roseberry, D., Rush, S., Schreiber, J., Simmons, H. M., Ptaszynski, M., and Sausville, E. A. (2015). First-in-human phase 1 study of filanesib (ARRY-520), a kinesin spindle protein inhibitor, in patients with advanced solid tumors. Invest New Drugs *33*, 440-449.

Lothe, R. A., Slettan, A., Saeter, G., Brogger, A., Borresen, A. L., and Nesland, J. M. (1995). Alterations at chromosome 17 loci in peripheral nerve sheath tumors. J Neuropathol Exp Neurol *54*, 65-73.

Lothe, R. A., Smith-Sorensen, B., Hektoen, M., Stenwig, A. E., Mandahl, N., Saeter, G., and Mertens, F. (2001). Biallelic inactivation of TP53 rarely contributes to the development of malignant peripheral nerve sheath tumors. Genes Chromosomes Cancer *30*, 202-206.

Luscan, A., Shackleford, G., Masliah-Planchon, J., Laurendeau, I., Ortonne, N., Varin, J., Lallemand, F., Leroy, K., Dumaine, V., Hivelin, M.*, et al.* (2014). The activation of the WNT signaling pathway is a Hallmark in neurofibromatosis type 1 tumorigenesis. Clin Cancer Res *20*, 358-371.

M

Ma, H. T., Erdal, S., Huang, S., and Poon, R. Y. (2014). Synergism between inhibitors of Aurora A and KIF11 overcomes KIF15-dependent drug resistance. Mol Oncol *8*, 1404-1418.

Maertens, O., Brems, H., Vandesompele, J., De Raedt, T., Heyns, I., Rosenbaum, T., De Schepper, S., De Paepe, A., Mortier, G., Janssens, S.*, et al.* (2006a). Comprehensive NF1 screening on cultured Schwann cells from neurofibromas. Hum Mutat *27*, 1030-1040.

Maertens, O., De Schepper, S., Vandesompele, J., Brems, H., Heyns, I., Janssens, S., Speleman, F., Legius, E., and Messiaen, L. (2007). Molecular dissection of isolated disease features in mosaic neurofibromatosis type 1. Am J Hum Genet *81*, 243-251.

Maertens, O., Legius, E., Speleman, F., Messiaen, L., and Vandesompele, J. (2006b). Real-time quantitative allele discrimination assay using 3' locked nucleic acid primers for detection of low-percentage mosaic mutations. Anal Biochem *359*, 144-146.

Maki, R. G., D'Adamo, D. R., Keohan, M. L., Saulle, M., Schuetze, S. M., Undevia, S. D., Livingston, M. B., Cooney, M. M., Hensley, M. L., Mita, M. M.*, et al.* (2009). Phase II study of sorafenib in patients with metastatic or recurrent sarcomas. J Clin Oncol *27*, 3133-3140.

Maksimovic, J., Gordon, L., and Oshlack, A. (2012). SWAN: Subset-quantile within array normalization for illumina infinium HumanMethylation450 BeadChips. Genome Biol *13*, R44.

Malumbres, M., and Barbacid, M. (2009). Cell cycle, CDKs and cancer: a changing paradigm. Nat Rev Cancer *9*, 153-166.

Mantripragada, K. K., Diaz de Stahl, T., Patridge, C., Menzel, U., Andersson, R., Chuzhanova, N., Kluwe, L., Guha, A., Mautner, V., Dumanski, J. P., and Upadhyaya, M. (2009). Genome-wide high-resolution analysis of DNA copy number alterations in NF1-associated malignant peripheral nerve sheath tumors using 32K BAC array. Genes Chromosomes Cancer *48*, 897-907.

Mantripragada, K. K., Spurlock, G., Kluwe, L., Chuzhanova, N., Ferner, R. E., Frayling, I. M., Dumanski, J. P., Guha, A., Mautner, V., and Upadhyaya, M. (2008). High-resolution DNA copy number profiling of malignant peripheral nerve sheath tumors using targeted microarray-based comparative genomic hybridization. Clin Cancer Res *14*, 1015-1024.

Mao, Y., Desai, A., and Cleveland, D. W. (2005). Microtubule capture by CENP-E silences BubR1-dependent mitotic checkpoint signaling. J Cell Biol *170*, 873-880.

Martens-de Kemp, S. R., Nagel, R., Stigter-van Walsum, M., van der Meulen, I. H., van Beusechem, V. W., Braakhuis, B. J., and Brakenhoff, R. H. (2013). Functional genetic screens identify genes essential for tumor cell survival in head and neck and lung cancer. Clin Cancer Res *19*, 1994-2003.

Martín, B. (2013). Caracterització epigenètica dels elements Alu i el seu paper en la regulació transcripcional. PhD thesis, Universitat de Barcelona.

Martin, G. A., Viskochil, D., Bollag, G., McCabe, P. C., Crosier, W. J., Haubruck, H., Conroy, L., Clark, R., O'Connell, P., Cawthon, R. M., and et al. (1990). The GAP-related domain of the neurofibromatosis type 1 gene product interacts with ras p21. Cell *63*, 843-849.

Martinez, I., and Dimaio, D. (2011). B-Myb, cancer, senescence, and microRNAs. Cancer Res *71*, 5370-5373.

Marullo, M., Zuccato, C., Mariotti, C., Lahiri, N., Tabrizi, S. J., Di Donato, S., and Cattaneo, E. (2010). Expressed Alu repeats as a novel, reliable tool for normalization of real-time quantitative RT-PCR data. Genome Biol *11*, R9.

Masayesva, B. G., Ha, P., Garrett-Mayer, E., Pilkington, T., Mao, R., Pevsner, J., Speed, T., Benoit, N., Moon, C. S., Sidransky, D*., et al.* (2004). Gene expression alterations over large chromosomal regions in cancers include multiple genes unrelated to malignant progression. Proc Natl Acad Sci U S A *101*, 8715-8720.

Mashour, G. A., Ratner, N., Khan, G. A., Wang, H. L., Martuza, R. L., and Kurtz, A. (2001). The angiogenic factor midkine is aberrantly expressed in NF1-deficient Schwann cells and is a mitogen for neurofibroma-derived cells. Oncogene *20*, 97-105.

Mawrin, C., Kirches, E., Boltze, C., Dietzmann, K., Roessner, A., and Schneider-Stock, R. (2002). Immunohistochemical and molecular analysis of p53, RB, and PTEN in malignant peripheral nerve sheath tumors. Virchows Arch *440*, 610-615.

Mechtersheimer, G., Otano-Joos, M., Ohl, S., Benner, A., Lehnert, T., Willeke, F., Moller, P., Otto, H. F., Lichter, P., and Joos, S. (1999). Analysis of chromosomal imbalances in sporadic and NF1-associated peripheral nerve sheath tumors by comparative genomic hybridization. Genes Chromosomes Cancer *25*, 362-369.

Menon, A. G., Anderson, K. M., Riccardi, V. M., Chung, R. Y., Whaley, J. M., Yandell, D. W., Farmer, G. E., Freiman, R. N., Lee, J. K., Li, F. P., and et al. (1990). Chromosome 17p deletions and p53 gene mutations associated with the formation of malignant neurofibrosarcomas in von Recklinghausen neurofibromatosis. Proc Natl Acad Sci U S A *87*, 5435-5439.

Mertens, F., Dal Cin, P., De Wever, I., Fletcher, C. D., Mandahl, N., Mitelman, F., Rosai, J., Rydholm, A., Sciot, R., Tallini, G*., et al.* (2000). Cytogenetic characterization of peripheral nerve sheath tumours: a report of the CHAMP study group. J Pathol *190*, 31-38.

Messiaen, L., and Wimmer, K. (2008). NF1 mutational spectrum. In: Kaufmann D, ed. Neurofibromatoses. Basel: Karger (Monographs in human genetics; vol. 16, p.63–77).

Michor, F., Iwasa, Y., and Nowak, M. A. (2004). Dynamics of cancer progression. Nat Rev Cancer *4*, 197-205.

Miki, H., Okada, Y., and Hirokawa, N. (2005). Analysis of the kinesin superfamily: insights into structure and function. Trends Cell Biol *15*, 467-476.

Miller, S. J., Jessen, W. J., Mehta, T., Hardiman, A., Sites, E., Kaiser, S., Jegga, A. G., Li, H., Upadhyaya, M., Giovannini, M*., et al.* (2009). Integrative genomic analyses of neurofibromatosis tumours identify SOX9 as a biomarker and survival gene. EMBO Mol Med *1*, 236-248.

Miller, S. J., Lan, Z. D., Hardiman, A., Wu, J., Kordich, J. J., Patmore, D. M., Hegde, R. S., Cripe, T. P., Cancelas, J. A., Collins, M. H., and Ratner, N. (2010). Inhibition of Eyes Absent Homolog 4 expression induces malignant peripheral nerve sheath tumor necrosis. Oncogene *29*, 368-379.

Miller, S. J., Rangwala, F., Williams, J., Ackerman, P., Kong, S., Jegga, A. G., Kaiser, S., Aronow, B. J., Frahm, S., Kluwe, L*., et al.* (2006). Large-scale molecular comparison of human schwann cells to malignant peripheral nerve sheath tumor cell lines and tissues. Cancer Res *66*, 2584-2591.

Mo, W., Chen, J., Patel, A., Zhang, L., Chau, V., Li, Y., Cho, W., Lim, K., Xu, J., Lazar, A. J*., et al.* (2013). CXCR4/CXCL12 mediate autocrine cell- cycle progression in NF1-associated malignant peripheral nerve sheath tumors. Cell *152*, 1077-1090.

Mohan, P., Castellsague, J., Jiang, J., Allen, K., Chen, H., Nemirovsky, O., Spyra, M., Hu, K., Kluwe, L., Pujana, M. A., *et al.* (2013). Genomic imbalance of HMMR/RHAMM regulates the sensitivity and response of malignant peripheral nerve sheath tumour cells to aurora kinase inhibition. Oncotarget *4*, 80-93.

Morin, A., Fritsch, L., Mathieu, J. R., Gilbert, C., Guarmit, B., Firlej, V., Gallou-Kabani, C., Vieillefond, A., Delongchamps, N. B., and Cabon, F. (2012). Identification of CAD as an androgen receptor interactant and an early marker of prostate tumor recurrence. FASEB J *26*, 460-467.

Muir, D., Neubauer, D., Lim, I. T., Yachnis, A. T., and Wallace, M. R. (2001). Tumorigenic properties of neurofibromin-deficient neurofibroma Schwann cells. Am J Pathol *158*, 501-513.

N

Nguyen, H. G., and Ravid, K. (2006). Tetraploidy/aneuploidy and stem cells in cancer promotion: The role of chromosome passenger proteins. J Cell Physiol *208*, 12-22.

Nielsen, G. P., Stemmer-Rachamimov, A. O., Ino, Y., Moller, M. B., Rosenberg, A. E., and Louis, D. N. (1999). Malignant transformation of neurofibromas in neurofibromatosis 1 is associated with CDKN2A/p16 inactivation. Am J Pathol *155*, 1879-1884.

NIH. (1988). Neurofibromatosis. Conference statement. National Institutes of Health Consensus Development Conference. Arch Neurol *45*, 575-578.

Nishi, T., Lee, P. S., Oka, K., Levin, V. A., Tanase, S., Morino, Y., and Saya, H. (1991). Differential expression of two types of the neurofibromatosis type 1 (NF1) gene transcripts related to neuronal differentiation. Oncogene *6*, 1555-1559.

Nislow, C., Lombillo, V. A., Kuriyama, R., and McIntosh, J. R. (1992). A plus-end-directed motor enzyme that moves antiparallel microtubules in vitro localizes to the interzone of mitotic spindles. Nature *359*, 543-547.

Nolan, T., Hands, R. E., and Bustin, S. A. (2006). Quantification of mRNA using real-time RT-PCR. Nat Protoc *1*, 1559-1582.

Nordlund, M., Gu, X., Shipley, M. T., and Ratner, N. (1993). Neurofibromin is enriched in the endoplasmic reticulum of CNS neurons. J Neurosci *13*, 1588-1600.

Novak, P., Jensen, T., Oshiro, M. M., Watts, G. S., Kim, C. J., and Futscher, B. W. (2008). Agglomerative epigenetic aberrations are a common event in human breast cancer. Cancer Res *68*, 8616-8625.

Nowicki, M. O., Pawlowski, P., Fischer, T., Hess, G., Pawlowski, T., and Skorski, T. (2003). Chronic myelogenous leukemia molecular signature. Oncogene *22*, 3952-3963.

O

O'Connor, O. A., Gerecitano, J., Van Deventer, H., Hainsworth, J., Zullo, K. M., Saikali, K., Seroogy, J., Wolff, A., and Escandon, R. (2015). The addition of granulocyte-colony stimulating factor shifts the dose limiting toxicity and markedly increases the maximum tolerated dose and activity of the kinesin spindle protein inhibitor SB-743921 in patients with relapsed or refractory lymphoma: results of an international, multicenter phase I/II study. Leuk Lymphoma *56*, 2585-2591.

Ohishi, J., Aoki, M., Nabeshima, K., Suzumiya, J., Takeuchi, T., Ogose, A., Hakozaki, M., Yamashita, Y., and Iwasaki, H. (2013). Imatinib mesylate inhibits cell growth of malignant peripheral nerve sheath tumors in vitro and in vivo through suppression of PDGFR-beta. BMC Cancer *13*, 224.

P

Park, G. H., Lee, S. J., Yim, H., Han, J. H., Kim, H. J., Sohn, Y. B., Ko, J. M., and Jeong, S. Y. (2014). TAGLN expression is upregulated in NF1-associated malignant peripheral nerve sheath tumors by hypomethylation in its promoter and subpromoter regions. Oncol Rep *32*, 1347-1354.

Park, J. H., Park, J., Choi, J. K., Lyu, J., Bae, M. G., Lee, Y. G., Bae, J. B., Park, D. Y., Yang, H. K., Kim, T. Y., and Kim, Y. J. (2011). Identification of DNA methylation changes associated with human gastric cancer. BMC Med Genomics *4*, 82.

Pasmant, E., de Saint-Trivier, A., Laurendeau, I., Dieux-Coeslier, A., Parfait, B., Vidaud, M., Vidaud, D., and Bieche, I. (2008). Characterization of a 7.6-Mb germline deletion encompassing the NF1 locus and about a hundred genes in an NF1 contiguous gene syndrome patient. Eur J Hum Genet *16*, 1459-1466.

Pasmant, E., Parfait, B., Luscan, A., Goussard, P., Briand-Suleau, A., Laurendeau, I., Fouveaut, C., Leroy, C., Montadert, A., Wolkenstein, P.*, et al.* (2015). Neurofibromatosis type 1 molecular diagnosis: what can NGS do for you when you have a large gene with loss of function mutations? Eur J Hum Genet *23*, 596-601.

Pasmant, E., Sabbagh, A., Spurlock, G., Laurendeau, I., Grillo, E., Hamel, M. J., Martin, L., Barbarot, S., Leheup, B., Rodriguez, D.*, et al.* (2010). NF1 microdeletions in neurofibromatosis type 1: from genotype to phenotype. Hum Mutat *31*, E1506-1518.

Patel, A. J., Liao, C. P., Chen, Z., Liu, C., Wang, Y., and Le, L. Q. (2014). BET bromodomain inhibition triggers apoptosis of NF1-associated malignant peripheral nerve sheath tumors through Bim induction. Cell Rep *6*, 81-92.

Patel, A. V., Eaves, D., Jessen, W. J., Rizvi, T. A., Ecsedy, J. A., Qian, M. G., Aronow, B. J., Perentesis, J. P., Serra, E., Cripe, T. P.*, et al.* (2012). Ras-driven transcriptome analysis identifies aurora kinase A as a potential malignant peripheral nerve sheath tumor therapeutic target. Clin Cancer Res *18*, 5020-5030.

Patwardhan, P. P., Surriga, O., Beckman, M. J., de Stanchina, E., Dematteo, R. P., Tap, W. D., and Schwartz, G. K. (2014). Sustained inhibition of receptor tyrosine kinases and macrophage depletion by PLX3397 and rapamycin as a potential new approach for the treatment of MPNSTs. Clin Cancer Res *20*, 3146-3158.

Peltonen, J., Jaakkola, S., Lebwohl, M., Renvall, S., Risteli, L., Virtanen, I., and Uitto, J. (1988). Cellular differentiation and expression of matrix genes in type 1 neurofibromatosis. Lab Invest *59*, 760-771.

Perez, M., Munoz-Galvan, S., Jimenez-Garcia, M. P., Marin, J. J., and Carnero, A. (2015). Efficacy of CDK4 inhibition against sarcomas depends on their levels of CDK4 and p16ink4 mRNA. Oncotarget.

Perrin, G. Q., Li, H., Fishbein, L., Thomson, S. A., Hwang, M. S., Scarborough, M. T., Yachnis, A. T., Wallace, M. R., Mareci, T. H., and Muir, D. (2007). An orthotopic xenograft model of intraneural NF1 MPNST suggests a potential association between steroid hormones and tumor cell proliferation. Lab Invest *87*, 1092-1102.

Perrone, F., Da Riva, L., Orsenigo, M., Losa, M., Jocolle, G., Millefanti, C., Pastore, E., Gronchi, A., Pierotti, M. A., and Pilotti, S. (2009). PDGFRA, PDGFRB, EGFR, and downstream signaling activation in malignant peripheral nerve sheath tumor. Neuro Oncol *11*, 725-736.

Perrone, F., Tabano, S., Colombo, F., Dagrada, G., Birindelli, S., Gronchi, A., Colecchia, M., Pierotti, M. A., and Pilotti, S. (2003). p15INK4b, p14ARF, and p16INK4a inactivation in sporadic and neurofibromatosis type 1-related malignant peripheral nerve sheath tumors. Clin Cancer Res *9*, 4132-4138.

Perry, A., Kunz, S. N., Fuller, C. E., Banerjee, R., Marley, E. F., Liapis, H., Watson, M. A., and Gutmann, D. H. (2002). Differential NF1, p16, and EGFR patterns by interphase cytogenetics (FISH) in malignant peripheral nerve sheath tumor (MPNST) and morphologically similar spindle cell neoplasms. J Neuropathol Exp Neurol *61*, 702-709.

Petek, E., Jenne, D. E., Smolle, J., Binder, B., Lasinger, W., Windpassinger, C., Wagner, K., Kroisel, P. M., and Kehrer-Sawatzki, H. (2003). Mitotic recombination mediated by the JJAZF1 (KIAA0160) gene causing somatic mosaicism and a new type of constitutional NF1 microdeletion in two children of a mosaic female with only few manifestations. J Med Genet *40*, 520-525.

Pfaffl, M. W. (2001). A new mathematical model for relative quantification in real-time RT-PCR. Nucleic Acids Res *29*, e45.

Phillips, J. L., Hayward, S. W., Wang, Y., Vasselli, J., Pavlovich, C., Padilla-Nash, H., Pezullo, J. R., Ghadimi, B. M., Grossfeld, G. D., Rivera, A.*, et al.* (2001). The consequences of chromosomal aneuploidy on gene expression profiles in a cell line model for prostate carcinogenesis. Cancer Res *61*, 8143-8149.

Pinna, V., Lanari, V., Daniele, P., Consoli, F., Agolini, E., Margiotti, K., Bottillo, I., Torrente, I., Bruselles, A., Fusilli, C.*, et al.* (2015). p.Arg1809Cys substitution in neurofibromin is associated with a distinctive NF1 phenotype without neurofibromas. Eur J Hum Genet *23*, 1068-1071.

Piotrowski, A., Xie, J., Liu, Y. F., Poplawski, A. B., Gomes, A. R., Madanecki, P., Fu, C., Crowley, M. R., Crossman, D. K., Armstrong, L.*, et al.* (2014). Germline loss-of-function mutations in LZTR1 predispose to an inherited disorder of multiple schwannomas. Nat Genet *46*, 182-187.

Plaat, B. E., Molenaar, W. M., Mastik, M. F., Hoekstra, H. J., te Meerman, G. J., and van den Berg, E. (1999). Computer-assisted cytogenetic analysis of 51 malignant peripheral-nerve-sheath tumors: sporadic vs. neurofibromatosis-type-1-associated malignant schwannomas. Int J Cancer *83*, 171-178.

Pollack, J. R., Sorlie, T., Perou, C. M., Rees, C. A., Jeffrey, S. S., Lonning, P. E., Tibshirani, R., Botstein, D., Borresen-Dale, A. L., and Brown, P. O. (2002). Microarray analysis reveals a major direct role of DNA copy number alteration in the transcriptional program of human breast tumors. Proc Natl Acad Sci U S A *99*, 12963-12968.

Purandare, S. M., Huntsman Breidenbach, H., Li, Y., Zhu, X. L., Sawada, S., Neil, S. M., Brothman, A., White, R., Cawthon, R., and Viskochil, D. (1995). Identification of neurofibromatosis 1 (NF1) homologous loci by direct sequencing, fluorescence in situ hybridization, and PCR amplification of somatic cell hybrids. Genomics *30*, 476-485.

Purcell, J. W., Davis, J., Reddy, M., Martin, S., Samayoa, K., Vo, H., Thomsen, K., Bean, P., Kuo, W. L., Ziyad, S.*, et al.* (2010). Activity of the kinesin spindle protein inhibitor ispinesib (SB-715992) in models of breast cancer. Clin Cancer Res *16*, 566-576.

R

Rahrmann, E. P., Moriarity, B. S., Otto, G. M., Watson, A. L., Choi, K., Collins, M. H., Wallace, M., Webber, B. R., Forster, C. L., Rizzardi, A. E.*, et al.* (2014). Trp53 haploinsufficiency modifies EGFR-driven peripheral nerve sheath tumorigenesis. Am J Pathol *184*, 2082-2098.

Rantala, J. K., Edgren, H., Lehtinen, L., Wolf, M., Kleivi, K., Vollan, H. K., Aaltola, A. R., Laasola, P., Kilpinen, S., Saviranta, P.*, et al.* (2010). Integrative functional genomics analysis of sustained polyploidy phenotypes in breast cancer cells identifies an oncogenic profile for GINS2. Neoplasia *12*, 877-888.

Rasmussen, S. A., Overman, J., Thomson, S. A., Colman, S. D., Abernathy, C. R., Trimpert, R. E., Moose, R., Virdi, G., Roux, K., Bauer, M.*, et al.* (2000). Chromosome 17 loss-of-heterozygosity studies in benign and malignant tumors in neurofibromatosis type 1. Genes Chromosomes Cancer *28*, 425-431.

Rath, O., and Kozielski, F. (2012). Kinesins and cancer. Nat Rev Cancer *12*, 527-539.

Riccardi, V. M. (1981). Cutaneous manifestation of neurofibromatosis: cellular interaction, pigmentation, and mast cells. Birth Defects Orig Artic Ser *17*, 129-145.

Riccardi, V.M. (1992). Neurofibromatosis: phenotype, natural history and pathogenesis. Baltimore: John Hopkins University Press.

Rihani, A., Van Maerken, T., Pattyn, F., Van Peer, G., Beckers, A., De Brouwer, S., Kumps, C., Mets, E., Van der Meulen, J., Rondou, P.*, et al.* (2013). Effective Alu repeat based RT-Qpcr normalization in cancer cell perturbation experiments. PLoS One *8*, e71776.

Rodenhiser, D. I., Coulter-Mackie, M. B., and Singh, S. M. (1993). Evidence of DNA methylation in the neurofibromatosis type 1 (NF1) gene region of 17q11.2. Hum Mol Genet *2*, 439-444.

Rodriguez, J., Vives, L., Jorda, M., Morales, C., Munoz, M., Vendrell, E., and Peinado, M. A. (2008). Genome-wide tracking of unmethylated DNA Alu repeats in normal and cancer cells. Nucleic Acids Res *36*, 770-784.

Rojnueangnit, K., Xie, J., Gomes, A., Sharp, A., Callens, T., Chen, Y., Liu, Y., Cochran, M., Abbott, M. A., Atkin, J.*, et al.* (2015). High Incidence of Noonan Syndrome Features Including Short Stature and Pulmonic Stenosis in Patients carrying NF1 Missense Mutations Affecting p.Arg1809: Genotype-Phenotype Correlation. Hum Mutat *36*, 1052-1063.

Rose, A. E., Satagopan, J. M., Oddoux, C., Zhou, Q., Xu, R., Olshen, A. B., Yu, J. Z., Dash, A., Jean-Gilles, J., Reuter, V.*, et al.* (2010). Copy number and gene expression differences between African American and Caucasian American prostate cancer. J Transl Med *8*, 70.

Rosenberg, C., Schut, T. B., Mostert, M. C., Tanke, H. J., Raap, A. K., Oosterhuis, J. W., and Looijenga, L. H. (1997). Comparative genomic hybridization in hypotriploid/hyperdiploid tumors. Cytometry *29*, 113-121.

Rouleau, G. A., Merel, P., Lutchman, M., Sanson, M., Zucman, J., Marineau, C., Hoang-Xuan, K., Demczuk, S., Desmaze, C., Plougastel, B., and et al. (1993). Alteration in a new gene encoding a putative membrane-organizing protein causes neuro-fibromatosis type 2. Nature *363*, 515-521.

Ruchaud, S., Carmena, M., and Earnshaw, W. C. (2007). Chromosomal passengers: conducting cell division. Nat Rev Mol Cell Biol *8*, 798-812.

S

Samur, M. K., Shah, P. K., Wang, X., Minvielle, S., Magrangeas, F., Avet-Loiseau, H., Munshi, N. C., and Li, C. (2013). The shaping and functional consequences of the dosage effect landscape in multiple myeloma. BMC Genomics *14*, 672.

Sawada, S., Florell, S., Purandare, S. M., Ota, M., Stephens, K., and Viskochil, D. (1996). Identification of NF1 mutations in both alleles of a dermal neurofibroma. Nat Genet *14*, 110-112.

Scanlan, M. J., Gout, I., Gordon, C. M., Williamson, B., Stockert, E., Gure, A. O., Jager, D., Chen, Y. T., Mackay, A., O'Hare, M. J., and Old, L. J. (2001). Humoral immunity to human breast cancer: antigen definition and quantitative analysis of mRNA expression. Cancer Immun *1*, 4.

Scheffzek, K., Ahmadian, M. R., Wiesmuller, L., Kabsch, W., Stege, P., Schmitz, F., and Wittinghofer, A. (1998). Structural analysis of the GAP-related domain from neurofibromin and its implications. EMBO J *17*, 4313-4327.

Schmidt, H., Taubert, H., Meye, A., Wurl, P., Bache, M., Bartel, F., Holzhausen, H. J., and Hinze, R. (2000). Gains in chromosomes 7, 8q, 15q and 17q are characteristic changes in malignant but not in benign peripheral nerve sheath tumors from patients with Recklinghausen's disease. Cancer Lett *155*, 181-190.

Schmidt, H., Wurl, P., Taubert, H., Meye, A., Bache, M., Holzhausen, H. J., and Hinze, R. (1999). Genomic imbalances of 7p and 17q in malignant peripheral nerve sheath tumors are clinically relevant. Genes Chromosomes Cancer *25*, 205-211.

Serra, E., Puig, S., Otero, D., Gaona, A., Kruyer, H., Ars, E., Estivill, X., and Lazaro, C. (1997). Confirmation of a double-hit model for the NF1 gene in benign neurofibromas. Am J Hum Genet *61*, 512-519.

Serra, E., Rosenbaum, T., Nadal, M., Winner, U., Ars, E., Estivill, X., and Lazaro, C. (2001). Mitotic recombination effects homozygosity for NF1 germline mutations in neurofibromas. Nat Genet *28*, 294-296.

Serra, E., Rosenbaum, T., Winner, U., Aledo, R., Ars, E., Estivill, X., Lenard, H. G., and Lazaro, C. (2000). Schwann cells harbor the somatic NF1 mutation in neurofibromas: evidence of two different Schwann cell subpopulations. Hum Mol Genet *9*, 3055-3064.

Sestini, R., Bacci, C., Provenzano, A., Genuardi, M., and Papi, L. (2008). Evidence of a four-hit mechanism involving SMARCB1 and NF2 in schwannomatosis-associated schwannomas. Hum Mutat *29*, 227-231.

Sharif, S., Moran, A., Huson, S. M., Iddenden, R., Shenton, A., Howard, E., and Evans, D. G. (2007). Women with neurofibromatosis 1 are at a moderately increased risk of developing breast cancer and should be considered for early screening. J Med Genet *44*, 481-484.

Sherman, L. S., Atit, R., Rosenbaum, T., Cox, A. D., and Ratner, N. (2000). Single cell Ras-GTP analysis reveals altered Ras activity in a subpopulation of neurofibroma Schwann cells but not fibroblasts. J Biol Chem *275*, 30740-30745.

Simsek-Kiper, P. O., Alanay, Y., Gulhan, B., Lissewski, C., Turkyilmaz, D., Alehan, D., Cetin, M., Utine, G. E., Zenker, M., and Boduroglu, K. (2013). Clinical and molecular analysis of RASopathies in a group of Turkish patients. Clin Genet *83*, 181-186.

Skotheim, R. I., Kallioniemi, A., Bjerkhagen, B., Mertens, F., Brekke, H. R., Monni, O., Mousses, S., Mandahl, N., Soeter, G., Nesland, J. M.*, et al.* (2003). Topoisomerase-II alpha is upregulated in malignant peripheral nerve sheath tumors and associated with clinical outcome. J Clin Oncol *21*, 4586-4591.

Sonobe, H., Takeuchi, T., Furihata, M., Taguchi, T., Kawai, A., Ohjimi, Y., Iwasaki, H., Kaneko, Y., and Ohtsuki, Y. (2000). A new human malignant peripheral nerve sheath tumour-cell line, HS-sch-2, harbouring p53 point mutation. Int J Oncol *17*, 347-352.

Sorensen, S. A., Mulvihill, J. J., and Nielsen, A. (1986). Long-term follow-up of von Recklinghausen neurofibromatosis. Survival and malignant neoplasms. N Engl J Med *314*, 1010-1015.

Steinmann, K., Cooper, D. N., Kluwe, L., Chuzhanova, N. A., Senger, C., Serra, E., Lazaro, C., Gilaberte, M., Wimmer, K., Mautner, V. F., and Kehrer-Sawatzki, H. (2007). Type 2 NF1 deletions are highly unusual by virtue of the absence of nonallelic homologous recombination hotspots and an apparent preference for female mitotic recombination. Am J Hum Genet *81*, 1201-1220.

Steinmann, K., Kluwe, L., Friedrich, R. E., Mautner, V. F., Cooper, D. N., and Kehrer-Sawatzki, H. (2009). Mechanisms of loss of heterozygosity in neurofibromatosis type 1-associated plexiform neurofibromas. J Invest Dermatol *129*, 615-621.

Stevenson, D. A., Zhou, H., Ashrafi, S., Messiaen, L. M., Carey, J. C., D'Astous, J. L., Santora, S. D., and Viskochil, D. H. (2006). Double inactivation of NF1 in tibial pseudarthrosis. Am J Hum Genet *79*, 143-148.

Stonecypher, M. S., Byer, S. J., Grizzle, W. E., and Carroll, S. L. (2005). Activation of the neuregulin-1/ErbB signaling pathway promotes the proliferation of neoplastic Schwann cells in human malignant peripheral nerve sheath tumors. Oncogene *24*, 5589-5605.

Storlazzi, C. T., Brekke, H. R., Mandahl, N., Brosjo, O., Smeland, S., Lothe, R. A., and Mertens, F. (2006). Identification of a novel amplicon at distal 17q containing the BIRC5/SURVIVIN gene in malignant peripheral nerve sheath tumours. J Pathol *209*, 492-500.

Stout, J. R., Yount, A. L., Powers, J. A., Leblanc, C., Ems-McClung, S. C., and Walczak, C. E. (2011). Kif18B interacts with EB1 and controls astral microtubule length during mitosis. Mol Biol Cell *22*, 3070-3080.

Stowe, I. B., Mercado, E. L., Stowe, T. R., Bell, E. L., Oses-Prieto, J. A., Hernandez, H., Burlingame, A. L., and McCormick, F. (2012). A shared molecular mechanism underlies the human rasopathies Legius syndrome and Neurofibromatosis-1. Genes Dev *26*, 1421-1426.

Stransky, N., Vallot, C., Reyal, F., Bernard-Pierrot, I., de Medina, S. G., Segraves, R., de Rycke, Y., Elvin, P., Cassidy, A., Spraggon, C.*, et al.* (2006). Regional copy number-independent deregulation of transcription in cancer. Nat Genet *38*, 1386-1396.

Stratton, M. R., Campbell, P. J., and Futreal, P. A. (2009). The cancer genome. Nature *458*, 719-724.

Strebhardt, K., and Ullrich, A. (2006). Targeting polo-like kinase 1 for cancer therapy. Nat Rev Cancer *6*, 321-330.

Stricker, T. P., Henriksen, K. J., Tonsgard, J. H., Montag, A. G., Krausz, T. N., and Pytel, P. (2013). Expression profiling of 519 kinase genes in matched malignant peripheral nerve sheath tumor/plexiform neurofibroma samples is discriminatory and identifies mitotic regulators BUB1B, PBK and NEK2 as overexpressed with transformation. Mod Pathol *26*, 930-943.

Subramanian, S., Thayanithy, V., West, R. B., Lee, C. H., Beck, A. H., Zhu, S., Downs-Kelly, E., Montgomery, K., Goldblum, J. R., Hogendoorn, P. C.*, et al.* (2010). Genome-wide transcriptome analyses reveal p53 inactivation mediated loss of miR-34a expression in malignant peripheral nerve sheath tumours. J Pathol *220*, 58-70.

Sun, D., Tainsky, M. A., and Haddad, R. (2012). Oncogene Mutation Survey in MPNST Cell Lines Enhances the Dominant Role of Hyperactive Ras in NF1 Associated Pro-Survival and Malignancy. Transl Oncogenomics *5*, 1-7.

Sun, W., Wright, F. A., Tang, Z., Nordgard, S. H., Van Loo, P., Yu, T., Kristensen, V. N., and Perou, C. M. (2009). Integrated study of copy number states and genotype calls using high-density SNP arrays. Nucleic Acids Res *37*, 5365-5377.

Suzuki, H., Ozawa, N., Taga, C., Kano, T., Hattori, M., and Sakaki, Y. (1994). Genomic analysis of a NF1-related pseudogene on human chromosome 21. Gene *147*, 277-280.

Szudek, J., Birch, P., Riccardi, V. M., Evans, D. G., and Friedman, J. M. (2000). Associations of clinical features in neurofibromatosis 1 (NF1). Genet Epidemiol *19*, 429-439.

Szudek, J., Evans, D. G., and Friedman, J. M. (2003). Patterns of associations of clinical features in neurofibromatosis 1 (NF1). Hum Genet *112*, 289-297.

Szudek, J., Joe, H., and Friedman, J. M. (2002). Analysis of intrafamilial phenotypic variation in neurofibromatosis 1 (NF1). Genet Epidemiol *23*, 150-164.

T

Tabone-Eglinger, S., Bahleda, R., Cote, J. F., Terrier, P., Vidaud, D., Cayre, A., Beauchet, A., Theou-Anton, N., Terrier-Lacombe, M. J., Lemoine, A.*, et al.* (2008). Frequent EGFR Positivity and Overexpression in High-Grade Areas of Human MPNSTs. Sarcoma *2008*, 849156.

Tajima, S., and Koda, K. (2015). A neurogenic tumor containing a low-grade malignant peripheral nerve sheath tumor (MPNST) component with loss of p16 expression and homozygous deletion of CDKN2A/p16: a case report showing progression from a neurofibroma to a high-grade MPNST. Int J Clin Exp Pathol *8*, 5113-5120.

Takahashi, S., Fusaki, N., Ohta, S., Iwahori, Y., Iizuka, Y., Inagawa, K., Kawakami, Y., Yoshida, K., and Toda, M. (2012). Downregulation of KIF23 suppresses glioma proliferation. J Neurooncol *106*, 519-529.

Tamborero, D., Gonzalez-Perez, A., Perez-Llamas, C., Deu-Pons, J., Kandoth, C., Reimand, J., Lawrence, M. S., Getz, G., Bader, G. D., Ding, L., and Lopez-Bigas, N. (2013). Comprehensive identification of mutational cancer driver genes across 12 tumor types. Sci Rep *3*, 2650.

Tan, B. T., Park, C. Y., Ailles, L. E., and Weissman, I. L. (2006). The cancer stem cell hypothesis: a work in progress. Lab Invest *86*, 1203-1207.

Tanaka, K., Matsumoto, K., and Toh, E. A. (1989). IRA1, an inhibitory regulator of the RAS-cyclic AMP pathway in Saccharomyces cerevisiae. Mol Cell Biol *9*, 757-768.

Tanaka, K., Nakafuku, M., Tamanoi, F., Kaziro, Y., Matsumoto, K., and Toh, E. A. (1990). IRA2, a second gene of Saccharomyces cerevisiae that encodes a protein with a domain homologous to mammalian ras GTPase-activating protein. Mol Cell Biol *10*, 4303-4313.

Tanenbaum, M. E., Macurek, L., Janssen, A., Geers, E. F., Alvarez-Fernandez, M., and Medema, R. H. (2009). Kif15 cooperates with eg5 to promote bipolar spindle assembly. Curr Biol *19*, 1703-1711.

Tanenbaum, M. E., Macurek, L., van der Vaart, B., Galli, M., Akhmanova, A., and Medema, R. H. (2011). A complex of Kif18b and MCAK promotes microtubule depolymerization and is negatively regulated by Aurora kinases. Curr Biol *21*, 1356-1365.

Tang, P. A., Siu, L. L., Chen, E. X., Hotte, S. J., Chia, S., Schwarz, J. K., Pond, G. R., Johnson, C., Colevas, A. D., Synold, T. W*., et al.* (2008). Phase II study of ispinesib in recurrent or metastatic squamous cell carcinoma of the head and neck. Invest New Drugs *26*, 257-264.

Taylor, B. S., Barretina, J., Maki, R. G., Antonescu, C. R., Singer, S., and Ladanyi, M. (2011). Advances in sarcoma genomics and new therapeutic targets. Nat Rev Cancer *11*, 541-557.

Tcherniuk, S., Skoufias, D. A., Labriere, C., Rath, O., Gueritte, F., Guillou, C., and Kozielski, F. (2010). Relocation of Aurora B and survivin from centromeres to the central spindle impaired by a kinesin-specific MKLP-2 inhibitor. Angew Chem Int Ed Engl *49*, 8228-8231.

Teinturier, C., Danglot, G., Slim, R., Pruliere, D., Launay, J. M., Bernheim, A. (1992). The neurofibromatosis 1 gene transcripts expressed in peripheral nerve and neurofibromas bear the additional exon located in the GAP domain. Biochem Biophys Res Commun *188*, 851-857

Terribas, E., Garcia-Linares, C., Lazaro, C., and Serra, E. (2013). Probe-based quantitative PCR assay for detecting constitutional and somatic deletions in the NF1 gene: application to genetic testing and tumor analysis. Clin Chem *59*, 928-937.

Thomas, L., Kluwe, L., Chuzhanova, N., Mautner, V., and Upadhyaya, M. (2010). Analysis of NF1 somatic mutations in cutaneous neurofibromas from patients with high tumor burden. Neurogenetics *11*, 391-400.

Thomas, L., Spurlock, G., Eudall, C., Thomas, N. S., Mort, M., Hamby, S. E., Chuzhanova, N., Brems, H., Legius, E., Cooper, D. N., and Upadhyaya, M. (2012). Exploring the somatic NF1 mutational spectrum associated with NF1 cutaneous neurofibromas. Eur J Hum Genet *20*, 411-419.

Tong, J., Hannan, F., Zhu, Y., Bernards, A., and Zhong, Y. (2002). Neurofibromin regulates G protein-stimulated adenylyl cyclase activity. Nat Neurosci *5*, 95-96.

Tonjes, M., Barbus, S., Park, Y. J., Wang, W., Schlotter, M., Lindroth, A. M., Pleier, S. V., Bai, A. H., Karra, D., Piro, R. M*., et al.* (2013). BCAT1 promotes cell proliferation through amino acid catabolism in gliomas carrying wild-type IDH1. Nat Med *19*, 901-908.

Torres, K. E., Zhu, Q. S., Bill, K., Lopez, G., Ghadimi, M. P., Xie, X., Young, E. D., Liu, J., Nguyen, T., Bolshakov, S*., et al.* (2011). Activated MET is a molecular prognosticator and potential therapeutic target for malignant peripheral nerve sheath tumors. Clin Cancer Res *17*, 3943-3955.

Trofatter, J. A., MacCollin, M. M., Rutter, J. L., Murrell, J. R., Duyao, M. P., Parry, D. M., Eldridge, R., Kley, N., Menon, A. G., Pulaski, K., and et al. (1993). A novel moesin-, ezrin-, radixin-like gene is a candidate for the neurofibromatosis 2 tumor suppressor. Cell *72*, 791-800.

Tsafrir, D., Bacolod, M., Selvanayagam, Z., Tsafrir, I., Shia, J., Zeng, Z., Liu, H., Krier, C., Stengel, R. F., Barany, F*., et al.* (2006). Relationship of gene expression and chromosomal abnormalities in colorectal cancer. Cancer Res *66*, 2129-2137.

Tucker, T., Wolkenstein, P., Revuz, J., Zeller, J., and Friedman, J. M. (2005). Association between benign and malignant peripheral nerve sheath tumors in NF1. Neurology *65*, 205-211.

U

Uchida, T., Matozaki, T., Suzuki, T., Matsuda, K., Wada, K., Nakano, O., Konda, Y., Nishisaki, H., Nagao, M., Sakamoto, C., *et al.* (1992). Expression of two types of neurofibromatosis type 1 gene transcripts in gastric cancers and comparison of GAP activities. Biochem Biophys Res Commun *187*, 332-339.

Upadhyaya, M., Huson, S. M., Davies, M., Thomas, N., Chuzhanova, N., Giovannini, S., Evans, D. G., Howard, E., Kerr, B., Griffiths, S*., et al.* (2007). An absence of cutaneous neurofibromas associated with a 3-bp inframe deletion in exon 17 of the NF1 gene (c.2970-2972 delAAT): evidence of a clinically significant NF1 genotype-phenotype correlation. Am J Hum Genet *80*, 140-151.

Upadhyaya, M., Kluwe, L., Spurlock, G., Monem, B., Majounie, E., Mantripragada, K., Ruggieri, M., Chuzhanova, N., Evans, D. G., Ferner, R*., et al.* (2008a). Germline and somatic NF1 gene mutation spectrum in NF1-associated malignant peripheral nerve sheath tumors (MPNSTs). Hum Mutat *29*, 74-82.

Upadhyaya, M., Spurlock, G., Monem, B., Thomas, N., Friedrich, R. E., Kluwe, L., and Mautner, V. (2008b). Germline and somatic NF1 gene mutations in plexiform neurofibromas. Hum Mutat *29*, E103-111.

Upadhyaya, M., Spurlock, G., Thomas, L., Thomas, N. S., Richards, M., Mautner, V. F., Cooper, D. N., Guha, A., and Yan, J. (2012). Microarray-based copy number analysis of neurofibromatosis type-1 (NF1)-associated malignant peripheral nerve sheath tumors reveals a role for Rho-GTPase pathway genes in NF1 tumorigenesis. Hum Mutat *33*, 763-776.

V

Van Loo, P., Nilsen, G., Nordgard, S. H., Vollan, H. K., Borresen-Dale, A. L., Kristensen, V. N., and Lingjaerde, O. C. (2012). Analyzing cancer samples with SNP arrays. Methods Mol Biol *802*, 57-72.

Vandenbroucke, I., Van Oostveldt, P., Coene, E., De Paepe, A., and Messiaen, L. (2004). Neurofibromin is actively transported to the nucleus. FEBS Lett *560*, 98-102.

Vandesompele, J., De Preter, K., Pattyn, F., Poppe, B., Van Roy, N., De Paepe, A., and Speleman, F. (2002). Accurate normalization of real-time quantitative RT-PCR data by geometric averaging of multiple internal control genes. Genome Biol *3*, RESEARCH0034.

Vanhauwaert, S., Van Peer, G., Rihani, A., Janssens, E., Rondou, P., Lefever, S., De Paepe, A., Coucke, P. J., Speleman, F., Vandesompele, J., and Willaert, A. (2014). Expressed repeat elements improve RT-qPCR normalization across a wide range of zebrafish gene expression studies. PLoS One *9*, e109091.

Vanneste, D., Takagi, M., Imamoto, N., and Vernos, I. (2009). The role of Hklp2 in the stabilization and maintenance of spindle bipolarity. Curr Biol *19*, 1712-1717.

Venere, M., Horbinski, C., Crish, J. F., Jin, X., Vasanji, A., Major, J., Burrows, A. C., Chang, C., Prokop, J., Wu, Q.*, et al.* (2015). The mitotic kinesin KIF11 is a driver of invasion, proliferation, and self-renewal in glioblastoma. Sci Transl Med *7*, 304ra143.

Venturin, M., Bentivegna, A., Moroni, R., Larizza, L., and Riva, P. (2005). Evidence by expression analysis of candidate genes for congenital heart defects in the NF1 microdeletion interval. Ann Hum Genet *69*, 508-516.

Verdijk, R. M., den Bakker, M. A., Dubbink, H. J., Hop, W. C., Dinjens, W. N., and Kros, J. M. (2010). TP53 mutation analysis of malignant peripheral nerve sheath tumors. J Neuropathol Exp Neurol *69*, 16-26.

Versteege, I., Sevenet, N., Lange, J., Rousseau-Merck, M. F., Ambros, P., Handgretinger, R., Aurias, A., and Delattre, O. (1998). Truncating mutations of hSNF5/INI1 in aggressive paediatric cancer. Nature *394*, 203-206.

Viskochil, D., Buchberg, A. M., Xu, G., Cawthon, R. M., Stevens, J., Wolff, R. K., Culver, M., Carey, J. C., Copeland, N. G., Jenkins, N. A., and et al. (1990). Deletions and a translocation interrupt a cloned gene at the neurofibromatosis type 1 locus. Cell *62*, 187-192.

Viskochil, D., Cawthon, R., O'Connell, P., Xu, G. F., Stevens, J., Culver, M., Carey, J., and White, R. (1991). The gene encoding the oligodendrocyte-myelin glycoprotein is embedded within the neurofibromatosis type 1 gene. Mol Cell Biol *11*, 906-912.

Vogel, K. S., Klesse, L. J., Velasco-Miguel, S., Meyers, K., Rushing, E. J., and Parada, L. F. (1999). Mouse tumor model for neurofibromatosis type 1. Science *286*, 2176-2179.

Vogt, J., Bengesser, K., Claes, K. B., Wimmer, K., Mautner, V. F., van Minkelen, R., Legius, E., Brems, H., Upadhyaya, M., Hogel, J.*, et al.* (2014). SVA retrotransposon insertion-associated deletion represents a novel mutational mechanism underlying large genomic copy number changes with non-recurrent breakpoints. Genome Biol *15*, R80.

Vossaert, L., O'Leary, T., Van Neste, C., Heindryckx, B., Vandesompele, J., De Sutter, P., and Deforce, D. (2013). Reference loci for RT-qPCR analysis of differentiating human embryonic stem cells. BMC Mol Biol *14*, 21.

Voz, M. L., Agten, N. S., Van de Ven, W. J., and Kas, K. (2000). PLAG1, the main translocation target in pleomorphic adenoma of the salivary glands, is a positive regulator of IGF-II. Cancer Res *60*, 106-113.

W

Walczak, C. E., Vernos, I., Mitchison, T. J., Karsenti, E., and Heald, R. (1998). A model for the proposed roles of different microtubule-based motor proteins in establishing spindle bipolarity. Curr Biol *8*, 903-913.

Wallace, M. R., Marchuk, D. A., Andersen, L. B., Letcher, R., Odeh, H. M., Saulino, A. M., Fountain, J. W., Brereton, A., Nicholson, J., Mitchell, A. L., and et al. (1990). Type 1 neurofibromatosis gene: identification of a large transcript disrupted in three NF1 patients. Science *249*, 181-186.

Wallace, M. R., Rasmussen, S. A., Lim, I. T., Gray, B. A., Zori, R. T., and Muir, D. (2000). Culture of cytogenetically abnormal schwann cells from benign and malignant NF1 tumors. Genes Chromosomes Cancer *27*, 117-123.

Wallander, M. L., Tripp, S., and Layfield, L. J. (2012). MDM2 amplification in malignant peripheral nerve sheath tumors correlates with p53 protein expression. Arch Pathol Lab Med *136*, 95-99.

Wang, H. U., Chen, Z. F., and Anderson, D. J. (1998). Molecular distinction and angiogenic interaction between embryonic arteries and veins revealed by ephrin-B2 and its receptor Eph-B4. Cell *93*, 741-753.

Wang, T. L., Diaz, L. A., Jr., Romans, K., Bardelli, A., Saha, S., Galizia, G., Choti, M., Donehower, R., Parmigiani, G., Shih Ie, M.*, et al.* (2004). Digital karyotyping identifies thymidylate synthase amplification as a mechanism of resistance to 5-fluorouracil in metastatic colorectal cancer patients. Proc Natl Acad Sci U S A *101*, 3089-3094.

Wang, T. L., Maierhofer, C., Speicher, M. R., Lengauer, C., Vogelstein, B., Kinzler, K. W., and Velculescu, V. E. (2002). Digital karyotyping. Proc Natl Acad Sci U S A *99*, 16156-16161.

Wang, X., He, C., and Hu, X. (2014a). LIM homeobox transcription factors, a novel subfamily which plays an important role in cancer (review). Oncol Rep *31*, 1975-1985.

Wang, X., Levin, A. M., Smolinski, S. E., Vigneau, F. D., Levin, N. K., and Tainsky, M. A. (2012). Breast cancer and other neoplasms in women with neurofibromatosis type 1: a retrospective review of cases in the Detroit metropolitan area. Am J Med Genet A *158A*, 3061-3064.

Wang, Y., Zhao, Z., Bao, X., Fang, Y., Ni, P., Chen, Q., Zhang, W., and Deng, A. (2014b). Borealin/Dasra B is overexpressed in colorectal cancers and contributes to proliferation of cancer cells. Med Oncol *31*, 248.

Wang, Z., Yin, B., Wang, B., Ma, Z., Liu, W., and Lv, G. (2013). MicroRNA-210 promotes proliferation and invasion of peripheral nerve sheath tumor cells targeting EFNA3. Oncol Res *21*, 145-154.

Wang, Z. Q., Faddaoui, A., Bachvarova, M., Plante, M., Gregoire, J., Renaud, M. C., Sebastianelli, A., Guillemette, C., Gobeil, S., Macdonald, E.*, et al.* (2015). BCAT1 expression associates with ovarian cancer progression: possible implications in altered disease metabolism. Oncotarget *6*, 31522-31543.

Watson, A. L., Anderson, L. K., Greeley, A. D., Keng, V. W., Rahrmann, E. P., Halfond, A. L., Powell, N. M., Collins, M. H., Rizvi, T., Moertel, C. L.*, et al.* (2014). Co-targeting the MAPK and PI3K/AKT/mTOR pathways in two genetically engineered mouse models of schwann cell tumors reduces tumor grade and multiplicity. Oncotarget *5*, 1502-1514.

Watson, A. L., Rahrmann, E. P., Moriarity, B. S., Choi, K., Conboy, C. B., Greeley, A. D., Halfond, A. L., Anderson, L. K., Wahl, B. R., Keng, V. W.*, et al.* (2013). Canonical Wnt/beta-catenin signaling drives human schwann cell transformation, progression, and tumor maintenance. Cancer Discov *3*, 674-689.

Welti, S., Fraterman, S., D'Angelo, I., Wilm, M., and Scheffzek, K. (2007). The sec14 homology module of neurofibromin binds cellular glycerophospholipids: mass spectrometry and structure of a lipid complex. J Mol Biol *366*, 551-562.

Wiest, V., Eisenbarth, I., Schmegner, C., Krone, W., and Assum, G. (2003). Somatic NF1 mutation spectra in a family with neurofibromatosis type 1: toward a theory of genetic modifiers. Hum Mutat *22*, 423-427.

Wimmer, K., Callens, T., Wernstedt, A., and Messiaen, L. (2011). The NF1 gene contains hotspots for L1 endonuclease-dependent de novo insertion. PLoS Genet *7*, e1002371.

Wood, K. W., Cornwell, W. D., and Jackson, J. R. (2001). Past and future of the mitotic spindle as an oncology target. Curr Opin Pharmacol *1*, 370-377.

Wood, K. W., Lad, L., Luo, L., Qian, X., Knight, S. D., Nevins, N., Brejc, K., Sutton, D., Gilmartin, A. G., Chua, P. R.*, et al.* (2010). Antitumor activity of an allosteric inhibitor of centromere-associated protein-E. Proc Natl Acad Sci U S A *107*, 5839-5844.

Wordeman, L. (2010). How kinesin motor proteins drive mitotic spindle function: Lessons from molecular assays. Semin Cell Dev Biol *21*, 260-268.

Wu, B. L., Austin, M. A., Schneider, G. H., Boles, R. G., and Korf, B. R. (1995). Deletion of the entire NF1 gene detected by the FISH: four deletion patients associated with severe manifestations. Am J Med Genet *59*, 528-535.

Wu, J., Patmore, D. M., Jousma, E., Eaves, D. W., Breving, K., Patel, A. V., Schwartz, E. B., Fuchs, J. R., Cripe, T. P., Stemmer-Rachamimov, A. O., and Ratner, N. (2014). EGFR-STAT3 signaling promotes formation of malignant peripheral nerve sheath tumors. Oncogene *33*, 173-180.

X

Xu, G. F., Lin, B., Tanaka, K., Dunn, D., Wood, D., Gesteland, R., White, R., Weiss, R., and Tamanoi, F. (1990). The catalytic domain of the neurofibromatosis type 1 gene product stimulates ras GTPase and complements ira mutants of S. cerevisiae. Cell *63*, 835-841.

Y

Yamashita, A. S., Baia, G. S., Ho, J. S., Velarde, E., Wong, J., Gallia, G. L., Belzberg, A. J., Kimura, E. T., and Riggins, G. J. (2014). Preclinical evaluation of the combination of mTOR and proteasome inhibitors with radiotherapy in malignant peripheral nerve sheath tumors. J Neurooncol *118*, 83-92.

Yan, J., Yan, F., Li, Z., Sinnott, B., Cappell, K. M., Yu, Y., Mo, J., Duncan, J. A., Chen, X., Cormier-Daire, V.*, et al.* (2014). The 3M complex maintains microtubule and genome integrity. Mol Cell *54*, 791-804.

Yang, F. C., Ingram, D. A., Chen, S., Hingtgen, C. M., Ratner, N., Monk, K. R., Clegg, T., White, H., Mead, L., Wenning, M. J.*, et al.* (2003). Neurofibromin-deficient Schwann cells secrete a potent migratory stimulus for Nf1+/- mast cells. J Clin Invest *112*, 1851-1861.

Yang, J., and Du, X. (2013). Genomic and molecular aberrations in malignant peripheral nerve sheath tumor and their roles in personalized target therapy. Surg Oncol *22*, e53-57.

Yang, J., Ylipaa, A., Sun, Y., Zheng, H., Chen, K., Nykter, M., Trent, J., Ratner, N., Lev, D. C., and Zhang, W. (2011). Genomic and molecular characterization of malignant peripheral nerve sheath tumor identifies the IGF1R pathway as a primary target for treatment. Clin Cancer Res *17*, 7563-7573.

Ye, X. S., Fan, L., Van Horn, R. D., Nakai, R., Ohta, Y., Akinaga, S., Murakata, C., Yamashita, Y., Yin, T., Credille, K. M.*, et al.* (2015). A Novel Eg5 Inhibitor (LY2523355) Causes Mitotic Arrest and Apoptosis in Cancer Cells and Shows Potent Antitumor Activity in Xenograft Tumor Models. Mol Cancer Ther *14*, 2463-2472.

Yen, T. J., Compton, D. A., Wise, D., Zinkowski, R. P., Brinkley, B. R., Earnshaw, W. C., and Cleveland, D. W. (1991). CENP-E, a novel human centromere-associated protein required for progression from metaphase to anaphase. EMBO J *10*, 1245-1254.

Yu, H., Zhao, X., Su, B., Li, D., Xu, Y., Luo, S., Xiao, C., and Wang, W. (2005). Expression of NF1 pseudogenes. Hum Mutat *26*, 487-488.

Z

Zhang, E. Y., Cristofanilli, M., Robertson, F., Reuben, J. M., Mu, Z., Beavis, R. C., Im, H., Snyder, M., Hofree, M., Ideker, T.*, et al.* (2013). Genome wide proteomics of ERBB2 and EGFR and other oncogenic pathways in inflammatory breast cancer. J Proteome Res *12*, 2805-2817.

Zhang, M., Wang, Y., Jones, S., Sausen, M., McMahon, K., Sharma, R., Wang, Q., Belzberg, A. J., Chaichana, K., Gallia, G. L.*, et al.* (2014). Somatic mutations of SUZ12 in malignant peripheral nerve sheath tumors. Nat Genet *46*, 1170-1172.

Zhang, P., Yang, X., Ma, X., Ingram, D. R., Lazar, A. J., Torres, K. E., and Pollock, R. E. (2015). Antitumor effects of pharmacological EZH2 inhibition on malignant peripheral nerve sheath tumor through the miR-30a and KPNB1 pathway. Mol Cancer *14*, 55.

Zheng, M., Zhou, Y., Yang, X., Tang, J., Wei, D., Zhang, Y., Jiang, J. L., Chen, Z. N., and Zhu, P. (2014). High GINS2 transcript level predicts poor prognosis and correlates with high histological grade and endocrine therapy resistance through mammary cancer stem cells in breast cancer patients. Breast Cancer Res Treat *148*, 423-436.

Zhou, W., Feng, X., Li, H., Wang, L., Zhu, B., Zhang, H., Yao, K., and Ren, C. (2007). Functional evidence for a nasopharyngeal carcinoma-related gene BCAT1 located at 12p12. Oncol Res *16*, 405-413.

Zhu, C., Zhao, J., Bibikova, M., Leverson, J. D., Bossy-Wetzel, E., Fan, J. B., Abraham, R. T., and Jiang, W. (2005). Functional analysis of human microtubule-based motor proteins, the kinesins and dyneins, in mitosis/cytokinesis using RNA interference. Mol Biol Cell *16*, 3187-3199.

Zhu, Y., Ghosh, P., Charnay, P., Burns, D. K., and Parada, L. F. (2002). Neurofibromas in NF1: Schwann cell origin and role of tumor environment. Science *296*, 920-922.

Zickler, A. M., Hampp, S., Messiaen, L., Bengesser, K., Mussotter, T., Roehl, A. C., Wimmer, K., Mautner, V. F., Kluwe, L., Upadhyaya, M.*, et al.* (2012). Characterization of the nonallelic homologous recombination hotspot PRS3 associated with type-3 NF1 deletions. Hum Mutat *33*, 372-383.

Zietsch, J., Ziegenhagen, N., Heppner, F. L., Reuss, D., von Deimling, A., and Holtkamp, N. (2010). The 4q12 amplicon in malignant peripheral nerve sheath tumors: consequences on gene expression and implications for sunitinib treatment. PLoS One *5*, e11858.

ANNEXE 1

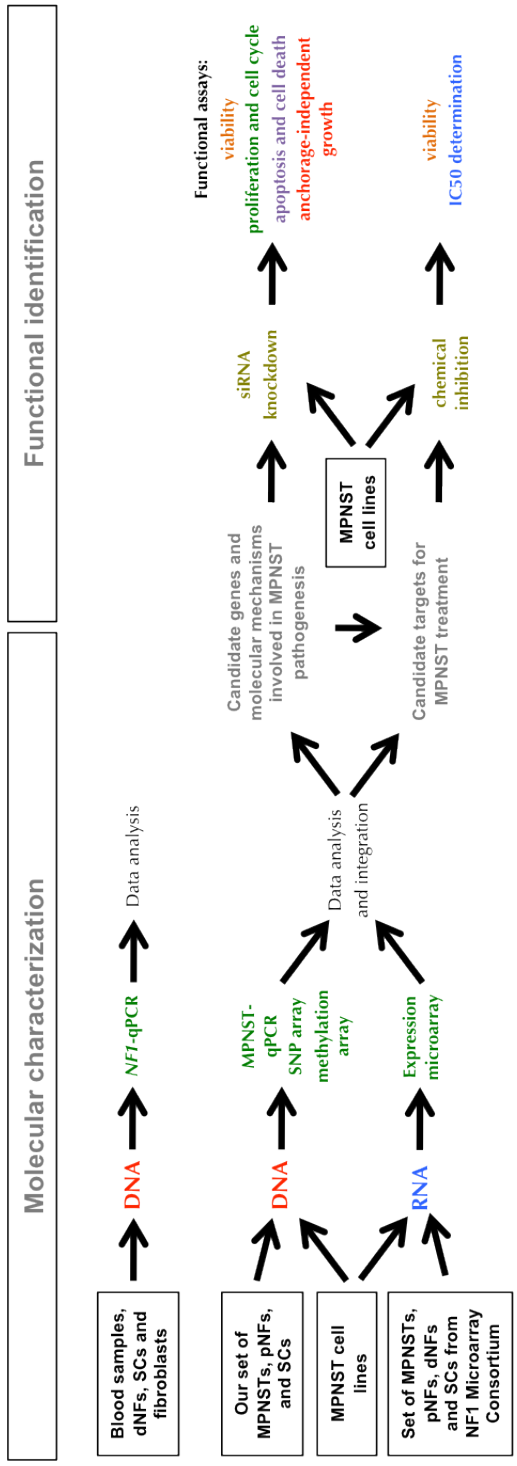

Figure A.1. Experimental design of the thesis project. Diagram including the experiments performed in the molecular characterization of NF1-associated tumours, MPNST cell lines and other samples and the *in vitro* experiments performed in the functional identification of candidate genes for MPNST pathogenesis.

A

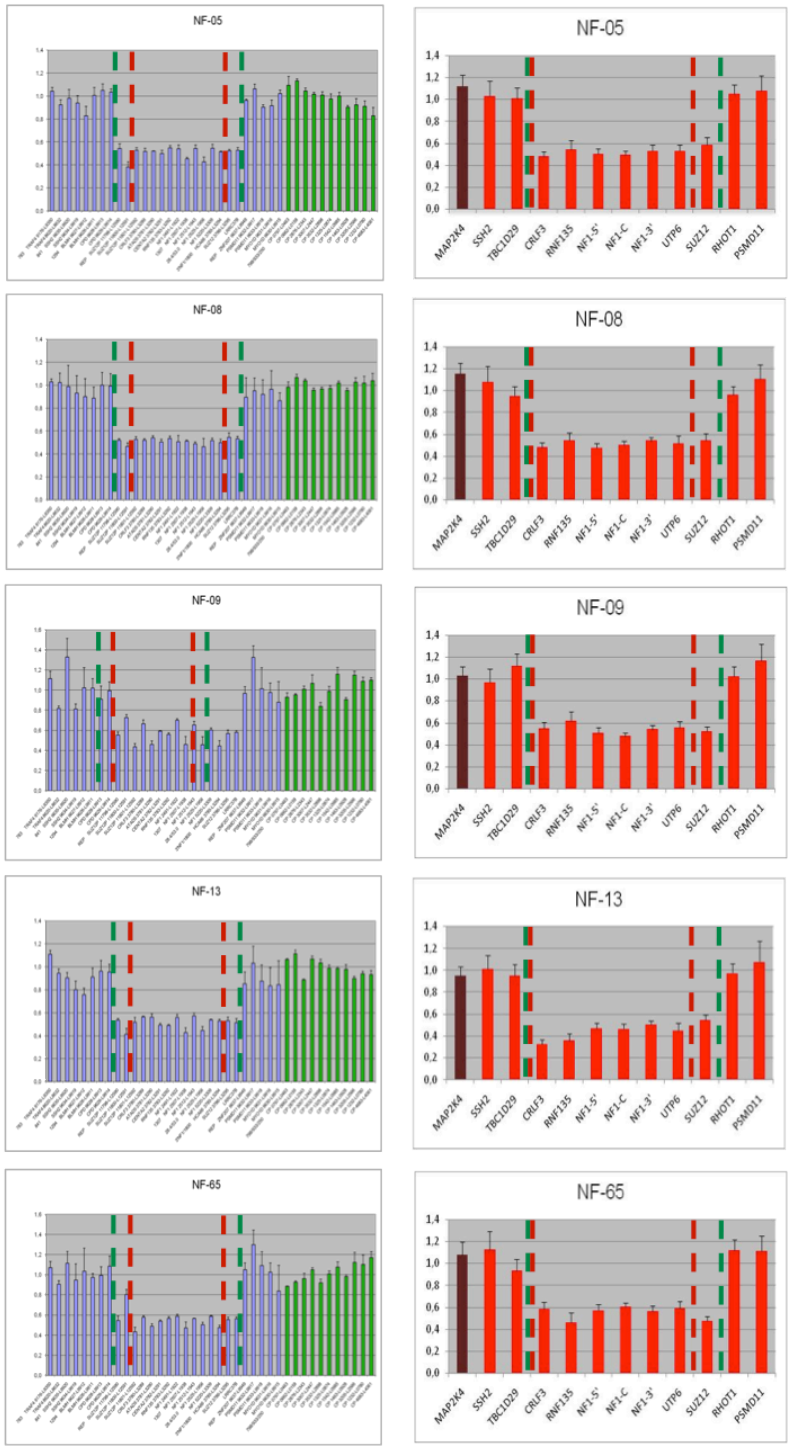
NF-05
NF-08
NF-09
NF-13
NF-65
MAP2K4
SSH2
TBC1D29
CRLF3
RNF135
NF1-5'
NF1-C
NF1-3'
UTP6
SUZ12
RHOT1
PSMD11

B

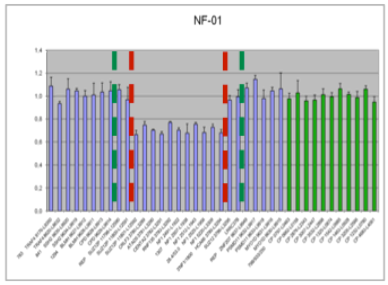
NF-01

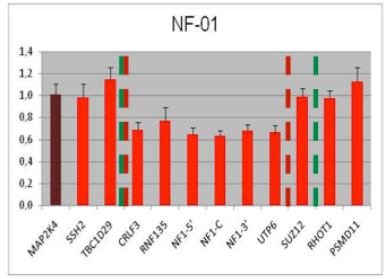
NF-01
MAP2K4
SSH2
TBC1D29
CRLF3
RNF135
NF1-5'
NF1-C
NF1-3'
UTP6
SUZ12
RHOT1
PSMD11

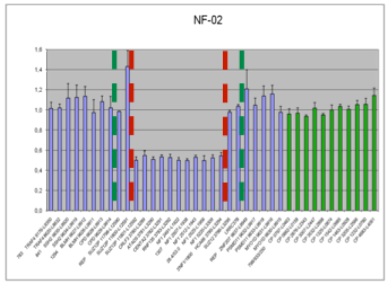
NF-02

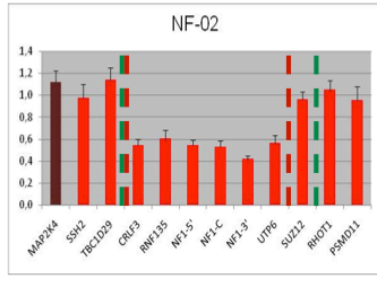
NF-02
MAP2K4
SSH2
TBC1D29
CRLF3
RNF135
NF1-5'
NF1-C
NF1-3'
UTP6
SUZ12
RHOT1
PSMD11

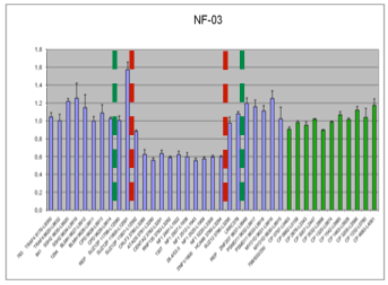
NF-03

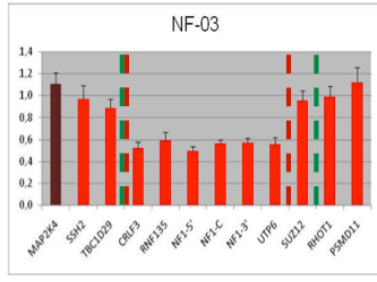
NF-03
MAP2K4
SSH2
TBC1D29
CRLF3
RNF135
NF1-5'
NF1-C
NF1-3'
UTP6
SUZ12
RHOT1
PSMD11

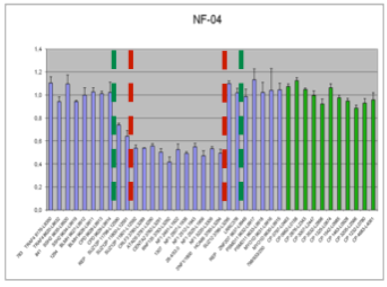
NF-04

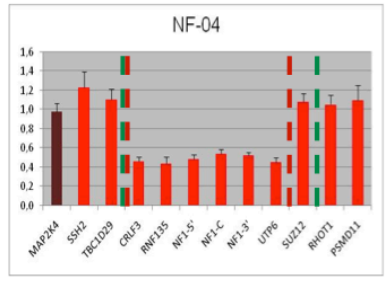
NF-04
MAP2K4
SSH2
TBC1D29
CRLF3
RNF135
NF1-5'
NF1-C
NF1-3'
UTP6
SUZ12
RHOT1
PSMD11

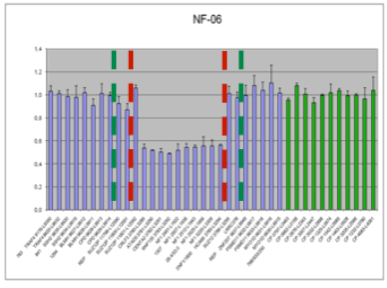
NF-06

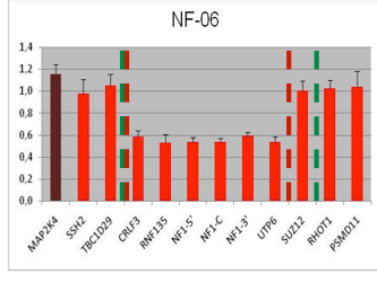
NF-06
MAP2K4
SSH2
TBC1D29
CRLF3
RNF135
NF1-5'
NF1-C
NF1-3'
UTP6
SUZ12
RHOT1
PSMD11

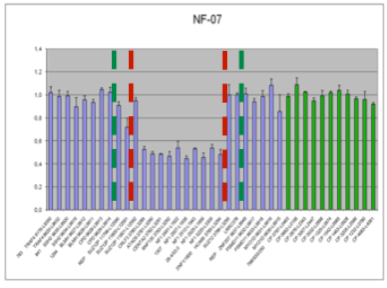
NF-07

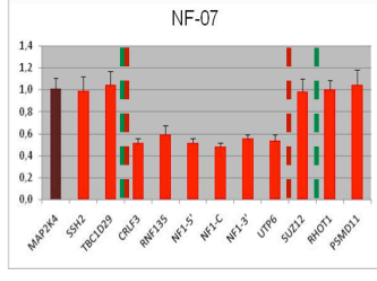
NF-07
MAP2K4
SSH2
TBC1D29
CRLF3
RNF135
NF1-5'
NF1-C
NF1-3'
UTP6
SUZ12
RHOT1
PSMD11

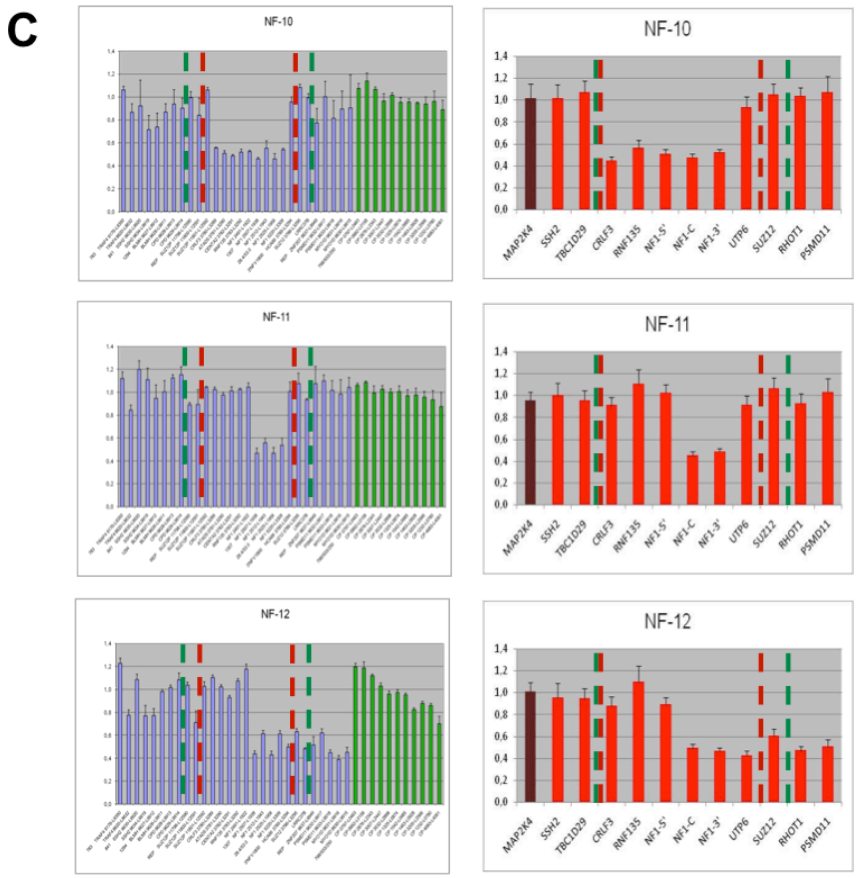

Figure A.2. Characterization of *NF1* constitutional deletions by MLPA and *NF1*-qPCR. Graphs showing the RCN±SD value (*y*-axis) calculated for each locus interrogated (*x*-axis) in MLPA and qPCR assays in the 5 Type-1 (A), 6 Type-2 (B) and 3 atypical (C) *NF1* microdeletions. Violet bars and red bars show the assessed loci within *NF1* region in MLPA and qPCR, respectively. Green bars and the brown bar are control loci placed in other sites within the genome in MLPA and qPCR, respectively. Dashed green and brown lines show, respectively, the extents of Type-1 and Type-2 microdeletions.

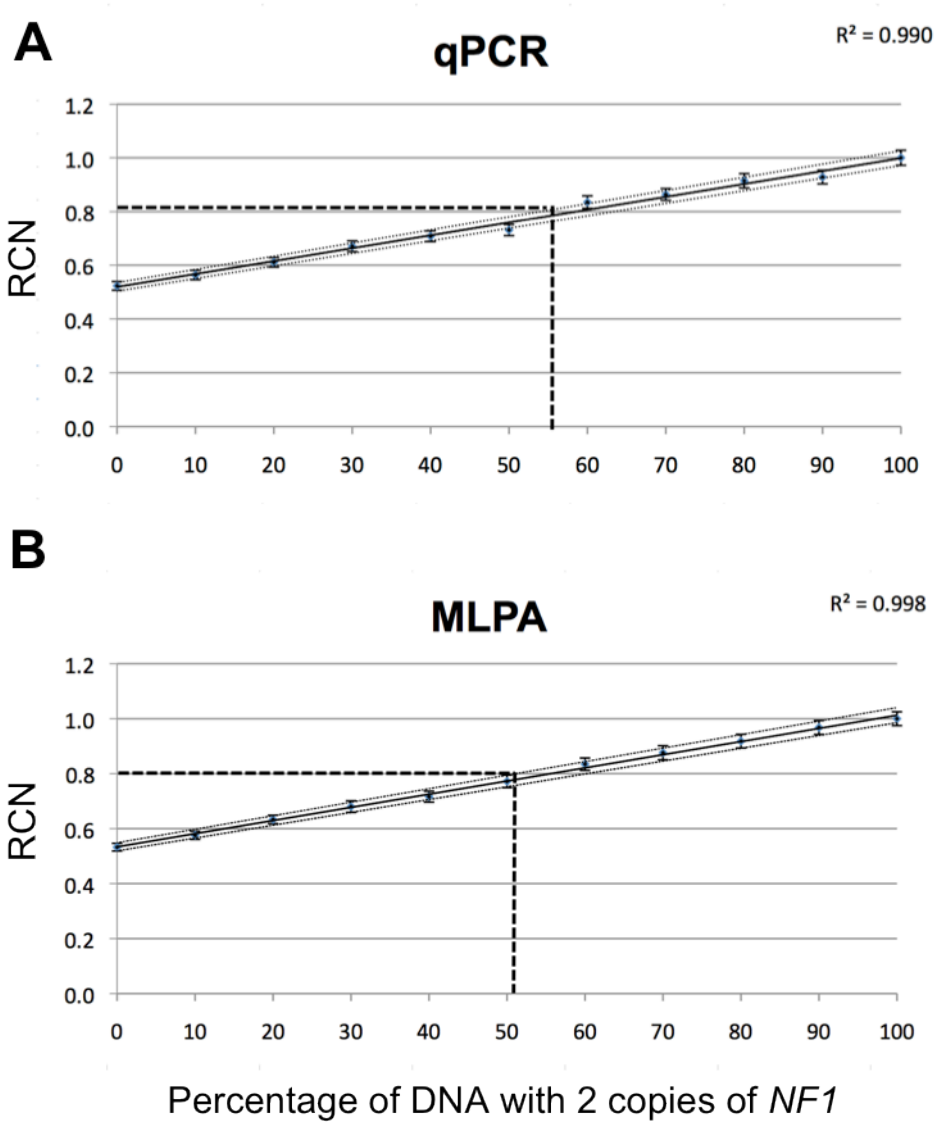

Figure A.3. Performance of the *NF1*-qPCR and MLPA assays in admixtures of 2 DNA samples with either 1 or 2 copies of *NF1*. Linear regression of RCN values (mean and SD; y-axis) of the percentage of DNA with 2 copies of *NF1* within the admixtures (x-axis). Separate calculations for the qPCR assay (A) and the MLPA assay (B). Dashed thick lines indicate the threshold for deletion detection: <56% for qPCR (A) and <51% for MLPA (B).

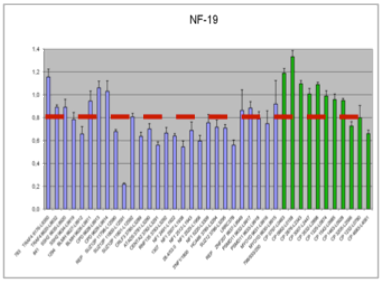
NF-19

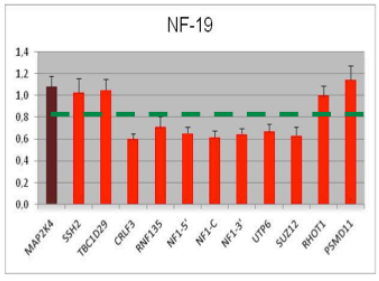
NF-19
MAP2K4
SSH2
TBC1D29
CRLF3
RNF135
NF1-5'
NF1-C
NF1-3'
UTP6
SUZ12
RHOT1
PSMD11

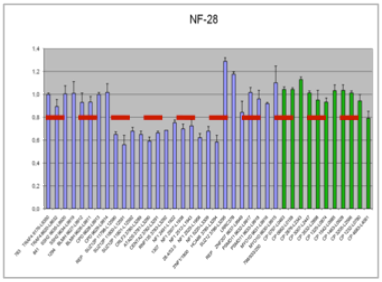
NF-28

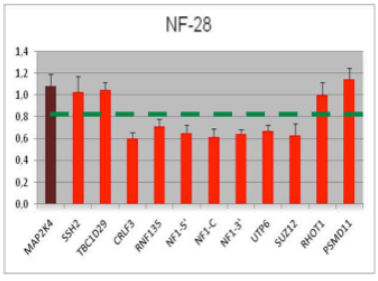
NF-28
MAP2K4
SSH2
TBC1D29
CRLF3
RNF135
NF1-5'
NF1-C
NF1-3'
UTP6
SUZ12
RHOT1
PSMD11

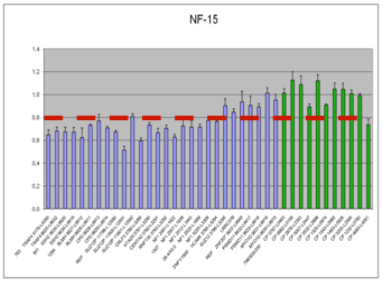
NF-15

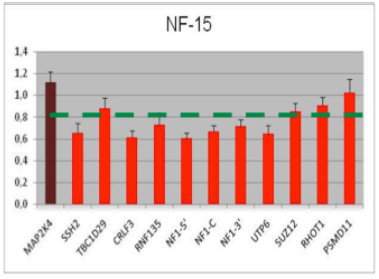
NF-15
MAP2K4
SSH2
TBC1D29
CRLF3
RNF135
NF1-5'
NF1-C
NF1-3'
UTP6
SUZ12
RHOT1
PSMD11

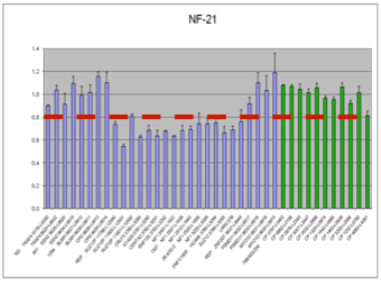
NF-21

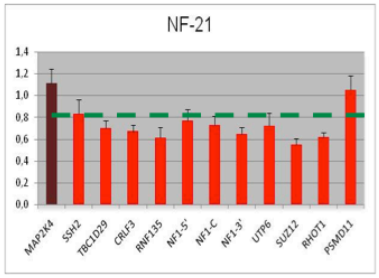
NF-21
MAP2K4
SSH2
TBC1D29
CRLF3
RNF135
NF1-5'
NF1-C
NF1-3'
UTP6
SUZ12
RHOT1
PSMD11

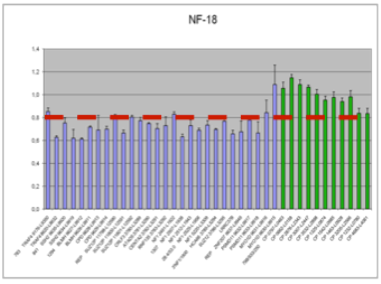
NF-18

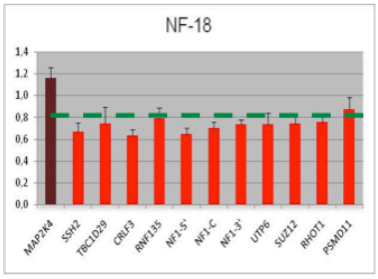
NF-18
MAP2K4
SSH2
TBC1D29
CRLF3
RNF135
NF1-5'
NF1-C
NF1-3'
UTP6
SUZ12
RHOT1
PSMD11

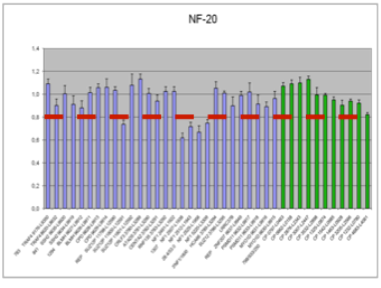
NF-20

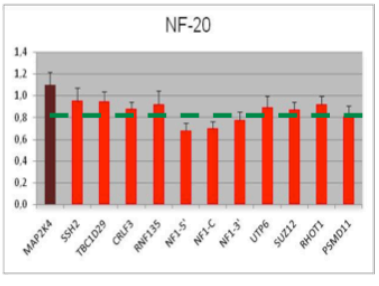
NF-20
MAP2K4
SSH2
TBC1D29
CRLF3
RNF135
NF1-5'
NF1-C
NF1-3'
UTP6
SUZ12
RHOT1
PSMD11

Figure A.4. Characterization of *NF1* somatic deletions by MLPA and *NF1*-qPCR. Graphs showing the RCN±SD value (*y*-axis) calculated for each locus interrogated (*x*-axis) in MLPA and qPCR assays in the 11 dNF samples containing 56% or less of *NF1*-deleted component. Violet bars and red bars show the assessed loci within *NF1* region in MLPA and qPCR, respectively. Green bars and the brown bar are control loci placed in other sites within the genome in MLPA and qPCR, respectively. Dashed green and brown lines show, respectively, the RCN cutoff values for qPCR (0.81) and MLPA (0.80) below which a deletion is considered.

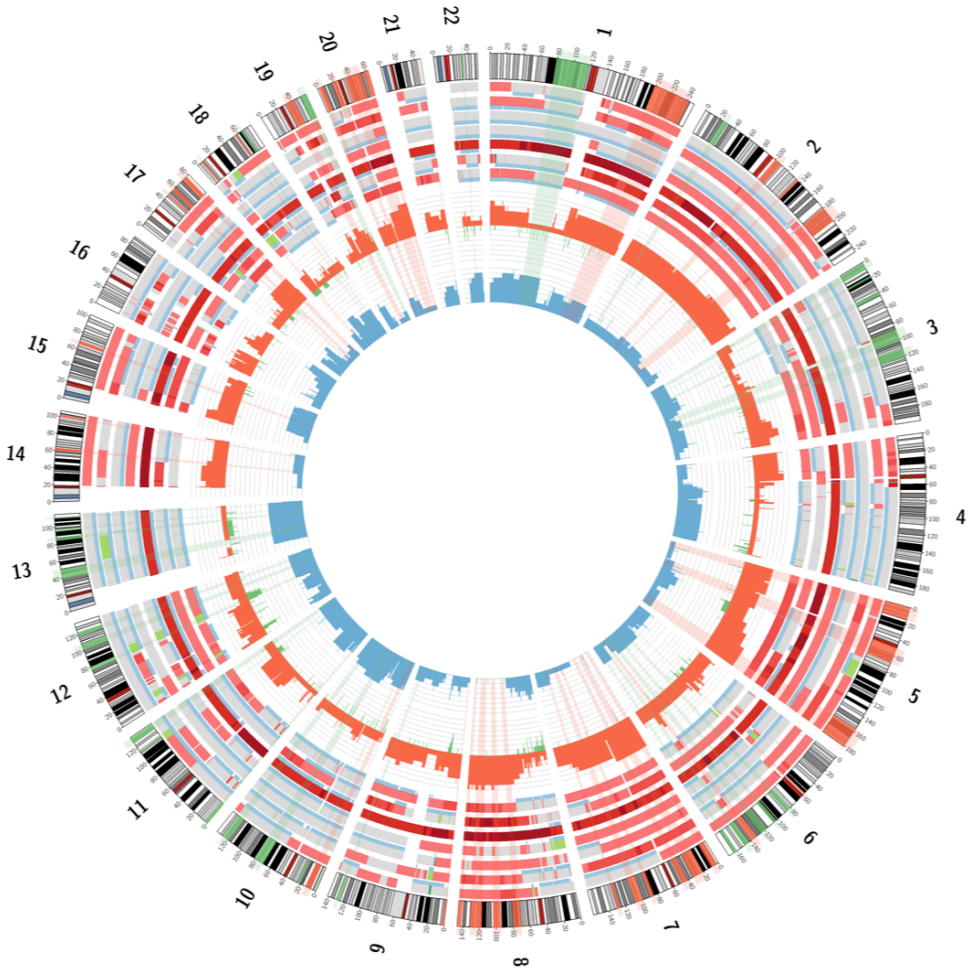

Figure A.5. Circos representation showing TIs and SCNAs found in MPNST cell lines. From outside to inside, idiograms of the 22 human autosomes with G-banding pattern are depicted. Over these idiograms red and green boxes show TIs of overexpression and underexpression, respectively, obtained from microarray expression data. The 7 consecutive circles summarize the SCNAs obtained from SNP array data in the 7 NF1-associated MPNST cell lines analyzed. Genomic gains are shown in red, and losses, in green. Colour intensity denotes the copy number of the alteration. MPNST cell lines showed a higher hyperploid genome than MPNSTs, with also some recurrent SCNAs. LOH of every MPNST cell line sample is also depicted in blue. In the inner part, the recurrence of the SCNAs (in red and green) and LOH (in blue) of all cell lines is shown.

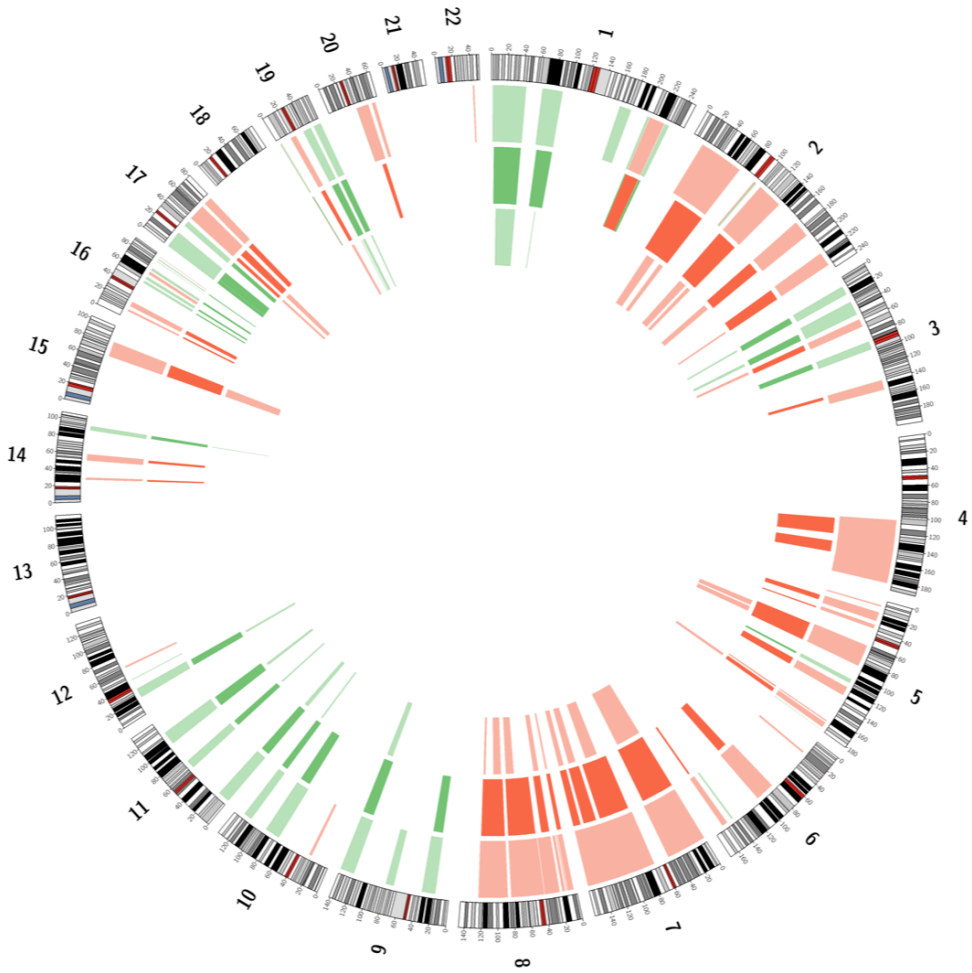

Figure A.6. Circos representation showing TIs found in MPNSTs considering three levels of significance with PREDA. From outside to inside, idiograms of the 22 human autosomes with G-banding pattern are depicted. The 3 consecutive circles show TIs of overexpression (red boxes) and TIs of underexpression (green boxes) obtained from microarray expression data and applying three levels of significance with PREDA: P=0.1, P=0.05 and P=0.01. A P=0.05 level of significance was chosen to delimit the boundaries of the TIs to be further studied (intense red and green boxes).

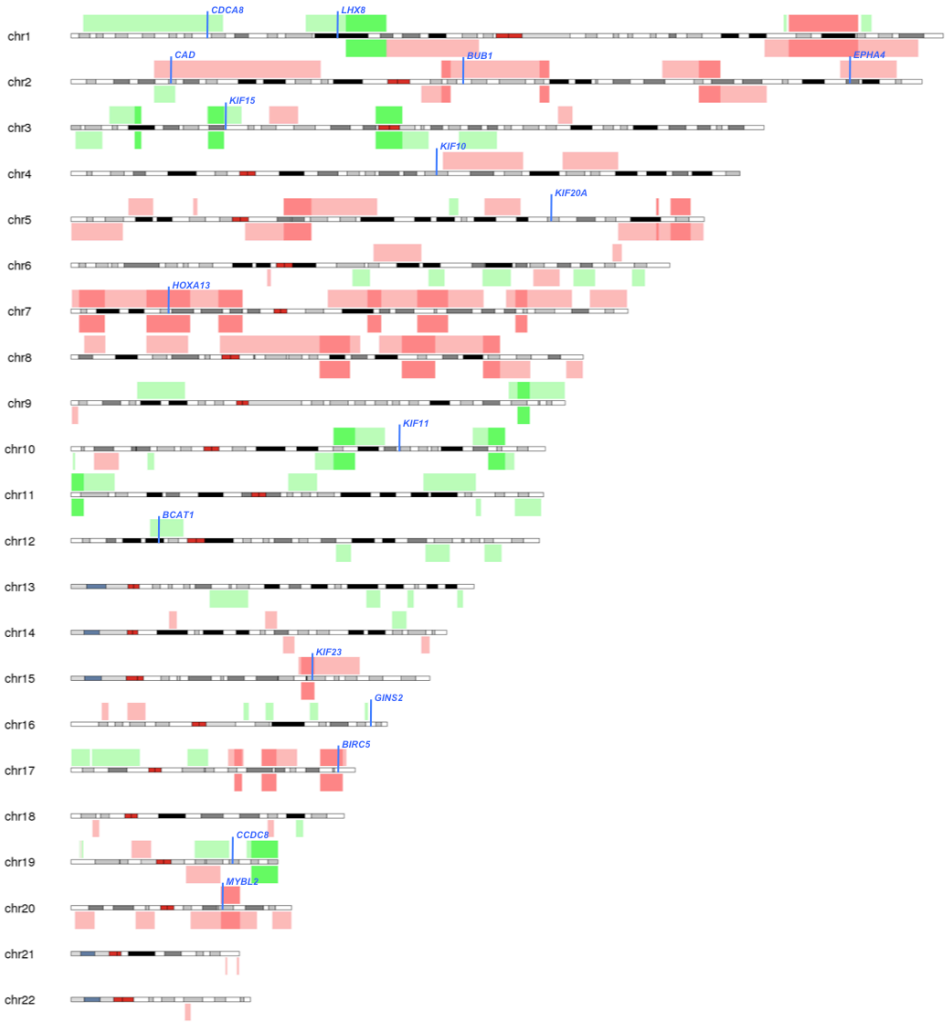

Figure A.7. Karyoplot showing TIs found in MPNSTs and TIs found in MPNST cell lines. A karyogram showing the idiograms of the 22 human autosomes with G-banding pattern is depicted. Red and green boxes represent, respectively, the 36 TIs of overexpression and 28 TIs of underexpression identified in MPNSTs (above the chromosomes), and the 35 TIs of overexpression and 31 TIs of underexpression identified in MPNST cell lines (below the chromosomes). Those TIs that are coincident for both tumours and cell lines (25.4% of TIs of overexpression from MPNSTs and 20.6% of TIs of underexpression from MPNSTs) are shown as intense red and green boxes. In blue are depicted the genes selected for the functional identification of genes involved in MPNST pathogenesis and their location in the genome.

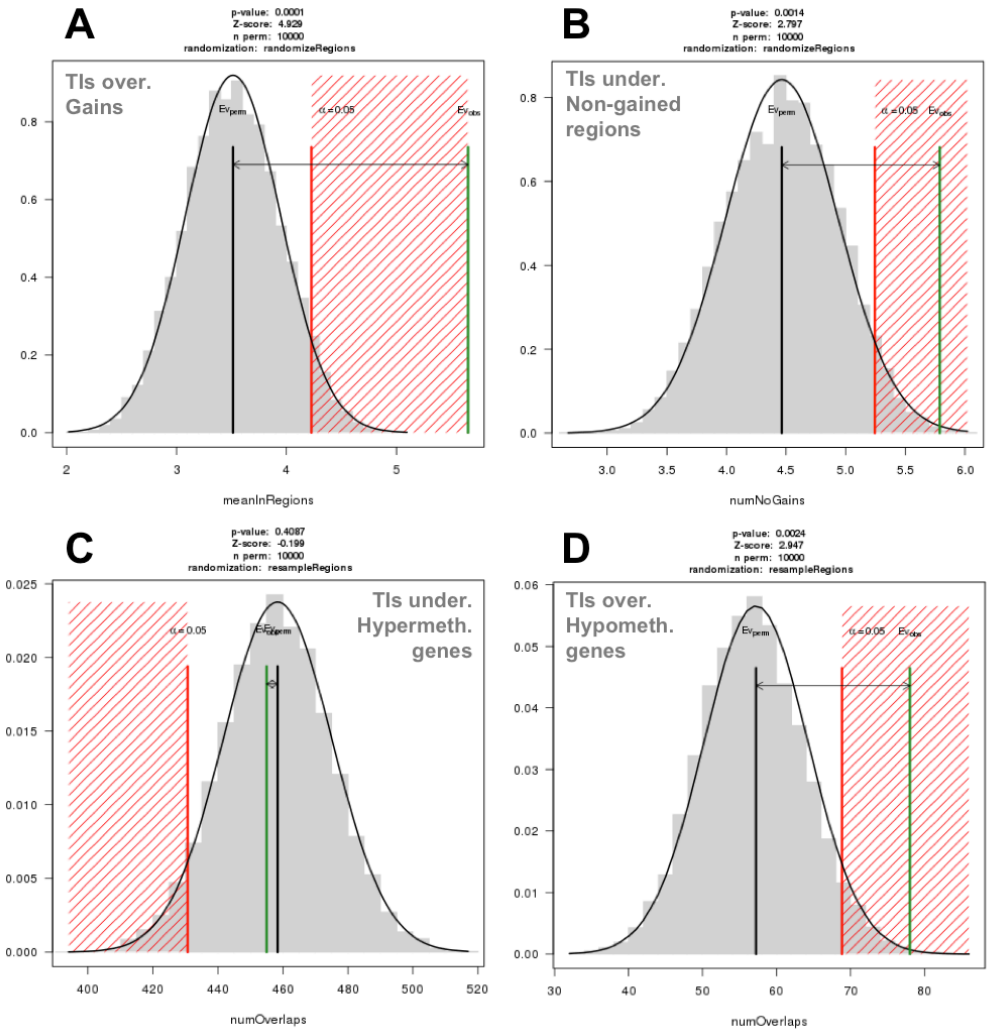

Figure A.8. Global association of TIs with SCNAs and with hypermethylated genes in MPNST cell lines by regioneR. regioneR plots showing the results of permutation tests. A. TIs of overexpression found in MPNST cell lines were significatively associated with genomic gains. B. TIs of underexpression found in MPNST cell lines were significatively associated with non-gained regions. C. TIs of underexpression found in MPNST cell lines were not enriched in hypermethylated genes. D. TIs of overexpression were significatively enriched in hypomethylated genes.

	Cell line					
Marker	**S462**	**T265**	**sNF96.2**	**NMS-2**	**90-8**	**STS26T**
D8S1179	10, 12	14	13	12, 13	10, 12	13, 14
D21S11	29	29, 32.3	30	30	30	30, 31
D7S820	8, 10	8	10, 11	9, 12	11	8, 11
CSF1PO	12	9, 12	12	12	12	10, 13
D3S1358	14, 17	15, 18	16	15, 16	15	14
TH01	7, 8	9	6	6	6	6, 9.3
D13S317	12	12	10	12	8	9, 10
D16S539	11, 13	13	11	9	9	12, 13
D2S1338	23	17, 23	17	18, 19	16, 24	20
D19S433	14	13, 14	13, 14	13.2, 14.2	13, 16	14
vWA	19	16	17, 19	14, 19	17	17
TPOX	8	11, 12	11	8, 9	11	8
D18S51	16	12	16	17	14, 18	17, 18
AMEL	X	X, Y	X	X, Y	X	X
D5S818	12	12, 13	11	12, 13	11	11, 12
FGA	20	21	22	21, 22	25	22, 23

Table A.1. STR profiles of MPNST cell lines. Information regarding the microsatellite profiles of MPNST cell lines obtained with the AmpFISTR Identifiler Plus Amplification kit.

		2q	17p		17q			*NF1* gene			17q							
Sample	**% of cells with 2 copies of *NF1***	**D2S2314**	**D17S1879**	**D17S1303**	**D17S783**	**D17S841**	**D17S1294**	**D17S1307**	**28.4**	**53.0**	**3'NF1**	**D17S1800**	**D17S798**	**D17S933**	**D17S250**	**D17S807**	**D17S789**	**PRA assay***	**SNP array***
NF-19	24																		
NF-28	37																		
NF-15	42																		
NF-17	49																	X	X
NF-18	44																	X	X
NF-20	44																	X	
NF-22	n/a																		
NF-25	45																		
NF-21	43																		X
NF-63	47																		
NF-24	44																		
NF-23	56																		
NF-27	52																	X	X
NF-29	68																		X
NF-16	61																		X
NF-26	71																	X	X

Table A.2. Characterization of *NF1* somatic deletions in dNFs by MMPA. Calculations obtained with the microsatellite multiplex PCR analysis (MMPA) of the percentage of cells with 2 copies of *NF1* present in each of the 16 dNFs analyzed (see Garcia-Linares et al., 2012 for details). For some samples deletion was also assessed by Paralog Ratio Analysis (PRA) and SNP array (Garcia-Linares et al., 2012). Green boxes show deleted loci; grey boxes show non-deleted loci; yellow boxes show non-informative microsatellites. n/a, not available.

Set	Sample	*AURKA / GLRX3*	*AURKA / ACSS1*	*AURKA / ADARB1*	*AURKA / L1*	*AURKA / L1PA*	*AURKA / NF*
MPNST cell lines	S462	1.30	1.38	2.16	1.41	1.39	**1.40**
	T265	4.01	2.40	2.92	2.56	2.77	**2.66**
	ST-8814	3.97	1.95	2.52	2.94	2.35	**2.63**
	S462-TY	1.43	1.33	2.29	1.62	1.40	**1.51**
	STS-26T	2.92	2.07	2.66	2.95	2.36	**2.64**
NF1-associated MPNSTs	MPNST_A	2.40	1.23	1.23	1.55	1.45	**1.50**
	MPNST-1	2.04	1.22	1.29	1.63	1.40	**1.51**
	MPNST_B	2.55	1.15	1.82	1.86	1.90	**1.88**
	MPNST_C	1.31	1.32	1.29	1.49	1.28	**1.38**
	MPNST_D	2.03	1.32	1.51	1.67	1.59	**1.63**
	MPNST_G	1.16	1.10	0.57	0.85	0.89	**0.87**
	MPNST_K	2.48	2.33	2.24	3.04	2.06	**2.50**
sporadic MPNSTs	M-23	1.28	1.31	1.28	1.68	1.37	**1.52**
	M-24	1.13	1.25	1.26	1.40	1.08	**1.23**
	M-25	1.37	1.03	1.18	1.05	1.10	**1.07**
	M-26	0.83	1.14	1.29	1.05	0.85	**0.94**
	M-27	2.58	1.27	1.29	1.23	1.41	**1.32**
benign neuro-fibromas	M-17	1.18	1.08	1.15	1.45	1.33	**1.39**
	M-10	1.04	1.15	1.08	1.16	1.09	**1.13**
	M-38	1.10	1.10	1.11	1.12	1.10	**1.11**
	M-39	1.22	1.13	1.28	1.16	1.25	**1.20**
	M-40	0.88	0.98	0.88	0.94	1.02	**0.98**
	M-46	0.94	1.26	1.06	1.09	1.00	**1.04**
	M-48	0.79	0.84	0.75	0.79	0.90	**0.85**
	M-49	0.89	0.96	0.88	1.00	0.83	**0.91**
control samples	M-18	1.14	1.01	1.11	1.11	1.19	**1.15**
	M-28	1.04	1.01	1.00	0.93	0.88	**0.91**
	M-29	0.85	0.93	0.90	1.18	0.99	**1.08**
	M-30	0.83	0.85	0.80	0.80	0.88	**0.84**
	M-31	1.04	0.96	1.01	0.89	0.95	**0.92**
	M-32	1.04	0.96	1.02	1.06	0.95	**1.00**
	NF-50	0.90	0.95	0.85	0.90	0.96	**0.93**
	NF-52	0.99	0.94	0.96	0.93	1.05	**0.98**
	NF-54	0.93	0.96	0.95	1.11	1.06	**1.09**
	NF-55	1.33	1.53	1.57	1.17	1.13	**1.15**

Table A.3. Comparison of copy number assessment using averaged LINEs or single genes as normalizers. RCN values of *AURKA* locus obtained for 5 MPNST cell lines, 12 MPNSTs (7 NF1-associated and 5 sporadic), 8 neurofibromas and 10 control samples with the MPNST-qPCR using as normalizers of copy number data the single loci *GLRX3*, *ACSS1*, *ADARB1*, *L1* or *L1PA*, or a nomalization factor (NF) averaging *L1* and *L1PA* relative quantities (RQ). Those RCN outside the 99% CI of a diploid status for *AURKA* (0.76 – 1.32) are considered to indicate a copy number change: either a genomic gain (red numbers in red boxes) or a copy number loss (green numbers in green boxes). RCN values of *AURKA* locus obtained with the NF are in bold.

ANNEXE 2

Clinical Chemistry 59:6
928–937 (2013)

Probe-Based Quantitative PCR Assay for Detecting Constitutional and Somatic Deletions in the *NF1* Gene: Application to Genetic Testing and Tumor Analysis

Ernest Terribas,[1] Carles Garcia-Linares,[1] Conxi Lázaro,[2] and Eduard Serra[1*]

BACKGROUND: About 5% of patients with neurofibromatosis type 1 (NF1) bear constitutional microdeletions that encompass *NF1* (neurofibromin 1) and neighboring genes. These patients are characterized by the development of a high number of dermal neurofibromas (dNFs), mental retardation, and an increased risk of developing a malignant peripheral nerve sheath tumor (MPNST). Additionally, 10% of somatic second hits identified in dNFs are caused by deletions involving the *NF1* gene. To detect constitutional and somatic deletions, we developed a probe-based quantitative PCR (qPCR) assay for interrogating the copy number status of 11 loci distributed along a 2.8-Mb region around the *NF1* gene.

METHODS: We developed the qPCR assay with Universal ProbeLibrary technology (Roche) and designed a Microsoft Excel spreadsheet to analyze qPCR data for copy number calculations. The assay fulfilled the essential aspects of the MIQE (minimum information for publication of quantitative real-time PCR experiments) guidelines and used the qBase relative quantification framework for calculations.

RESULTS: The assay was validated with a set of DNA samples with known constitutional or somatic *NF1* deletions. The assay showed high diagnostic sensitivity and specificity and distinguished between Type-1, Type-2, and atypical constitutional microdeletions in 14 different samples. It also identified 16 different somatic deletions in dNFs. These results were confirmed by multiplex ligation-dependent probe amplification.

CONCLUSIONS: The qPCR assay provides a methodology for detecting constitutional *NF1* microdeletions that could be incorporated as an additional technique in a genetic-testing setting. It also permits the identification of somatic *NF1* deletions in tissues with a high percentage of cells bearing 2 copies of the *NF1* gene.

Neurofibromatosis type 1 (NF1)[3] is an autosomal dominant genetic disorder caused by mutations in *NF1*[4] (neurofibromin 1) (MIM 613113; NG 009018.1), a tumor suppressor gene located at 17q11.2. This disease affects approximately 1 in 3500 individuals. One of the most important clinical manifestations is the development of multiple dermal neurofibromas (dNFs), which are benign tumors of the peripheral nervous system. NF1 patients show a wide spectrum of constitutional mutations that affect the *NF1* gene. Most of the mutations (93%) are point mutations, including nonsense, missense, insertion/deletions, and splicing mutations. The

[1] Institute of Predictive and Personalized Medicine of Cancer (IMPPC), Badalona, Barcelona, Spain; [2] Molecular Diagnostics Unit, Hereditary Cancer Program, Catalan Institute of Oncology (ICO-IDIBELL), L'Hospitalet de Llobregat, Barcelona, Spain.

* Address correspondence to this author at: Institute of Predictive and Personalized Medicine of Cancer (IMPPC), Program on Hereditary Cancer, Carretera de Can Ruti, Camí de les Escoles s/n, 08916 Badalona, Barcelona, Spain. Fax +34-93-465-1472; e-mail eserra@imppc.org.

Received August 16, 2012; accepted January 18, 2013.
Previously published online at DOI: 10.1373/clinchem.2012.194217

[3] Nonstandard abbreviations: NF1, neurofibromatosis type 1; dNF, dermal neurofibroma; REP, low-copy repeat; MPNST, malignant peripheral nerve sheath tumor; SC, Schwann cell; FISH, fluorescence in situ hybridization; MLPA, multiplex ligation-dependent probe amplification; SNP, single-nucleotide polymorphism; qPCR, quantitative real-time PCR; UPL, Universal ProbeLibrary (Roche); LDR, linear dynamic range; LINE, long interspersed repeat element; L1PA, LINE in the L1 family; Cq, quantification cycle; RQ, relative quantity; NRQ, normalized relative quantity; NF, normalization factor; RCN, relative copy number; RF, rescaling factor; MMPA, microsatellite multiplex PCR analysis; MIQE, minimum information for publication of quantitative real-time PCR experiments.

[4] Human genes: *NF1*, neurofibromin; *SUZ12*, suppressor of zeste 12 homolog (*Drosophila*); *SUZ12P1*, suppressor of zeste 12 homolog pseudogene 1; *ADARB1*, adenosine deaminase, RNA-specific, B1; *TBC1D29*, TBC1 domain family, member 29; *CRLF3*, cytokine receptor-like factor 3; *RNF135*, ring finger protein 135; *UTP6*, UTP6, small subunit (SSU) processome component, homolog (yeast); *RHOT1*, ras homolog family member T1; *SSH2*, slingshot homolog 2 (*Drosophila*); *PSMD11*, proteasome (prosome, macropain) 26S subunit, non-ATPase, 11; *MAP2K4*, mitogen-activated protein kinase kinase 4; *OMG*, oligodendrocyte myelin glycoprotein; *EVI2B*, ecotropic viral integration site 2B; *EVI2A*, ecotropic viral integration site 2A; *EFCAB5*, EF-hand calcium binding domain 5; *NSRP1*, nuclear speckle splicing regulatory protein 1; *SLC6A4*, solute carrier family 6 (neurotransmitter transporter, serotonin), member 4; *BLMH*, bleomycin hydrolase; *TMIGD1*, transmembrane and immunoglobulin domain containing 1; *CPD*, carboxypeptidase D; *GOSR1*, golgi SNAP receptor complex member 1; *LRRC37BP1*, leucine rich repeat containing 37B pseudogene 1; *ATAD5*, ATPase family, AAA domain containing 5; *TEFM*, transcription elongation factor, mitochondrial; *ADAP2*, ArfGAP with dual PH domains 2; *RAB11FIP4*, RAB11 family interacting protein 4 (class II); *COPRS*, coordinator of PRMT5, differentiation stimulator (formerly *C17orf79*); *LRRC37B*, leucine rich repeat containing 37B; *RHBDL3*, rhomboid, veinlet-like 3 (*Drosophila*); *C17orf75*, chromosome 17 open reading frame 75; *ZNF207*, zinc finger protein 207.

remaining mutations consist of intragenic deletions/duplications (approximately 2%) and microdeletions that span *NF1* and neighboring genes (approximately 5%) *(1)*. Approximately 90% of *NF1* microdeletions (Types-1, -2, and -3) are recurrent and arise via nonallelic homologous recombination between low-copy repeats (REPs), which are paralogous regions flanking the *NF1* gene. REP-A and REP-C regions mediate Type-1 deletions, which are the most frequent. These regions span 1.4 Mb and contain *NF1* and 14 other protein-coding genes *(2–4)*. Type 2 deletions are less frequent and typically appear in the context of somatic mosaicism. The distance between their breakpoints, which are located at the *SUZ12* [suppressor of zeste 12 homolog (*Drosophila*)] gene and its pseudogene *SUZ12P1* (suppressor of zeste 12 homolog pseudogene 1), spans 1.2 Mb *(5)*. The REP-B and REP-C regions are involved in the rare Type-3 deletions, which are 1.0 Mb in length *(6–8)*. In the remaining approximately 10% of constitutional *NF1* microdeletions, the so-called atypical deletions, the REPs are not involved in generating the breakpoint *(7, 9)*. Individuals bearing a *NF1* microdeletion present a more severe clinical phenotype, including dysmorphic features, learning disabilities, cardiovascular malformations, childhood overgrowth, a higher number of dNFs, and a higher lifetime risk for the development of malignant peripheral nerve sheath tumors (MPNSTs) *(10–12)*.

Deletions of the *NF1* gene also occur somatically, e.g., in tumors such as dNFs arising in patients with NF1. A key event in the initiation of neurofibroma development is biallelic inactivation of the *NF1* gene *(13–15)*. dNFs are composed of different cell types, but only Schwann cells (SCs) bear a double inactivation of the *NF1* gene *(16–18)*. Approximately 75% of the somatic mutational spectrum of the *NF1* gene in NF1-associated dNFs is accounted for by point mutations (i.e., nonsense, missense, small insertion/deletion, and splicing mutations) and intragenic deletions. The remainder (approximately 25%) present as a loss of heterozygosity in large genomic regions that include the *NF1* gene *(19, 20)*. The mechanistic causes of loss of heterozygosity are mitotic recombination in 62% of cases and genomic deletions of 80 kb to 8 Mb in the remaining 38% *(20)*.

To date, *NF1* constitutional deletions have been identified with multiple techniques, such as microsatellite analysis with intragenic markers *(21–23)*, interphase fluorescence in situ hybridization (FISH) analysis via the use of probes within and flanking the *NF1* gene *(11, 22, 24, 25)*, multiplex ligation-dependent probe amplification (MLPA) with commercially available kits *(23, 26)*, and array comparative genomic hybridization *(27)*. Microsatellite analysis *(20, 28, 29)*, FISH *(30)*, MLPA *(19, 20, 29, 31)*, and array comparative genomic hybridization *(32)* have also been used to characterize somatic deletions encompassing the *NF1* gene, together with other techniques, such as single-nucleotide polymorphism (SNP) analysis *(32)*, paralog ratio analysis *(20, 32)*, and SNP array *(20)*.

Quantitative real-time PCR (qPCR) has been used to confirm intragenic constitutional deletions in *NF1 (26);* however, qPCR has not been used routinely to detect constitutional *NF1* microdeletions. qPCR represents an alternative methodology because of its high analytical sensitivity and low imprecision, its relatively low screening cost, and its fast assay-development time. We describe a probe-based qPCR assay for detecting all 4 types of *NF1* constitutional microdeletions and somatic deletions that affect the *NF1* region. We also compare our qPCR results with those obtained via other techniques.

Materials and Methods

PATIENTS AND SAMPLES

This study included 59 samples: 14 venous blood samples previously tested by FISH and microsatellite markers and found to carry a constitutional deletion of *NF1* in each case *(21, 33)*; 16 samples from surgically excised dNFs; and 5 samples from selective SC cultures ($SC^{NF1-/-}$) derived from dNFs, previously analyzed by MLPA, paralog ratio analysis, and SNP array and found to bear a somatic *NF1* deletion in each case [*(20)* and data not shown]. In addition, we used a set of 24 control samples, each of which presents 2 copies of the *NF1* gene: 10 dNF samples, 5 blood samples, 4 skin samples, 3 fibroblast samples, and 2 $SC^{NF1+/-}$ samples. All patients gave written informed consent for the molecular studies performed.

Total DNA was extracted from blood samples with different methodologies: the salting-out procedure, the Wizard Genomic DNA Purification Kit (Promega), and the FlexiGene DNA Kit (Qiagen). DNA was extracted from dNFs and skin with the Gentra Puregene Kit (Qiagen). The QIAamp DNA Mini Kit (Qiagen) was used to extract DNA from cells (SCs and fibroblasts). All extractions were performed according to the manufacturer's instructions. A NanoDrop® spectrophotometer was used to quantify DNA and to measure purity and quality. DNA integrity was assessed by gel electrophoresis. All DNA samples included in this study presented with high purity and integrity.

qPCR EXPERIMENTAL SETUP

Primers and probes for the qPCR assay were developed with Roche Universal ProbeLibrary (UPL) technology. UPLs are hydrolysis probes of 8- to 9-nucleotide locked nucleic acid that are labeled at the 5′ end with the flu-

orescent dye 6-carboxyfluorescein and at the 3′ end with a quencher dye. The combination of the hydrolysis probe and the primer pair provided the specificity required for each particular genomic locus of interest. The design of each of the primers (desalted and purified; Sigma Life Science) was subjected to an in silico PCR and BLAT search analysis to evaluate their specificity, which was later assessed experimentally by PCR and agarose gel electrophoresis before qPCR experiments were conducted. The sequences of the primers and probes used in this study are listed in Table 1 of the Data Supplement that accompanies the online version of this article at http://www.clinchem.org/content/vol59/issue6.

qPCR experiments were performed in a LightCycler® 480 Real-Time PCR System with white Multiwell Plate 384 plates (Roche Diagnostics). Conditions for amplification were as follows: 95 °C for 10 min; 45 cycles of 95 °C for 10 s, 60 °C for 30 s, and 72 °C for 1 s; and 40 °C for 30 s. The linear dynamic range (LDR) and efficiency (*E*) of the primers were evaluated (see Table 1 in the online Data Supplement). Then, to minimize technical variation between runs, we divided all samples under study into 3 panels of 20 samples each according to the sample-maximization method *(34, 35)*. Each reaction in all experiments included 5 ng DNA template, 4 μL of 2× LightCycler 480 Probes Master Mix (Roche Diagnostics), 0.1 μmol/L UPL probe, and 0.75 μmol/L of each primer, in a total volume of 8 μL [except for reactions for the L1PA locus—a long interspersed repeat element (LINE) in the L1 family—which included 0.2 μmol/L UPL probe and 1.2 μmol/L of each primer]. PCRs for each primer set and sample were performed in triplicate. Each set of PCR assays included both negative controls without template and a dilution series of a particular template for calculating the *E* value of the primer pair in each run. In addition, a calibrator sample of known copy number was included in triplicate in every assay.

qPCR DATA ANALYSIS

We designed a Microsoft Excel spreadsheet to analyze qPCR data for copy number calculations. We used formulas from the qBase relative quantification framework *(34)*, which are based on the Pfaffl method *(36)*. In brief, we averaged the 3 quantification cycle (Cq) numbers obtained from each triplicate with the second-derivative maximum method in the LightCycler® 480 software [as long as the difference in Cq between the replicate with the highest value and the replicate with lowest value was <0.3 for all genes and <0.2 for the L1PA locus *(35)*]. We then calculated the ΔCq value for the difference between the unknown sample and the calibrator sample ($\Delta Cq = Cq_{unknown} - Cq_{calibrator}$). The relative quantity (RQ) was later calculated as: $RQ = E^{-\Delta Cq}$. We calculated the normalized relative quantity (NRQ) as: NRQ = RQ/NF, where NF is the normalization factor. The NF in turn is the geometric mean of the RQ values for the 2 selected reference loci—the *ADARB1* (adenosine deaminase, RNA-specific, B1) gene and the L1PA locus—for the particular sample. The value for the stability parameter, *M (37)*, for this particular NF was previously calculated for the entire set of samples and was <0.2 ($M = 0.168$) *(35)*. Finally, we calculated relative copy number (RCN) as: RCN = NRQ/RF, where RF is a rescaling factor. The RF is the geometric mean of the NRQ values of a set of 24 control samples bearing 2 *NF1* copies. RCN values close to 1 indicate the presence of 2 *NF1* copies, and RCN values close to 0.5 indicate an *NF1* deletion. A 99% CI for RCN values indicating 2 *NF1* copies was calculated for each interrogated locus (see Table 1 in the online Data Supplement).

MLPA ANALYSIS

We also used the MLPA technique to assess the *NF1* copy number status of both samples with constitutional and somatic deletions. We performed MLPA reactions in duplicate with the SALSA MLPA Kit P122-C1 NF1 Area (MRC-Holland) and 40 ng DNA, in accordance with the manufacturer's instructions. Once ligated and amplified, PCR fragments were separated by capillary electrophoresis (ABI 3130xl Genetic Analyzer; Applied Biosystems). Peak intensities were analyzed with Peak Scanner Software (Applied Biosystems) and normalized for peak heights, as described elsewhere *(20)*. In brief, peak height values were exported to an Excel spreadsheet. Relative probe signals were calculated for a particular sample by dividing the peak height of each of the 28 pairs of probes encompassing the *NF1* region by the sum of the peak heights of the 11 pairs of reference probes (not located in the *NF1* region). The ratio obtained for each individual relative probe height was then normalized for that specific probe to the mean obtained with 3 control samples (with 2 copies of the *NF1* region). For genomic regions present in 2 copies in a sample, these calculations were expected to yield an RCN value of approximately 1.0. A value <0.8 was considered to indicate a deletion.

MICROSATELLITE MULTIPLEX PCR ANALYSIS

In parallel, we used microsatellite multiplex PCR analysis (MMPA) as previously developed in our laboratory *(28)* to assess the *NF1* copy number status of tumor samples with *NF1* somatic deletions and to calculate the percentage of cells within the tumors with 2 *NF1* copies. This technique allows the simultaneous amplification of 16 microsatellite markers. MMPA reactions were performed in duplicate with

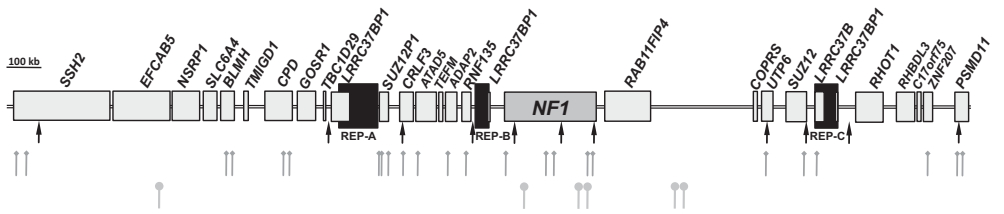

Fig. 1. Schematic representation of the *NF1* region at 17q11.2 assessed with the qPCR assay.

Protein-coding genes [except for *OMG* (oligodendrocyte myelin glycoprotein), *EVI2B* (ecotropic viral integration site 2B), and *EVI2A* (ecotropic viral integration site 2A)] are represented by gray boxes; REPs are represented by black boxes. Indicated are the positions of the 11 qPCR probes (black arrows), the 24 MLPA probes ("tailed" small gray circles), and the 6 MMPA microsatellites ("tailed" large gray circles) within the *NF1* region. *EFCAB5*, EF-hand calcium binding domain 5; *NSRP1*, nuclear speckle splicing regulatory protein 1; *SLC6A4*, solute carrier family 6 (neurotransmitter transporter, serotonin), member 4; *BLMH*, bleomycin hydrolase; *TMIGD1*, transmembrane and immunoglobulin domain containing 1; *CPD*, carboxypeptidase D; *GOSR1*, golgi SNAP receptor complex member 1; *LRRC37BP1*, leucine rich repeat containing 37B pseudogene 1; *ATAD5*, ATPase family, AAA domain containing 5; *TEFM*, transcription elongation factor, mitochondrial; *ADAP2*, ArfGAP with dual PH domains 2; *RAB11FIP4*, RAB11 family interacting protein 4 (class II); *COPRS*, coordinator of PRMT5, differentiation stimulator (formerly *C17orf79*); *LRRC37B*, leucine rich repeat containing 37B; *RHBDL3*, rhomboid, veinlet-like 3 (*Drosophila*); *C17orf75*, chromosome 17 open reading frame 75; *ZNF207*, zinc finger protein 207. See human genes footnote for the names of the other genes identified in this figure.

the Multiplex PCR Kit (Qiagen) and 50 ng DNA. Information regarding the amplification protocol, data analysis, and calculations is described elsewhere *(28)*.

Results

DEVELOPMENT AND VALIDATION OF THE qPCR ASSAY

The qPCR assay was set up with UPL probes and their corresponding specific primer pairs. For copy number assessment, we selected 11 genomic loci distributed along a 2.8-Mb region encompassing the *NF1* gene (Fig. 1). To distinguish Type-1, Type-2, Type-3, and atypical *NF1* microdeletions specifically, we decided to interrogate 3 regions within the *NF1* gene (*NF1*-5′, *NF1*-C, and *NF1*-3′), 5 loci that closely flank REP-A, REP-B, REP-C, *SUZ12*, and its pseudogene (*SUZ12P1*) [*TBC1D29*, TBC1 domain family, member 29; *CRLF3*, cytokine receptor-like factor 3; *RNF135*, ring finger protein 135; *UTP6*, UTP6, small subunit (SSU) processome component, homolog (yeast); *RHOT1*, ras homolog family member T1], and 1 locus within *SUZ12P1* (SUZ12P1). Two other loci located distal to the *NF1* gene [*SSH2*, slingshot homolog 2 (*Drosophila*); *PSMD11*, proteasome (prosome, macropain) 26S subunit, non-ATPase, 11] were also included. In addition, the *MAP2K4* (mitogen-activated protein kinase kinase 4) gene, located in 17p, was selected as a control (i.e., a locus with 2 copies). Moreover, we selected 2 reference genes, *ADARB1* (21q22.3) and the LINE repetitive sequence L1PA (which is interspersed through the genome) to further normalize copy number data, as has been suggested *(35)*. We chose UPL probes for our study because of their advantages of higher specificity, higher PCR *E* values, and avoidance of primer-dimer signal that hydrolysis probes show, in contrast to fluorescent dyes such as SYBR Green. We also chose UPL probes for their flexibility of use and their reduced cost compared with DNA-sequenced hydrolysis probes.

Some experiments were performed to validate the qPCR assay. First, a set of 2-fold dilutions of pooled DNA samples (80 to 0.156 ng per reaction in triplicate) was used to determine the LDR and the *E* value of the primers used *(34)*. All designed primers showed a large LDR (at least 9 orders of magnitude) and high *E* values, which ranged from 1.88 to 2.11 for the loci analyzed (see Table 1 in the online Data Supplement).

Then, we determined the range of RCN values for a 2-copy status of the *NF1* gene by analyzing 24 control samples. The mean (SD) NRQ for the 12 loci and 24 samples interrogated was 0.99 (0.08) (Fig. 2). The mean calculated 99% CI of RCN for the 12 loci was 0.81–1.23. An RCN value below the lower limit of the CI for a locus was considered to indicate deletion of that particular locus.

The qPCR assay also showed low intraassay and interassay imprecision (see Table 1 in the online Data Supplement).

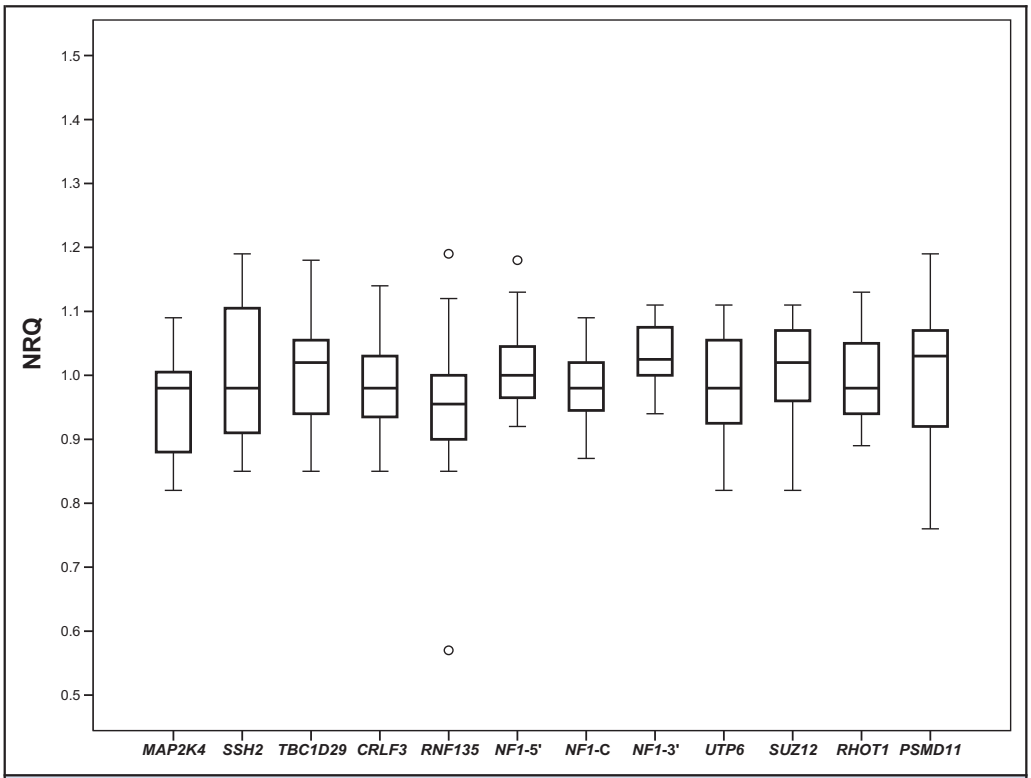

Fig. 2. Distribution of NRQ values for each of the 12 interrogated loci in a set of 24 control samples (with 2 copies of *NF1*).

Box plots with NRQ values plotted on the *y* axis and the different interrogated loci on the *x* axis. Outlier values are indicated (○). Data for box plots are presented as the median, interquartile range, and range.

DETECTION OF *NF1* CONSTITUTIONAL DELETIONS

After validating the qPCR assay with a panel of 24 control samples, we tested the performance of the qPCR assay by using a set of 14 DNA samples previously characterized and bearing a constitutional deletion of the *NF1* gene: 5 Type-1 deletions, 6 Type-2 deletions, and 3 atypical deletions. No Type-3 deletion was tested. All deletions were detected with the qPCR assay (Fig. 3; see Fig. 1 in the online Data Supplement). The mean (SD) RCN value within the deleted loci was 0.53 (0.07). Patient NF-01 bears a type 2 microdeletion. The DNA sample from this patient showed a mean RCN value of 0.68 (0.05) within the deleted loci. This result could reflect the presence of mosaicism for this microdeletion. Thus, when we considered all of the loci known to be deleted in our sample set, the qPCR assay showed 100% diagnostic sensitivity and 99.2% diagnostic specificity (see Table 2 in the online Data Supplement). The *SUZ12* locus, which is essential for distinguishing a Type-1 deletion from a Type-2 deletion, showed 100% diagnostic sensitivity and 96.9% diagnostic specificity. These results were confirmed in a parallel analysis of these samples with the MLPA technique (see Fig. 1 in the online Data Supplement).

DETECTION OF *NF1* SOMATIC DELETIONS

We also tested the performance of the qPCR assay for detecting somatic copy number losses by using samples from tumors and cells bearing different known somatic *NF1* deletions. Because the $NF1^{-/-}$ cellular component is not total, not only within a dNF (and other NF1-associated traits) *(17)* but also in tissues showing mosaicism for a constitutional *NF1* deletion, we first checked the reliability of the qPCR assay for detecting deletions in the context of mosaicism.

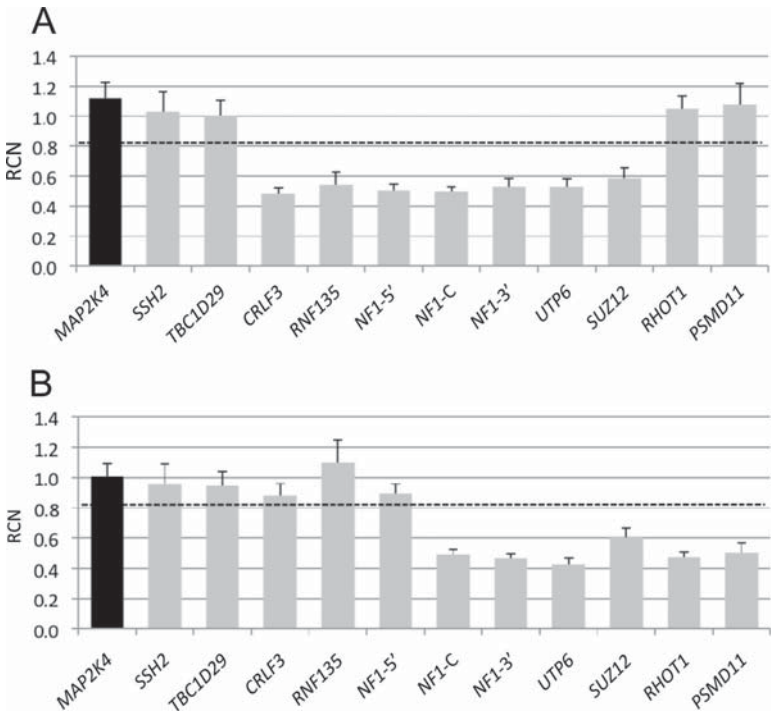

Fig. 3. Characterization of *NF1* constitutional deletions.

Mean (SD) RCN values for the 11 loci located in the *NF1* region (gray columns) and the *MAP2K4* control locus (black bar) for sample NF-05 (type 1 microdeletion) (A) and sample NF-12 (atypical microdeletion) (B). Dashed line indicates the RCN cutoff for deletion detection. For information on all constitutional deletions, see Fig. 1 and Table 2 in the online Data Supplement.

To assess the performance of the qPCR assay in admixtures of *NF1*-deleted and -nondeleted DNA samples, we set a cutoff value for the maximum percentage of *NF1*-nondeleted cells present in a tumor (or tissue) that the qPCR assay could tolerate and still detect the presence of a somatic *NF1* deletion. To choose this cutoff, we checked the performance of the qPCR assay with several admixtures of 2 DNA samples, one with 2 *NF1* copies and the other with a single *NF1* copy. We prepared 11 serial dilutions of NF-59 (*NF1* constitutional deletion) and NF-60 (sample with 2 *NF1* copies) with different DNA percentages of the 2 samples in quintuplicate (i.e., 0% to 100% of the sample with 2 *NF1* copies). For each admixture, the mean (SD) of the calculated RCN for the 6 loci (*NF1*-5′, *NF1*-C, *NF1*-3′, *CRLF3*, *RNF135*, and *UTP6*) was plotted against the percentage of DNA with 2 *NF1* copies present in the DNA admixture (Fig. 4A). To calculate the cutoff value for the percentage of cells with 2 *NF1* copies that the qPCR assay could tolerate and still detect the presence of an *NF1* deletion, we used the mean lower 99% confidence limit for all loci (0.81) (Fig. 4A). Hence, the qPCR assay detected *NF1* somatic deletions in dNFs containing less than 56% of *NF1*-nondeleted DNA.

We also set a cutoff value for the MLPA technique by using the same serial DNA admixtures used for the qPCR. These samples were analyzed in duplicate, and for each admixture we plotted the mean (SD) of the calculated copy number of the 11 loci (from the *CRLF3* 3780 probe to the *SUZ12* 3786 probe) against the percentage of DNA with 2 *NF1* copies present in the DNA admixture (Fig. 4B). We used an RCN value of 0.8 to obtain the cutoff value for the highest percentage of *NF1*-nondeleted cells in tumors at which the MLPA assay was able to detect the presence of an *NF1* deletion. This percentage was approximately 51%, similar to that of the qPCR assay.

To evaluate the ability of the qPCR assay to detect somatic deletions in dNFs and $SC^{NF1-/-}$ cells, we ana-

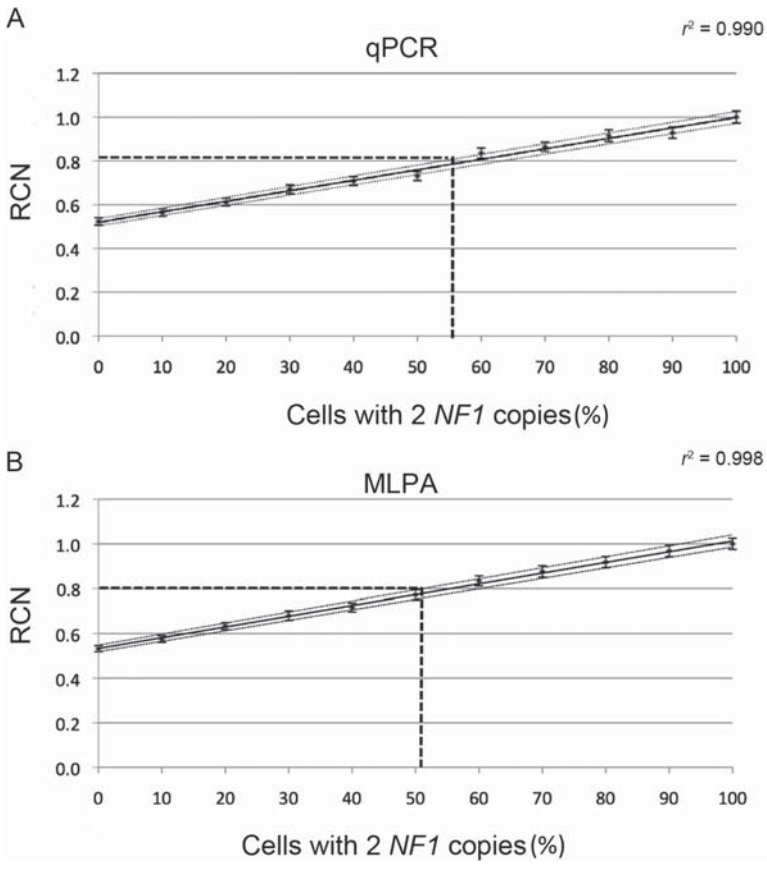

Fig. 4. Performance of the qPCR and MLPA assays in admixtures of 2 DNA samples with either 1 or 2 *NF1* copies.
Linear regression of RCN values (mean and SD) (*y* axis) on the percentage of DNA with 2 *NF1* copies within admixtures (*x* axis). Separate calculations for the qPCR assay (A) and the MLPA assay (B). Dashed thick lines indicate the threshold for deletion detection.

lyzed 16 DNA samples from dNFs and 5 $SC^{NF1-/-}$ samples bearing an *NF1* somatic deletion. First, we used MMPA to calculate the percentage of DNA with 2 *NF1* copies within tumor samples and cell cultures, as described elsewhere *(28)*. The results with this technique also confirmed the presence of deletions in the *NF1* region in these samples *(28)* (see Table 3 in the online Data Supplement).

The qPCR assay detected the presence of deletions in the *NF1* region in all 16 dNF and $SC^{NF1-/-}$ samples tested that contained <56% of the *NF1*-nondeleted component (Fig. 5; see Fig. 2 in the online Data Supplement). When all loci known to be deleted in this sample set were considered, the qPCR assay showed 90.5% diagnostic sensitivity and 98.9% diagnostic specificity (see Table 2 in the online Data Supplement). The technique was still able to detect a deleted locus in all 4 tumor samples with >56% of *NF1*-nondeleted DNA, but the diagnostic sensitivity and specificity values were lower (see Table 2 in the online Data Supplement). The mean RCN value within the deleted loci in $SC^{NF1-/-}$ samples was 0.62 (0.11); this result probably denotes the presence of cells with *NF1*-nondeleted DNA in the SC cultures.

All qPCR results for the detection of somatic *NF1* deletions in dNFs were confirmed with the results obtained with the parallel MLPA analysis (see Fig. 2 in the online Data Supplement).

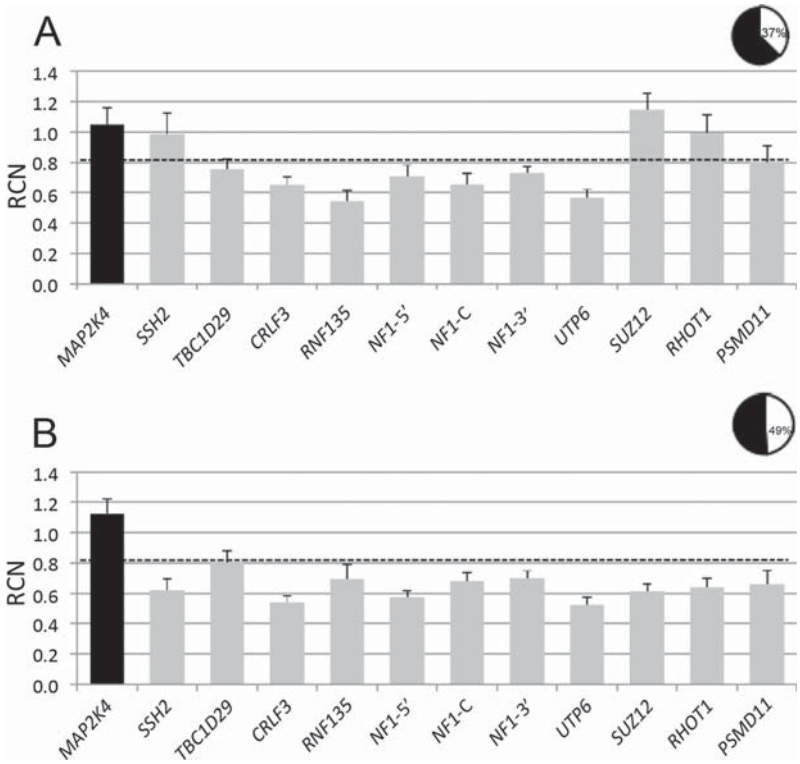

Fig. 5. Characterization of *NF1* somatic deletions.

RCN values (mean and SD) are shown for the 12 interrogated loci for 2 samples with somatic deletions: NF-28, containing 37% of cells (A) and NF-17, with 49% of cells with 2 *NF1* copies (B). Dashed line indicates the RCN cutoff for deletion detection. For information on all somatic deletions, see Fig. 2 and Table 2 in the online Data Supplement.

Discussion

Different techniques, including FISH, MLPA, and array comparative genomic hybridization, are currently being used to assess the presence of microdeletions involving the *NF1* locus. A qPCR approach has also been developed to validate deletions involving specific exons within the *NF1* gene that have previously been detected with MLPA analysis *(26)*. In addition, qPCR has been used to detect low percentages of somatic *NF1* point mutations *(38)*; however, until the present study qPCR analysis had not been used to detect and distinguish between different types of *NF1* microdeletions or to check for somatic second-hit deletions. We have developed a probe-based qPCR assay that detects both constitutional and somatic *NF1* deletions in samples from NF1 patients by interrogating the copy number of an approximately 2.8-Mb region that includes the *NF1* gene.

Our assay fulfills all of the essential aspects of the MIQE (minimum information for publication of quantitative real-time PCR experiments) guidelines *(39)* and most of the desirable information (see Table 4 in the online Data Supplement). Our adherence to these criteria strengthens the reliability of the developed qPCR assay and the results we have obtained. The assay requires small amounts of DNA: Each reaction is performed in just 8 μL, and only 15 ng per interrogated locus is required. qPCR reactions are highly efficient ($E > 1.88$) and amplify at similar rates with a large LDR. We used 5 ng DNA per PCR reaction, although smaller DNA quantities may be analyzed. Given all of the interrogated loci and replicates, a total of 210 ng is required per sample.

This assay enabled the detection of the 14 constitutional microdeletions and the 16 somatic deletions in dNFs containing <56% of *NF1*-nondeleted cells. The diagnostic sensitivity and specificity of our assay were near or at 100% when all of the interrogated loci were considered. For somatic deletions, the diagnostic sensitivity was around 90%, because the qPCR assay detected 2 copies for a few loci known to have a deletion. The presence of a deletion event in a dNF sample was considered, however, because most of the deleted loci within the 2.8-Mb *NF1* region in that sample were detected as single copies. In addition, to increase diagnostic specificity and minimize the false-positive rate, we applied a stringent CI (99%) to assess for the absence of a deletion.

qPCR is a highly analytically sensitive, specific, and precise technique that has several advantages over other methodologies. It is cheap and fast. Determining the copy number status of different loci in several samples can be performed in just 3 h, including plate preparation, PCR amplification, and data analysis. Detecting copy number changes in samples of DNA extracted with different methodologies and kits or from different tissues and tumors can be challenging for many techniques, such as MLPA. qPCR, however, is very robust with respect to the DNA quality, thereby permitting the screening and comparison of DNA samples from different sources.

The reliable design of the qPCR assay we have described, along with the specific locations of the 11 interrogated loci within the *NF1* region, allow accurate detection of Type-1, Type-2, and atypical *NF1* microdeletions and are suitable for detecting the rare Type-3 microdeletions. The assay could be expanded, if required, to incorporate more loci for assessment. This qPCR assay is also capable of detecting deletions in the context of mosaicism, a feature important for constitutional Type-2 microdeletions and for somatic deletions found in dNFs.

We believe this qPCR assay could be incorporated into a genetic-testing setting as a useful diagnostic tool, either as a first screening step or as a validation technique for *NF1* microdeletions (approximately 5% of NF1 cases). In addition, the assay allows the identification of somatic deletions in neurofibromas and other NF1 traits that require the double inactivation of the *NF1* gene, when the deletion is present in at least 44% of the tissue sample.

Author Contributions: *All authors confirmed they have contributed to the intellectual content of this paper and have met the following 3 requirements: (a) significant contributions to the conception and design, acquisition of data, or analysis and interpretation of data; (b) drafting or revising the article for intellectual content; and (c) final approval of the published article.*

Authors' Disclosures or Potential Conflicts of Interest: *Upon manuscript submission, all authors completed the author disclosure form. Disclosures and/or potential conflicts of interest:*

Employment or Leadership: None declared.
Consultant or Advisory Role: None declared.
Stock Ownership: None declared.
Honoraria: None declared.
Research Funding: Spanish Health Research Foundation: Instituto de Salud Carlos III (grant nos. PI081871, PI11/01609, and ISCIII-RTICC RD06/0020/1051), Government of Catalonia (grant no. 2009SGR290), and Asociación Española Contra el Cáncer (AECC).
Expert Testimony: None declared.
Patents: None declared.

Role of Sponsor: The funding organizations played no role in the design of study, choice of enrolled patients, review and interpretation of data, or preparation or approval of manuscript.

Acknowledgments: We thank Dr. S. Villatoro for technical advice, H. Evans for manuscript correction, Serra laboratory members, NF ICO-IMPPC group members, and the Asociación Española de Afectados de Neurofibromatosis for their constant support of our research.

References

1. Messiaen L, Wimmer K. NF1 mutational spectrum. In: Kaufmann D, ed. Neurofibromatoses. Basel: Karger; 2008. p 63–77. (Monographs in human genetics; vol. 16).
2. Jenne DE, Tinschert S, Reimann H, Lasinger W, Thiel G, Hameister H, Kehrer-Sawatzki H. Molecular characterization and gene content of breakpoint boundaries in patients with neurofibromatosis type 1 with 17q11.2 microdeletions. Am J Hum Genet 2001;69:516–27.
3. Dorschner MO, Sybert VP, Weaver M, Pletcher BA, Stephens K. NF1 microdeletion breakpoints are clustered at flanking repetitive sequences. Hum Mol Genet 2000;9:35–46.
4. Lopez Correa C, Brems H, Lazaro C, Marynen P, Legius E. Unequal meiotic crossover: a frequent cause of NF1 microdeletions. Am J Hum Genet 2000;66:1969–74.
5. Petek E, Jenne DE, Smolle J, Binder B, Lasinger W, Windpassinger C, et al. Mitotic recombination mediated by the JJAZF1 (KIAA0160) gene causing somatic mosaicism and a new type of constitutional NF1 microdeletion in two children of a mosaic female with only few manifestations. J Med Genet 2003;40:520–5.
6. Bengesser K, Cooper DN, Steinmann K, Kluwe L, Chuzhanova NA, Wimmer K, et al. A novel third type of recurrent NF1 microdeletion mediated by nonallelic homologous recombination between LRRC37B-containing low-copy repeats in 17q11.2. Hum Mutat 2010;31:742–51.
7. Pasmant E, Sabbagh A, Spurlock G, Laurendeau I, Grillo E, Hamel MJ, et al. NF1 microdeletions in neurofibromatosis type 1: from genotype to phenotype. Hum Mutat 2010;31:E1506–18.
8. Zickler AM, Hampp S, Messiaen L, Bengesser K, Mussotter T, Roehl AC, et al. Characterization of the nonallelic homologous recombination hotspot PRS3 associated with type-3 NF1 deletions. Hum Mutat 2012;33:372–83.
9. Steinmann K, Kluwe L, Cooper DN, Brems H, De Raedt T, Legius E, et al. Copy number variations in the NF1 gene region are infrequent and do not predispose to recurrent type-1 deletions. Eur J Hum Genet 2008;16:572–80.
10. Kayes LM, Burke W, Riccardi VM, Bennett R, Ehrlich P, Rubenstein A, Stephens K. Deletions spanning the neurofibromatosis 1 gene: identification and phenotype of five patients. Am J Hum Genet 1994;54:424–36.
11. Wu BL, Austin MA, Schneider GH, Boles RG, Korf BR. Deletion of the entire NF1 gene detected by the FISH: four deletion patients associated with severe manifestations. Am J Med Genet 1995;59:

528–35.
12. De Raedt T, Brems H, Wolkenstein P, Vidaud D, Pilotti S, Perrone F, et al. Elevated risk for MPNST in NF1 microdeletion patients. Am J Hum Genet 2003;72:1288–92.
13. Colman SD, Williams CA, Wallace MR. Benign neurofibromas in type 1 neurofibromatosis (NF1) show somatic deletions of the NF1 gene. Nat Genet 1995;11:90–2.
14. Sawada S, Florell S, Purandare SM, Ota M, Stephens K, Viskochil D. Identification of NF1 mutations in both alleles of a dermal neurofibroma. Nat Genet 1996;14:110–2.
15. Serra E, Puig S, Otero D, Gaona A, Kruyer H, Ars E, et al. Confirmation of a double-hit model for the NF1 gene in benign neurofibromas. Am J Hum Genet 1997;61:512–9.
16. Kluwe L, Friedrich R, Mautner VF. Loss of NF1 allele in Schwann cells but not in fibroblasts derived from an NF1-associated neurofibroma. Genes Chromosomes Cancer 1999;24:283–5.
17. Serra E, Rosenbaum T, Winner U, Aledo R, Ars E, Estivill X, et al. Schwann cells harbor the somatic NF1 mutation in neurofibromas: evidence of two different Schwann cell subpopulations. Hum Mol Genet 2000;9:3055–64.
18. Maertens O, Brems H, Vandesompele J, De Raedt T, Heyns I, Rosenbaum T, et al. Comprehensive NF1 screening on cultured Schwann cells from neurofibromas. Hum Mutat 2006;27:1030–40.
19. Thomas L, Spurlock G, Eudall C, Thomas NS, Mort M, Hamby SE, et al. Exploring the somatic NF1 mutational spectrum associated with NF1 cutaneous neurofibromas. Eur J Hum Genet 2012;20:411–9.
20. Garcia-Linares C, Fernandez-Rodriguez J, Terribas E, Mercade J, Pros E, Benito L, et al. Dissecting loss of heterozygosity (LOH) in neurofibromatosis type 1-associated neurofibromas: importance of copy neutral LOH. Hum Mutat 2011;32:78–90.
21. Lopez Correa C, Brems H, Lazaro C, Estivill X, Clementi M, Mason S, et al. Molecular studies in 20 submicroscopic neurofibromatosis type 1 gene deletions. Hum Mutat 1999;14:387–93.
22. Kluwe L, Siebert R, Gesk S, Friedrich RE, Tinschert S, Kehrer-Sawatzki H, Mautner VF. Screening 500 unselected neurofibromatosis 1 patients for deletions of the NF1 gene. Hum Mutat 2004;23:111–6.
23. Wimmer K, Yao S, Claes K, Kehrer-Sawatzki H, Tinschert S, De Raedt T, et al. Spectrum of single- and multiexon NF1 copy number changes in a cohort of 1,100 unselected NF1 patients. Genes Chromosomes Cancer 2006;45:265–76.
24. Messiaen LM, Callens T, Mortier G, Beysen D, Vandenbroucke I, Van Roy N, et al. Exhaustive mutation analysis of the NF1 gene allows identification of 95% of mutations and reveals a high frequency of unusual splicing defects. Hum Mutat 2000;15:541–55.
25. Riva P, Corrado L, Natacci F, Castorina P, Wu BL, Schneider GH, et al. NF1 microdeletion syndrome: refined FISH characterization of sporadic and familial deletions with locus-specific probes. Am J Hum Genet 2000;66:100–9.
26. De Luca A, Bottillo I, Dasdia MC, Morella A, Lanari V, Bernardini L, et al. Deletions of NF1 gene and exons detected by multiplex ligation-dependent probe amplification. J Med Genet 2007;44:800–8.
27. Pasmant E, Sabbagh A, Masliah-Planchon J, Haddad V, Hamel MJ, Laurendeau I, et al. Detection and characterization of NF1 microdeletions by custom high resolution array CGH. J Mol Diagn 2009;11:524–9.
28. Garcia-Linares C, Mercade J, Gel B, Biayna J, Terribas E, Lazaro C, Serra E. Applying microsatellite multiplex PCR analysis (MMPA) for determining allele copy-number status and percentage of normal cells within tumors. PLoS One 2012;7:e42682.
29. Thomas L, Kluwe L, Chuzhanova N, Mautner V, Upadhyaya M. Analysis of NF1 somatic mutations in cutaneous neurofibromas from patients with high tumor burden. Neurogenetics 2010;11:391–400.
30. De Luca A, Bernardini L, Ceccarini C, Sinibaldi L, Novelli A, Giustini S, et al. Fluorescence in situ hybridization analysis of allelic losses involving the long arm of chromosome 17 in NF1-associated neurofibromas. Cancer Genet Cytogenet 2004;150:168–72.
31. Steinmann K, Kluwe L, Friedrich RE, Mautner VF, Cooper DN, Kehrer-Sawatzki H. Mechanisms of loss of heterozygosity in neurofibromatosis type 1-associated plexiform neurofibromas. J Invest Dermatol 2009;129:615–21.
32. De Raedt T, Maertens O, Chmara M, Brems H, Heyns I, Sciot R, et al. Somatic loss of wild type NF1 allele in neurofibromas: comparison of NF1 microdeletion and non-microdeletion patients. Genes Chromosomes Cancer 2006;45:893–904.
33. Steinmann K, Cooper DN, Kluwe L, Chuzhanova NA, Senger C, Serra E, et al. Type 2 NF1 deletions are highly unusual by virtue of the absence of nonallelic homologous recombination hotspots and an apparent preference for female mitotic recombination. Am J Hum Genet 2007;81:1201–20.
34. Hellemans J, Mortier G, De Paepe A, Speleman F, Vandesompele J. qBase relative quantification framework and software for management and automated analysis of real-time quantitative PCR data. Genome Biol 2007;8:R19.
35. D'Haene B, Vandesompele J, Hellemans J. Accurate and objective copy number profiling using real-time quantitative PCR. Methods 2010;50:262–70.
36. Pfaffl MW. A new mathematical model for relative quantification in real-time RT-PCR. Nucleic Acids Res 2001;29:e45.
37. Vandesompele J, De Preter K, Pattyn F, Poppe B, Van Roy N, De Paepe A, Speleman F. Accurate normalization of real-time quantitative RT-PCR data by geometric averaging of multiple internal control genes. Genome Biol 2002;3:RESEARCH0034.
38. Maertens O, Legius E, Speleman F, Messiaen L, Vandesompele J. Real-time quantitative allele discrimination assay using 3′ locked nucleic acid primers for detection of low-percentage mosaic mutations. Anal Biochem 2006;359:144–6.
39. Bustin SA, Benes V, Garson JA, Hellemans J, Huggett J, Kubista M, et al. The MIQE guidelines: minimum information for publication of quantitative real-time PCR experiments. Clin Chem 2009;55:611–22.